frontiers | Research Topics

Insights in functional plant ecology 2022

Edited by
Boris Rewald, Jianshuang Wu and Antonio Montagnoli

Published in
Frontiers in Plant Science

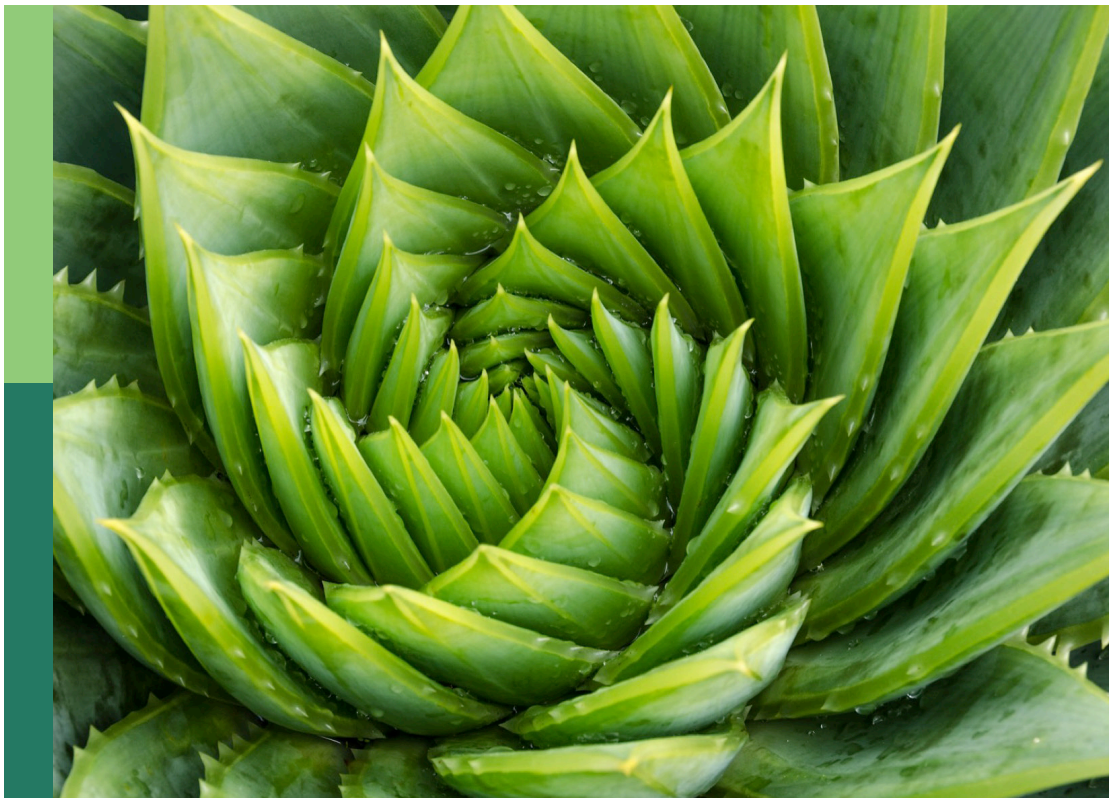

ISSN 1664-8714
ISBN 978-2-8325-3702-2
DOI 10.3389/978-2-8325-3702-2

About Frontiers

Frontiers is more than just an open access publisher of scholarly articles: it is a pioneering approach to the world of academia, radically improving the way scholarly research is managed. The grand vision of Frontiers is a world where all people have an equal opportunity to seek, share and generate knowledge. Frontiers provides immediate and permanent online open access to all its publications, but this alone is not enough to realize our grand goals.

Frontiers journal series

The Frontiers journal series is a multi-tier and interdisciplinary set of open-access, online journals, promising a paradigm shift from the current review, selection and dissemination processes in academic publishing. All Frontiers journals are driven by researchers for researchers; therefore, they constitute a service to the scholarly community. At the same time, the *Frontiers journal series* operates on a revolutionary invention, the tiered publishing system, initially addressing specific communities of scholars, and gradually climbing up to broader public understanding, thus serving the interests of the lay society, too.

Dedication to quality

Each Frontiers article is a landmark of the highest quality, thanks to genuinely collaborative interactions between authors and review editors, who include some of the world's best academicians. Research must be certified by peers before entering a stream of knowledge that may eventually reach the public - and shape society; therefore, Frontiers only applies the most rigorous and unbiased reviews. Frontiers revolutionizes research publishing by freely delivering the most outstanding research, evaluated with no bias from both the academic and social point of view. By applying the most advanced information technologies, Frontiers is catapulting scholarly publishing into a new generation.

What are Frontiers Research Topics?

Frontiers Research Topics are very popular trademarks of the *Frontiers journals series*: they are collections of at least ten articles, all centered on a particular subject. With their unique mix of varied contributions from Original Research to Review Articles, Frontiers Research Topics unify the most influential researchers, the latest key findings and historical advances in a hot research area.

Find out more on how to host your own Frontiers Research Topic or contribute to one as an author by contacting the Frontiers editorial office: frontiersin.org/about/contact

Insights in functional plant ecology 2022

Topic editors

Boris Rewald — University of Natural Resources and Life Sciences Vienna, Austria
Jianshuang Wu — Institute of Environment and Sustainable Development in Agriculture, Chinese Academy of Agricultural Sciences, China
Antonio Montagnoli — University of Insubria, Italy

Citation

Rewald, B., Wu, J., Montagnoli, A., eds. (2023). *Insights in functional plant ecology 2022*. Lausanne: Frontiers Media SA. doi: 10.3389/978-2-8325-3702-2

Table of contents

frontiers | Frontiers in Plant Science

TYPE Original Research
PUBLISHED 07 October 2022
DOI 10.3389/fpls.2022.978299

OPEN ACCESS

EDITED BY
Boris Rewald,
University of Natural Resources and Life Sciences Vienna, Austria

REVIEWED BY
Wen Xing Long,
Hainan University, China
Junpeng Mu,
Mianyang Normal University, China

*CORRESPONDENCE
Celina Ben Saadi
celina.bensaadi@gmail.com

SPECIALTY SECTION
This article was submitted to Functional Plant Ecology, a section of the journal Frontiers in Plant Science

RECEIVED 25 June 2022
ACCEPTED 15 September 2022
PUBLISHED 07 October 2022

CITATION
Ben Saadi C, Cayuela L, Bañares de Dios G, de Aledo JG, Matas-Granados L, Salinas N, La Torre Cuadros MdlÁ and Macía MJ (2022) Latitudinal patterns and environmental drivers of taxonomic, functional, and phylogenetic diversity of woody plants in western Amazonian *terra firme* forests. *Front. Plant Sci.* 13:978299. doi: 10.3389/fpls.2022.978299

Latitudinal patterns and environmental drivers of taxonomic, functional, and phylogenetic diversity of woody plants in western Amazonian *terra firme* forests

Celina Ben Saadi[1]*, Luis Cayuela[2], Guillermo Bañares de Dios[2], Julia G. de Aledo[1,3], Laura Matas-Granados[1,3], Norma Salinas[4,5], María de los Ángeles La Torre Cuadros[6,7] and Manuel J. Macía[1,3]

[1]Departamento de Biología, Área de Botánica, Universidad Autónoma de Madrid, Madrid, Spain, [2]Departmento de Biología y Geología, Física y Química Inorgánica, Universidad Rey Juan Carlos, Móstoles, Spain, [3]Centro de Investigación en Biodiversidad y Cambio Global (CIBC-UAM), Universidad Autónoma de Madrid, Madrid, Spain, [4]Sección Quíimica, Pontificia Universidad Católica del Perú, Lima, Peru, [5]School of Geography and Environment, University of Oxford, Oxfordshire, United Kingdom, [6]Departamento de Ciencias Agrarias, Universidad Científica del Sur, Villa el Salvador, Peru, [7]Departamento de Manejo Forestal, Universidad Nacional Agraria La Molina, Lima, Peru

Elucidating how environmental factors drive plant species distributions and how they affect latitudinal diversity gradients, remain essential questions in ecology and biogeography. In this study we aimed: 1) to investigate the relationships between all three diversity attributes, *i.e.*, taxonomic diversity (TD), functional diversity (FD), and phylogenetic diversity (PD); 2) to quantify the latitudinal variation in these diversity attributes in western Amazonian *terra firme* forests; and 3) to understand how climatic and edaphic drivers contribute to explaining diversity patterns. We inventoried *ca.* 15,000 individuals from *ca.* 1,250 species, and obtained functional trait records for *ca.* 5,000 woody plant individuals in 50 plots of 0.1 ha located in five *terra firme* forest sites spread over a latitudinal gradient of 1200 km covering *ca.* 10°C in latitude in western Amazonia. We calculated all three diversity attributes using Hill numbers: $q = 0$ (richness), $q = 1$ (richness weighted by relative abundance), and $q = 2$ (richness weighted by dominance). Generalized linear mixed models were constructed for each diversity attribute to test the effects of different uncorrelated environmental predictors comprising the temperature seasonality, annual precipitation, soil pH and soil bulk density, as well as accounting for the effect of spatial autocorrelation, *i.e.*, plots aggregated within sites. We confirmed that TD ($q = 0$, $q = 1$, and $q = 2$), FD ($q = 0$, $q = 1$, and $q = 2$), and PD ($q = 0$) increased monotonically towards the Equator following the latitudinal diversity gradient. The importance of rare species could explain the lack of a pattern for PD ($q = 1$ and $q = 2$). Temperature seasonality, which

was highly correlated with latitude, and annual precipitation were the main environmental drivers of variations in TD, FD, and PD. All three diversity attributes increased with lower temperature seasonality, higher annual precipitation, and lower soil pH. We confirmed the existence of latitudinal diversity gradients for TD, FD, and PD in hyperdiverse Amazonian *terra firme* forests. Our results agree well with the predictions of the environmental filtering principle and the favourability hypothesis, even acting in a 10°C latitudinal range within tropical climates.

KEYWORDS

latitudinal diversity gradient, taxonomic diversity (TD), functional diversity (FD), phylogenetic diversity (PD), environmental filtering, favourability hypothesis, tropical *terra firme* forest, woody plant

Introduction

Environmental drivers are key factors that determine plant diversity patterns at different spatial scales (McGill et al., 2006; HilleRisLambers et al., 2012; Arellano et al., 2016), but we still lack a comprehensive understanding of how environmental drivers act in hyperdiverse tropical forests (Wieczynski et al., 2019; Mori et al., 2021; Bañares de Dios et al., 2022). Diversity patterns have been traditionally explored in terms of taxonomic diversity (TD), *i.e.*, species identity (Swenson, 2011; Swenson et al., 2012c). TD provides insights into the distribution of diversity and its underlying mechanisms (Gentry, 1982) but it does not consider two important diversity attributes: functional adaptations and evolutionary history (Swenson, 2011; Dawson et al., 2013; Chao et al., 2014; López et al., 2016). Functional diversity (FD) provides information about phenotypic adaptation to the environment and it is measured through functional traits (Cornelissen et al., 2003; Pérez-Harguindeguy et al., 2013; Córdova-Tapia & Zambrano, 2015). Due to the adaptive information provided, the functional perspective has increased in importance compared with the classic taxonomic approach for answering questions about the interactions between communities and their surrounding environment (Cornelissen et al., 2003; Violle et al., 2007; Swenson, 2012a; Poorter et al., 2017; Poorter et al., 2018). In addition, phylogenetic diversity (PD) is defined as the degree of phylogenetic relatedness among co-occurring species (López et al., 2016; Pellens & Grandcolas, 2016; Massante et al., 2019). The use of PD has grown in popularity in recent decades because the evolutionary history of communities provide insights into species relationships and functional trait evolution (Lean & Maclaurin, 2016; Pellens & Grandcolas, 2016).

Environmental drivers such as climate and edaphic properties contribute to explaining diversity patterns in tropical *terra firme* forests, *i.e.*, non-flooding. Water availability and soil fertility are abiotic factors with key effects on favouring plant growth, and thus are the main drivers of variations in spatial diversity in lowland tropical forests (Gentry, 1988; Fortunel et al., 2014; Honorio Coronado et al., 2015; Poorter et al., 2017). The available water depends mainly on temperature, precipitation, and soil texture (Sollins, 1998; Clarholm & Skyllberg, 2013; Moles et al., 2014). Crucially, tropical rainforests experience important changes in water availability throughout the year due to precipitation and temperature seasonality (Malhi & Wright, 2004; Moles et al., 2014; Malizia et al., 2020). Therefore, the main climatic constraint on plant growth and survival is usually the severity and duration of the dry season (Malhi & Wright, 2004; Aubry-Kientz et al., 2015; Honorio Coronado et al., 2015), even under tropical climates. This seasonality follows a latitudinal pattern where it intensifies towards higher latitudes. Accordingly, climatic seasonality is the main driver of the global latitudinal diversity gradient, which is one of the most widely accepted diversity patterns on Earth, where TD increases from the poles towards the Equator as a result of climatic favourability (Fischer, 1960; Gentry, 1982; Willig et al., 2003; Weiser et al., 2007; Swenson et al., 2012c; Malizia et al., 2020). FD has also been shown to increase with decreasing latitude (Swenson et al., 2012b; Wieczynski et al., 2019), where the number of functional strategies increases as the climatic conditions become more benign (Fischer, 1960; Swenson et al., 2012b; Moles et al., 2014; Wieczynski et al., 2019). In woody angiosperms, PD also increases towards the Equator (Qian et al., 2013; Kerkhoff et al., 2014; Qian et al., 2017; Massante et al., 2019), partly due to the favourable climatic conditions found at lower latitudes.

Another important aspect of water availability is the soil water content, which depends greatly on the soil texture because it controls aeration, drainage and humidity retention capacity (Sollins, 1998; Rodrigues et al., 2019; Hofhansl et al., 2020). In addition, variability in soil fertility directly affects plant diversity

(Sanford & Cuevas, 1996; Garibaldi et al., 2014; Bañares de Dios et al., 2022). Most *terra firme* tropical soils are oligotrophic but they are rich in nitrogen (Sollins, 1998) with quite acidic pH values (Herrera et al., 1978; Medina & Cuevas, 1989; Sollins, 1998). The fertility of tropical soils depends on pH because it determines the availability of base-metal cations and toxicity of aluminum (Herrera et al., 1978; Sollins, 1998; Nelson & Su, 2010; Bañares de Dios et al., 2022). Nevertheless, species seem to tolerate these low nutrient, acidic, and high aluminum conditions (Herrera et al., 1978; Medina & Cuevas, 1989; Mori et al., 2021). Hence, both the soil nutrient availability and water content play critical roles in environmental filtering (Katabuchi et al., 2012; Rodrigues et al., 2019; Hofhansl et al., 2020), which is mainly dependent on the soil pH and texture (Sollins, 1998; Nelson & Su, 2010). In addition, the soil organic matter content favours moisture retention, cation exchange and nutrient turnover, thereby affecting the soil texture and fertility and thus improving soil quality (Craswell & Lefroy, 2001; Athira et al., 2019; Bañares de Dios et al., 2022). The bulk density is determined by the soil texture and it has an inverse relationship with the soil organic matter content, so it can be used as a proxy for the soil quality (Bauer, 1974; Athira et al., 2019; de la Cruz-Amo et al., 2020).

The main goal of the present study was to investigate the patterns of woody plant diversity in western Amazonian *terra firme* forests along a 1,200 km latitudinal gradient. Amazonian rainforests, specifically western Amazonian forests, harbour among the most hyperdiverse floras worldwide (Gentry, 1988; Wright, 2002; Honorio Coronado et al., 2015; Brooks, 2018). Amazonian rainforests are characterized by high abundance and diversity of woody angiosperms, where a limited number of species dominate the community (Pitman et al., 2013; Draper et al., 2021). The relatively low number of dominant taxa means that tropical communities usually harbour extremely large numbers of rare species (Ter Steege et al., 2013; Leitão et al., 2016; Draper et al., 2021; Cazzolla Gatti et al., 2022). Many studies have been conducted in Amazonian rainforests over the last century, but none analysed the latitudinal gradients of woody plants within tropical regions by considering all three diversity attributes comprising TD, FD, and PD. In this study we specifically aimed: 1) to investigate the relationship between all three diversity attributes; 2) to quantify the latitudinal variations in TD, FD and PD; and 3) to understand how climatic and edaphic drivers contribute to explaining diversity patterns. We hypothesized that all three diversity attributes would increase towards equatorial latitudes, mainly due to a reduction in seasonality harshness, with differential contributions of climatic drivers and soil properties, in agreement with environmental filtering.

Materials and methods

Study area and taxonomic characterization of plant communities

This study was conducted in western Amazonian forests which comprise several forest types, but the most extended are *terra firme* forests (Herrera et al., 1978). *Terra firme* forests are highly diverse and can contain up to 300 tree species per hectare (Gentry, 1988; Valencia et al., 1994). Western Amazonian forests formed on Pliocene and Pleistocene sediments from the Andes, which are fairly young and fertile soils compared with those in central and eastern Amazonia (Pitman et al., 2001; Hoorn et al., 2010; Lamarre et al., 2012; Honorio Coronado et al., 2015; Nobre et al., 2019). These forests have low annual thermal variability, high precipitation, and relatively well-drained fertile soils (Gentry, 1988; Burnham & Johnson, 2004; Brooks, 2018).

The study area encompassed 50 plots sampled throughout five western Amazonian regions in Peru spanning a 1,200 km latitudinal gradient from –2.9496°C to –12.8270°C and covering *ca*. 10°C in latitude (Figure 1, Table S1). The study regions corresponded to the protected areas of Tambopata National Reserve (Madre de Dios), Buffer Zone of Yanesha Communal Reserve (Pasco), Buffer Zone of Cordillera Azul National Park (Ucayali), Río Abiseo National Park (San Martín), and Maijuna-Kichwa Regional Conservation Area (Loreto). In each region 10 plots of 0.1 ha (50 × 20 m) were established according to Arellano et al. (2016). Plots were located in areas of well conserved *terra firme* lowland and submontane forests according to the biome classification of Britto (2017), and they were established at least 300 m apart from each other to minimize spatial autocorrelation. All woody plant individuals, including trees, lianas, and hemiepiphytes, rooting inside the plot limits with a diameter at breast height (DBH) ≥ 2.5 cm were included. Plot based studies usually apply an inclusion criterion of DBH ≥ 10 cm, so our study included a high number of juvenile and understory individuals that are rarely considered (Gentry, 1982; Arellano et al., 2016; Draper et al., 2021), which could increase the TD and PD by including typically smaller species, as well as FD by considering more understory individuals that grow in shadier conditions (Niinemets, 2010; Weerasinghe et al., 2014). Up to three individuals from each taxon were sampled in each region to obtain herbarium sheet duplicates and replicates to measure functional traits. Collected vouchers specimens were identified and stored primarily in the USM herbarium, with some duplicates at MOL herbarium. The herbarium acronyms followed Thiers (2021). Taxonomic names were standardized using the 'Taxostand' package in R (Cayuela et al., 2012).

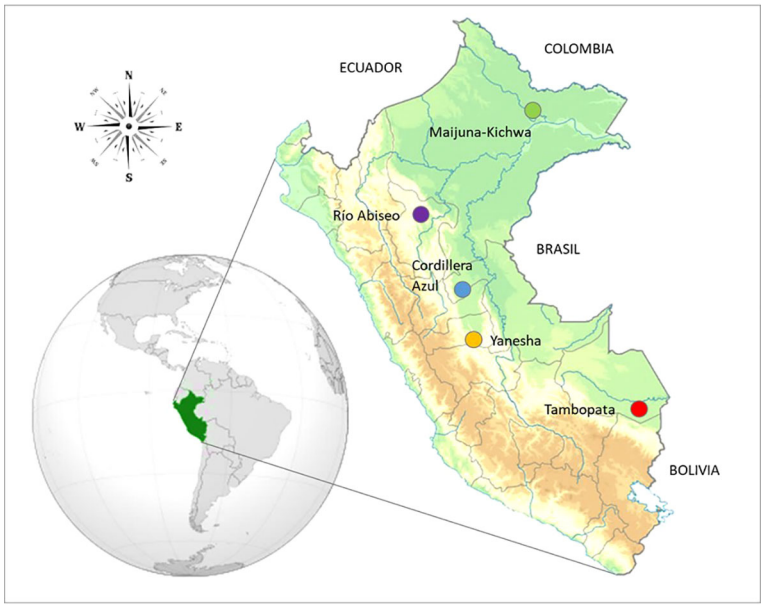

FIGURE 1
Map of Peru with coloured dots indicating the five regions studied in Western Amazonia. Top to bottom: Maijuna-Kichwa Regional Conservation Area, Río Abiseo National Park, Buffer Zone of Cordillera Azul National Park, Yanesha Comunal Reserve and Tambopata National Reserve.

Climatic and edaphic characterisation of study sites

Climatic data for each plot were retrieved from the CHELSA database (Karger et al., 2019). All 19 CHELSA temperature and precipitation related bioclimatic variables were considered (Table S2).

Five soil subsamples were collected in a zigzag pattern within the plot limits and mixed to obtain one representative sample for each plot. A metallic cylinder was used to extract subsamples of the first 15 cm of the soil layer below plant debris. After mixing and air drying, the soil samples were sieved through a 2 mm mesh to separate the organic fraction comprising organic matter debris, such as leaves and roots, and the coarse fraction. The remaining soil corresponded to the fine fraction which was used for chemical and textural analyses (Table S3). The pH was measured in distilled water as the real acidity and in KCl as the potential acidity. The organic carbon content and total N, S, and C contents were measured using the LECO/Dumas direct combustion method. The available Al contents and those of macronutrients (P, Ca, Mg, Na, and K) and micronutrients (Fe, Co, Cu, Mn, Ni, and Zn) were measured by extraction with the Melich III method followed by an inductively coupled plasma mass spectrometry. Textural analyses were performed using the hydrometer method after adding dispersal solution. Soil mineralogy and clay contents were measured by X-ray diffraction. The soil sampling and characterization analyses were based on the protocols described by Arellano et al. (2016).

To avoid collinearity, we calculated Pearson's correlation coefficients *(r)* between all environmental variables (Figure S1), *i.e.*, climate, soil, and latitude. Most of the environmental variables were highly correlated, so we selected two climatic and two edaphic uncorrelated variables based on previous studies. The selected climatic factors comprised the temperature seasonality (°C) and annual precipitation (mm/year) because they reflect climatic limitations on plant growth (Malhi & Wright, 2004; Aubry-Kientz et al., 2015). The selected edaphic factors comprised the pH as an approximation of soil fertility (Sollins, 1998; Nelson & Su, 2010) and the soil bulk density (g/cm^3) to consider the soil texture and organic matter content (Bauer, 1974; Motavalli et al., 1995; Athira et al., 2019).

Functional characterization of plant communities

Three functional traits comprising the specific leaf area (SLA), leaf thickness (LT) and wood density (WD) were measured for each individual collected. These traits are used extensively because they are robust indicators of the functional strategies of woody plants in the leaf (Wright et al., 2004) and wood economy spectrum (Chave et al., 2009). Five mature leaves were used to measure the foliar traits. SLA (mm^2/mg) was calculated as the ratio between the leaf surface area measured with a CI-202 Portable Laser Leaf Area Meter (CID Bio-Science, WA, USA) and dry mass after drying for 48 h at 80°CC. SLA

measurements included all of the leaf structures. LT (mm) was measured with a digital calliper. The branch wood density was used as an approximation for WD (Swenson & Enquist, 2008). For each individual collected, a 10 cm branch section was peeled to remove the bark and its dimensions were measured with a digital calliper to calculate the fresh volume. WD (g/cm^3) was calculated as the ratio between the dry mass after drying for 48 h at 80°CC and the fresh volume. All measurements and calculations followed standardized protocols (Cornelissen et al., 2003). Only individuals with records for all three functional traits were included for functional characterization. Mean trait values were calculated for each taxon.

Phylogenetic characterization of plant communities

We obtained a phylogenetic tree using the *V.PhyloMaker* package in R (Jin & Qian, 2019). This package allowed us to prune a pre-existing mega-tree of vascular plants based on the phylogenies of Smith and Brown (2018) and Zanne et al. (2014) for seed plants and pteridophytes, respectively, with a given list of species. The 'phylo.maker' function was used with the arguments *nodes=nodes.info.1* and *scenarios=S3*.

Diversity measurements

We calculated Hill numbers for TD, FD and PD. Hill numbers only differ in terms of the parameter q, which determines the sensitivity to relative abundances (Hill, 1973). For TD (Chao et al., 2014): $q = 0$ denotes the species richness (*i.e.*, number of species), $q = 1$ represents the richness considering relative abundance (*i.e.*, Shannon's diversity), and $q = 2$ is the richness considering dominance (*i.e.*, inverse of Simpson's index). Hence, the contribution of rare species to diversity decreases as the value of the parameter q increases. Hill numbers were typically only used for TD but Chao et al. (2010) extended them to PD based on the phylogenetic distances between species, and Chiu and Chao (2014) extended them to FD based on the functional distances between species traits.

By considering the Hill numbers for all three diversity attributes we can obtain a unified framework of attribute diversity, where each component is measured in different units or entities (Chao et al., 2014). TD is measured as the effective number of taxonomic entities, so the attribute value is unity for each taxon. For FD, the attribute value is the functional distance between each pair of taxa based on functional traits, and thus it is measured as the effective number of functional entities. PD is measured as the effective number of phylogenetic entities, where the attribute value is the length of each branch segment. All entities are treated as taxonomically, functionally and phylogenetically equally distinct. Hill numbers for $q = 0$, $q = 1$, and $q = 2$ were obtained for the three diversity attributes using the 'renyi' function in the *vegan* package for TD, with the code provided by Chiu and Chao (2014) for FD, and with the 'ChaoPD' function in the *entropart* package (Chao et al., 2010) for PD. Using different Hill numbers to explore diversity allowed us to examine how rare, abundant, and dominant species responded to the environmental factors and latitude.

Data analyses

First, we explored the relationships between different Hill numbers as well as between Hill numbers and latitude using negative binomial generalized linear models (GLMs). To fit these models, we used the 'glm.nb' function in the *MASS* package (Venables & Ripley, 2002). To account for the variance explained by the models, we calculated Cragg and Uhler's pseudo-R-squared (pR^2) using the 'pR2' function in the *pscl* package (Jackman, 2020). We then constructed negative binomial generalized linear mixed models (GLMMs) to assess the effects of climatic and edaphic variables on the Hill numbers for each diversity attribute by using the 'glmer.nb' function in the *lme4* package (Bates et al., 2015). Environmental variables comprising the temperature seasonality, annual precipitation, soil pH and soil bulk density were included as fixed effects, whereas region (n = 5) was treated as a random factor to account for potential spatial autocorrelation among plots sampled within the same region. The latitude was not a factor itself but instead it was a surrogate for climatic gradients (Willig et al., 2003), so it was not included in the models. Nevertheless, it was indirectly considered because it was significantly negatively correlated with temperature seasonality. Temperature and seasonality have been shown to reflect the effects of latitudinal variation (Willig et al., 2003; Swenson et al., 2012b), thereby justifying our approach of using temperature seasonality as an accurate proxy for latitude in the models. Interaction terms between predictors were not included. Model selection was conducted based on Akaike's Information Criterion corrected for small sample size (AICc). When models had a difference in AICc ≥ 2, the model with the highest AICc was considered less than optimal and rejected. When two or more models had a difference in AICc< 2, we selected the most complex to generate model predictions. We calculated two components of the pseudo-R-squared for GLMMs: marginal (R^2_m) and conditional (R^2_c) coefficients, which represent the variance explained by fixed effects and by both random and fixed effects, respectively (Nakagawa & Schielzeth, 2013). We used the 'r.squaredGLMM' function in the *MuMIn* R package (Barton, 2013). All analyses were conducted in R v4.2.1 (R Core Team, 2021).

Results

Environmental and taxonomic overview

The temperature seasonality ranged from 4.16°C in Maijuna to 9.30°C in Tambopata (Table S1) and it had a strong significant

correlation with latitude (r = –0.97; Table S4). The maximum annual precipitation was recorded at Cordillera Azul with 3948 mm and the minimum at Río Abiseo with 1756 mm (Table S1), and it had no significant correlation with latitude (r = –0.09; Table S4). Among the edaphic properties, the soil bulk density and pH were not correlated with each other (r = –0.26; Table S4). Both variables were weakly correlated with the annual precipitation (bulk density: r = 0.40; pH: r = –0.29; Table S4), but not with the temperature seasonality (bulk density: r = 0.25; pH: r = –0.18; Table S4) or latitude (bulk density: r = –0.20; pH: r = 0.11; Table S4). The bulk density ranged from 0.61 to 1.00 g/cm^3 and it varied fairly heterogeneously among the sites. The pH ranged from 3.78 to 5.46 (Table S1), although all of the pH values above 5.0 were determined in white sand soils in seven plots in Río Abiseo.

Overall, 14,681 individuals were inventoried in five regions belonging to 2,211 species (See Table S5 for the list of species). A total of 302 taxa were identified in Tambopata, 467 taxa in Yanesha, 511 taxa in Cordillera Azul, 154 taxa in Río Abiseo and 542 taxa in Maijuna (Table S6). Among the functional data, 274 taxa had records for all functional traits in Tambopata, 442 taxa in Yanesha, 466 taxa in Cordillera Azul, 269 taxa in Río Abiseo and 450 taxa in Maijuna (Table S6). The generated phylogenetic tree included 302 taxa present in Tambopata, 467 taxa in Yanesha, 511 taxa in Cordillera Azul, 292 taxa in Río Abiseo and 542 taxa in Maijuna (Table S6).

Correlation between diversity attributes

When all sites were considered together in the analysis, TD and FD were positively and significantly correlated with each other for all three Hill numbers q = 0 (pR^2 = 0.71), q = 1 (pR^2 = 0.66), and q = 2 (pR^2 = 0.50) (Figure 2A; Table 1). However, when PD was considered with either TD or FD, the only Hill numbers with positive and significant correlations were q = 0 (with TD: pR^2 = 0.90; with FD: pR^2 = 0.81) and q = 1 (with TD: pR^2 = 0.51; with FD: pR^2 = 0.53) (Figures 2B, C; Table 1).

Latitudinal patterns

When the TD patterns were explored across latitude, significant positive relationships were found for all three Hill numbers: q = 0 (pR^2 = 0.27), q = 1 (pR^2 = 0.34), and q = 2 (pR^2 = 0.28) (Figure 3A; Table 2), thereby indicating that diversity increases towards the Equator. For FD, all of the Hill numbers exhibited significant positive trends, but latitude explained a lower proportion of the variability in FD: q = 0 (pR^2 = 0.10), q = 1 (pR^2 = 0.12), and q = 2 (pR^2 = 0.10) (Figure 3B; Table 2). The only Hill number for PD that had a significant positive latitudinal trend was q = 0 (pR^2 = 0.27) (Figure 3C; Table 2).

Effects of environmental variables on TD, FD and PD

Our results indicated monotonic increases in all diversity attributes towards lower latitudes, except when we considered relative abundances (q = 1) and dominance (q = 2) for PD (Figure 3B). Analysis of the contributions of environmental variables to diversity indicated that climatic factors seemed to be responsible for the latitudinal diversity pattern, whereas the edaphic properties appeared to have different effects on common and rare species (Figure 4). The effect of temperature seasonality was significant for all diversity attributes irrespective of whether relative abundances and dominance were considered (Figure 4).

The best-fit model was selected for each diversity attribute and each Hill number based on the AICc values. All of the best-fit models for TD, FD, and PD included temperature seasonality, which was highly correlated with latitude (r = –0.97; Table S4), and annual precipitation as fixed terms (Figure 4; Table 3). Both the soil pH and density appeared in the best-fit models for TD with q = 0, and PD with q = 0 and q = 1 (Figure 4; Table 3). In addition, pH was also present in TD with q = 1 and all three best-fit models for FD (Figure 4; Table 3). The best-fit model for PD with q = 2 (Table 3) had no explanatory variables except for the random factor, *i.e.*, null model.

Discussion

Correlations between diversity attributes

The relationship between TD and FD is clear because, a larger potential range of functional strategies can be found when more species are present (Kooyman et al., 2012). We found that TD and FD were positively and significantly correlated (Figure 2A) even when more weight was given to abundant and dominant taxa (q = 1 and especially q = 2), thereby suggesting that although dominant species exhibited a narrower spectrum of functional strategies compared with rare species, they were not limited to the same suite of functional strategies, and thus FD increased as the number of dominant species increased (Figure 2A, q = 2). The relationship between TD and FD was in agreement with previous studies conducted at a global scale (Li et al., 2018), in the New World (Swenson et al., 2012b; Lamanna et al., 2014), and North America (Swenson & Weiser, 2014).

In addition, TD is closely related to PD, and thus they should be strongly positively correlated (Honorio Coronado et al., 2015). However, local speciation or extinction events could lead to the adaptive radiation of a few lineages and the opposite trend, *i.e.*, high TD and low PD (Losos, 2008; Massante et al., 2019). Our results showed that TD and PD increased together (Figure 2B, q = 0 and q = 1), so there seemed

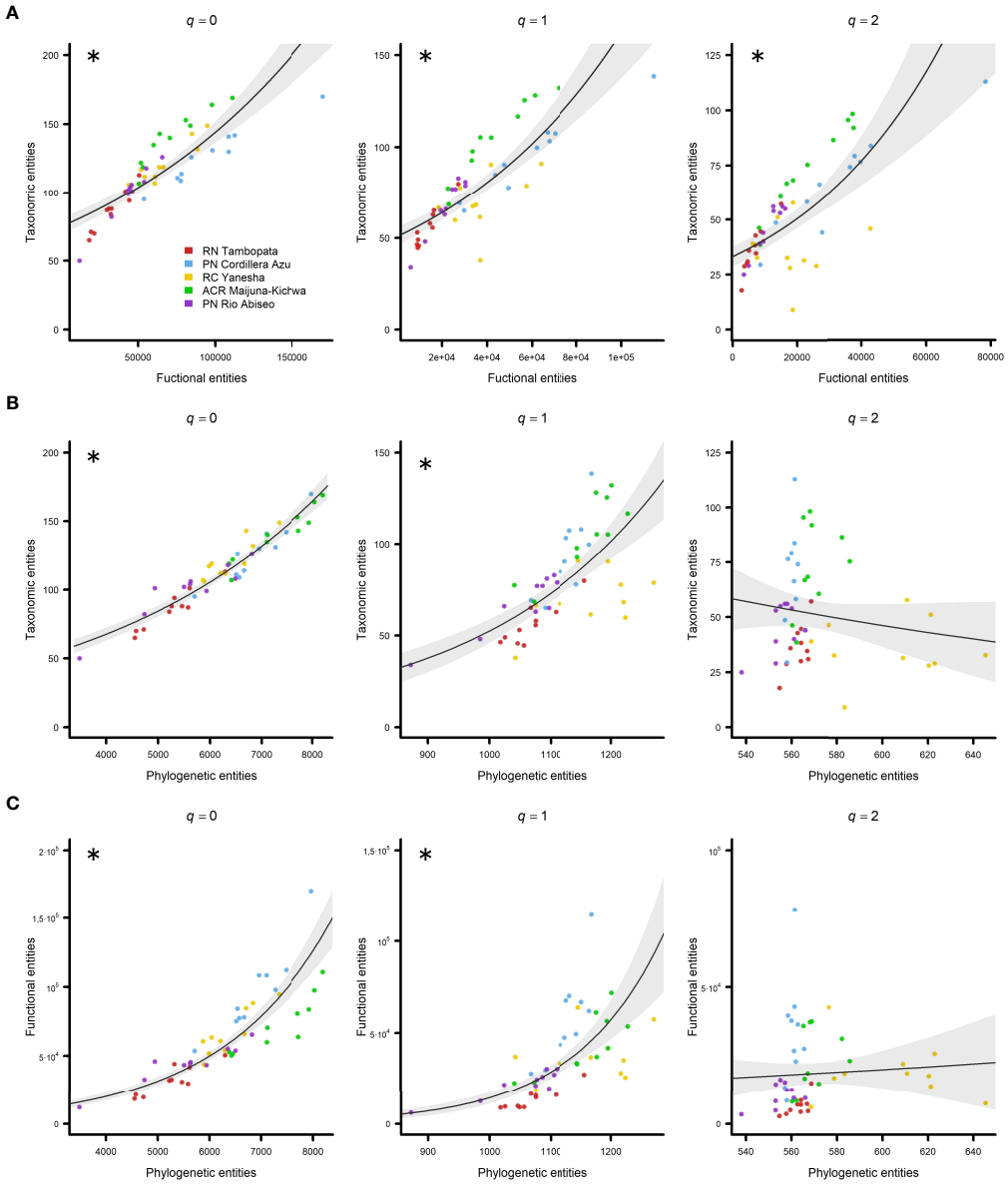

FIGURE 2
Relationship between diversity attributes in all five regions studied in Western Amazonia represented by negative binomial generalized linear models (GLMs) with 95% confidence intervals. **(A)** Taxonomic vs. functional entities, **(B)** taxonomic vs. phylogenetic entities, and **(C)** functional vs. phylogenetic entities. Hill numbers were considered as diversity indexes: q = 0 (left column), q = 1 (central column), and q = 2 (right column). Regions are represented by different colours (see the legend). Significant pseudo R-squared (pR^2) values are marked with asterisks.

to be no indication of high diversification by a few lineages as shown in a previous study (Giehl & Jarenkow, 2012). However, this was not the case when we considered dominance (Figure 2B, $q = 2$) because a few clades appeared to account for many of the dominant species (Draper et al., 2021).

Finally, phylogenetic relatedness involves some degree of evolutionary preservation of the adaptive strategies reflected in functional traits (Swenson et al., 2012c; López et al., 2016; Coelho de Souza et al., 2019). Thus, if FD is strongly influenced by a shared evolutionary history, there should be a positive correlation between phylogenetic proximity and ecological similarity (Webb, 2000; Webb et al., 2008; Kooyman et al., 2012). However, not all functional traits are necessarily phylogenetically conserved (Cavender-Bares et al., 2004; Swenson & Enquist, 2009; López et al., 2016), and strong adaptation of related lineages to a heterogeneous environment leads to high FD and low PD, thereby inverting the trend (Losos, 2008; López et al., 2016). The positive relationship between FD and PD (Figure 2C, $q = 0$ and $q =$

TABLE 1 Pseudo R-squared (pR^2) values for negative binomial generalized linear models (GLMs) between diversity attributes for different Hill numbers: taxonomic diversity (TD), functional diversity (FD), and phylogenetic diversity (PD).

Study areas	Hill numbers	TD vs. FD	TD vs. PD	FD vs. PD
All sites	*q = 0*	0.71***	0.90***	0.81***
	q = 1	0.66***	0.51***	0.53***
	q = 2	0.50***	0.02	0.00
Tambopata	*q = 0*	0.81***	0.80***	0.78***
	q = 1	0.75***	0.70***	0.85***
	q = 2	0.76***	0.47**	0.62***
Cordillera Azul	*q = 0*	0.84***	0.84***	0.93***
	q = 1	0.87***	0.64***	0.77***
	q = 2	0.78***	0.03	0.13
Yanesha	*q = 0*	0.71***	0.67***	0.76***
	q = 1	0.21	0.26	0.07
	q = 2	0.01	0.00	0.07
Maijuna	*q = 0*	0.79***	0.82***	0.86***
	q = 1	0.86***	0.76***	0.75***
	q = 2	0.90***	0.13	0.10
Río Abiseo	*q = 0*	0.89***	0.83***	0.78***
	q = 1	0.88***	0.85***	0.88***
	q = 2	0.83***	0.33*	0.29*

Significance levels represented by: (*) when p<0.05, (**) when p<0.01 and (***) when p<0.001.

1) suggested that the functional traits in our study were phylogenetically conserved. However, when dominance was considered (q = 2), the dominant clades probably had a limited set of functional adaptations and/or these traits were not phylogenetically conserved. The absence of significant relationships between TD–PD and FD–PD when considering dominance (Figures 2B, C, q = 2) were probably due to seven plots in Yanesha with surprisingly high PD but relatively low TD, *i.e.*, a few species from distant lineages dominated the community, and FD, *i.e.*, a few functional strategies that appeared in distant lineages dominated the community.

Regardless of the causes, the positive relationships between the three diversity attributes showed that if we take action to preserve and conserve communities with high TD, we are also indirectly preserving FD and PD, at least in western Amazonian *terra firme* forests.

Latitudinal patterns

Overall, our results indicated that the three diversity attributes increased monotonically towards the Equator in western Amazonian *terra firme* forests (Figure 3), where they consistently followed the latitudinal diversity gradient. These findings agree well with the predictions of the environmental filtering principle, which states that communities are shaped by abiotic deterministic factors (Götzenberger et al., 2012; López et al., 2016; Poorter et al., 2017), and the favourability hypothesis, which maintains that the effect of environmental filtering becomes more restrictive when the environmental conditions are less favourable (Swenson et al., 2012b; Lamanna et al., 2014; Wieczynski et al., 2019), and thus they forecast that TD, FD, and PD will increase towards lower latitudes due to climatic favourability (Fischer, 1960; Weiser et al., 2007; Swenson et al., 2012c; Qian et al., 2013; Qian et al., 2017; Kubota et al., 2018; Massante et al., 2019; Wieczynski et al., 2019). In addition, our results showed that the latitudinal decrease in all three diversity attributes was noticeable within tropical areas, even in a 10°C latitudinal gradient. Thus, although tropical environments have benign climatic conditions in global terms, environmental filtering and climatic favourability are still important for these species-rich communities (Fortunel et al., 2014). In fact, several studies found that environmental filtering had a stronger effect in species-rich communities, such as tropical forests, compared with species-poor communities (Lamanna et al., 2014; Swenson & Weiser, 2014; Li et al., 2018)

We found a monotonic increase in TD with decreasing latitude, which was consistent for all Hill numbers (Figure 3A), thereby indicating that this pattern remained regardless of whether the relative abundances (q = 1) and dominance (q = 2) of taxa were considered. Our results showed that TD increased towards the Equator, which is a widely accepted trend (Fischer, 1960; Gentry, 1982; Willig et al., 2003; Weiser et al., 2007). Some recent studies of

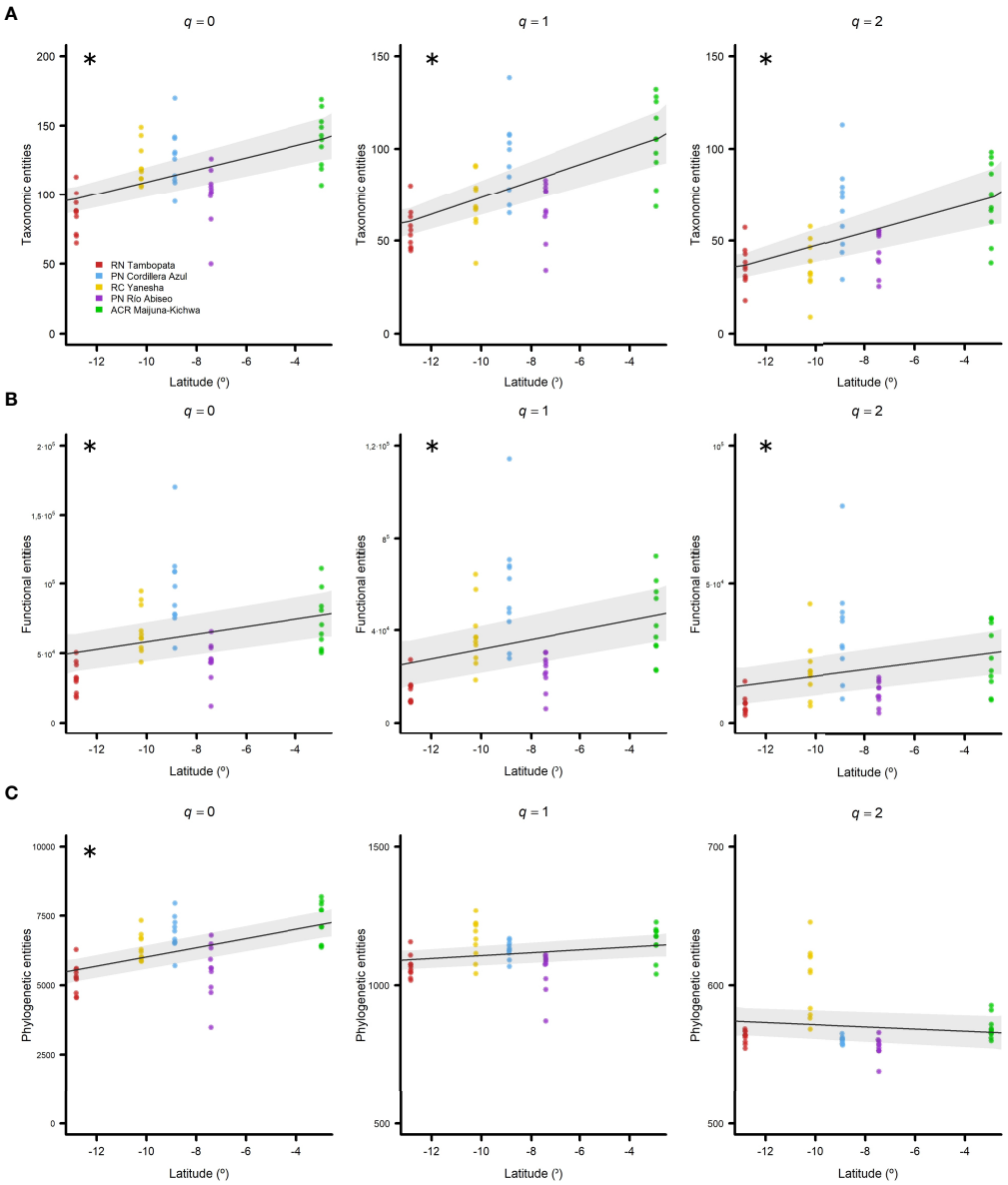

FIGURE 3
Diversity latitudinal trends for all five regions studied in Western Amazonia represented by negative binomial generalized linear models (GLMs) with 95% confidence intervals. **(A)** Taxonomic, **(B)** functional, and **(C)** phylogenetic entities found against latitude in decimal degrees. Hill numbers were considered as diversity indexes: q = 0 (left column), q = 1 (central column), and q = 2 (right column). Regions are represented by different colours (see the legend). Significant pseudo R-squared (pR^2) values are marked with asterisks.

latitudinal gradients obtained similar results in terms of the species richness in North America (Qian et al., 2013) and South America (Cazzolla Gatti et al., 2022).

Our results indicated a monotonic increase in FD with decreasing latitude (Figure 3B), which is in agreement with previous studies of woody plants in the New World (Swenson et al., 2012b; Lamanna et al., 2014). This finding was consistent for all Hill numbers, thereby indicating that this pattern remained regardless of whether relative abundances (q = 1) and dominance (q = 2) were considered. The reduction in functional entities when abundance and dominance were considered could be explained by the absence of rare species with rare ecological strategies, *i.e.*, uncommon combinations of functional traits, which were greatly responsible for the FD of the community (Mouillot et al., 2013; Leitão et al., 2016).

Finally, we found a monotonic increase in PD of woody plants with decreasing latitude only for the Hill number of q = 0 (Figure 3C). This pattern is consistent with recent studies of woody angiosperms in the New World (Kerkhoff et al., 2014), North America (Qian et al., 2013), and even at a global scale

TABLE 2 Pseudo R-squared (pR^2) values for negative binomial generalized linear models (GLMs) between latitude and diversity attributes for different Hill numbers: taxonomic diversity (TD), functional diversity (FD) and phylogenetic diversity (PD).

Diversity atributes	Hill numbers	pR^2
TD	$q = 0$	0.27***
	$q = 1$	0.34***
	$q = 2$	0.28***
FD	$q = 0$	0.10*
	$q = 1$	0.12**
	$q = 2$	0.10**
PD	$q = 0$	0.27***
	$q = 1$	0.05
	$q = 2$	0.01

Significance levels represented by: (*) when p<0.05, (**) when p<0.01 and (***) when p<0.001.

(Qian et al., 2017). The results obtained by Massante et al. (2019) appear to contradict ours because they found a worldwide increase in PD of woody plants towards higher latitudes. However, they also considered gymnosperms in their analyses, which usually have greater tolerance of harsher conditions at high latitudes, and the trend inverted when they were excluded. In addition, no significant trend was found between PD and latitude when relative abundances and dominance were considered (Figure 3C, $q = 1$ and $q = 2$, respectively), which remained fairly constant along the latitudinal gradient. The decrease in phylogenetic entities and loss of the latitudinal pattern can be explained by the high contribution of rare species to diversity in species-rich tropical communities (Leitão et al., 2016; Lamanna et al., 2017; Cazzolla Gatti et al., 2022).

The presence and persistence of rare species is inversely correlated with latitude in tropical forests worldwide (Lamanna et al., 2017). In addition, the diversity of all species increases towards lower latitudes, but the diversity of rare species appears to increase more steeply than those of common or dominant species when approaching the Equator (Stevens & Willig, 2002; Lamanna et al., 2017). Thus, the loss of a significant latitudinal pattern for PD ($q = 1$ and $q = 2$) in the present study suggests important contributions of rare species to the maintenance of PD in western Amazonian *terra firme* forests (Leitão et al., 2016).

Effects of environmental variables on TD, FD, and PD

The overall diversity tended to increase as the temperature seasonality decreased, annual precipitation increased, soil pH

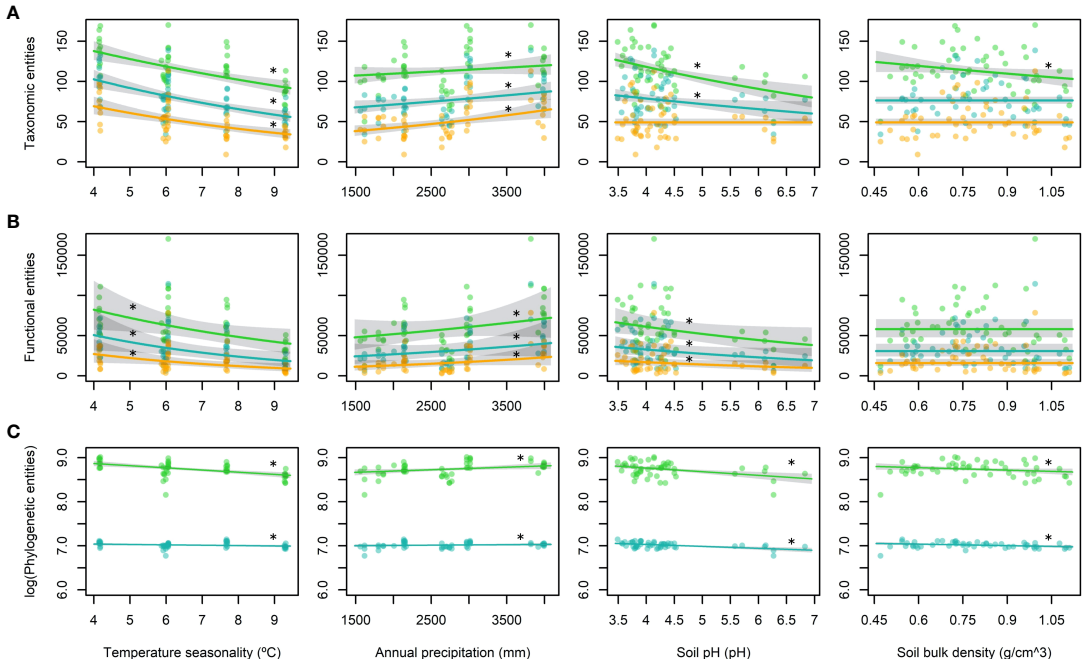

FIGURE 4
Predictions of the best-fit generalized linear mixed models (GLMMs) with 95% confidence intervals for each diversity attribute: **(A)** taxonomic entities, **(B)** functional entities, and **(C)** phylogenetic entities. Hill numbers are shown in different colours: $q = 0$ in green, $q = 1$ in blue, and $q = 2$ in yellow. Each column corresponds to one of the terms included in the models: temperature seasonality (left column), annual precipitation (central left column), soil pH (central right column), and soil bulk density (right column). Terms included in the best-fit model are marked with asterisks.

TABLE 3 Comparison of the best alternative models for Hill numbers of taxonomic diversity (TD), functional diversity (FD), and phylogenetic diversity (PD) as functions of temperature seasonality, annual precipitation, soil pH, and soil bulk density.

Diversity attribute	Hill numbers	Formulae for the best models	df	AICc	R^2_m	R^2_c
TD	q = 0	TD.q0 ~ (1|Region) + Temperature seasonality + Soil pH + Soil density	8	446.90	0.540	0.540
		TD.q0 ~ (1|Region) + Temperature seasonality + Annual precipitation + Soil pH + Soil density	**9**	**448.11**	**0.555**	**0.555**
	q = 1	TD.q1 ~ (1|Region) + Temperature seasonality + Soil pH	7	433.66	0.507	0.512
		TD.q1 ~ (1|Region) + Temperature seasonality + Annual precipitation + Soil pH	**8**	**433.17**	**0.556**	**0.556**
	q = 2	**TD.q2 ~ (1|Region) + Temperature seasonality + Annual precipitation**	**7**	**426.32**	**0.482**	**0.482**
FD	q = 0	FD.q0 ~ (1|Region) + Soil pH	6	1140.76	0.066	0.596
		FD.q0 ~ (1|Region) + Temperature seasonality + Soil pH	7	1139.81	0.329	0.583
		FD.q0 ~ (1|Region) + Temperature seasonality + Annual precipitation + Soil pH	**8**	**1141.35**	**0.415**	**0.584**
	q = 1	FD.q1 ~ (1|Region) + Soil pH	6	1098.98	0.045	0.623
		FD.q1 ~ (1|Region) + Temperature seasonality + Soil pH	7	1097.58	0.362	0.612
		FD.q1 ~ (1|Region) + Temperature seasonality + Annual precipitation + Soil pH	**8**	**1099.14**	**0.438**	**0.616**
	q = 2	FD.q2 ~ (1|Region) + Soil pH	6	1055.47	0.035	0.533
		FD.q2 ~ (1|Region) + Temperature seasonality + Annual precipitation	7	1054.37	0.378	0.538
		FD.q2 ~ (1|Region) + Temperature seasonality + Annual precipitation + Soil pH	**8**	**1055.04**	**0.407**	**0.535**
PD	q = 0	PD.q0 ~ (1|Region) + Temperature seasonality + Annual precipitation + Soil pH	8	812.56	0.533	0.533
		PD.q0 ~ (1|Region) + Temperature seasonality + Annual precipitation + Soil pH + Soil density	**9**	**812.27**	**0.560**	**0.560**
	q = 1	PD.q1 ~ (1|Region) + Soil pH	6	563.00	0.141	0.319
		PD.q1 ~ (1|Region) + Temperature seasonality + Soil pH	7	562.85	0.276	0.323
		PD.q1 ~ (1|Region) + Temperature seasonality + Soil pH + Soil density	**8**	561.65	0.377	0.377
		PD.q1 ~ (1|Region) + Temperature seasonality + Annual precipitation + Soil pH + Soil density	**9**	**563.48**	**0.388**	**0.388**
	q = 2	**PD.q2 ~ (1|Region)**	**5**	**440.80**	**0.000**	**0.290**
		PD.q2 ~ (1|Region) + Soil pH	6	442.12	0.033	0.250
		PD.q2 ~ (1|Region) + Soil density	6	442.44	0.023	0.260
		PD.q2 ~ (1|Region) + Soil pH + Soil density	7	442.12	0.200	0.229

Region is included as a random factor. df , degrees of freedom; AICc , Akaike's Information Criterion corrected for small sample sizes;R^2_m , pseudo-R-squared accounting for fixed effects; R^2_c , pseudo-R-squared accounting for both random and fixed effects. The best-fit models are highlighted in bold. Significant terms for the best-fit models are underlined.

decreased, and soil bulk density decreased, although to a lesser extent for the latter (Figure 4). Temperature seasonality seemed to be the most important environmental driver for shaping diversity trends because it was included as a significant factor in all of the best-fit models for all three diversity attributes, where the only exception was PD with q = 2 (Table 3). Annual precipitation was also included in all of the models but it was a significant factor only for TD with q = 1 and q = 2, and PD with q = 0 (Table 3), thereby suggesting that seasonal temperature variation was more important for shaping diversity than total water discharge. Similarly, previous studies consistently found that temperature variables had greater power for explaining diversity patterns than precipitation variables (Giehl & Jarenkow, 2012; Moles et al., 2014; Chen et al., 2015). Our findings are also consistent with environmental filtering and the favourability hypothesis for all diversity attributes because diversity increases with lower temperature seasonality and higher precipitations (Fischer, 1960; Swenson et al., 2012b; Qian et al., 2013; Asefa et al., 2017; Wieczynski et al., 2019).

Among the edaphic factors, the soil pH was present in all of the best-fit models, except for TD with q = 2, and it was a significant fixed factor in the best-fit models for TD with q = 0 and q = 1, FD with q = 0, and PD with q = 0 and q = 1 (Table 3). Our results showed that the diversity was greater when the soil was more acidic, which suggests that these communities are adapted to high soil acidity conditions (pH 3.5–4.5), although soils with a pH under 5.3 are characterized by low availability of base metal cation and toxic aluminium concentrations (Sollins, 1998; Bañares de Dios et al., 2022). In addition, the soil bulk density only appeared in the best-fit models for TD with q = 0, and PD with q = 0 and q = 1 (Table 3). Diversity increased as the bulk density decreased and the soils had lower bulk density values of 0.47 to 1.11 g/cm^3 than average ones for fully mineral soils, *i.e.*, clay = 1.0 to 1.6 g/cm^3 and sand = 1.2 to 1.8 g/cm^3 (Athira et al., 2019), which suggests that the organic matter content increased as the bulk density decreased (Bauer, 1974; Athira et al., 2019; de la Cruz-Amo et al., 2020). Therefore, the soil organic matter content may have facilitated the adaptation

of tropical plants to soils with low nutrient contents, high aluminium concentrations and low pH. Tropical soils are regarded as depleted of organic matter but large amounts of organic material are continuously supplied by decaying vegetation and its breakdown usually occurs very fast in the tropics, with rapid mineralization and availability for uptake (Herrera et al., 1978; Craswell & Lefroy, 2001; de la Cruz-Amo et al., 2020).

Overall, we found that TD increased as the temperature seasonality decreased, precipitation increased, and soil acidity increased (Figure 4A). Previous studies have demonstrated that the species richness of woody plants is negatively correlated with temperature seasonality, and positively correlated with the mean annual temperature and soil water content (Hofhansl et al., 2020). When we considered dominance (q = 2), only climatic factors were included in the best-fit model. This suggests that dominant species with wider tolerances and more widespread distributions were more dependent on the climate than the soils compared with rarer or less abundant species, which seemed more related to the local edaphic conditions (Pitman et al., 2013; Arellano et al., 2014).

According to our results, FD was affected by the temperature seasonality, annual precipitation and soil pH (Figure 4B), even when relative abundances and dominance were considered (q = 1 and q = 2, respectively). These results confirm that functional strategies are a consequence of environmental filtering because abiotic factors affect FD of both rare and common species in a similar manner. Therefore, although tropical climatic conditions are benign, they still strongly condition the successful functional strategies (Fortunel et al., 2014; Lamanna et al., 2014), thereby agreeing with the predictions of the favourability hypothesis in tropical environments. Recent studies obtained similar results for climatic and edaphic drivers (Swenson, 2012a; Molina-Venegas et al., 2018; Hofhansl et al., 2020).

We found that PD increased as the temperature seasonality decreased, precipitation increased, soil acidity increased, and bulk density decreased (Figure 4C). When traits are phylogenetically conserved, PD increases with decreasing environmental harshness, *i.e.*, increasing temperature or precipitation (Qian et al., 2013; Satdichanh et al., 2015; Qian et al., 2017). Therefore, environmental filtering and the favourability hypothesis are consistent with our results for PD with q = 0 and q = 1. Recent studies also showed that climatic filtering and soil fertility shaped PD of woody angiosperms (Honorio Coronado et al., 2015; Kubota et al., 2018). The lack of a best-fit model other than the null model for PD with q = 2 could be explained by the fact that dominant clades probably appeared and expanded under conditioning by their dispersion abilities and historical factors which are not reflected in the actual environmental conditions (Pitman et al., 2001; Arellano et al., 2016).

Conclusions

The latitudinal diversity gradient is explained by the environmental filtering principle and favourability hypothesis through climatic factors. Increases in temperature and precipitation seasonality are found in tropical regions towards higher latitudes (Fortunel et al., 2014), thereby leading to a noticeable latitudinal diversity gradient on a global scale but also within narrower latitudinal ranges such as the tropics. We found that temperature seasonality was still a relevant driver of all diversity attributes comprising TD, FD, and PD within a 10°C latitudinal gradient in the Neotropics. Therefore, our results support environmental filtering and the favourability hypothesis within hyperdiverse tropical regions.

In addition, the positive relationships found between the three diversity attributes indicate that if we take measures to protect and conserve TD, we also indirectly protect FD and PD, at least in western Amazonian *terra firme* forests. Furthermore, several studies found effects of TD, FD, and PD on productivity, and thus preserving forests with multiple functional strategies and a great evolutionary legacy will also protect their vital ecosystem functions (Balvanera et al., 2006; Gamfeldt et al., 2008; Cadotte, 2013; Coelho de Souza et al., 2019). Future studies should aim to understand diversity from this holistic perspective.

Data availability statement

The raw data supporting the conclusions of this article will be made available by the authors, without undue reservation.

Author contributions

CB, GB, MM and LC conceived the ideas. CB, JA and GB collected the data. NS and MTC provided bureaucratic, logistic and field support. CB and GB analyzed the data. CS led the writing. GB, JA, LM-G, LC, and MM gave continuous input to the manuscript writing and statistical analyses. All authors contributed to the article and approved the submitted version.

Funding

The appropriate permits were obtained to collect material in the field: Área de Conservación Regional Maijuna-Kichwa No. 003-2019-GLR-GGR-ARA, Parque Nacional Río Abiseo No. 001-2016-SERNANP-PNRA-JEF, Zona de Amortiguamientó Parque Nacional Cordillera Azul No. 315-2017-SERFOR-DGGSPFFS, Zona de Amortiguamiento Reserva Comunal

Yanesha No. 401-2018-MINAGRISERFOR-DGGSPFFS, Reserva Nacional Tambopata No. 35-2017-SERNANP-DGANP.

Acknowledgments

We would like to express our most sincere gratitude to the native communities of Nueva Vida, Leoncio Prado, San Carlos, Yamino and Infierno for receiving us so kindly in their homes and forests, and for their crucial assistance in the field. We would also like to thank the Peruvian local authorities of Servicio Nacional de Áreas Naturales Protegidas por el Estado (SERNANP), Servicio Nacional Forestal (SERFOR), and Autoridad Regional Ambiental del Gobierno Regional de Loreto (ARA-GOREL) for assistance and support that made the expeditions possible in the sampled protected areas. We offer our most sincere gratitude to Victoria Cala, who performed the edaphic analyses, for her much appreciated contribution. We show our special appreciation to Luis Torres Montenegro for its valuable taxonomic and logistic work; Mara Paneghel for her crucial and most valuable help; Manuel Marca for his assistance in the field; Camino Monsalve for her contribution to the functional traits; and Iñigo Gómez, Maaike Pyck and Silvia Aguado for their much appreciated volunteer work.

Conflict of interest

The authors declare that the research was conducted in the absence of any commercial or financial relationships that could be construed as a potential conflict of interest.

Publisher's note

Supplementary material

The Supplementary Material for this article can be found online at: https://www.frontiersin.org/articles/10.3389/fpls.2022.978299/full#supplementary-material

References

Arellano, G., Cala, V., Fuentes, A., Cayola, L., Jørgensen, P. M., and Macía, M. J. (2016). A standard protocol for woody plant inventories and soil characterisation using temporary 0.1-ha plots in tropical forests. *J. Trop. For. Sci.* 28 (4), 508–516.

Arellano, G., Cala, V., and Macía, M. J. (2014). Niche breadth of oligarchic species in Amazonian and Andean rain forests. *J. Veg. Sci.* 25 (6), 1355–1366. doi: 10.1111/jvs.12180

Arellano, G., Jørgensen, P. M., Fuentes, A. F., Loza, M. I., Torrez, V., and Macía, M. J. (2016). Oligarchic patterns in tropical forests: Role of the spatial extent, environmental heterogeneity and diversity. *J. Biogeogr.* 43 (3), 616–626. doi: 10.1111/jbi.12653

Arellano, G., Tello, J. S., Jørgensen, P. M., Fuentes, A. F., Loza, M. I., Torrez, V., et al. (2016). Disentangling environmental and spatial processes of community assembly in tropical forests from local to regional scales. *Oikos* 125 (3), 326–335. doi: 10.1111/oik.02426

Asefa, M., Cao, M., Zhang, G., Ci, X., Li, J., and Yang, J. (2017). Environmental filtering structures tree functional traits combination and lineages across space in tropical tree assemblages. *Sci. Rep.* 7 (1), 1–11. doi: 10.1038/s41598-017-00166-z

Athira, M., Jagadeeswaran, R., and Kumaraperumal, R. (2019). Influence of soil organic matter on bulk density in coimbatore soils. *Int. J. Chem. Stud.* 7 (3), 3520–3523.

Aubry-Kientz, M., Rossi, V., and Wagner, F. (2015). Identifying climatic drivers of tropical forest dynamics. *Biogeosciences* 12 (19), 5583–5596. doi: 10.5194/bgd-12-1-2015

Balvanera, P., Pfisterer, A. B., Buchmann, N., He, J. S., Nakashizuka, T., Raffaelli, D., et al. (2006). Quantifying the evidence for biodiversity effects on ecosystem functioning and services. *Ecol. Lett.* 9 (10), 1146–1156. doi: 10.1111/j.1461-0248.2006.00963.x

Bañares-de-Dios, G., Macía, M. J., de Carvalho, G. M., Arellano, G., and Cayuela, L. (2022). Soil and climate drive floristic composition in tropical Forests : A literature review. *Front. Ecol. Evol.* 10, 866905. doi: 10.3389/fevo.2022.866905

Barton, K. (2013). *MuMIn: Multi-model inference*. R package version1.43.17. Available at: https://CRAN.Rproject.org/package=MuMIn.

Bates, D., Mächler, M., Ben, B., and Walker, S. (2015). Fitting linear mixed-effects models using lme4. *J. Stat. Softw.* 67 (1), 1–48. doi: 10.18637/jss.v067.i01.Corresponding

Bauer, A. (1974). Influence of soil organic matter on bulk density and available water capacity of soils. *Farm Res.* 31 (5), 44–52.

Britto, B. (2017). Actualización de las ecorregiones terrestres de perú propuestas en el libro rojo de plantas endémicas del perú. *Gayana Botánica* 74 (1), 15–29. doi: 10.4067/s0717-66432017005000318

Brooks, D. (2018). *Tropical and subtropical moist broadleaf forests. World Wildlife Fund (WWF)*, Central South America: Bolivia and Argentina. Available at: https://www. worldwildlife. org/ecoregions/nt0165.

Burnham, R. J., and Johnson, K. R. (2004). South American palaeobotany and the origins of neotropical rainforests. *Philos. Trans. R. Soc. B: Biol. Sci.* 359 (1450), 1595–1610. doi: 10.1098/rstb.2004.1531

Cadotte, M. W. (2013). Experimental evidence that evolutionarily diverse assemblages result in higher productivity. *Proc. Natl. Acad. Sci. United States America* 110 (22), 8996–9000. doi: 10.1073/pnas.1301685110

Cavender-Bares, J., Ackerly, D. D., Baum, D. A., and Bazzaz, F. A. (2004). Phylogenetic overdispersion in Floridian oak communities. *Am. Nat.* 163 (6), 823–843. doi: 10.1086/386375

Cayuela, L., Granzow-de la Cerda, Í., Albuquerque, F. S., and Golicher, D. J. (2012). Taxonstand: An r package for species names standardisation in vegetation databases. *Methods Ecol. Evol.* 3 (6), 1078–1083. doi: 10.1111/j.2041-210X.2012.00232.x

Cazzolla Gatti, R., Reich, P. B., Gamarra, J. G., Crowther, T., Hui, C., Morera, A., et al. (2022). The number of tree species on earth. *Proc. Natl. Acad. Sci.* 119 (6), 1–11. doi: 10.1073/pnas.2115329119/-/DCSupplemental.Published

Chao, A., Chiu, C. H., and Jost, L. (2010). Phylogenetic diversity measures based on hill numbers. *Philos. Trans. R. Soc. B: Biol. Sci.* 365 (1558), 3599–3609. doi: 10.1098/rstb.2010.0272

Chao, A., Chiu, C. H., and Jost, L. (2014). Unifying species diversity, phylogenetic diversity, functional diversity, and related similarity and differentiation measures through hill numbers. *Annu. Rev. Ecol. Evol. Syst.* 45, 297–324. doi: 10.1146/annurev-ecolsys-120213-091540

Chave, J., Coomes, D., Jansen, S., Lewis, S. L., Swenson, N. G., and Zanne, A. E. (2009). Towards a worldwide wood economics spectrum. *Ecol. Lett.* 12 (4), 351–366. doi: 10.1111/j.1461-0248.2009.01285.x

Chen, S.B., Ferry Slik, J. W., Gao, J., Mao, L. F., Bi, M. J., Shen, M. W., et al. (2015). Latitudinal diversity gradients in bryophytes and woody plants: Roles of

temperature and water availability. *J. Syst. Evol.* 53 (6), 535–545. doi: 10.1111/jse.12158

Chiu, C. H., and Chao, A. (2014). Distance-based functional diversity measures and their decomposition: A framework based on hill numbers. *PloS One* 9 (7), 1–17. doi: 10.1371/journal.pone.0100014

Clarholm, M., and Skyllberg, U. (2013). Translocation of metals by trees and fungi regulates pH, soil organic matter turnover and nitrogen availability in acidic forest soils. *Soil Biol Biochem* 63 (2013), 142–153. doi: 10.1016/j.soilbio.2013.03.019

Coelho de Souza, F., Dexter, K. G., Phillips, O. L., Pennington, R. T., Neves, D., Sullivan, M. J. P., et al. (2019). Evolutionary diversity is associated with wood productivity in Amazonian forests. *Nat. Ecol. Evol.* 3 (12), 1754–1761. doi: 10.1038/s41559-019-1007-y

Córdova-Tapia, F., and Zambrano, L. (2015). La diversidad funcional en la ecología de comunidades. *Ecosistemas* 24 (3), 78–87. doi: 10.7818/ecos.2015.24-3.10

Cornelissen, J. H. C., Lavorel, S., Garnier, E., Díaz, S., Buchmann, N., Gurvich, D. E., et al. (2003). A handbook of protocols for standardised and easy measurement of plant functional traits worldwide. *Aust. J. Bot.* 51 (4), 335–380. doi: 10.1071/BT02124

Craswell, E. T., and Lefroy, R. D. B. (2001). The role and function of organic matter in tropical soils. *NIn Managing organic matter in tropical soils: Scope and limitations*. Dordrecht: Springer pp. 7–18. doi: 1978-1-4613-1163-8_10/978-94-017-2172-1_2

Dawson, M. N., Algar, A. C., Antonelli, A., Dávalos, L. M., Davis, E., Early, R., et al. (2013). An horizon scan of biogeography. *Front. Biogeogr.* 5 (2), 130–157. doi: 10.21425/f5fbg18854

de la Cruz-Amo, L., Bañares-de-Dios, G., Cala, V., Granzow-de la Cerda, Í., Espinosa, C. I., Ledo, A., et al. (2020). Trade-offs among aboveground, belowground, and soil organic carbon stocks along altitudinal gradients in Andean tropical montane forests. *Front. Plant Sci.* 11. doi: 10.3389/fpls.2020.00106

Draper, F. C., Costa, F. R. C., Arellano, G., Phillips, O. L., Duque, A., Macía, M. J., et al. (2021). Amazon Tree dominance across forest strata. *Nat. Ecol. Evol.* 5 (6), 757–767. doi: 10.1038/s41559-021-01418-y

Fischer, A. G. (1960). Latitudinal variations in organic diversity. *Evolution* 14 (1), 64–81. doi: 10.2307/2405923

Fortunel, C., Paine, C. E. T., Fine, P. V. A., Kraft, N. J. B., and Baraloto, C. (2014). Environmental factors predict community functional composition in Amazonian forests. *J. Ecol.* 102 (1), 145–155. doi: 10.1111/1365-2745.12160

Gamfeldt, L., Hillebrand, H., and Jonsson, P. R. (2008). Multiple functions increase the importance of biodiversity for overall ecosystem functioning. *Ecology* 89 (5), 1223–1231. doi: 10.1890/06-2091.1

Garibaldi, C., Nieto-Ariza, B., Macía, M. J., and Cayuela, L. (2014). Soil and geographic distance as determinants of floristic composition in the azuero peninsula (Panama). *Biotropica* 46 (6), 687–695. doi: 10.1111/btp.12174

Gentry, A. H. (1982). Patterns of Neotropical plant species diversity. *Evol. Biol.*, 1–84. Springer, Boston, MA. doi: 1978-1-4613-1163-8_10/978-1-4615-6968-8_1

Gentry, A. H. (1988). Tree species richness of upper Amazonian forests. *Proc. Natl. Acad. Sci.* 85 (1), 156–159. doi: 10.1073/pnas.85.1.156

Giehl, E. L. H., and Jarenkow, J. A. (2012). Niche conservatism and the differences in species richness at the transition of tropical and subtropical climates in south America. *Ecography* 35 (10), 933–943. doi: 10.1111/j.1600-0587.2011.07430.x

Götzenberger, L., de Bello, F., Bråthen, K. A., Davison, J., Dubuis, A., Guisan, A., et al. (2012). Ecological assembly rules in plant communities-approaches, patterns and prospects. *Biol. Rev.* 87 (1), 111–127. doi: 10.1111/j.1469-185X.2011.00187.x

Herrera, R., Klinge, H., and Medina, E. (1978). Amazon Ecosystems: their structure and functioning with particular emphasis on nutrients. *Interciencia* 3 (4), 223–231.

Hill, M. O. (1973). Diversity and Evenness : A unifying notation and its consequences. *Ecology* 54(2), 427–432. doi: 10.2307/1934352

HilleRisLambers, J., Adler, P. B., Harpole, W. S., Levine, J. M., and Mayfield, M. M. (2012). Rethinking community assembly through the lens of coexistence theory. *Annu. Rev. Ecol. Evol. Syst.* 43 (1), 227–248. doi: 10.1146/annurev-ecolsys-110411-160411

Hofhansl, F., Chacón-Madrigal, E., Fuchslueger, L., Jenking, D., Morera-Beita, A., Plutzar, C., et al. (2020). Climatic and edaphic controls over tropical forest diversity and vegetation carbon storage. *Sci. Rep.* 10 (1), 1–11. doi: 10.1038/s41598-020-61868-5

Honorio Coronado, E. N., Dexter, K. G., Pennington, R. T., Chave, J., Lewis, S. L., Alexiades, M. N., et al (2015) Phylogenetic diversity of Amazonian tree communities *Diversity Distrib.* 21(11), 1295–1307. doi: 10.1111/ddi.12357

Hoorn, C., Wesselingh, F. P., ter Steege, H., Bermudez, M. A., Mora, A., Sevink, J., et al. (2010). Amazonia Through Time : Andean uplift, climate change, landscape evolution, and biodiversity. *Science* 330, 927–931. doi: 10.1126/science.1194585

Jackman, S. (2020). *pscl: Classes and methods for R. Department of Political Science* (Stanford, CA: Stanford University).

Jin, Y., and Qian, H. (2019). V.PhyloMaker: an r package that can generate very large phylogenies for vascular plants. *Ecography* 42 (8), 1353–1359. doi: 10.1111/ecog.04434

Karger, D. N., Conrad, O., Böhner, J., Kawohl, T., Kreft, H., Soria-Auza, R. W., et al. (2019). Climatologies at high resolution for the earth land surface areas. *CHELSA V1. 2: Technical specification*. Swiss Federal Research Institute WSL, Switzerland. doi: 10.1594/WDCC/CHELSA

Katabuchi, M., Kurokawa, H., Davies, S. J., Tan, S., and Nakashizuka, T. (2012). Soil resource availability shapes community trait structure in a species-rich dipterocarp forest. *J. Ecol.* 100 (3), 643–651. doi: 10.1111/j.1365-2745.2011.01937.x

Kerkhoff, A. J., Moriarty, P. E., and Weiser, M. D. (2014). The latitudinal species richness gradient in new world woody angiosperms is consistent with the tropical conservatism hypothesis. *Proc. Natl. Acad. Sci. United States America* 111 (22), 8125–8130. doi: 10.1073/pnas.1308932111

Kooyman, R., Rossetto, M., Allen, C., and Cornwell, W. (2012). Australian Tropical and subtropical rain forest community assembly: Phylogeny, functional biogeography, and environmental gradients. *Biotropica* 44 (5), 668–679. doi: 10.1111/j.1744-7429.2012.00861.x

Kubota, Y., Kusumoto, B., Shiono, T., and Ulrich, W. (2018). Environmental filters shaping angiosperm tree assembly along climatic and geographic gradients. *J. Veg. Sci.* 29 (4), 607–618. doi: 10.1111/jvs.12648

Lamanna, C., Blonder, B., Violle, C., Kraft, N. J. B., Sandel, B., Šímová, I., et al. (2014). Functional trait space and the latitudinal diversity gradient. *Proc. Natl. Acad. Sci. U. S. A.* 111 (38), 13745–13750. doi: 10.1073/pnas.1317722111

Lamanna, J. A., Mangan, S. A., Alonso, A., Bourg, N. A., Brockelman, W. Y., Bunyavejchewin, S., et al. (2017). Plant diversity increases with the strength of negative density dependence at the global scale. *Science* 356 (6345), 1389–1392. doi: 10.1126/science.aam5678

Lamarre, G. P. A., Baraloto, C., Fortunel, C., Dávila, N., Mesones, I., Rios, J. G., et al. (2012). Herbivory, growth rates, and habitat specialization in tropical tree lineages: Implications for Amazonian beta-diversity. *Ecology* 93 (sp8), 195–210. doi: 10.1890/11-0397.1

Lean, C., and Maclaurin, J. (2016). The value of phylogenetic diversity. *In Biodiversity conservation and phylogenetic systematics*. Cham: Springer. (pp. 19–37).

Leitão, R. P., Zuanon, J., Villéger, S., Williams, S. E., Baraloto, C., Fortune, C., et al. (2016). Rare species contribute disproportionately to the functional structure of species assemblages. *Proc. R. Soc. B: Biol. Sci.* 283 (1828), 1–9. doi: 10.1098/rspb.2016.0084

Li, Y., Shipley, B., Price, J. N., Dantas, V., de, L., Tamme, R., et al. (2018). Habitat filtering determines the functional niche occupancy of plant communities worldwide. *J. Ecol.* 106 (3), 1001–1009. doi: 10.1111/1365-2745.12802

López, B. E., Burgio, K. R., Carlucci, M. B., Palmquist, K. A., Parada, A., Weinberger, V. P., et al. (2016). A new framework for inferring community assembly processes using phylogenetic information, relevant traits and environmental gradients. *One Ecosyst.* 1, 1–24. doi: 10.3897/oneeco.1.e9501

Losos, J. B. (2008). Phylogenetic niche conservatism, phylogenetic signal and the relationship between phylogenetic relatedness and ecological similarity among species. *Ecol. Lett.* 11 (10), 995–1003. doi: 10.1111/j.1461-0248.2008.01229.x

Malhi, Y., and Wright, J. (2004). Spatial patterns and recent trends in the climate of tropical rainforest regions. *Philos. Trans. R. Soc. B: Biol. Sci.* 359 (1443), 311–329. doi: 10.1098/rstb.2003.1433

Malizia, A., Blundo, C., Carilla, J., Acosta, O. O., Cuesta, F., Duque, A., et al. (2020). Elevation and latitude drives structure and tree species composition in Andean forests: Results from a large-scale plot network. *PloS One* 15 (4), 1–18. doi: 10.1371/journal.pone.0231553

Massante, J. C., Götzenberger, L., Takkis, K., Hallikma, T., Kaasik, A., Laanisto, L., et al. (2019). Contrasting latitudinal patterns in phylogenetic diversity between woody and herbaceous communities. *Sci. Rep.* 9 (1), 1–10. doi: 10.1038/s41598-019-42827-1

McGill, B. J., Enquist, B. J., Weiher, E., and Westoby, M. (2006). Rebuilding community ecology from functional traits. *Trends Ecol. Evol.* 21 (4), 178–185. doi: 10.1016/j.tree.2006.02.002

Medina, E., and Cuevas, E. (1989). Patterns of nutrient accumulation and release in Amazonian forests of the upper Rio Negro basin. In *Mineral nutrients in tropical forest and savanna ecosystems*. Melbourne: Blackwell Scientific Publications. 217–240.

Moles, A. T., Perkins, S. E., Laffan, S. W., Flores-Moreno, H., Awasthy, M., Tindall, M. L., et al. (2014). Which is a better predictor of plant traits: Temperature or precipitation? *J. Veg. Sci.* 25 (5), 1167–1180. doi: 10.1111/jvs.12190

Molina-Venegas, R., Aparicio, A., Lavergne, S., and Arroyo, J. (2018). Soil conditions drive changes in a key leaf functional trait through environmental filtering and facilitative interactions. *Acta Oecologica* 86, 1–8. doi: 10.1016/j.actao.2017.11.008

Mori, G. B., Poorter, L., Schietti, J., and Piedade, M. T. F. (2021). Edaphic characteristics drive functional traits distribution in Amazonian floodplain forests. *Plant Ecol.* 222 (3), 349–360. doi: 1978-1-4613-1163-8_10/s11258-020-01110-4

Motavalli, P. P., Palm, C. A., Parton, W. J., Elliott, E. T., and Frey, S. D. (1995). Soil pH and organic c dynamics in tropical forest soils: Evidence from laboratory and simulation studies. *Soil Biol. Biochem.* 27 (12), 1589–1599. doi: 10.1016/0038-0717(95)00082-P

Mouillot, D., Bellwood, D. R., Baraloto, C., Chave, J., Galzin, R., Harmelin-Vivien, M., et al. (2013). Rare species support vulnerable functions in high-diversity ecosystems. *PloS Biol.* 11 (5), 1–11. doi: 10.1371/journal.pbio.1001569

Nakagawa, S., and Schielzeth, H. (2013). A general and simple method for obtaining R2 from generalized linear mixed-effects models. *Methods Ecol. Evol.* 4 (2), 133–142. doi: 10.1111/j.2041-210x.2012.00261.x

Nelson, P. N., and Su, N. (2010). Soil pH buffering capacity: A descriptive function and its application to some acidic tropical soils. *Aust. J. Soil Res.* 48 (3), 201–207. doi: 10.1071/SR09150

Niinemets, Ü. (2010). A review of light interception in plant stands from leaf to canopy in different plant functional types and in species with varying shade tolerance. *Ecol. Res.* 25 (4), 693–714. doi: 1978-1-4613-1163-8_10/s11284-010-0712-4

Nobre, C. A., Berenguer, E., Brando, P. M., and Poveda, G. (2019). Scientific framework to save the amazon. doi: 10.13140/RG.2.2.24053.12009

Pellens, R., and Grandcolas, P. (2016). Phylogenetics and conservation biology: Drawing a path into the diversity of life. *In Biodivers. Conserv. Phylogenet. Syst.* 14, 1–15. doi: 1978-1-4613-1163-8_10/978-3-319-22461-9

Pérez-Harguindeguy, N., Díaz, S., Garnier, E., Lavorel, S., Poorter, H., Jaureguiberry, P., et al. (2013). New handbook for standardised measurement of plant functional traits worldwide. *Aust. J. Bot.* 61 (3), 167–234. doi: 10.1071/BT12225

Pitman, N. C. A., Silman, M. R., and Terborgh, J. W. (2013). Oligarchies in Amazonian tree communities: A ten-year review. *Ecography* 36 (2), 114–123. doi: 10.1111/j.1600-0587.2012.00083.x

Pitman, N. C. A., Terborgh, J. W., Silman, M. R., Núñez, P. V., Neill, D. A., Cerón, C. E., et al. (2001). Dominance and distribution of tree species in upper Amazonian terra firme forests. *Ecology* 82 (8), 2101–2117. doi: 10.1890/0012-9658(2001)082[2101:DADOTS]2.0.CO;2

Poorter, L., Castilho, C. V., Schietti, J., Oliveira, R. S., and Costa, F. R. C. (2018). Can traits predict individual growth performance? a test in a hyperdiverse tropical forest. *New Phytol.* 219 (1), 109–121. doi: 10.1111/nph.15206

Poorter, L., van der Sande, M. T., Arets, E. J. M. M., Ascarrunz, N., Enquist, B., Finegan, B., et al. (2017). Biodiversity and climate determine the functioning of Neotropical forests. *Global Ecol. Biogeogr.* 26 (12), 1423–1434. doi: 10.1111/geb.12668

Qian, H., Jin, Y., and Ricklefs, R. E. (2017). Patterns of phylogenetic relatedness of angiosperm woody plants across biomes and life-history stages. *J. Biogeogr.* 44 (6), 1383–1392. doi: 10.1111/jbi.12936

Qian, H., Zhang, Y., Zhang, J., and Wang, X. (2013). Latitudinal gradients in phylogenetic relatedness of angiosperm trees in north America. *Global Ecol. Biogeogr.* 22 (11), 1183–1191. doi: 10.1111/geb.12069

R Core Team (2021). *R: A language and environment for statistical computing* (R Foundation for Statistical Computing, Vienna, Austria). Available at: http://www.R-project. org/

Rodrigues, P. M. S., Silva, J. O., and Schaefer, C. E. G. R. (2019). Edaphic properties as key drivers for woody species distributions in tropical savannic and forest habitats. *Aust. J. Bot.* 67 (1), 70–80. doi: 10.1071/BT17241

Sanford, R. L., and Cuevas, E. (1996). Root growth and rhizosphere interactions in tropical forests. *In Tropical forest plant ecophysiology*. Boston, MA: Springer. (pp. 268–300) doi: 1978-1-4613-1163-8_10/978-1-4613-1163-8_10

Satdichanh, M., Millet, J., Heinimann, A., Nanthavong, K., and Harrison, R. D. (2015). Using plant functional traits and phylogenies to understand patterns of plant community assembly in a seasonal tropical forest in. *PloS One* 10 (6), 1–15. doi: 10.1371/journal.pone.0130151

Smith, S. A., and Brown, J. W. (2018). Constructing a broadly inclusive seed plant phylogeny. *Am. J. Bot.* 105 (3), 302–314. doi: 10.1002/ajb2.1019

Sollins, P. (1998). Factors influencing species composition in tropical lowland rain forest: Does soil matter? *Ecology* 79 (1), 23–30. doi: 10.1890/0012-9658(1998)079[0023:FISCIT]2.0.CO;2

Stevens, R. D., and Willig, M. R. (2002). Geographical ecology at the community level: Perspectives on the diversity of new world bats. *Ecology* 83 (2), 545–560. doi: 10.1890/0012-9658(2002)083[0545:GEATCL]2.0.CO;2

Swenson, N. G. (2011). The role of evolutionary processes in producing biodiversity patterns, and the interrelationships between taxonomic, functional and phylogenetic biodiversity. *Am. J. Bot.* 98 (3), 472–480. doi: 10.3732/ajb.1000289

Swenson, N. G. (2012a). The functional ecology and diversity of tropical tree assemblages through space and time: From local to regional and from traits to transcriptomes. *ISRN forestry*. 2012, 1–16. doi: 10.5402/2012/743617

Swenson, N. G., and Enquist, B. J. (2008). The relationship between stem and branch wood specific gravity and the ability of each measure to predict leaf area. *Am. J. Bot.* 95 (4), 516–519. doi: 10.3732/ajb.95.4.516

Swenson, N. G., and Enquist, B. J. (2009). Opposing assembly mechanisms in a Neotropical dry forest: Implications for phylogenetic and functional community ecology. *Ecology* 90 (8), 2161–2170. doi: 10.1890/08-1025.1

Swenson, N. G., Enquist, B. J., Pither, J., Kerkhoff, A. J., Boyle, B. , Weiser, M. D., et al. (2012b). The biogeography and filtering of woody plant functional diversity in north and south America. *Global Ecol. Biogeogr.* 21 (8), 798–808. doi: 10.1111/j.1466-8238.2011.00727.x

Swenson, N. G., Erickson, D. L., Mi, X., Bourg, N. A., Forero-Montana, J., Ge, X., et al. (2012c). Phylogenetic and functional alpha and beta diversity in temperate and tropical tree communities. *Ecology* 93, 112–125. doi: 10.1890/11-0402.1

Swenson, N. G., and Weiser, M. D. (2014). On the packing and filling of functional space in eastern north American tree assemblages. *Ecography* 37 (11), 1056–1062. doi: 10.1111/ecog.00763

Ter Steege, H., Pitman, N. C. A., Sabatier, D., Baraloto, C., Salomão, R. P., Guevara, J. E., et al. (2013). Hyperdominance in the Amazonian tree flora. *Science* 342 (6156), 1–43. doi: 10.1126/science.1243092

Thiers, B. (2021). *Index herbariorum: A global directory of public herbaria and associated staff*. New York, USA: New York Botanical Garden's Virtual Herbarium.

Valencia, R., Balslev, H., and Paz Y Miño C, G. (1994). High tree alpha-diversity in Amazonian Ecuador. *Biodivers. Conserv.* 3 (1), 21–28. doi: 10.1007/BF00115330

Venables, W., and Ripley, B. (2002). *Modern applied statistics with s* (Springer US, New York, NY). doi: 10.1007/978-0-387-21706-2_10

Violle, C., Navas, M.-L., Vile, D., Kazakou, E., Fortunel, C., Hummel, I., et al. (2007). Let the concept of trait be functional! *Oikos* 116 (5), 882–892. doi: 10.1111/j.2007.0030-1299.15559.x

Webb, C. O. (2000). Exploring the phylogenetic structure of ecological communities: An example for rain forest trees. *Am. Nat.* 156 (2), 145–155. doi: 10.1086/303378

Webb, C. O., Cannon, C. H., and Davies, S. J. (2008). Ecological organization, biogeography, and the phylogenetic structure of tropical forest tree communities. tropical forest community ecology. In *Tropical forest community ecology*, Blackwell Publishing Ltd. West Sussex (UK): Blackwell Publishing Ltd. 79–97

Weerasinghe, L. K., Creek, D., Crous, K. Y., Xiang, S., Liddell, M. J., Turnbull, M. H., et al. (2014). Canopy position affects the relationships between leaf respiration and associated traits in a tropical rainforest in far north Queensland. *Tree Physiol.* 34 (6), 564–584. doi: 10.1093/treephys/tpu016

Weiser, M. D., Enquist, B. J., Boyle, B., Killeen, T. J., Jørgensen, P. M., Fonseca, G., et al. (2007). Latitudinal patterns of range size and species richness of new world woody plants. *Global Ecol. Biogeogr.* 16 (5), 679–688. doi: 10.1111/j.1466-8238.2007.00323.x

Wieczynski, D. J., Boyle, B., Buzzard, V., Duran, S. M., Henderson, A. N., Hulshof, C. M., et al. (2019). Climate shapes and shifts functional biodiversity in forests worldwide. *Proc. Natl. Acad. Sci. United States America* 116 (2), 587–592. doi: 10.1073/pnas.1813723116

Willig, M. R., Kaufman, D. M., and Stevens, R. D. (2003). Latitudinal gradients of biodiversity: Pattern, process, scale, and synthesis. *Annu. Rev. Ecol. Evol. Syst.* 34, 273–309. doi: 10.1146/annurev.ecolsys.34.012103.144032

Wright, S. J. (2002). Plant diversity in tropical forests: A review of mechanisms of species coexistence. *Oecologia* 130 (1), 1–14. doi: 10.1007/s004420100809

Wright, I. J., Reich, P. B., Westoby, M., Ackerly, D. D., Baruch, Z., Bongers, F., et al. (2004). The worldwide leaf economics spectrum. *Nature* 428 (6985), 821–827. doi: 10.1038/nature02403

Zanne, A. E., Tank, D. C., Cornwell, W. K., Eastman, J. M., Smith, S. A., Fitzjohn, R. G., et al. (2014). Three keys to the radiation of angiosperms into freezing environments. *Nature* 506 (7486), 89–92. doi: 10.1038/nature12872

frontiers | Frontiers in Plant Science

TYPE Original Research
PUBLISHED 07 October 2022
DOI 10.3389/fpls.2022.993051

OPEN ACCESS

EDITED BY
Boris Rewald,
University of Natural Resources and Life Sciences Vienna, Austria

REVIEWED BY
Daniel Nadal-Sala,
Karlsruhe Institute of Technology (KIT), Germany
Tim Seipel,
Montana State University, United States

*CORRESPONDENCE
José Dorado
jose.dorado@csic.es

SPECIALTY SECTION
This article was submitted to Functional Plant Ecology, a section of the journal Frontiers in Plant Science

RECEIVED 13 July 2022
ACCEPTED 15 September 2022
PUBLISHED 07 October 2022

CITATION
Guerra JG, Cabello F, Fernández-Quintanilla C, Peña JM and Dorado J (2022) Plant functional diversity is affected by weed management through processes of trait convergence and divergence. *Front. Plant Sci.* 13:993051. doi: 10.3389/fpls.2022.993051

Plant functional diversity is affected by weed management through processes of trait convergence and divergence

Jose G. Guerra[1,2], Félix Cabello[3], César Fernández-Quintanilla[1], José M. Peña[1] and José Dorado[1]*

[1]Instituto de Ciencias Agrarias (CSIC), Madrid, Spain, [2]Escuela Técnica Superior de Ingeniería Agronómica, Alimentaria y de Biosistemas (ETSIAAB), Universidad Politécnica de Madrid, Madrid, Spain, [3]Instituto Madrileño de Investigación y Desarrollo Rural, Agrario y Alimentario (IMIDRA), Finca El Encín, Madrid, Spain

Weed management involving tillage and/or herbicides has generally led to a decline of plant diversity in agroecosystems, with negative impacts on ecosystem services provision. The use of plant covers has become the predominant alternative in vineyard management, with numerous studies focusing on analyzing the advantages and disadvantages of plant covers compared to the aforementioned management. Although the impacts of weed management on taxonomic diversity have been widely studied, many gaps remain on their effects on plant functional diversity. As plant functional diversity is linked to the delivery of key ecosystem services in agroecosystems, understanding these effects could enable the development of more sustainable practices. From 2008 to 2018, a long-term trial was carried out in a Mediterranean vineyard to assess different agricultural practices. In this article, we examined how weed management, as well as irrigation use, could affect plant functional diversity. Based on 10 functional traits, such as plant height, specific leaf area or seed mass, we measured different indices of functional diversity and used null models to detect processes of trait convergence and divergence. Our results revealed that weed management and irrigation use had a significant effect on plant functional diversity. Mown plots showed the highest functional richness but were functionally convergent, since mowing was a strong functional filter on most of the traits. Tillage also behaved as a functional filter on some vegetative traits, but favored the divergence of certain reproductive traits. Herbicide-treated and irrigated plots showed the highest values of functional divergence by promoting more competitive species with more divergent trait values. The effect of weed management on these community assembly processes was shaped by the use of irrigation in vineyard rows, leading to functional divergence in those vegetative traits related to resource acquisition and seed mass. These results suggest that greater functional diversity may be associated with the bias caused by higher occurrence of competitive species (e.g. *Convolvulus arvensis*, *Sonchus asper*) with contrasting values for certain traits. Therefore, since

these species are considered harmful to crops, higher plant functional diversity might not be a desirable indicator in agroecosystems.

KEYWORDS

biodiversity, agricultural management, spontaneous plant cover, mowing, tillage, herbicide, Mediterranean vineyards

1 Introduction

Agricultural intensification is the main process driving the widespread biodiversity loss observed in European farmland in recent decades (Emmerson et al., 2016). This intensification process has caused a marked decline in European arable weeds (Storkey et al., 2012), decreasing both taxonomic and functional diversity (José-María et al., 2010; Carmona et al., 2020), which could have negative impacts on the provision of key ecosystem services in agroecosystems such as crop pollination (Bretagnolle and Gaba, 2015) or pest control (Martínez-Uña et al., 2013; Crowder and Jabbour, 2014). In this context of agricultural intensification, since crop losses due to weeds can be substantial (Oerke, 2006), weed management has targeted weed eradication using recurrent tillage and/or herbicides (MacLaren et al., 2020). These weed management practices have led to environmental impacts such as soil erosion and soil fertility decline, which pose a serious threat to Mediterranean agroecosystems (Novara et al., 2011; Prosdocimi et al., 2016). To deal with these problems, greener weed management practices have been promoted over the past few years. In vineyards, plant cover (usually mown) has become widespread as a viable option to conventional management based on soil tillage, with positive effects such as the improvement of soil properties or the enhancement of biodiversity (Winter et al., 2018; Novara et al., 2019; Guerra et al., 2022), although exhibiting in some cases a reduction on vineyard vigor and yield (Monteiro and Lopes, 2007; Celette and Gary, 2013). The impact of weed management on weed communities has been extensively documented, revealing that management practices such as tillage, herbicide or mowing can exert selective pressure on these communities, altering their composition and/or taxonomic diversity (Doradoand López-Fando, 2006; José-María et al., 2010; Grundy et al., 2011; Larson et al., 2021; Guerra et al., 2022). However, gaps remain on how these management practices might affect plant functional diversity.

Plant functional diversity can be defined as the value, range, distribution and relative abundance of plant functional traits present in a given ecosystem (Díaz et al., 2007), being closely related to ecosystem properties and provision of key ecosystem services such as carbon sequestration or maintenance of soil fertility (Díaz and Cabido, 2001; Díaz et al., 2007; Conti and Díaz, 2013). Thus, plant functional diversity can explain variations in ecosystem functions even when species richness does not (Cadotte et al., 2011). These links to ecosystem processes has made plant functional diversity a central issue for ecology in the last two decades, leading to the proposal of numerous indices for its estimation in different ecosystems (Petchey and Gaston, 2002; Botta-Dukát, 2005; Mason et al., 2005; Villéger et al., 2008).

In agroecosystems, previous works have shown how agricultural intensification reduces functional diversity of weed communities in arable systems (Carmona et al., 2020) and olive groves (Tarifa et al., 2021), although only Carmona et al. (2020) explored in depth the effect on several indicators of functional diversity. However, these studies did not analyze potential differences due to different weed managements. In vineyards, recent short-term studies have partially analyzed the effects of weed management on some aspects of plant functional diversity. Thus, Kazakou et al. (2016) estimated functional richness, one of the three indices proposed by Villéger et al. (2008) to measure functional diversity, finding that spontaneous cover showed higher functional richness than tillage. Hall et al. (2020) estimated functional diversity using Rao's quadratic entropy (Rao, 1982), observing higher functional diversity in vineyards managed with permanent vegetation cover compared to those observed in bare soil management (herbicide or tillage). Mainardis et al. (2020) found that functional diversity, estimated by functional dispersion and functional divergence, was higher under mowing than under tillage.

Plant functional diversity indices combined with null models have also been used to identify community assembly processes driven by functional traits (Götzenberger et al., 2012; Botta-Dukát and Czúcz, 2016), testing the existence of the two main mechanisms underlying the assemblage of plant communities: habitat filtering and limiting similarity. Trait convergence is usually related to habitat filtering mechanisms (Keddy, 1992), in which environmental or management factors act as abiotic filters restricting the range of species trait values (e.g. Lhotsky et al., 2016). In recent years, it has been described that weed management can affect the functional structure of weed communities favoring one set of functional traits over others (Fried et al., 2012; Guerra et al., 2021) which could be indicative, although not proven, of trait convergence caused by habitat

filtering. In contrast, trait divergence could occur according to the principle of limiting similarity (Macarthur and Levins, 1967) which suggests that species can coexist more easily if they diverge in their traits, thereby decreasing competition between them (e.g. Thompson et al., 2010). Nevertheless, convergent and divergent patterns can occur simultaneously within the same community (Bernard-Verdier et al., 2012; Spasojevic and Suding, 2012) and may differ between traits, with convergence being more common for vegetative traits while divergence is more likely for reproductive traits (Grime, 2006). In agroecosystems, the study of these processes that condition plant functional diversity has been limited to grasslands (e.g. Mason et al., 2011; Bernard-Verdier et al., 2012), lacking studies that test the existence of such processes according to weed management.

The aim of this study was to examine how weed management, as well as irrigation use, might affect functional diversity of weed communities. In particular, we have focused on analyzing the relationship between weed management and trait convergence or divergence patterns. Based on previous studies (Guerra et al., 2021; Guerra et al., 2022), we further hypothesize that functional diversity could also vary depending on the management adjacent to each plot studied. For example, Guerra et al. (2022) reported that species richness was higher in herbicide-treated plots close to mowing than in plots close to tillage. In addition, we have recently observed that at herbicide-treated and irrigated rows, with intermediate values of bare soil, the most competitive species were favored (Guerra et al., 2021; 2022). Given that competition is a factor that can shape plant functional diversity (Navas and Violle, 2009), this work also studied the relationship between functional diversity and competitiveness (CSR strategy; Grime, 1974). Therefore, the purpose of this article is to contribute to increase the knowledge on the influence of agronomic management on plant functional diversity, so that implications for agroecological weed management can be analyzed.

2 Materials and methods

2.1 Study site and experimental design

Research was carried out in an experimental vineyard at the IMIDRA farm El Socorro (Colmenar de Oreja, Madrid), located at 755 m in the central plateau of the Iberian Peninsula, developed on a clay-loam soil of type Calcic Haploxeralf. Climate is Mediterranean, with mean annual temperature of 13.7°C and annual precipitation of 421.4 mm (data from the farm weather station for the period 2001–2021). Grapevines (c.v. Tempranillo) were grown on trellises, with deficit drip irrigation applied from June to September in vineyard rows.

In 2008, a randomized block trial with four replications was set up to assess different vineyard management systems. Based on this trial, a study was designed in 2015 to examine how different weed management (herbicide, tillage, mowing), as a function of irrigation within the vineyard (non-irrigated inter-rows, irrigated rows) could affect the functional diversity of plant communities (Figure 1). Irrigation was considered since the deficit irrigation applied during the dry period generates clearly contrasting conditions between inter-rows (non-irrigated) and rows (irrigated) that could have a significant effect on plant functional diversity. Accordingly, five types of plots were identified: a) herbicide-treated rows (irrigated); b) mown inter-rows (non-irrigated); c) mown rows (irrigated); d) tilled inter-rows (non-irrigated); e) tilled rows (irrigated). Herbicide-treated inter-rows (non-irrigated) were not included in the original design as this is a very unusual praxis in Mediterranean vineyards, where herbicide application is restricted to rows. Herbicide treatment consisted of two applications of glyphosate (1440 g ai ha^{-1}) throughout the grapevine growth cycle (Figure 1). Mowing of the spontaneous plant cover (two passes) was performed with a flail mower in vineyard inter-rows and with an inter-vine mower in rows. Tillage (two-three passes) was carried out with a cultivator in vineyard inter-rows and with an inter-vine tiller in vineyard rows.

According to our initial hypothesis that the functional diversity of a plot could vary as a function of adjacent management, we distinguished eight different environmental sites in the experimental design (Figure 1). For example, it was considered that the functional diversity in herbicide-treated rows next to mowing (site 6) might be different from that found in herbicide-treated rows next to tillage (site 2). For further details on study site and experimental design, see Guerra et al. (2022).

2.2 Vegetation sampling

In each of the 32 plots (4 blocks × 8 sites), six sampling points separated by a distance of 5.5 m were fixed (Figure 1). Sampling points were placed in pairs (inter-row and row, respectively) spaced 1 m apart. In each of them, a 33 × 66 cm frame was placed, identifying all plant species and assessing the coverage percent of each species (Andújar et al., 2010), as well as the percentage of bare soil. For each species, mean percentage cover was calculated by pooling the data obtained in the six sampling points of each plot. Castroviejo (1986-2012) was used for species identification, updating the species name according to the International Plant Names Index (IPNI, 2022).

2.3 Plant traits

In order to measure functional diversity, 10 functional traits previously associated with plant response to weed management (Guerra et al., 2021), were selected: five vegetative traits related

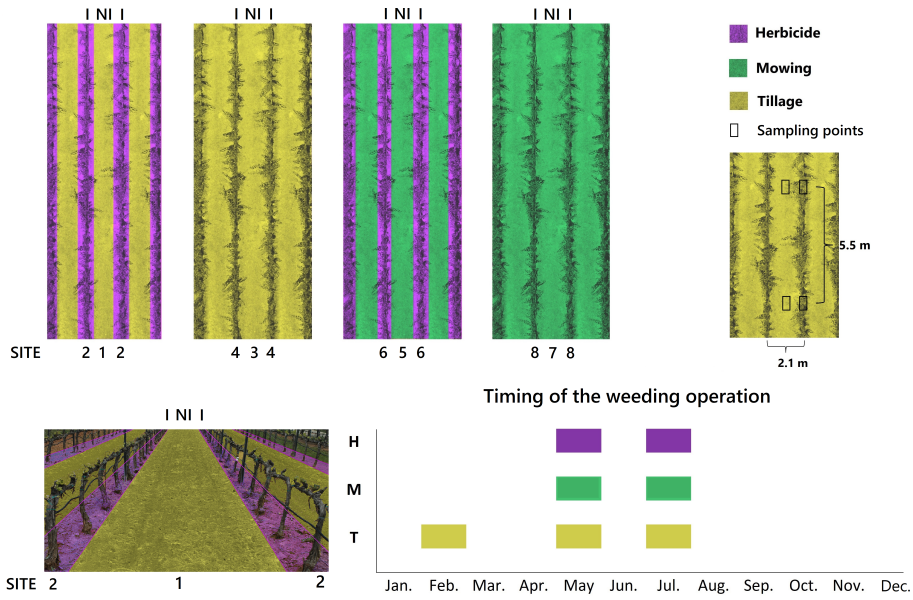

FIGURE 1
Diagram of the experimental design and location of the sampling points (upper part), 3D image depicting sites 2-1-2 (lower left) and schematic chronogram of the weeding operations carried out in the study field (lower right). Irrigation treatment: I: irrigated row; NI, non-irrigated inter-row. Site: 1, tilled inter-rows adjacent to herbicide-treated plots; 2, herbicide-treated rows adjacent to tilled plots; 3, tilled inter-rows adjacent to tilled plots; 4, tilled rows; 5, mown inter-rows adjacent to herbicide-treated plots; 6, herbicide-treated rows adjacent to mown plots; 7, mown inter-rows adjacent to mown plots; 8, mown rows.

to resource-acquiring capacity (Raunkiaer life form [RLF], plant height vegetative [PHV], specific leaf area [SLA], leaf dry matter content [LDMC], leaf area [LA]), and five reproductive traits related to regenerative ability (seed mass [SM], seed bank longevity index [SLI], onset of flowering [OFL], duration of flowering period [DFP], dispersal syndrome [DS]). An overview of the traits used can be found in Table 1.

This study included only species with a significant presence, excluding in the analyses those with less than 0.25% relative cover based on the overall value of all plots. Then, plant trait data

TABLE 1 Brief description of the functional traits used tocompute the functional diversity indexes.

Code	Name	Units	Explanation
RLF	Raunkiaer life form	–	The life form of a plant defined by the position and degree of protection of its perennating bud (Raunkiaer, 1934). Qualitative trait with four levels: therophyte, therophyte/hemicryptophyte, hemicryptophyte, geophyte.
PHV	Plant height (vegetative)	cm	The shortest distance between the upper-boundary of the main photosynthetic tissues (excluding inflorescences) on a plant and the ground level (Cornelissen et al., 2003).
SLA	Specific leaf area	$mm^2\ mg^{-1}$	The one-sided area of a fresh leaf divided by its oven-dry mass (Cornelissen et al., 2003).
LDMC	Leaf dry matter content	$mg\ g^{-1}$	The oven-dry mass (mg) of a leaf divided by its water-saturated fresh mass (g) (Cornelissen et al., 2003).
LA	Leaf area	mm^2	Area of a leaf.
SM	Seed mass	mg	The oven-dry mass of an average seed of a species (Cornelissen et al., 2003).
SLI	Seed bank longevity index	–	The ratio of the number of records that classify the species as persistent to the number of all records for the species (Thompson et al., 1998). SLI can take any value from 0, when all records are transient, to 1, when all records are persistent.
OFL	Onset of flowering	–	Species classification according to month of beginning of flowering period: earlier (January, February), medium (March, April), late (May, June).
DFP	Duration of flowering period	months	Months during which the flowering occurs.
DS	Dispersal syndrome	–	Species grouped according to their dispersal mechanisms into three categories: unspecialized, refers to autochorous species or species without any specific dispersal mechanism; anemochorous, dispersed by wind; zoochorous, dispersed by animals.

were compiled from plant trait databases such as TRY Database (Kattge et al., 2020) and stored in a new database (Guerra et al., 2021). Further details on the traits and database used can be found in Guerra et al. (2021).

2.4 Functional diversity analysis

2.4.1 Functional diversity estimation

Functional diversity based on three components, i.e. functional richness, functional evenness and functional divergence (Mason et al., 2005), were analyzed in this work. Functional richness and functional evenness were computed according to two indices proposed by Villéger et al. (2008): FRic, which quantifies the functional space volume filled by the community based on the calculation of the convex hull volume (see Cornwell et al., 2006); and FEve, which measures the uniformity of abundance distribution in this volume to quantify the regularity with which the different species, weighted by their abundance, fill this functional space.

Functional divergence was measured from Rao's quadratic entropy (RaoQ), which is often used as an index of functional divergence (Schleuter et al., 2010) although encompasses both richness and functional divergence (Mouchet et al., 2010). Hence, RaoQ is the mean distance between species weighted by species abundance (Botta-Dukát, 2005). This index is strongly related to functional dispersion index (FDis) proposed by Laliberté and Legendre (2010) and to the community weighted variance (CWV) defined by Sonnier et al. (2010). It should be noted that FDis and CWV were initially calculated, yielding very similar results to RaoQ (Supplementary Figure 1). ConsequentlRaoQ was used because it is a more common index than the previous ones in plant functional diversity studies.

For computing functional diversity indices, a functional distance matrix based on trait values for each species was initially generated using the Gower distance (Gower, 1971). On this functional matrix, a principal coordinate analysis (PCoA) was performed and the resulting PCoA axes were used as new "traits" to compute in each plot the indices mentioned above, using the function *dbFD* from the R package *FD* (Laliberté and Legendre, 2010).

2.4.2 Null models: Estimating effect size FRic and effect size RaoQ

Thereafter, a null model approach was applied for functional diversity indices (except for FEve, which was excluded according to Mason et al., 2013), testing whether observed FRic and RaoQ values, the latter calculated for the set of traits and also for each trait individually, differed from random expected values. This approach was implemented for two purposes: Firstly, to remove any trivial effect of species richness on functional diversity indices (in line with Mason et al., 2013; Pakeman et al., 2017; Carmona et al., 2020). This is particularly relevant for FRic, given its strong positive correlation with species richness (Villéger et al., 2008; Mouchet et al., 2010) such as was revealed in a preliminary analysis (Supplementary Figure 2). After removing this effect, RaoQ becomes a "pure measure" of functional divergence (Mason et al., 2013). Secondly, null models were developed to test changes in community assembly processes (similarly to Bernard-Verdier et al., 2012; Mason et al., 2012; Mason et al., 2013). Although both RaoQ and FRic have proven to be reliable measures for this purpose, RaoQ seems to be the most suitable for detecting trait convergence and divergence (Botta-Dukát and Czúcz, 2016).

Implemented null models were selected based on previous work (Mason et al., 2013; Botta-Dukát and Czúcz, 2016; Götzenberger et al., 2016). For FRic, randomized matrix was obtained with the independent swap algorithm (function "independentswap" in *picante*) while maintaining the occurrence frequency of the species and the species richness of each plot. For RaoQ, species abundance within each plot was shuffling maintaining sample species richness (function "richness" in *picante*). Null models were generated from randomized matrices using the R package *picante* (Kembel et al., 2010), performing 1000 randomizations for each model to ensure an accurate estimate (Gotelli, 2000).

Subsequently, functional diversity indices were calculated from randomized matrices, measuring the degree to which the observed values of a variable were different from its expected values and later calculating the effect size. The standard method for measuring effect size in a null model is to compute standardized effect size (SES; Gotelli and McCabe, 2002), but Botta-Dukát (2018) has recently pointed out that this method is not suitable when, as in our case, the symmetry assumption is not satisfied. For this reason, it was decided to measure the effect size (ES) according to Chase et al. (2011) as has been performed previously for other cases with not-symmetric distribution of the null model (e.g. Bernard-Verdier et al., 2012; Lhotsky et al., 2016):

$$ES = (p - 0.5) \times 2$$

where

$$p = \frac{number\ (NULL < obs) + \frac{number\ (NULL=obs)}{2}}{1000}$$

being *number (NULL< obs)* the number of occasions in which the value obtained from the null model (*NULL*, expected value) was less than the observed value (*obs*) and *number (NULL = obs)* the number of occasions in which the value obtained from the null model was equal to the observed value. This procedure was performed separately for both FRic and RaoQ. Thus, two new indices were obtained from the effect sizes of FRic (ES FRic) and RaoQ (ES RaoQ) with values ranging from +1 to -1, where positive values indicate a higher observed value than expected, and vice versa. Trait convergence or divergence were assumed if the observed RaoQ values were, respectively, lower or higher than the estimated RaoQ values by the null model (similarly to

Bernard-Verdier et al., 2012; Boonman et al., 2021). Since sometimes community assemblage patterns cannot be described by a single multivariate trait index (Spasojevic and Suding, 2012; Carmona et al., 2015), ES RaoQ has been calculated for the set of all traits (multi-trait) and for each single trait. Besides, although RaoQ (and by extension, ES RaoQ) is less affected by trait outliers than FRic (Cornwell and Ackerly, 2009), functional divergence will be higher the closer the abundant species are located to the boundary of the functional trait space (Botta-Dukát and Czúcz, 2016). Taking this into account, it was assumed that the occurrence of abundant species with extreme values for certain traits could be associated with trait divergence. Abundant species were considered to be those dominant and subordinate species (Grime, 1998) with a relative cover of more than 3% (arbitrary value), which could fundamentally govern the community assemblage processes under the mass ratio hypothesis (Grime, 1998; Díaz and Cabido, 2001). Therefore, the relationship between the most abundant species and ES RaoQ was also analyzed.

2.5 Competitiveness index

The CSR theory (Grime, 1974), which has been extensively applied to the study of plant communities (e.g. Cerabolini et al., 2010; Guerra et al., 2021), categorizes plant species within a triangular scheme consisting of three dimensions: a competitiveness dimension (C-dimension), a stress-tolerance dimension (S-dimension) and a ruderality dimension (R-dimension). The competitive dimension is related to the ability of plant species to compete with their neighbors, with competitor plants typically being large herbaceous species with rapid resource acquisition (Grime, 1974; Hodgson et al., 1999). Building on this theoretical framework, Hodgson et al. (1999) developed a method for CSR classification based on functional traits of herbaceous plants.

Recently, a correlation between the functional structure of weed communities and the CSR strategy has been observed (Guerra et al., 2021). In order to analyze the relationship between competitiveness and functional diversity, we applied a procedure similar to that used by Ricotta et al. (2016) to calculate here a competitiveness index (C_{index}). For this purpose, the competitiveness dimension (C-dimension) of each of the selected species was firstly estimated according to Hodgson et al. (1999). Then, community-weighted mean (CWM; Garnier et al., 2004) of C-dimension values were computed with the R package *FD* for each of the plots (i.e. plot-level C-dimension values weighted by species abundance). Thus, C_{index} was calculated as:

$$C_{index} = \sum_{i=1}^{n} p_i \times \text{C-dimension}_i$$

where p_i is the relative abundance of species *i*, and C-dimension$_i$ is the C-dimension value of species *i*.

2.6 Statistical analyses

The effect of weed management (WM) and irrigation (I) on functional diversity indices was analyzed by means of linear mixed models with the R package *lme4* (Bates et al., 2015), except for RaoQ models which were fitted *via* beta regressions models, with "loglog" as link function, using the R package *betareg* (Cribari-Neto and Zeileis, 2010). Due to the inherent constraints of the experimental design, WM and I were always considered as nested fixed factors (WM:I), although the individual effects of WM and I were also explored. In addition, the influence that adjacent management might have on each plot was examined by fitting alternative models with "site" as a fixed effect. In all fitted models, year and block were considered as random effects.

To screen the best models for each variable, the corrected Akaike's information criterion (AICc) was used, choosing the model with the lowest AICc value (Burnham and Anderson, 2002). Model fit was estimated by mean of pseudo R^2 (only for beta regression models), marginal R^2 (variance explained by fixed effects) and conditional R^2 (variance explained by the whole model) using the R package *performance* (Lüdecke et al., 2021). To test whether fixed effects of the selected models were statistically significant, type-III ANOVA tests were performed using the R package *car* (Fox and Weisberg, 2019). When a significant effect was observed, a *post-hoc* analysis was performed using the pairwise t-test adjusted for Bonferroni correction for pairwise comparison.

In order to detect trait convergence or divergence patterns, values of ES RaoQ were tested as to whether they were significantly different from zero using a one-sample t-test (for normally distributed data) and a Wilcoxon signed-ranks test (for non-normally distributed data). In addition, to analyse the impact of the most abundant species on trait divergence, the relationships between ES RaoQ (both multi-trait and single-trait estimations) and relative cover of these species were assessed using Pearson's correlation test (when data were fitted to a normal distribution) and Spearman's correlation test (for non-normally distributed data).

Finally, the relationship between C_{index} and ES RaoQ was explored through linear regression models using ES RaoQ as the response variable. All analyses were carried out in R 4.1.0 (R Core Team, 2022).

3 Results

A total of 59 plant species were detected, of which 29 showed a significant occurrence (Supplementary Table 1). Complete trait information for these 29 species, reported elsewhere (Guerra et al., 2021), was employed to compute functional diversity indices. Nonetheless, trait data for the most abundant species

10.3389/fpls.2022.993051

are provided (see Supplementary Tables 2, 3). All models except the one constructed for ES FRic showed lower AICc values when WM:I was used as predictor variable (Table 2).

3.1 Effects of weed management and irrigation on functional diversity

A moderate influence of WM:I on functional richness (R^2_m = 0.16) was observed (Table 2). Thus, functional richness was significantly higher in mown irrigated plots compared to tilled irrigated plots, while intermediate values were reached in herbicide-treated irrigated plots (Table 3). However, when the influence of species richness was removed (i.e. ES FRic), opposite values were obtained. Model for ES FRic was best fitted when "site" was used as predictor variable (R^2_m= 0.44). Thus, herbicide-treated sites (site 2 and 6) showed significantly different ES FRic values between them (Figure 2A). Indeed, herbicide-treated rows next to tillage (i.e. site 2), showed similar values to tilled plots but significantly greater than herbicide-treated rows next to mowing (i.e. site 6). A slightly lower effect of WM:I on functional evenness was found (R^2_m = 0.10), with no significant differences observed among managements. In contrast, a marked influence of WM:I on functional divergence (RaoQ) was observed (pseudo R^2 = 0.43), reaching significantly greater values in herbicide-treated irrigated plots than in mown irrigated plots (Table 3). This effect is even more marked for ES RaoQ (R^2_m = 0.55). Besides, irrigation also had a significant effect on functional divergence (Table 2). Thus, higher RaoQ and ES RaoQ values were observed in irrigated plots, although for RaoQ, these differences were only significant when comparing among mown plots (Table 3).

3.2 Trait convergence and divergence as a function of weed management and irrigation

Results related to ES RaoQ for the whole set of traits showed a process of trait convergence in tilled non-irrigated plots and in mown plots, being especially marked in mown non-irrigated plots, while trait divergence was observed in herbicide-treated irrigated plots (Figure 2B). Therefore, mowing significantly promoted trait convergence while trait divergence was enhanced in irrigated plots, supporting what was observed in the exploratory analysis (Supplementary Tables 4, 5). The results of ES RaoQ values for each single trait provided more detailed information (Figure 3; Table 4). Trait convergence observed in tilled non-irrigated plots was mainly due to the negative ES RaoQ values detected for RLF, PHV and LA. In mown plots, convergence was found for all traits except for RLF and, in the case of mown irrigated plots, also for LA and SM. In contrast, a trend towards trait divergence was observed in most traits in

TABLE 2 Summary of models built to analyze the effect of weed management (WM) and irrigation (I) on functional diversity indices.

	FRic				FEve				RaoQ				ES FRic				ES RaoQ			
	WM	I	WM:I	Site	WM	I	WM:I	Site	WM	I	WM:I	Site	WM	I	WM:I	Site	WM	I	WM:I	Site
P-value	**	*ns*	**	**	*	*ns*	*	*	***	***	***	***	***	*ns*	***	***	***	***	***	***
R^2_c	0.17	0.09	0.20	0.26	0.10	0.03	0.11	0.18	-	-	-	-	-	-	-	-	0.49	0.33	0.60	0.62
R^2_m	0.12	0.00	0.16	0.16	0.08	0.03	0.10	0.16	-	-	-	-	0.26	0.03	0.29	0.42	0.45	0.30	0.55	0.56
pseudo R^2	-	-	-	-	-	-	-	-	0.33	0.26	0.43	0.43	-	-	-	-	-	-	-	-
AICc	-	-	-31.91	-14.81	-	-	-70.98	-61.07	-	-	-525.72	-487.97	-	-	169.89	162.07	-	-	119.83	127.35

FRic, functional richness; Feve, functional evenness; RaoQ, Rao's quadratic entropy; ES FRic, effect size functional richness; ES RaoQ, effect size Rao's quadratic entropy.
The significance levels of the fixed terms were assessed from a type-III ANOVA (*ns*, non-significant, $^*P < 0.05$, $^{**}P < 0.01$, $^{***}P < 0.001$). For mixed models, R^2_c and R^2_m provide the proportion of variance explained by the whole model and by the fixed effects, respectively. Pseudo R^2 was estimated for beta regression models.

TABLE 3 Mean values (± SE) by plots of functional diversity indices based on the interaction of weed management and irrigation (WM:I).

	FRic	FEve	RaoQ	ES FRic	ES RaoQ
HI	0.41 ± 0.03 **ab**	0.58 ± 0.03 **a**	0.06 ± 0.00 **a**	-0.05 ± 0.15 **a**	0.31 ± 0.13 **a**
MNI	0.45 ± 0.03 **ab**	0.49 ± 0.02 **a**	0.03 ± 0.00 **c**	-0.71 ± 0.08 **b**	-0.94 ± 0.01 **c**
MI	0.54 ± 0.04 **a**	0.52 ± 0.04 **a**	0.04 ± 0.00 **b**	-0.41 ± 0.17 **ab**	-0.50 ± 0.15 **b**
TNI	0.36 ± 0.05 **b**	0.56 ± 0.03 **a**	0.04 ± 0.00 **b**	0.12 ± 0.12 **a**	-0.38 ± 0.09 **b**
TI	0.29 ± 0.04 **b**	0.61 ± 0.04 **a**	0.06 ± 0.00 **ab**	0.17 ± 0.14 **a**	0.10 ± 0.13 **a**

HI, herbicide – irrigation; MNI, mowing – non-irrigation; MI, mowing – irrigation; TNI, tillage – non-irrigation; TI, tillage – irrigation.
FRic, functional richness; Feve, functional evenness; RaoQ, Rao's quadratic entropy; ES FRic, effect size of functional richness; ES RaoQ, effect size of Rao's quadratic entropy.
Means within the same column with the same letters are not significantly different.

herbicide-treated irrigated plots, but this divergence was only significant for LA and SM. It should be noted that a strong functional convergence was observed for PHV in all plots except in herbicide-treated irrigated plots, where the median value was above zero. In tilled irrigated plots, high functional divergence was also observed for SM and, to a lesser extent, for SLI and OFL. However, the ES RaoQ value for the whole set of traits was not significantly higher than zero, since trait convergence was detected for leaf traits and PHV. In addition, when the effect of irrigation on the divergence of single traits was explored, it was revealed that irrigation only had a significant effect on divergence for RLF, PHV, LA and SM (Supplementary Table 5). Thus, for these traits, irrigated plots were more functionally divergent than non-irrigated plots.

The highest ES RaoQ values found for PHV, LA and SM were strongly associated with two species having more extreme values for these traits: *Sonchus asper* (for PHV and LA) and *Convolvulus arvensis* (for SM) (Supplementary Figure 4). An increased occurrence of *S. asper* caused a substantial increase in ES RaoQ for PHV and especially for LA, with ES RaoQ values above 0.5 for plots with a relative cover above 20% for this species (Figure 4A); while a small increase in the percentage of *C. arvensis* caused an exponential increase in ES RaoQ for SM (Figure 4B), with ES RaoQ higher than 0.5 from a percentage of *C. arvensis* of 4%. For further details, see Supplementary Figures 5, 6.

3.3 Links between competitiveness and functional diversity

A strong correlation was found between C_{index} and ES RaoQ (R^2 = 0.80, P< 0.001), which was best fitted using a cubic regression model (Figure 5). Hence, functional divergence was greater the higher the competitiveness, but with a slight drop for C_{index} above 0.45. An analysis of the ES RaoQ values for each single trait showed how there was a significant positive correlation between ES RaoQ and competitiveness for all traits

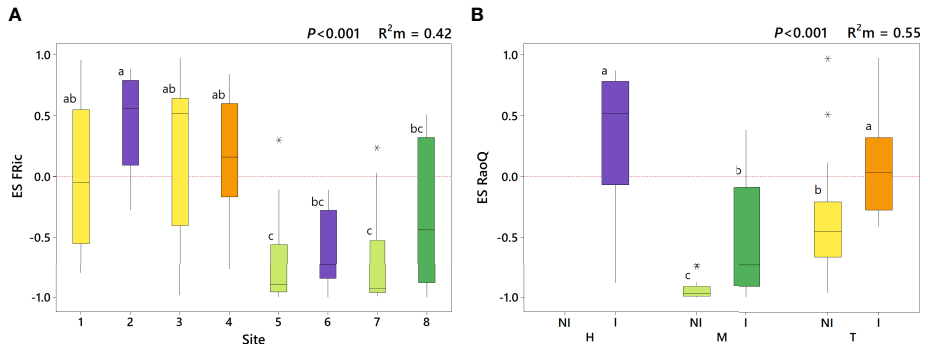

FIGURE 2
Effect size of FRic (ES FRic) depending on site **(A)** and effect size of RaoQ (ES RaoQ) depending on the interaction of weed management and irrigation (WM:I) **(B)**. Marginal R^2 (R^2m) provides the variance explained by the fixed effects. Same letters on the boxes indicate no significant differences. H, herbicide; M, mowing; T, tillage; NI, non-irrigation; I, irrigation. Sites: 1, tilled inter-rows adjacent to herbicide-treated plots; 2, herbicide-treated rows adjacent to tilled plots; 3, tilled inter-rows adjacent to tilled plots; 4, tilled rows; 5, mown inter-rows adjacent to herbicide-treated plots; 6, herbicide-treated rows adjacent to mown plots; 7, mown inter-rows adjacent to mown plots; 8, mown rows. Outliers are indicated with an asterisk (*).

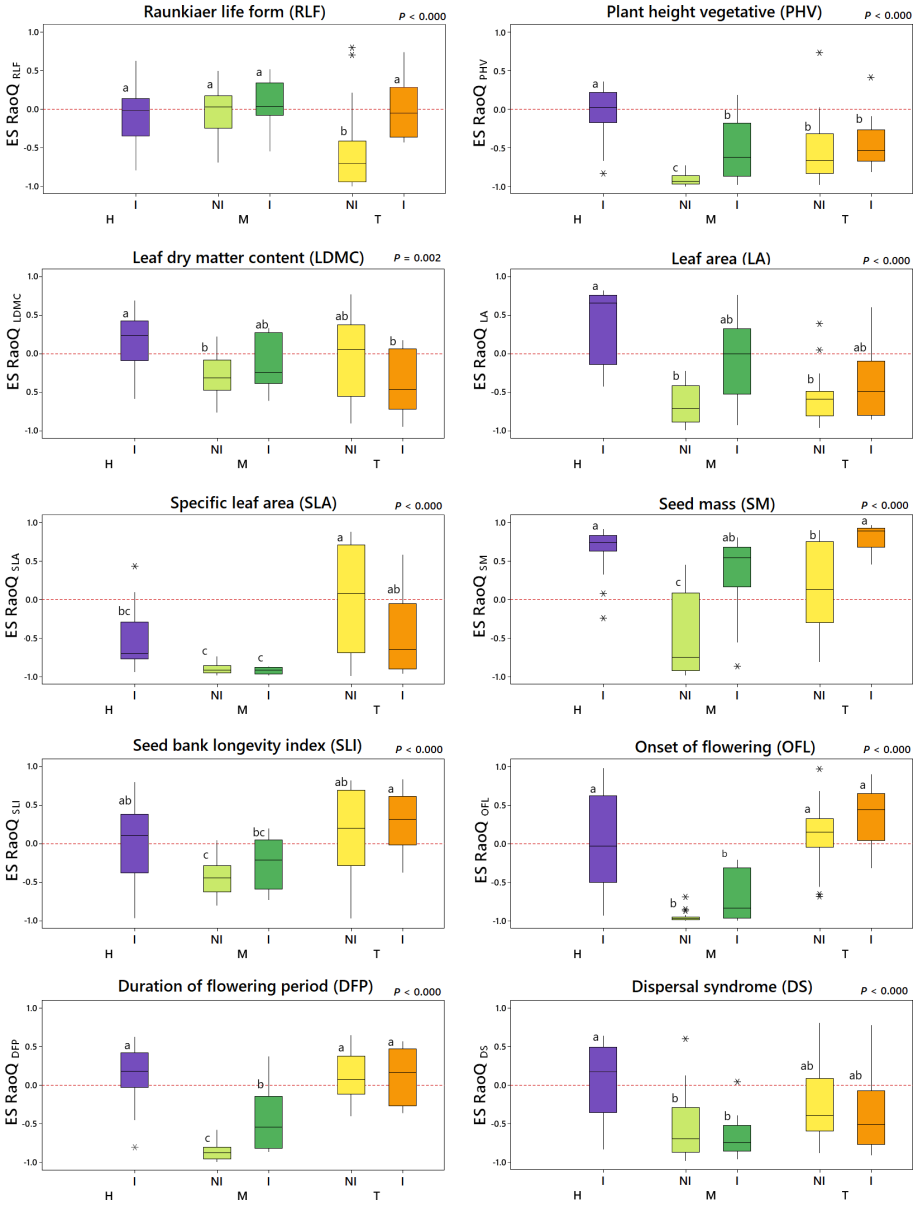

FIGURE 3
Effect size of RaoQ (ES RaoQ) for each single trait depending on the interaction of weed management and irrigation (WM:I). H, herbicide; M, mowing; T, tillage; NI, non-irrigation; I, irrigation. For pairwise comparison, a Student's t-test was conducted, with *P*-values adjusted using the Bonferroni correction. Same letters on the boxes indicate no significant differences. Trait code indicated in the subscripts: RLF, Raunkiær Life Form; PHV, plant height; LDMC, leaf dry matter content; LA, leaf area; SLA, specific leaf area; SM, seed mass; SLI, seed bank longevity index; OFL, onset of flowering; DFP, duration of flowering period; DS, dispersal syndrome. Outliers are indicated with an asterisk (*)

except for LDMC and SLA (Supplementary Table 6). This correlation was particularly strong for PHV, LA and SM.

4 Discussion

To our knowledge, this is the first long-term study addressing how plant functional diversity is shaped by weed management and the first work to evidence trait convergence and divergence processes linked to weed management. Our results revealed that weed management affected different dimensions of functional diversity, with significant major impact on functional divergence. Indeed, trait divergence was observed in herbicide-treated irrigated plots, while trait convergence patterns were detected in tilled plots and especially in mown plots. Irrigation use, which implies different ecological conditions within the vineyard, also affected

10.3389/fpls.2022.993051

TABLE 4 Results of tests on ES RaoQ values to analyze trait convergence or divergence, using a one-sample t-test (for normally distributed data) and a Wilcoxon signed-rank test (for non-normally distributed data) to test whether ES RaoQ values are significantly different from 0.

	ES RaoQ	ES RaoQ $_{RLF}$	ES RaoQ $_{PHV}$	ES RaoQ $_{LDMC}$	ES RaoQ $_{LA}$	ES RaoQ $_{SLA}$	ES RaoQ $_{SM}$	ES RaoQ $_{SLI}$	ES RaoQ $_{OFL}$	ES RaoQ $_{DFP}$	ES RaoQ $_{DS}$
HI	*0,52**	-0,08	*0,02*	0,16	*0,66***	*-0,70****	*0,74****	0,01	*-0,03*	*0,18*	*0,18*
MNI	*-0,97****	0,03	*-0,93****	*-0,29****	*-0,71****	*-0,91****	*-0,74****	*-0,43****	*-0,98****	*-0,88****	*-0,69****
MI	*-0,73***	0,10	*-0,54****	-0,12	-0,08	*-0,92****	*0,55*	*-0,25**	*-0,83****	*-0,43***	*-0,75****
TNI	*-0,46***	*-0,70****	*-0,67****	-0,06	*-0,59****	*0,08*	*0,13*	*0,20*	0,16	0,09	*-0,39**
TI	0,01	0,02	-0,43**	*-0,37***	-0,40**	*-0,41**	*0,81****	*0,29**	*0,44***	0,14	-0,34

HI, herbicide – irrigation; MNI, mowing – non-irrigation; MI, mowing – irrigation; TNI, tillage – non-irrigation; TI, tillage – irrigation. Trait code indicated in the subscripts: RLF, Raunkiaer Life Form; PHV, plant height; LDMC, leaf dry matter content; LA, leaf area; SLA, specific leaf area; SM, seed mass; SLI, seed bank longevity index; OFL, onset of flowering; DFP, duration of flowering period; DS, dispersal syndrome.
For normally distributed data, mean values are indicated. For non-normally distributed data, median values are reported (in italics). Significance levels are indicated by *P*-values: $^{*}P < 0.05$; $^{**}P < 0.01$; $^{***}P < 0.001$

functional diversity with higher functional divergence in irrigated plots with respect to non-irrigated plots.

4.1 Effects of weed management and irrigation on plant functional diversity

The findings obtained for functional richness were within expectations since, as the literature states, a significant positive correlation exists between functional and species richness (Villéger et al., 2008). In our study, mown plots with higher species richness (Guerra et al., 2022) were also those that filled a larger functional space, which is in consonance with the findings of Kazakou et al. (2016). However, when the effect of species richness on functional richness was removed (i.e. ES FRic), the results were reversed. For instance, in mown inter-rows the observed functional richness values were much lower than expected from the null model (ES FRic = -0.71), evidencing high functional redundancy, thus revealing the occurrence in these plots of a large number of species with similar traits. Herbicide effect on ES FRic differed according to adjacent management (Figure 2A), similar to that observed for species richness in Guerra et al. (2022). In this previous work it was noted that herbicide-treated plots next to mowing (site 6) showed higher number of species than herbicide-treated plots next to tillage (site 2). Taking this into account, the low ES FRic values observed at site 6 highlight that higher species richness did not lead in this case to a significant increase in functional richness (Supplementary Figure 3), suggesting that added species are functionally redundant.

Likewise, functional evenness was also lower in mown plots. These findings are in line with Carmona et al. (2020), who observed the lowest values of functional evenness and SES FRic (very similar to ES FRic) in less intensively managed plots. In addition, the lower values observed for ES FRic and FEve in mown plots suggest the existence of habitat filtering mechanisms (Mouchet et al., 2010; Pakeman, 2011), which is in line with the lower values of ES RaoQ found in these plots. Hence, mowing seems to be acting as an abiotic filter that promotes a process of functional convergence in the vast majority of traits, in line with previous work in meadows (Mudrák et al., 2016; Halassy et al., 2019). These results are in agreement with those discussed by Guerra et al. (2021), who observed a distinct suite of plant traits in response to mowing (species with higher stress tolerance, lower vegetative height, lower SLA and higher LDMC). Nonetheless, our findings are not consistent with previous studies reporting the highest values of RaoQ (or similar index FDis) in spontaneous plant covers (Hall et al., 2020) or mown rows (Mainardis et al., 2020). This could be explained by the fact that mowing effects on plant communities depend on the time scale considered, as we will discuss below. Hence, plant communities tend to become more homogeneous and functionally convergent after years of adopting conservation

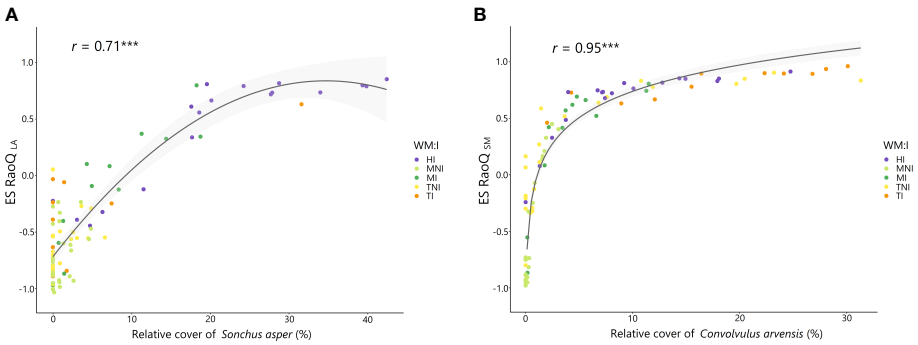

FIGURE 4
Relationship between the relative cover of *Sonchus asper* and effect size of RaoQ for leaf area (ES RaoQ $_{LA}$) **(A)** and between the relative cover of *Convolvulus arvensis* and effect size of RaoQ for seed mass (ES RaoQ $_{SM}$) **(B)**. Dots, corresponding to plots, have been filled in by the interaction of weed management and irrigation (WM:I): HI, herbicide – irrigation; MNI, mowing – non-irrigation; MI, mowing – irrigation; TNI, tillage – non-irrigation; TI, tillage – irrigation. For each correlation, Spearman correlation coefficient (*r*) and its level of significance (***P< 0.000) are shown. Confidence intervals (95%) are shaded in light gray.

agriculture practices (Derrouch et al., 2021). In particular, mowing can lead over time to a homogeneous species composition (Lepš, 2014) and to functional convergence in some traits such as plant height (Halassy et al., 2019).

In tilled inter-rows, although in a more attenuated form, it was also possible to detect a process of functional convergence in some vegetative traits (RLF, PHV, LA), due to the abundant occurrence of short ruderal therophytes with small leaves such as *Lamium amplexicaule*, which are favored by tillage (Hall et al., 2020; Guerra et al., 2021). However, contrary to expectations, no trait convergence was observed in tilled non-irrigated plots for leaf economics traits (LDMC, SLA), which had been previously associated with tillage and agricultural intensification (Carmona et al., 2020; Hall et al., 2020; Guerra et al., 2021). Although tillage may be acting as a functional filter enhancing traits related to fast-growing ruderal species (Guerra et al., 2021), this habitat filtering process may have been hidden in tilled non-irrigated plots by two independent processes. Firstly, the high abundance of *Stellaria media* in these plots, with an extreme value for SLA, led to an increase in functional divergence (Supplementary Figures 5D and 6D). High SLA values are associated with high growth rates (Hunt and Cornelissen, 1997), enabling species to

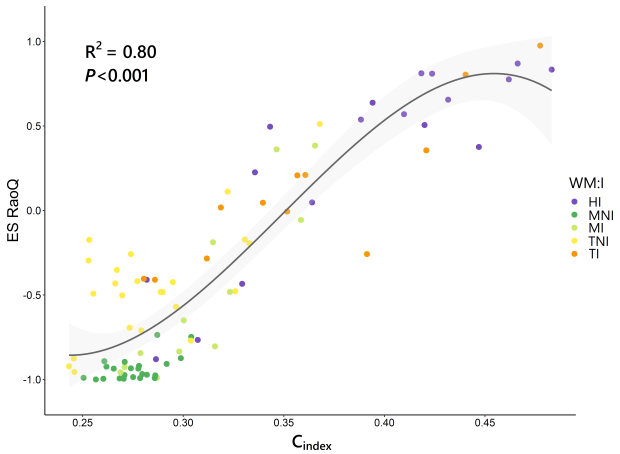

FIGURE 5
Relationship between competitiveness index (C_{index}) and the effect size of RaoQ (ES RaoQ). Dots, corresponding to plots, have been filled in by the interaction of weed management and irrigation (WM:I): HI, herbicide – irrigation; MNI, mowing – non-irrigation; MI, mowing – irrigation; TNI, tillage – non-irrigation; TI, tillage – irrigation. R-squared (R^2) provides the proportion of variance explained by C_{index}. Confidence intervals (95%) are shaded in light gray.

complete their life cycle in a short time (Grime and Hunt, 1975). This would give *S. media* an adaptive advantage to proliferate in environments subject to recurrent disturbances, such as tilled fields (Jernigan et al., 2017). Therefore, tillage could be exerting habitat filtering at the lower margin of the functional range by limiting the occurrence of species with low SLA, while not necessarily limiting the occurrence of species with more extreme values at the upper margin of the functional range, since high SLA values provide an adaptive advantage over tillage. Secondly, the habitat filtering could be hidden here by the abundance of species that are not typical of tillage (e.g. *Medicago minima*, *Bromus madritensis*) but which colonize these tilled spaces due to their massive occurrence in nearby mown plots, compatible with a spatial mass effect (Shmida and Wilson, 1985). Thus, the abundance in tilled non-irrigated plots of *M. minima and B. madritensis*, with LDMC values substantially higher than those of typical tillage species (e.g. *L. amplexicaule*), caused a marked increase in functional divergence (Supplementary Figure 6D).

The observed convergence in vegetative traits (PHV, LDMC, SLA) in tilled irrigated plots, would suggest a process of habitat filtering due to tillage. However, trait convergence was counterbalanced here by divergence patterns observed for certain reproductive traits (SM, SLI, OFL), which were markedly high for SM. Trait divergence for SLI and OFL was a consequence of the coexistence in these plots of tillage specialist species with a persistent seed bank and early flowering (e.g. *L. amplexicaule*, *Veronica hederifolia*) together with species with a transient seed bank (e.g. *Diplotaxis erucoides*, *M. minima*) and later flowering (e.g. *C. arvensis*, *B. madritensis*). This suggests the existence of a partitioning of phenological and regeneration niches (Grubb, 1977), with different reproductive strategies, similar to what has been documented in previous studies (Cornwell and Ackerly, 2009; Bernard-Verdier et al., 2012). Likewise, the greatest functional divergence observed for SM was mainly due to the occurrence of a single species, *C. arvensis*, with a vastly higher SM than the others (Figure 4B). This higher SM may provide *C. arvensis* a greater ability to compete for establishment sites (Turnbull et al., 2004), increase success in colonization and survival after tillage or herbicide application (Kazakou et al., 2021) and establish a persistent soil seed bank with physically dormant seeds (Xiong et al., 2018), enabling its permanence on arable land.

Similarly, the higher abundance of *C. arvensis* in irrigated plots also led to a significantly higher functional divergence for SM compared to non-irrigated plots. This was also the cause of the higher divergence observed in irrigated plots for RLF, as the geophyte life form of *C. arvensis* contrasts with the vast majority of therophytes in these communities.

Overall, our results revealed that functional divergence was greater in irrigated than in non-irrigated plots, since beyond RLF and SM, trait divergence was detected in irrigated plots for PHV and LA. This is consistent with the literature, which states that functional divergence may increase with increasing water availability, particularly in vegetative traits related to resource acquisition (Spasojevic and Suding, 2012; Carmona et al., 2015; Nogueira et al., 2018). Divergence for PHV and LA was mainly driven by the increased abundance in irrigated plots of more competitive species such as *S. asper* or *D. erucoides* (Guerra et al., 2021), which had a significantly greater vegetative height and leaf size than the rest. The PHV and LA are closely associated with competitive ability (Grime, 1974; Keddy et al., 2002). On this basis, a tall and large-leaved species such as *S. asper* could compete more effectively for resources, especially for light capture and water. These trait divergence patterns observed for these vegetative traits would indicate a partitioning of light interception strategies, in line with previous work in herbaceous communities (Spasojevic and Suding, 2012).

From the above, irrigation favored more competitive species that showed markedly divergent values for certain traits. This led to an overdispersion of these traits and thus to an increase in functional divergence indices, as clearly reflected by the strong positive correlation found between ES RaoQ and C_{index} (Figure 5), albeit with a slight downward trend in functional divergence was observed at higher C_{index} values. This is consistent with former studies indicating that functional divergence may be maximal at intermediate levels of competition, whereas when competitive processes are maximized, as in undisturbed productive habitats, trait convergence may occur as weaker competitors are excluded and traits that confer plant species greater competitive ability are enhanced (Grime, 2006; Navas and Violle, 2009; Mayfield and Levine, 2010).

In our study, competitiveness was significantly greater in herbicide-treated irrigated plots, where a significant trait divergence was detected for the whole set of traits. The higher abundance of *S. asper* in these plots, where it is the dominant species together with *B. madritensis*, would explain the higher functional divergence observed. But to understand why, it is first necessary to describe the particular dynamics that occur in these herbicide-treated irrigated plots. Except for cases of herbicide resistance (Heap and Duke, 2018), which are not reported in our study field, the application of non-residual herbicide glyphosate removes almost the totality of weeds, thus resulting in a completely bare soil. But in our case, after the last summer application there was a time window between applications of 8-9 months (see Figure 1) during which different species were able to colonize, germinate and grow in gaps caused by the herbicide treatment. Under these particular conditions, the two dominant species were *S. asper* and *B. madritensis*, in our opinion due to two reasons: (a) the most abundant species in nearby plots might have colonized the herbicide-generated gaps more profusely. In fact, the two most abundant species in mown plots, *M. minima* and *B. madritensis*, were respectively the third and the first most

abundant species in herbicide-treated irrigated plots (Supplementary Figure 5); (b) both tillage and mowing seem to be more successful in limiting the occurrence of *S. asper* (Guerra et al., 2022). During the months between the last herbicide application and the following year sampling, these dominant species initiate an annual process of resource competition which, as mentioned above, would be enhanced in irrigated plots. In this competition for resources, in line with the "limiting similarity" theory (Macarthur and Levins, 1967), two species are more likely to coexist if they have differentiated niches, as in the case of *S. asper* and *B. madritensis*, with markedly different functional traits (see Supplementary Table 3). Thus, with respect to vegetative traits, *S. asper* is a noticeably taller species, with much larger leaves, lower LDMC and lower SLA than *B. madritensis*. These species also differ in all reproductive traits, with *S. asper* having much lighter seeds, a markedly higher SLI, different phenological traits and a different dispersal syndrome than *B. madritensis*. Considering the evidence of two clearly divergent species within the multi-trait functional space, which was also reflected in significant trait divergence detected through null models, would confirm the existence of niche differentiation processes in herbicide-treated irrigated plots.

4.2 Synthesis and implications for agroecological weed management

Our study has evidenced how plant functional diversity can be affected by weed management through processes of trait convergence and divergence, also revealing that these processes can occur simultaneously, affecting both vegetative and reproductive plant traits. Trait divergence was significant in herbicide-treated irrigated plots, where marked differences between the two dominant species provided clear evidence of a process of niche differentiation. The effect of weed management on these processes was shaped by the application of irrigation in vineyard rows, leading primarily to functional divergence for vegetative traits linked to the ability to acquire resources.

On the whole, these community assembly processes were reflected in the estimated functional diversity indices. Hence, mown plots exhibited the highest functional richness. However, when species abundance was considered (i.e. RaoQ), herbicide-treated irrigated plots showed the highest functional diversity. Since ecosystem functions may be further conditioned by dominant plant species (mass-ratio hypothesis), RaoQ may be a more appropriate index to measure plant functional diversity. Indeed, higher functional diversity might not be a desirable indicator in agroecosystems, since higher RaoQ values were associated in this study with the occurrence of dominant species such as *S. asper* and *C. arvensis*, which are considered as noxious grapevine weeds (Guerra et al., 2022) and cause yield losses in a wide variety of crops (Boldt et al., 1998). Based on these assumptions, it would be advisable to propose agroecological weed management aimed not at maximizing functional diversity, but at favoring a certain range of plant trait values, reducing disservices (e.g. crop competition, pest hosting) and enhancing ecosystem services (e.g. pollination, carbon sequestration). For this purpose, CWM of plant traits could be a more useful tool than functional diversity indices (Lavorel, 2013; Weil et al., 2021). Therefore, further studies are required to clarify the relationship between weed management, plant functional traits and the provision of ecosystem services. This relationship should be the central core of agroecological weed management.

Data availability statement

The original contributions presented in the study are included in the article/Supplementary Material. Further inquiries can be directed to the corresponding author.

Author contributions

JG, FC, CF-Q and JD conceived and designed the research; JG and JD conducted the plant surveys; JG processed the data, obtained abundance matrix and collected data on plant traits; JG analysed the data with support from JP and JD; JG led the writing of the manuscript under the supervision of JD. All authors contributed critically to the drafts and gave final approval for publication.

Funding

This work was supported by FEDER/MICINN-AEI, grant number AGL2017-83325-C4-1-R and by MICINN-AEI, grant number PID2020-113229RB-C41/AEI/10.13039/501100011033. The lead author has been granted a predoctoral research fellowship FPI-INIA2016-00035.

Acknowledgments

We would like to thank the great support provided by J.M. Martín and D. Campos, CSIC technical staff who participated in the field sampling. We also acknowledge support of the publication fee by the CSIC Open Access Publication Support Initiative through its Unit of Information Resources for Research (URICI).

Conflict of interest

The authors declare that the research was conducted in the absence of any commercial or financial relationships that could be construed as a potential conflict of interest.

Publisher's note

All claims expressed in this article are solely those of the authors and do not necessarily represent those of their affiliated organizations, or those of the publisher, the editors and the reviewers. Any product that may be evaluated in this article, or claim that may be made by its manufacturer, is not guaranteed or endorsed by the publisher.

Supplementary material

The Supplementary Material for this article can be found online at: https://www.frontiersin.org/articles/10.3389/fpls.2022.993051/full#supplementary-material

References

Andújar, D., Ribeiro, A., Carmona, R., Fernández-Quintanilla, C., and Dorado, J. (2010). An assessment of the accuracy and consistency of human perception of weed cover. *Weed Res.* 50, 638–647. doi: 10.1111/j.1365-3180.2010.00809.x

Bates, D., Mächler, M., Bolker, B., and Walker, S. (2015). Fitting linear mixed-effects models using lme4. *J. Stat. Software* 67, 1–48. doi: 10.18637/jss.v067.i01

Bernard-Verdier, M., Navas, M.-L., Vellend, M., Violle, C., Fayolle, A., and Garnier, E. (2012). Community assembly along a soil depth gradient: contrasting patterns of plant trait convergence and divergence in a Mediterranean rangeland. *J. Ecol.* 100, 1422–1433. doi: 10.1111/1365-2745.12003

Boldt, P. E., Rosenthal, S. S., and Srinivasan, R. (1998). Distribution of field bindweed and hedge bindweed in the USA. *J. Prod. Agric.* 11, 377–381. doi: 10.2134/jpa1998.0377

Boonman, C. C. F., Santini, L., Robroek, B. J. M., Hoeks, S., Kelderman, S., Dengler, J., et al. (2021). Plant functional and taxonomic diversity in European grasslands along climatic gradients. *J. Veg. Sci.* 32, e13027. doi: 10.1111/jvs.13027

Botta-Dukát, Z. (2005). Rao's quadratic entropy as a measure of functional diversity based on multiple traits. *J. Veg. Sci.* 16, 533–540. doi: 10.1111/j.1654-1103.2005.tb02393.x

Botta-Dukát, Z. (2018). Cautionary note on calculating standardized effect size (SES) in randomization test. *Community Ecol.* 19, 77–83. doi: 10.1556/168.2018.19.1.8

Botta-Dukát, Z., and Czúcz, B. (2016). Testing the ability of functional diversity indices to detect trait convergence and divergence using individual-based simulation. *Methods Ecol. Evol.* 7, 114–126. doi: 10.1111/2041-210X.12450

Bretagnolle, V., and Gaba, S. (2015). Weeds for bees? a review. *Agron. Sustain. Dev.* 35, 891–909. doi: 10.1007/s13593-015-0302-5

Burnham, K. P., and Anderson, D. R. (2002). *Model selection and multimodel inference* (New York: Springer).

Cadotte, M. W., Carscadden, K., and Mirotchnick, N. (2011). Beyond species: functional diversity and the maintenance of ecological processes and services. *J. Appl. Ecol.* 48, 1079–1087. doi: 10.1111/j.1365-2664.2011.02048.x

Carmona, C. P., Guerrero, I., Peco, B., Morales, M. B., Oñate, J. J., Pärt, T., et al. (2020). Agriculture intensification reduces plant taxonomic and functional diversity across European arable systems. *Funct. Ecol.* 34, 1448–1460. doi: 10.1111/1365-2435.13608

Carmona, C. P., Mason, N. W. H., Azcárate, F. M., and Peco, B. (2015). Inter-annual fluctuations in rainfall shift the functional structure of Mediterranean grasslands across gradients of productivity and disturbance. *J. Veg. Sci.* 26, 538–551. doi: 10.1111/jvs.12260

Castroviejo, S (1986-2012). *Flora iberica* (CSIC, Madrid: Real Jardín Botánico).

Celette, F., and Gary, C. (2013). Dynamics of water and nitrogen stress along the grapevine cycle as affected by cover cropping. *Eur. J. Agron.* 45, 142–152. doi: 10.1016/j.eja.2012.10.001

Cerabolini, B. E. L., Brusa, G., Ceriani, R. M., De Andreis, R., Luzzaro, A., and Pierce, S. (2010). Can CSR classification be generally applied outside Britain? *Plant Ecol.* 210, 253–261. doi: 10.1007/s11258-010-9753-6

Chase, J. M., Kraft, N. J. B., Smith, K. G., Vellend, M., and Inouye, B. D. (2011). Using null models to disentangle variation in community dissimilarity from variation in α-diversity. *Ecosphere* 2, art24. doi: 10.1890/ES10-00117.1

Conti, G., and Díaz, S. (2013). Plant functional diversity and carbon storage – an empirical test in semi-arid forest ecosystems. *J. Ecol.* 101, 18–28. doi: 10.1111/1365-2745.12012

Cornelissen, J. H. C., Lavorel, S., Garnier, E., Díaz, S., Buchmann, N., Gurvich, D. E., et al. (2003). A handbook of protocols for standardised and easy measurement of plant functional traits worldwide. *Aust. J. Bot.* 51, 335–380. doi: 10.1071/bt02124

Cornwell, W. K., and Ackerly, D. D. (2009). Community assembly and shifts in plant trait distributions across an environmental gradient in coastal California. *Ecol. Monogr.* 79, 109–126. doi: 10.1890/07-1134.1

Cornwell, W. K., Schwilk, D. W., and Ackerly, D. D. (2006). A trait-based test for habitat filtering: Convex Hull volume. *Ecology* 87, 1465–1471. doi: 10.1890/0012-9658(2006)87[1465:ATTFHF]2.0.CO;2

Cribari-Neto, F., and Zeileis, A. (2010). Beta regression in R.. *J. Stat. Softw* 34, 1–24. doi: 10.18637/jss.v034.i02

Crowder, D. W., and Jabbour, R. (2014). Relationships between biodiversity and biological control in agroecosystems: Current status and future challenges. *Biol. Control* 75, 8–17. doi: 10.1016/j.biocontrol.2013.10.010

Daane, K. M., Hogg, B. N., Wilson, H., and Yokota, G. Y. (2018). Native grass ground covers provide multiple ecosystem services in Californian vineyards. *J. Appl. Ecol.* 55, 2473–2483. doi: 10.1111/1365-2664.13145

Derrouch, D., Dessaint, F., Fried, G., and Chauvel, B. (2021). Weed community diversity in conservation agriculture: Post-adoption changes. *Agric. Ecosyst. Environ.* 312, 107351. doi: 10.1016/j.agee.2021.107351

Díaz, S., Lavorel, S., Bello, F., Quétier, F., Grigulis, K., and Robson, T. M. (2007). Incorporating plant functional diversity effects in ecosystem service assessments. *Proc. Natl. Acad. Sci. U. S. A.* 104, 20684–20689. doi: 10.1073/pnas.0704716104

Díaz, S., and Cabido, M. (2001). Vive la différence: plant functional diversity matters to ecosystem processes. *Trends Ecol. Evol.* 16, 646–655. doi: 10.1016/S0169-5347(01)02283-2

Dorado, J., and López-Fando, C. (2006). The effect of tillage system and use of a paraplow on weed flora in a semiarid soil from central Spain. *Weed Res.* 46, 424–431. doi: 10.1111/j.1365-3180.2006.00526.x

Emmerson, M., Morales, M. B., Oñate, J. J., Batáry, P., Berendse, F., Liira, J., et al. (2016). "Chapter two - how agricultural intensification affects biodiversity and ecosystem services,", in *Advances in ecological research Large-scale ecology: Model systems to global perspectives*. Eds. A. J. Dumbrell, R. L. Kordas and G. Woodward (Cambridge, MA: Academic Press), 43–97. doi: 10.1016/bs.aecr.2016.08.005

Fox, J., and Weisberg, S. (2019). *An r companion to applied regression, third edition* (Thousand Oaks CA: Sage). Available at: https://socialsciences.mcmaster.ca/jfox/Books/Companion/.

Fried, G., Kazakou, E., and Gaba, S. (2012). Trajectories of weed communities explained by traits associated with species' response to management practices. *Agric. Ecosyst. Environ.* 158, 147–155. doi: 10.1016/j.agee.2012.06.005

Garnier, E., Cortez, J., Billès, G., Navas, M.-L., Roumet, C., Debussche, M., et al. (2004). Plant functional markers capture ecosystem properties during secondary succession. *Ecology* 85, 2630–2637. doi: 10.1890/03-0799

Gotelli, N. J. (2000). Null model analysis of species Co-occurrence patterns. *Ecology* 81, 2606–2621. doi: 10.1890/0012-9658(2000)081[2606:NMAOSC]2.0.CO;2

Gotelli, N. J., and McCabe, D. J. (2002). Species Co-occurrence: A meta-analysis of j. m. diamond's assembly rules model. *Ecology* 83, 2091–2096. doi: 10.1890/0012-9658(2002)083[2091:SCOAMA]2.0.CO;2

Götzenberger, L., Botta-Dukát, Z., Lepš, J., Pärtel, M., Zobel, M., and de Bello, F. (2016). Which randomizations detect convergence and divergence in trait-based community assembly? A test of commonly used null models. *J. Veg. Sci.* 27, 1275–1287. doi: 10.1111/jvs.12452

Götzenberger, L., de Bello, F., Bråthen, K. A., Davison, J., Dubuis, A., Guisan, A., et al. (2012). Ecological assembly rules in plant communities–approaches, patterns and prospects. *Biol. Rev.* 87, 111–127. doi: 10.1111/j.1469-185X.2011.00187.x

Gower, J. C. (1971). A general coefficient of similarity and some of its properties. *Biometrics* 27, 857–871. doi: 10.2307/2528823

Grime, J. P. (1974). Vegetation classification by reference to strategies. *Nature* 250, 26–31. doi: 10.1038/250026a0

Grime, J. P. (1998). Benefits of plant diversity to ecosystems: immediate, filter and founder effects. *J. Ecol.* 86, 902–910. doi: 10.1046/j.1365-2745.1998.00306.x

Grime, J. P. (2006). Trait convergence and trait divergence in herbaceous plant communities: Mechanisms and consequences. *J. Veg. Sci.* 17, 255–260. doi: 10.1111/j.1654-1103.2006.tb02444.x

Grime, J. P., and Hunt, R. (1975). Relative growth-rate: Its range and adaptive significance in a local flora. *J. Ecol.* 63, 393. doi: 10.2307/2258728

Grubb, P. J. (1977). The maintenance of species-richness in plant communities: The importance of the regeneration niche. *Biol. Rev.* 52, 107–145. doi: 10.1111/j.1469-185X.1977.tb01347.x

Grundy, A. C., Mead, A., Bond, W., Clark, G., and Burston, S. (2011). The impact of herbicide management on long-term changes in the diversity and species composition of weed populations. *Weed Res.* 51, 187–200. doi: 10.1111/j.1365-3180.2010.00831.x

Guerra, J. G., Cabello, F., Fernández-Quintanilla, C., and Dorado, J. (2021). A trait-based approach in a Mediterranean vineyard: Effects of agricultural management on the functional structure of plant communities. *Agric. Ecosyst. Environ.* 316, 107465. doi: 10.1016/j.agee.2021.107465

Guerra, J. G., Cabello, F., Fernández-Quintanilla, C., Peña, J. M., and Dorado, J. (2022). How weed management influence plant community composition, taxonomic diversity and crop yield: A long-term study in a Mediterranean vineyard. *Agric. Ecosyst. Environ.* 326, 107816. doi: 10.1016/j.agee.2021.107816

Halassy, M., Botta-Dukát, Z., Csecserits, A., Szitár, K., and Török, K. (2019). Trait-based approach confirms the importance of propagule limitation and assembly rules in old-field restoration. *Restor. Ecol.* 27, 840–849. doi: 10.1111/rec.12929

Hall, R. M., Penke, N., Kriechbaum, M., Kratschmer, S., Jung, V., Chollet, S., et al. (2020). Vegetation management intensity and landscape diversity alter plant species richness, functional traits and community composition across European vineyards. *Agric. Syst.* 177, 102706. doi: 10.1016/j.agsy.2019.102706

Heap, I., and Duke, S. O. (2018). Overview of glyphosate-resistant weeds worldwide. *Pest Manage. Sci.* 74, 1040–1049. doi: 10.1002/ps.4760

Hodgson, J. G., Wilson, P. J., Hunt, R., Grime, J. P., and Thompson, K. (1999). Allocating c-S-R plant functional types: A soft approach to a hard problem. *Oikos* 85, 282–294. doi: 10.2307/3546494

Hunt, R., and Cornelissen, J. H. C. (1997). Components of relative growth rate and their interrelations in 59 temperate plant species. *New Phytol.* 135, 395–417. doi: 10.1046/j.1469-8137.1997.00671.x

IPNI (2022) *International plant names index* (Kew, Harvard University Herbaria and Libraries and Australian National Botanic Gardens: The Royal Botanic Gardens). Available at: http://www.ipni.org (Accessed April 2022).

Jernigan, A. B., Caldwell, B. A., Cordeau, S., DiTommaso, A., Drinkwater, L. E., Mohler, C. L., et al. (2017). Weed abundance and community composition following a long-term organic vegetable cropping systems experiment. *Weed Sci.* 65, 639–649. doi: 10.1017/wsc.2017.33

José-María, L., Armengot, L., Blanco-Moreno, J. M., Bassa, M., and Sans, F. X. (2010). Effects of agricultural intensification on plant diversity in Mediterranean dryland cereal fields. *J. Appl. Ecol.* 47, 832–840. doi: 10.1111/j.1365-2664.2010.01822.x

Kattge, J., Bönisch, G., Díaz, S., Lavorel, S., Prentice, I. C., Leadley, P., et al. (2020). TRY plant trait database – enhanced coverage and open access. *Glob. Change Biol.* 26, 119–188. doi: 10.1111/gcb.14904

Kazakou, E., Fried, G., Cheptou, P.-O., and Gimenez, O. (2021). Does seed mass drive interspecies variation in the effect of management practices on weed demography? *Ecol. Evol.* 11, 13166–13174. doi: 10.1002/ece3.8038

Kazakou, E., Fried, G., Richarte, J., Gimenez, O., Violle, C., and Metay, A. (2016). A plant trait-based response-and-effect framework to assess vineyard inter-row soil management. *Bot. Lett.* 163, 373–388. doi: 10.1080/23818107.2016.1232205

Keddy, P. A. (1992). Assembly and response rules: two goals for predictive community ecology. *J. Veg. Sci.* 3, 157–164. doi: 10.2307/3235676

Keddy, P., Nielsen, K., Weiher, E., and Lawson, R. (2002). Relative competitive performance of 63 species of terrestrial herbaceous plants. *J. Veg. Sci.* 13, 5–16. doi: 10.1111/j.1654-1103.2002.tb02018.x

Kembel, S. W., Cowan, P. D., Helmus, M. R., Cornwell, W. K., Morlon, H., Ackerly, D. D., et al. (2010). Picante: R tools for integrating phylogenies and ecology. *Bioinformatics* 26, 1463–1464. doi: 10.1093/bioinformatics/btq166

Laliberté, E., and Legendre, P. (2010). A distance-based framework for measuring functional diversity from multiple traits. *Ecology* 91, 299–305. doi: 10.1890/08-2244.1

Larson, C. D., Menalled, F. D., Lehnhoff, E. A., and Seipel, T (2021). Plant community responses to integrating livestock into a reduced-till organic cropping system. *Ecosphere* 12, e03412. doi: 10.1002/ecs2.3412

Lavorel, S. (2013). Plant functional effects on ecosystem services. *J. Ecol.* 101, 4–8. doi: 10.1111/1365-2745.12031

Lepš, J. (2014). Scale- and time-dependent effects of fertilization, mowing and dominant removal on a grassland community during a 15-year experiment. *J. Appl. Ecol.* 51, 978–987. doi: 10.1111/1365-2664.12255

Lhotsky, B., Kovács, B., Ónodi, G., Csecserits, A., Rédei, T., Lengyel, A., et al. (2016). Changes in assembly rules along a stress gradient from open dry grasslands to wetlands. *J. Ecol.* 104, 507–517. doi: 10.1111/1365-2745.12532

Lüdecke, D., Ben-Shachar, M. S., Patil, I., Waggoner, P., and Makowski, D. (2021). Performance: An r package for assessment, comparison and testing of statistical models. *J. Open Source Software* 6, 3139. doi: 10.21105/joss.03139

Macarthur, R., and Levins, R. (1967). The limiting similarity, convergence, and divergence of coexisting species. *Am. Nat.* 101, 377–385. doi: 10.1086/282505

MacLaren, C., Storkey, J., Menegat, A., Metcalfe, H., and Dehnen-Schmutz, K. (2020). An ecological future for weed science to sustain crop production and the environment. a review. *Agron. Sustain. Dev.* 40, 24. doi: 10.1007/s13593-020-00631-6

Mainardis, M., Boscutti, F., Rubio Cebolla, M. D. M., and Pergher, G. (2020). Comparison between flaming, mowing and tillage weed control in the vineyard: Effects on plant community, diversity and abundance. *PloS One* 15, e0238396. doi: 10.1371/journal.pone.0238396

Martínez-Uña, A., Martín, J. M., Fernández-Quintanilla, C., and Dorado, J. (2013). Provisioning floral resources to attract aphidophagous hoverflies (Diptera: Syrphidae) useful for pest management in central Spain. *J. Econ. Entomol.* 106, 2327–2335. doi: 10.1603/EC13180

Mason, N. W. H., Bello, F., Mouillot, D., Pavoine, S., and Dray, S. (2013). A guide for using functional diversity indices to reveal changes in assembly processes along ecological gradients. *J. Veg. Sci.* 24, 794–806. doi: 10.1111/jvs.12013

Mason, N. W. H., de Bello, F., Doležal, J., and Lepš, J. (2011). Niche overlap reveals the effects of competition, disturbance and contrasting assembly processes in experimental grassland communities. *J. Ecol.* 99, 788–796. doi: 10.1111/j.1365-2745.2011.01801.x

Mason, N. W. H., Mouillot, D., Lee, W. G., and Wilson, J. B. (2005). Functional richness, functional evenness and functional divergence: the primary components of functional diversity. *Oikos* 111, 112–118. doi: 10.1111/j.0030-1299.2005.13886.x

Mason, N. W. H., Richardson, S. J., Peltzer, D. A., Bello, F., Wardle, D. A., and Allen, R. B. (2012). Changes in coexistence mechanisms along a long-term soil chronosequence revealed by functional trait diversity. *J. Ecol.* 100, 678–689. doi: 10.1111/j.1365-2745.2012.01965.x

Mayfield, M. M., and Levine, J. M. (2010). Opposing effects of competitive exclusion on the phylogenetic structure of communities. *Ecol. Lett.* 13, 1085–1093. doi: 10.1111/j.1461-0248.2010.01509.x

Monteiro, A., and Lopes, C. M. (2007). Influence of cover crop on water use and performance of vineyard in Mediterranean Portugal. *Agric. Ecosyst. Environ.* 121, 336–342. doi: 10.1016/j.agee.2006.11.016

Mouchet, M. A., Villéger, S., Mason, N. W. H., and Mouillot, D. (2010). Functional diversity measures: an overview of their redundancy and their ability to discriminate community assembly rules. *Funct. Ecol.* 24, 867–876. doi: 10.1111/j.1365-2435.2010.01695.x

Mudrák, O., Janeček, Š., Götzenberger, L., Mason, N. W. H., Horník, J., de Castro, I., et al. (2016). Fine-scale coexistence patterns along a productivity gradient in wet meadows: shifts from trait convergence to divergence. *Ecography* 39, 338–348. doi: 10.1111/ecog.01723

Navas, M., and Violle, C. (2009). Plant traits related to competition: how do they shape the functional diversity of communities? *Community Ecol.* 10, 131–137. doi: 10.1556/comec.10.2009.1.15

Nogueira, C., Nunes, A., Bugalho, M. N., Branquinho, C., McCulley, R. L., and Caldeira, M. C. (2018). Nutrient addition and drought interact to change the structure and decrease the functional diversity of a Mediterranean grassland. *Front. Ecol. Evol.* 6. doi: 10.3389/fevo.2018.00155

Novara, A., Gristina, L., Saladino, S. S., Santoro, A., and Cerdà, A. (2011). Soil erosion assessment on tillage and alternative soil managements in a Sicilian vineyard. *Soil Tillage Res.* 117, 140–147. doi: 10.1016/j.still.2011.09.007

Novara, A., Minacapilli, M., Santoro, A., Rodrigo-Comino, J., Carrubba, A., Sarno, M., et al. (2019). Real cover crops contribution to soil organic carbon sequestration in sloping vineyard. *Sci. Total Environ.* 652, 300–306. doi: 10.1016/j.scitotenv.2018.10.247

Oerke, E.-C. (2006). Crop losses to pests. *J. Agric. Sci.* 144, 31–43. doi: 10.1017/S0021859605005708

Pakeman, R. J. (2011). Functional diversity indices reveal the impacts of land use intensification on plant community assembly. *J. Ecol.* 99, 1143–1151. doi: 10.1111/j.1365-2745.2011.01853.x

Pakeman, R. J., Hewison, R. L., Riach, D., Fisher, J. M., Hurskainen, S., Fielding, D. A., et al. (2017). Long-term functional structure and functional diversity changes in Scottish grasslands. *Agric. Ecosyst. Environ.* 247, 352–362. doi: 10.1016/j.agee.2017.06.033

Petchey, O. L., and Gaston, K. J. (2002). Functional diversity (FD), species richness and community composition. *Ecol. Lett.* 5, 402–411. doi: 10.1046/j.1461-0248.2002.00339.x

Prosdocimi, M., Cerdà, A., and Tarolli, P. (2016). Soil water erosion on Mediterranean vineyards: A review. *CATENA* 141, 1–21. doi: 10.1016/j.catena.2016.02.010

Rao, C. R. (1982). Diversity and dissimilarity coefficients: A unified approach. *Theor. Popul. Biol.* 21, 24–43. doi: 10.1016/0040-5809(82)90004-1

Raunkiaer, C. (1934). *The life forms of plants and statistical plant geography* (Oxford: Oxford University Press).

R Core Team (2022). *R: A language and environment for statistical computing* (Vienna. Austria: R Foundation for Statistical Computing). Available at: https://www.R-project.org/.

Ricotta, C., de Bello, F., Moretti, M., Caccianiga, M., Cerabolini, B. E. L., and Pavoine, S. (2016). Measuring the functional redundancy of biological communities: a quantitative guide. *Methods Ecol. Evol.* 7, 1386–1395. doi: 10.1111/2041-210X.12604

Schleuter, D., Daufresne, M., Massol, F., and Argillier, C. (2010). A user's guide to functional diversity indices. *Ecol. Monogr.* 80, 469–484. doi: 10.1890/08-2225.1

Shmida, A., and Wilson, M. V. (1985). Biological determinants of species diversity. *J. Biogeogr.* 12, 1–20. doi: 10.2307/2845026

Sonnier, G., Shipley, B., and Navas, M.-L. (2010). Plant traits, species pools and the prediction of relative abundance in plant communities: a maximum entropy approach. *J. Veg. Sci.* 21, 318–331. doi: 10.1111/j.1654-1103.2009.01145.x

Spasojevic, M. J., and Suding, K. N. (2012). Inferring community assembly mechanisms from functional diversity patterns: the importance of multiple assembly processes. *J. Ecol.* 100, 652–661. doi: 10.1111/j.1365-2745.2011.01945.x

Storkey, J., Meyer, S., Still, K. S., and Leuschner, C. (2012). The impact of agricultural intensification and land-use change on the European arable flora. *Proc. R. Soc B Biol. Sci.* 279, 1421–1429. doi: 10.1098/rspb.2011.1686

Tarifa, R., Martínez-Núñez, C., Valera, F., González-Varo, J. P., Salido, T., and Rey, P. J. (2021). Agricultural intensification erodes taxonomic and functional diversity in Mediterranean olive groves by filtering out rare species. *J. Appl. Ecol.* 58, 2266–2276. doi: 10.1111/1365-2664.13970

Thompson, K., Petchey, O. L., Askew, A. P., Dunnett, N. P., Beckerman, A. P., and Willis, A. J. (2010). Little evidence for limiting similarity in a long-term study of a roadside plant community. *J. Ecol.* 98, 480–487. doi: 10.1111/j.1365-2745.2009.01610.x

Thompson, K., Bakker, J. P., Bekker, R. M., and Hodgson, J. G (1998). Ecological correlates of seed persistence in soil in the north-west European flora. *J. Ecol.* 86, 163–169. doi: 10.1046/j.1365-2745.1998.00240.x

Turnbull, L. A., Coomes, D., Hector, A., and Rees, M. (2004). Seed mass and the competition/colonization trade-off: competitive interactions and spatial patterns in a guild of annual plants. *J. Ecol.* 92, 97–109. doi: 10.1111/j.1365-2745.2004.00856.x

Villéger, S., Mason, N. W. H., and Mouillot, D. (2008). New multidimensional functional diversity indices for a multifaceted framework in functional ecology. *Ecology* 89, 2290–2301. doi: 10.1890/07-1206.1

Weil, S.-S., Martinez-Almoyna, C., Piton, G., Renaud, J., Boulangeat, L., Foulquier, A., et al. (2021). Strong links between plant traits and microbial activities but different abiotic drivers in mountain grasslands. *J. Biogeogr.* 48, 2755–2770. doi: 10.1111/jbi.14235

Winter, S., Bauer, T., Strauss, P., Kratschmer, S., Paredes, D., Popescu, D., et al. (2018). Effects of vegetation management intensity on biodiversity and ecosystem services in vineyards: A meta-analysis. *J. Appl. Ecol.* 55, 2484–2495. doi: 10.1111/1365-2664.13124

Xiong, R., Wang, Y., Wu, H., Ma, Y., Jiang, W., Ma, X., et al. (2018). Seed treatments alleviate dormancy of field bindweed (Convolvulus arvensis L.). *Weed Technol.* 32, 564–569. doi: 10.1017/wet.2018.46

frontiers | Frontiers in Plant Science

TYPE Original Research
PUBLISHED 07 October 2022
DOI 10.3389/fpls.2022.925296

OPEN ACCESS

EDITED BY
Boris Rewald,
University of Natural Resources and Life Sciences Vienna, Austria

REVIEWED BY
Robbie Hart,
Missouri Botanical Garden, United States
Jinlong Zhang,
Kadoorie Farm and Botanic Garden, Hong Kong SAR, China

*CORRESPONDENCE
Bo Song
songbo@mail.kib.ac.cn
Hang Sun
sunhang@mail.kib.ac.cn

†These authors have contributed equally to this work

SPECIALTY SECTION
This article was submitted to Functional Plant Ecology, a section of the journal Frontiers in Plant Science

RECEIVED 21 April 2022
ACCEPTED 15 September 2022
PUBLISHED 07 October 2022

CITATION
Rana SK, Rana HK, Stöcklin J, Ranjitkar S, Sun H and Song B (2022) Global warming pushes the distribution range of the two alpine 'glasshouse' *Rheum* species north- and upwards in the Eastern Himalayas and the Hengduan Mountains. *Front. Plant Sci.* 13:925296. doi: 10.3389/fpls.2022.925296

Global warming pushes the distribution range of the two alpine 'glasshouse' *Rheum* species north- and upwards in the Eastern Himalayas and the Hengduan Mountains

Santosh Kumar Rana[1,2†], Hum Kala Rana[1†], Jürg Stöcklin[3], Sailesh Ranjitkar[4,5,6], Hang Sun[1*] and Bo Song[1,7*]

[1]Key Laboratory for Plant Diversity and Biogeography of East Asia, Kunming Institute of Botany, Chinese Academy of Sciences, Kunming, China, [2]Department of Ecosystem Science and Management, Pennsylvania State University, University Park, PA, United States, [3]Institute of Botany, University of Basel, Basel, Switzerland, [4]N. Gene Solution of Natural Innovation, Kathmandu, Nepal, [5]School of Development Studies, Lumbini Buddhist University, Devdaha, Nepal, [6]MICD, Faculty of Humanities and Social Science, Mid-West University, Lalitpur, Nepal, [7]Yunnan Key Laboratory for Integrative Conservation of Plant Species with Extremely Small Populations, Kunming Institute of Botany, Chinese Academy of Sciences, Kunming, China

Alpine plants' distribution is being pushed higher towards mountaintops due to global warming, finally diminishing their range and thereby increasing the risk of extinction. Plants with specialized 'glasshouse' structures have adapted well to harsh alpine environments, notably to the extremely low temperatures, which makes them vulnerable to global warming. However, their response to global warming is quite unexplored. Therefore, by compiling occurrences and several environmental strata, we utilized multiple ensemble species distribution modeling (eSDM) to estimate the historical, present-day, and future distribution of two alpine 'glasshouse' species *Rheum nobile* Hook. f. & Thomson and *R. alexandrae* Batalin. *Rheum nobile* was predicted to extend its distribution from the Eastern Himalaya (EH) to the Hengduan Mountains (HM), whereas *R. alexandrae* was restricted exclusively in the HM. Both species witnessed a northward expansion of suitable habitats followed by a southerly retreat in the HM region. Our findings reveal that both species have a considerable range shift under different climate change scenarios, mainly triggered by precipitation rather than temperature. The model predicted northward and upward migration for both species since the last glacial period which is mainly due to expected future climate change scenarios. Further, the observed niche overlap between the two species presented that they are more divergent depending on their habitat, except for certain regions in the HM. However, relocating appropriate habitats to the north and high elevation may not ensure the species' survival, as it needs to adapt to the extreme climatic circumstances in alpine habitats. Therefore, we advocate for more conservation efforts in these biodiversity hotspots.

KEYWORDS

biodiversity hotspots, biomod2, climate change, glasshouse, range shifts, *Rheum*

Introduction

"*Unless we move quickly to protect global biodiversity, we will soon lose most of the species composing life on Earth.*" —Edward O. Wilson (1929–2021).

Global biodiversity hotspots (Myers et al., 2000) harbor high levels of species richness and endemism (Sun et al., 2017; Rahbek et al., 2019), yet they are vulnerable to large-scale climatic change (Baker and Moseley, 2007). Two biodiversity hotspots, i.e., the Himalayas and the Mountains of Southwest China (also known as the Hengduan Mountains) (Myers et al., 2000; Mittermeier et al., 2011) known to be the biodiversity reservoir of 'the Third Pole', can't remain intangible by present-day global warming (Qiu, 2008). The alpine areas of this region are characterized by low temperatures, intense solar radiation, strong winds, dense cloudiness, frequent precipitation, and a short growing season (He et al., 2006). Several plant species in this area have evolved specific phenotypes, such as "downy plant", "cushion plant", and "glasshouse plant" (Tsukaya and Tsuge, 2001; Körner, 2003) . But those plants, which are well adapted to extreme environments through specialized structures, might be susceptible to climate warming (Doiron et al., 2014). Nevertheless, plant species are known to respond to changes in climate by altering their phenology (Cleland et al., 2007) or shifting their distribution range (Parmesan and Yohe, 2003; Chen et al., 2011). Meanwhile, in the past plant species in the Himalaya-Hengduan Mountains (HHM) have been transformed by quaternary climatic oscillations (Sandel et al., 2011; Muellner-Riehl et al., 2019).

Global warming pushes the plant populations to upslope along elevation and poleward along latitude to track isotherms (Lenoir and Svenning, 2013; Zu et al., 2021). As mountain species migrate upslope to cooler climatic conditions to avoid rising temperatures, it results in a smaller inhabited area and population reduction (Morueta-Holme et al., 2015; Freeman et al., 2018). As they ascend higher in elevation towards mountaintops, the elevational range becomes progressively constrained, perhaps increasing the risk of extinction (Manne et al., 1999; Freeman et al., 2018). Warming temperature drives lowlands species to move upwards, and there may be no record for species adapted to higher temperatures to compensate for the loss (Colwell et al., 2008). Indeed, lowland species from warmer microhabitats may relocate to cooler refuges at the same elevation due to global warming (Bush et al., 2004). However, alpine plants might face summit trap phenomena (Rana et al., 2017; Salick et al., 2019). Due to climate change, plant distribution patterns are changing, with species expanding in more suitable areas and declining in increasingly hostile ones (Kelly and Goulden, 2008). Notably, past temperature rise presented an unusual and persistent upward movement of tree lines for about 1000 m in the Himalayan alpine meadows (Schickhoff et al., 2014) or the HM coniferous forest (Lenoir et al., 2008; Wang et al., 2018; Yao et al., 2020). In line with these predictions, several alpine plants (for instance, *Anemone rivularis*, *Abies delavayi*) have shifted their ranges upward, north-westward (Liang et al., 2018), or upslope (Kelly and Goulden, 2008; Lenoir et al., 2008; Rumpf et al., 2018). However, on the other hand, the alpine glasshouse species are rarely explored for their range shifts.

The genus *Rheum* (Polygonaceae) has around 60 species widely distributed across the QTP's high latitudes. Only a few species make it to Central and Western Asia and Europe (Losina-Losinskaya, 1936; Kao and Cheng, 1975). Owing to the therapeutic and pharmacological properties of *Rheum*, the increased market demand has impaired the survival and existence of wild species (Chen et al., 2018). The majority of *Rheum* species have evolved specific morphologies to cope with the harsh climate (Tsukaya and Tsuge, 2001). The 'glasshouse' plants, with their large upper translucent bracts covering the inflorescences, are examples of such adaptations (Ohba, 1988). Despite the fact 'glasshouse' morphology may be found in more than ten plant families, including Ranunculaceae, Caryophyllaceae, Lamiaceae, Asteraceae, and Polygonaceae (Yoshida, 2002), the most known alpine 'glasshouse' plant species that have piqued the interest of evolutionary and conservation biologists are *R. nobile* Hook. f. & Thomson and *R. alexandrae* Batalin. The multifunctional translucent bracts of such plants are likely to have evolved independently in the Himalayas as a response to low temperatures and high irradiance, facilitating an upward range shift in response to climate change (Tsukaya and Tsuge, 2001; Tsukaya, 2002; Sun et al., 2012; Song et al., 2013c; Song et al., 2015; Song et al., 2020a). On the other hand, cold-adapted alpine plants may experience range contractions and/or local extinctions (Giménez-Benavides et al., 2011; Wiens, 2016) due to a slower rate of adaptation than that of climate change (Quintero and Wiens, 2013). Therefore, to fill the unprecedented research gap in *Rheum* species and to develop a scientific strategy to protect

alpine glasshouse species (i.e., *R. nobile* and *R. alexandrae*) from the negative consequences of global warming, we used species distribution models and assessed the geographical distribution range shift.

The species distribution models (SDM) combined with geographic information systems have ushered in a new era of research into the consequences of climate change on species ecology, biogeography, and conservation (Guisan and Thuiller, 2005; Warren et al., 2008). Ensemble SDM (eSDM) can discover geographic places with a high possibility of having a focal species present by focusing on biological niche demands (Guisan and Thuiller, 2005). With the recent advancement in SDM approaches (Miller, 2010), multi-model projections have been widely utilized to identify the climatic envelope and range shift for endemic and endangered species (Pearson et al., 2007; Robinson et al., 2018).

This research looks at how global warming affects the distribution ranges of the geographically co-occurring alpine 'glasshouse' species *R. nobile* and *R. alexandrae* (Polygonaceae). With the following precise goals in mind, we adopted multiple eSDM approaches to 1) characterize the realized niche underpinning the distribution of the two focal species, 2) predict range shifts of the two focal species under various climatic scenarios, and 3) discuss potential adaptive responses to changes in the distributional range of the two focal species in response to global warming for biodiversity conservation.

Materials and methods

Focal species

Rheum nobile and *R. alexandrae* are two species that have evolved specific adaptations to cope with the cold-foggy and damp conditions prevalent at high elevations in the HHM, respectively. Both species (Figure 1A) are giant perennial herbs endemic to the Eastern Himalayas (EH) and the Hengduan Mountains (HM) (Figure 1D), growing at elevations between 3,400 and 6,000 m a.s.l. (Li and Gao, 1998; Chowdhery and Agrawala, 2009). *Rheum nobile* is a monocarpic herb with individuals dying after a single reproductive event after ca. 33 years of vegetative growth (Song et al., 2020b), whereas *R. alexandrae* is a multi-stemmed polycarpic perennial (Song et al. unpublished). Despite their relatedness and morphological similarity (Sun et al., 2012), they have distinct habitat and range distributions. *Rheum nobile* is found chiefly on alpine open scree and occasionally in open patches of alpine meadows, i.e., in well-drained habitats (Chowdhery and Agrawala, 2009; Song et al., 2013c), whereas the partly sympatric *R. alexandrae* is found mainly on alpine wetlands, including marshes, swampy meadows, and lakeshores (Chen, 1993).

Rarefaction of species occurrence

We focused on the entire geographic distribution ranges of the two species (Figure 1D). For this, the past field (1937–2020) (Supplementary Table S1) datasets were compiled and cross-checked with the herbarium records from the National Herbarium and Plant Laboratories (KATH, Nepal) and Kunming Institute of Botany, CAS (KUN, China) to construct the geographic distribution of both species. In addition to past field and herbarium collections, we also ground-validated occurrence points (from 2015 to 2022) through GPS in the field and cross-checked with the online databases of the Chinese National Herbarium (PE; http://pe.ibcas.ac.cn/en/), Chinese Virtual Herbarium (CVH; http://www.cvh.ac.cn/), the Global Biodiversity Information Facility (GBIF.org, 2021), the Royal Botanical Garden at Edinburgh (RBGE, United Kingdom; http://data.rbge.org.uk/search/herbarium/) and the Herbarium at the University of Tokyo (TI, Japan; http://umdb.um.u-tokyo.ac.jp/DShokubu/). While compiling the occurrence datasets, we mainly focused on geographic coordinates recorded by the different resource persons during the field. So, the occurrence points from the other herbarium specimens and online databases were discarded in the datasets. Following Barbet-Massin et al. (2012), the background points were randomly chosen within a 25–50 km radius of the occurrence points.

Overfitting or biases in eSDM may result from geo-coding errors in the herbarium label and spatially clustered localities (Hijmans, 2012; Boria et al., 2014; Rana et al., 2021), making it challenging to forecast range distribution and climatic suitability accurately. Therefore, we spatially rarefied the gathered geographic occurrences to avoid model bias (Boria et al., 2014; Rana et al., 2017; Rana et al., 2020b). Due to the filter distances' effectiveness in spatially high heterogeneous regions, like mountains, the occurrences were rarefied using a 10-km spatial grid (Veloz, 2009; Boria et al., 2014; Rana et al., 2021). Finally, the models were developed using 56 out of 79 *R. nobile* occurrences and 54 out of 77 *R. alexandrae* occurrences after rarefaction.

Explanatory environmental variables

The potential distribution of the two focal species was modeled for the present-day (ca. 1990–2000) and projected to the paleo (LIG: last inter-glacial ca. 120,000–140,000 years BP; the LGM: last glacial maximum ca. 22,000 years BP) and future (2070, Representative Concentration Pathways, RCPs4.5) climatic scenarios. The climatic projection was created using a multi-model median (MMM) ensemble of General Circulation Models (GCMs) (Rana et al., 2021) (see Supplementary Table S2 for GCMs).

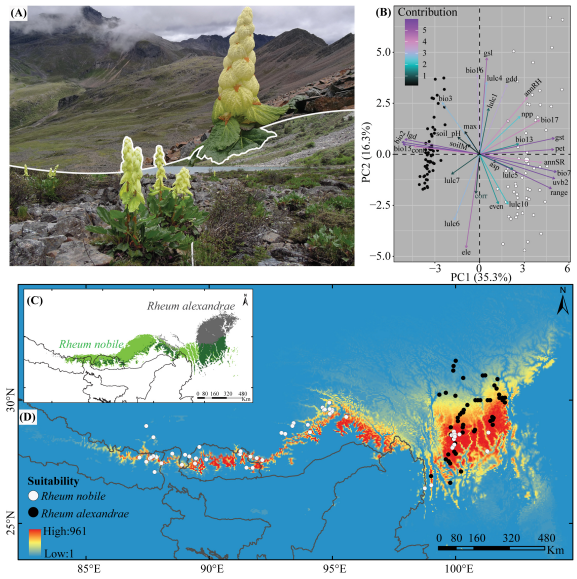

FIGURE 1
(A) Images of *Rheum nobile* (above) and *Rheum alexandrae* (below) in their respective habitats. **(B)** The relative contribution of the predictive environmental variables (colored arrows) to the two axes of biplots from principal components analysis (PCA). The distribution area of both species as a function of **(C)** raster overlay and **(D)** fuzzy overlay depicts their present-day bio-climatically suitable niche in the Eastern Himalaya (EH) and the Hengduan Mountains (HM). The two dots in **(B, D)** represent the occurrence points for *R. nobile* (white dot) and *R. alexandrae* (black dot).

We used three different eSDM in different environmental strata, each with its unique set of predictive variables. Firstly, bioclimatic variables (http://www.worldclim.org/version2) were used to forecast under paleo climatic (LIG, LGM), present-day, and future scenarios. Secondly, all environmental variables were pooled and forecasted. Finally, ensemble forecasting was performed by combining bioclimatic variables with other environmental variable categories such as geo-climatic (http://www.worldclim.org/version2; http://nelson.wisc.edu/sage; http://www.cgiar-csi.org), habitat heterogeneity (Tuanmu and Jetz, 2015; http://www.earthenv.org/texture), growing days (https://chelsa-climate.org/), ultra-violet radiation (Beckmann et al., 2014; https://www.ufz.de/gluv/) and consensus land-cover (Tuanmu and Jetz, 2014; http://www.earthenv.org/landcover). All these climatic variables (Hijmans et al., 2005) and other environmental variables were used with a spatial resolution of 2.5 arc-min (Table 1).

The elimination of highly correlated and/or redundant variables reduces the high collinearity, uncertainties, and predictive errors associated with clustered variables (Ranjitkar et al., 2014). Therefore, we used successive steps of variable selection. Firstly, variables were selected category-wise; secondly, all variables from each category were pooled together (for combined ensemble forecasting); and finally, bioclimatic variables were combined with environmental variables from other categories. Initially screened global consensus landcover variables were analyzed with species occurrences larger than a 30% threshold out of all occurrences (Supplementary Table S3). We used the variance inflation factor (VIF; Fox and Weisberg, 2011) (calculated using the R-package 'car' fixing elevation as a response variable) in conjunction with a Pearson correlation matrix as the significant core of variable selection. In VIF, the linear function of the model employs numeric response variables and is expressed as VIFj=1/(1–R^2j), where R^2j is the R^2-value obtained by regressing the j^{th} predictor on the remaining predictors (Jackson et al., 2009). Variables with VIFj >10 indicate strong multi-collinearity (Quinn and Keough, 2002), and variables with a high VIFj have a negative impact on the modeling output. Several tests were run with extracted values of occurrences for bioclimatic and other environmental variables until a set of predictors with VIFj values less than 10 was retained. The selection of explanatory variables includes Pearson correlation values of < |0.8| (see Supplementary Tables S4, S5 for correlation analysis results) and VIFj values of < 10 (see Supplementary Tables S6–S10 for VIFj analysis results). Initially, variables were selected based on the Pearson correlation (Supplementary Tables S4, S5) and VIFj analysis (Supplementary Tables S6, S7). In contrast, the remaining steps used VIF (Supplementary Tables S8–S10) as the primary function of the variable selection for both focal species. Several species-specific and environmental variables were used as a subset of predictive variables for forecasting the suitable range (Table 1).

TABLE 1 Multi-step selection of predictive environmental variables for ensemble species distribution modeling (eSDM) of two alpine 'glasshouse' herbs, *Rheum nobile* and *Rheum alexandrae*.

Environmental variables	*Rheum nobile*				*Rheum alexandrae*			
	1st	2nd	3rd		1st	2nd	3rd	
Bioclimatic variables (*V1*)								
Mean diurnal range (°C)	–	–			bio2	bio2		
Isothermality [(bio2/bio7) × 100]	bio3	bio3			bio3	bio3		
Temperature Annual Range (bio5-bio6) (°C)	bio7	bio7			–	–		
Mean Temperature of Wettest Quarter (°C)	–	–			bio8	–		
Mean Temperature of Warmest Quarter (°C)	bio10	–			–	–		
Precipitation of Wettest Month (mm)	bio13	bio13			bio13	bio13		
Precipitation Seasonality (Coefficient of Variation)	bio15	–			bio15	bio15		
Precipitation of Wettest Quarter (mm)	bio16	bio16			bio16	bio16		
Precipitation of Driest Quarter (mm)	bio17	bio17			bio17	–		
Precipitation of Coldest Quarter (mm)	bio19	–			–	–		
Geo-climatic (*V2*)								
Elevation (m)	ele	ele	ele	bio3, bio7 bio10, bio13 bio16, bio17 bio19	ele	ele	ele	bio2, bio3 bio8, bio13 bio15, bio16
Aspect (degree)	asp	asp	asp		asp	asp	asp	
Net primary productivity (kg-carbon/m²/year)	npp	npp	npp		npp	npp	npp	
Annual aridity (ratio)	ai	–	–		ai	–	–	
Soil moisture (mm based on 150 mm water holding capacity)	soilM	soilM	soilM		soilM	soilM	soilM	
Potential evapotranspiration (mm)	pet	pet	pet		pet	–	pet	
Annual Relative Humidity (%)	annRH	annRH	annRH		annRH	annRH	annRH	
Annual solar radiation (kJ/m²/day)	annSR	annSR	annSR		annSR	annSR	annSR	
Soil pH (acidity-alkaline level)	soil_pH	soil_pH	soil_pH		soil_pH	soil_pH	soil_pH	
Soil carbon (Kg-Carbon/m² to 1 m depth)	soilC	–	soilC		soilC	–	–	
Annual water vapour (kPa)	–	–	–		annWV	–	–	
Habitat heterogeneity (*V3*)								
Correlation (linear dependency of EVI on adjacent pixels, 1≥ x ≥-1)	corr	corr	corr	bio3, bio7 bio10, bio13 bio15, bio16 bio17, bio19	corr	corr	corr	bio2, bio3 bio8, bio13 bio15, bio16 bio17
Coefficient of variation (normalized dispersion of EVI, x ≥0)	cv	–	cv		cv	–	cv	
Evenness (evenness of EVI, 1≥ x ≥0)	even	even	even		even	even	even	
Homogeneity (similarity of EVI between adjacent pixels, 1≥ x ≥0)	homo	–	homo		homo	–	homo	
Maximum (dominance of EVI combinations between adjacent pixels, 1≥ x ≥0)	max	max	max		max	max	max	
Range (Range of EVI, x ≥0)	range	range	range		–	–	–	
Contrast (exponentially weighted difference in EVI between adjacent pixels, x ≥0)	–	–	–		cont	cont	cont	
Growing days (*V4*)								
Growing degree days (°C based on 5-degree base temperature)	gdd	gdd	gdd	bio3, bio7 bio13, bio15 bio16, bio17 bio19	gdd	gdd	gdd	bio2, bio3 bio8, bio13 bio15, bio16 bio17
Growing season length (number of days)	gsl	gsl	gsl		gsl	gsl	gsl	
Growing season temperature (°C/10)	gst	gst	gst		gst	–	–	
Last day of growing season (Julian day)	–	–	–		lgd	lgd	lgd	
Ultra-violet radiations (*V5*)								
UV-B seasonality (J/m²/day)	uvb2	uvb2	uvb2	bio3, bio7 bio10, bio13 bio15, bio16 bio17, bio19	uvb2	uvb2	uvb2	bio2, bio3 bio8, bio13 bio15, bio16 bio17
Mean UV-B of lowest month (J/m²/day)	uvb4	–	uvb4		–	–	–	
Sum of monthly mean UV-B during lowest quarter	uvb6	–	–		uvb6	–	–	

(Continued)

TABLE 1 Continued

Environmental variables	*Rheum nobile*				*Rheum alexandrae*			
	1st	2nd	3rd		1st	2nd	3rd	
Consensus landcover (*V6*)								
Evergreen/deciduous Needleleaf trees (%)	lulc1	lulc1	lulc1	bio3, bio7 bio10, bio13 bio15, bio16 bio17, bio19	lulc1	lulc1	lulc1	bio2, bio3 bio8, bio13 bio15, bio16 bio17
Mixed/other trees (%)	lulc4	lulc4	lulc4		lulc4	lulc4	lulc4	
Shrubs (%)	lulc5	lulc5	lulc5		–	–	–	
Herbaceous vegetation (%)	lulc6	lulc6	lulc6		lulc6	lulc6	lulc6	
Cultivated and managed vegetation (%)	lulc7	lulc7	lulc7		lulc7	lulc7	lulc7	
Snow/ice (%)	lulc10	lulc10	lulc10					

1st, categories-wise selection; 2nd, all categories combinedly (for combined eSDM); 3rd, Bioclimatic variables with other environmental variables categories.

Furthermore, principal component analysis (PCA) was performed to group the occurrences according to the predictive bioclimatic and environmental variables of *R. nobile* and *R. alexandrae* using the R-package '*factoextra*' (Kassambara and Mundt, 2020).

Ensemble model development and validation

For a given species distribution model, we used the standardized approach in ODMAP (Overview, Data, Model, Assessment and Prediction) (Zurell et al., 2020) protocol structure (Supplementary Methods). The ensemble of SDMs was implemented using the R-package '*Biomod2*' (Thuiller et al., 2020). *Biomod2* outperforms single algorithms by incorporating simulations across multi-model classes, parameters, and climatic conditions (Araujo and New, 2007). Moreover, the consistent modeling approach was applied throughout the different strategies implemented for *R. nobile* and *R. alexandrae*. The assessment of SDM using niche-based modeling techniques allows for different modeling approaches such as bioclimatic envelopes, regression, classification methods, and machine learning methods (Thuiller et al., 2020) (Table 2). Except for MaxEnt with a maximum iteration of 5000 (Maximum Entropy Models; Phillips et al., 2006), all other models in *Biomod2* were run with the default settings.

Apart from analyzing significant variables, the essential steps in modeling are ensemble model development and validation for consensus mapping, which is generally done using a four-step modeling procedure in *Biomod2*. The initial step was calibrating ten sub-models with the '*BIOMOD_Modelling*' function, which defined 4-fold cross-validation using 75% of the data to train the models. The remaining 25% were used to assess the predictive power using True Skill Statistics (TSS), Cohen's Kappa, and Area Under Curve-Receiver Operating characteristics (AUC) statistics (Araujo et al., 2005; Allouche et al., 2006). The threshold-dependent model accuracy matrices, i.e., TSS and Cohen's kappa, are independent of prevalence–the ratio of presence to pseudo-absence data in presence-absence predictions (Allouche et al., 2006). It considers both sensitivity and specificity, with the values ranging from −1 to +1, with +1 denoting perfect agreement. Scores between 0.6 to 0.9 suggest medium to good model performance (Allouche et al., 2006). The threshold-independent model evaluation indicator AUC, on the other hand, is likewise independent of prevalence (Phillips et al., 2006) and examines the models' discriminating abilities. AUC values of less than 0.6 were regarded as poor, 0.6–0.9 were rated moderate, and >0.9 were considered excellent (Phillips et al., 2006). We applied the '*BIOMOD_EnsembleModeling*' function in the second step, with sub-model weights > 0.9 assessed by TSS for ensemble modeling. The sampling procedure was replicated five times. We then used '*BIOMOD_Projection*' for projecting the calibrated sub-models into a new space or time. Finally, the '*BIOMOD_EnsembleForecasting*' function was used to forecast and generate the consensus mapping of species over time and space. The consensus model was then projected onto the past (LIG, LGM) and future (2070) climatic scenarios. Each model's contribution to the final ensemble model was proportional to its goodness-of-fit statistics.

Mapping the ensemble species distribution model

The spatial conversion of the consensus ensemble model to a binary model (presence/absence) was based on the thresholds (50% of suitable habitats) that suit the present-day distribution of the focal species (Forester et al., 2013; Rana et al., 2020a; Rana et al., 2021). The spatial analyses were carried out in ArcMap 10.4.1 (Environmental Systems Resource Institute (ESRI), 2016) using the extension Spatial Analysis to reclassify changes in LIG, LGM, and future conditions compared to present-day suitability into reduction, stable, and expanded areas of the focal species. The predicted suitable habitat maps of the two focal species were then overlapped to locate overlapping regions under present-day climatic scenarios.

TABLE 2 Model evaluation indices for the ensemble species distribution modeling (eSDM) of *Rheum nobile* and *Rheum alexandrae* using Biomod2 in R-programming language.

R. nobile/R. alexandrae	**V1**			**V1 + V2**			**V1+ V3**			**V1+V4**			**V1+ V5**			**V1+ V6**			**Environmental**		
Algorithms	*Kappa*	*TSS*	*AUC*	*Kappa*	*TSS*	*AUC*	*Kappa*	*TSS*	*AUC*	*Kappa*	*TSS*	*AUC*	*Kappa*	*TSS*	*AUC*	*Kappa*	*TSS*	*AUC*	*Kappa*	*TSS*	*AUC*
Generalized additive model (GAM)	0.92/1	0.98/1	1/1	1/1	1/1	1/1	1/1	1/1	1/1	1/1	1/1	1/1	0.95/1	0.99/1	1/1	1/1	1/1	1/1	1/1	1/1	1/1
Generalized boosting model (GBM)	0.96/ 0.97	1/1	1/1	0.99/ 0.97	1/1	1/1	0.97/ 0.99	1/1	1/1	0.97/ 0.96	1/1	1/1	0.97/ 0.98	1/1	1/1	0.96/ 0.98	1/1	1/1	0.98/ 0.99	1/1	1/1
Generalized linear model (GLM)	0.84/ 0.75	0.94/ 0.91	1/0.99	0.89/ 0.94	0.97/ 0.99	1/1	0.85/ 0.83	0.93/ 0.94	1/0.99	0.89/ 0.92	0.95/ 0.95	1/1	0.86/ 0.82	0.93/ 0.94	1/1	0.88/ 0.83	0.94/ 0.92	1/0.99	0.91/1	0.99/1	1/1
Classification tree analysis (CTA)	0.91/ 0.93	0.93/ 0.94	0.97/ 0.99	0.91/ 0.93	0.91/ 0.99	0.97/1	0.88/ 0.91	0.85/ 0.94	0.96/ 0.97	0.9/ 0.88	0.89/ 0.85	0.96/ 0.93	0.9/ 0.92	0.91/ 0.92	0.97/ 0.99	0.91/ 0.91	0.93/ 0.94	0.97/ 0.97	0.9/ 0.88	0.85/ 0.85	0.94/ 0.93
Artificial neural network (ANN)	0.84/ 0.99	0.8/ 0.98	0.96/ 0.99	0.98/ 0.95	0.98/ 0.98	1/1	0.91/ 0.85	0.93/ 0.97	0.99/ 0.98	0.85/ 0.97	0.97/ 0.98	0.99/1	0.89/ 0.97	0.89/ 0.96	0.96/ 0.99	0.92/1	0.93/1	0.99/1	0.79/ 0.86	0.82/ 0.85	0.93/ 0.98
Flexible discriminant analysis (FDA)	0.87/ 0.89	0.93/ 0.98	0.98/1	0.84/ 0.87	0.89/ 0.99	0.95/1	0.87/ 0.86	0.89/ 0.98	0.96/1	0.9/ 0.87	0.97/ 0.94	1/0.99	0.85/ 0.88	0.94/ 0.97	0.98/1	0.86/ 0.9	0.91/ 0.98	0.96/1	0.92/ 0.94	0.97/ 0.98	0.99/ 0.99
Multiple adaptive regression splines (MARS)	0.9/ 0.95	0.97/ 0.98	1/1	1/0.91	1/0.89	1/0.94	0.9/ 0.96	0.97/ 0.98	1/0.99	0.94/ 0.94	0.97/ 0.99	1/1	0.9/ 0.95	0.94/ 0.98	0.99/1	0.92/ 0.98	0.95/1	1/1	1/1	1/1	1/1
Random forest (RF)	1/0.99	1/1	1/1	1/1	1/1	1/1	0.99/1	1/1	1/1	1/0.99	1/1	1/1	1/0.99	1/1	1/1	0.99/1	1/1	1/1	1/1	1/1	1/1
Surface range envelops (SRE)	0.7/ 0.82	0.62/ 0.72	0.81/ 0.86	0.65/ 0.69	0.52/ 0.56	0.76/ 0.78	0.6/ 0.67	0.48/ 0.52	0.74/ 0.76	0.7/ 0.81	0.6/0.7	0.8/ 0.85	0.67/ 0.81	0.55/ 0.7	0.78/ 0.85	0.61/ 0.77	0.48/ 0.65	0.74/ 0.82	0.46/ 0.62	0.32/ 0.46	0.66/ 0.73
Maximum Entrophy (MaxEnt)	0.93/ 0.96	0.98/ 0.97	1/0.99	0.99/ 0.95	1/0.98	1/1	0.95/ 0.99	0.99/1	1/1	0.95/ 0.95	0.97/ 0.98	1/1	0.92/ 0.95	0.97/ 0.98	1/1	0.97/ 0.97	0.97/ 0.98	1/0.99	1/1	0.9/1	1/1

Kappa, Cohen's kappa; TSS, True Skill Statistics; AUC, Area Under the Curve; V1, Bioclimatic variables; V2, Geo-climatic; V3, Habitat-heterogeneity; V4, Growing days; V5, Ultra-violet radiations; V6, Consensus landcover

10.3389/fpls.2022.925296

Niche equivalency test

Under the current bioclimatic scenario, we used the *ecospat* test in R-package '*ENMTools*' (Warren and Dinnage, 2021) for the two focal species, *R. nobile*, and *R. alexandrae*, to test the hypothesis that the environmental niche model formed by population occurrences is identical. The R version of *ENMTools* has a more straightforward user interface of *ecospat* hypothesis testing with *enmtools.species* objects. It further conducts principal component analysis for multiple predictor variables to reduce them to a two-dimensional environment space (Warren et al., 2021). The bioclimatic niches were measured and validated using Schoener's '*D*' and Hellinger's-based '*I*' through *enmtools.ecospat.id* function of identity test and *enmtools.ecospat.bg* function of background test (symmetric and asymmetric) (Warren et al., 2010; Warren et al., 2021). Schoener's *D* is a formula that calculates the appropriate range depending on the probability of occupied grid cells. Hellinger's-based *I* works in a similar way as Schoener's *D*, but without the assumption (Warren and Seifert, 2011). The pairwise similarity values of *D* and *I* indices ranged from 0 (complete divergence/no overlap) to 1 (high similarity/complete overlap), indicating that as the score increases, so does the niche overlap.

Results

Explanatory variables analysis and model performance

The series of variable selection resulted in a robust set of bioclimatic and other environmental variables to predict the environmental niche of the two species. Initially screened variable selection through Pearson correlations ($r < |0.8|$) and VIF (VIF*j* <10) yielded 36 and 34 least correlated and non-redundant variables for *R. nobile* and *R. alexandrae*, respectively. These variables are species-specific to determine the distribution of *R. nobile* and *R. alexandrae* (refer to Table 1 for details on predictive variables). Landcover, being an influential factor in determining species range for SDM (Bucklin et al., 2015), we chose the number of occurrences found within each landcover variable (Supplementary Table S3). The first model employs bioclimatic variables, including eight for *R. nobile* (three temperature-dependent, five precipitations dependent) and seven for *R. alexandrae* (three temperature-dependent, four precipitations-dependent). Highly contributing algorithm with TSS >0.9 (Table 2) were selected to estimate the response curves of the variables, notably for bioclimatic variables from eSDM (Figure 2) and *ENMTools* (see Supplementary Figure S1).

The suitability of *R. nobile* is more favored by temperature annual range (bio7: ca. 28 °C), mean temperature of warmest quarter (bio10: ca. 10 °C), precipitation of coldest quarter (bio19: ca. 12 mm) than that of *R. alexandrae* by mean diurnal range (bio2: ca. 14 °C), mean temperature of the wettest quarter (bio8: 8 °C) (Figure 2; Supplementary Figure S1). Furthermore, the co-existing niches for both focal species are characterized by isothermality (bio3; ca. 45), precipitation of wettest month (bio13, ca. 200 mm), precipitation seasonality (bio15; ca. 100 mm), precipitation of wettest quarter (bio16; 300–500 mm), and precipitation of driest quarter (bio17; ca. 12 mm) (Figure 2; Supplementary Figure S1). However, other environmental variables contributed to forecasting suitable habitats for the two focal species. When all predictive environmental variables were combined as in the second modeling, robust comparable model algorithms were produced (Table 2). Also, in the third modeling when all these environmental variables were independently modeled with bioclimatic variables only, suitability was found to be predictive.

Meanwhile, the first two components of a PCA with all predictive variables explained 51.6% (PC1: 35.3% and PC2: 16.3%) of the observed variance for the two focal species, and their environmental niches were demarcated from each other in biplots (Figure 1B; Supplementary Figure S2). Bioclimatically (*V1*), bio2, bio3, and bio15 are the most important for *R. alexandrae*, whereas bio7 and bio17 are the most important for *R. nobile*. Although the contributions of the different variables in the biplots are species-specific, *R. nobile*'s niche is characterized by an assembly of most variables. When compared to *R. alexandrae*, the niche of *R. nobile* is characterized largely by environmental variables (refer to Figure 1B and Table 1 for more details on variables contribution). The model evaluation indices AUC and Cohen's kappa value varied from 0.66 to 1 and 0.46 to 1. The SRE algorithm scored the lowest, and the RF, GAM, and GBM algorithms scored the highest (Table 2). Finally, the consensus model was evaluated and calibrated for all three modelings, with TSS >0.9 (details in Table 2). The result indicates that the consensus models were highly predictive and accurate regarding AUC, Cohen's kappa, and TSS (Table 2).

Ecological niche analysis

Quantitatively, the average weight of the identity test (*D, I* < 0.82; Figure 3A) and the low weight of the background test (*D, I*<0.6; Figures 3B, C) show that the two focal species *R. nobile* and *R. alexandrae*, have quite different environmental niches. The ENM similarity score for the present-day occurrence of two species is average compared to what would be expected based on the null hypothesis of niche equivalency, indicating that the two species' environmental niches may not be similar (Figure 3A). However, the observed overlap between the two species in

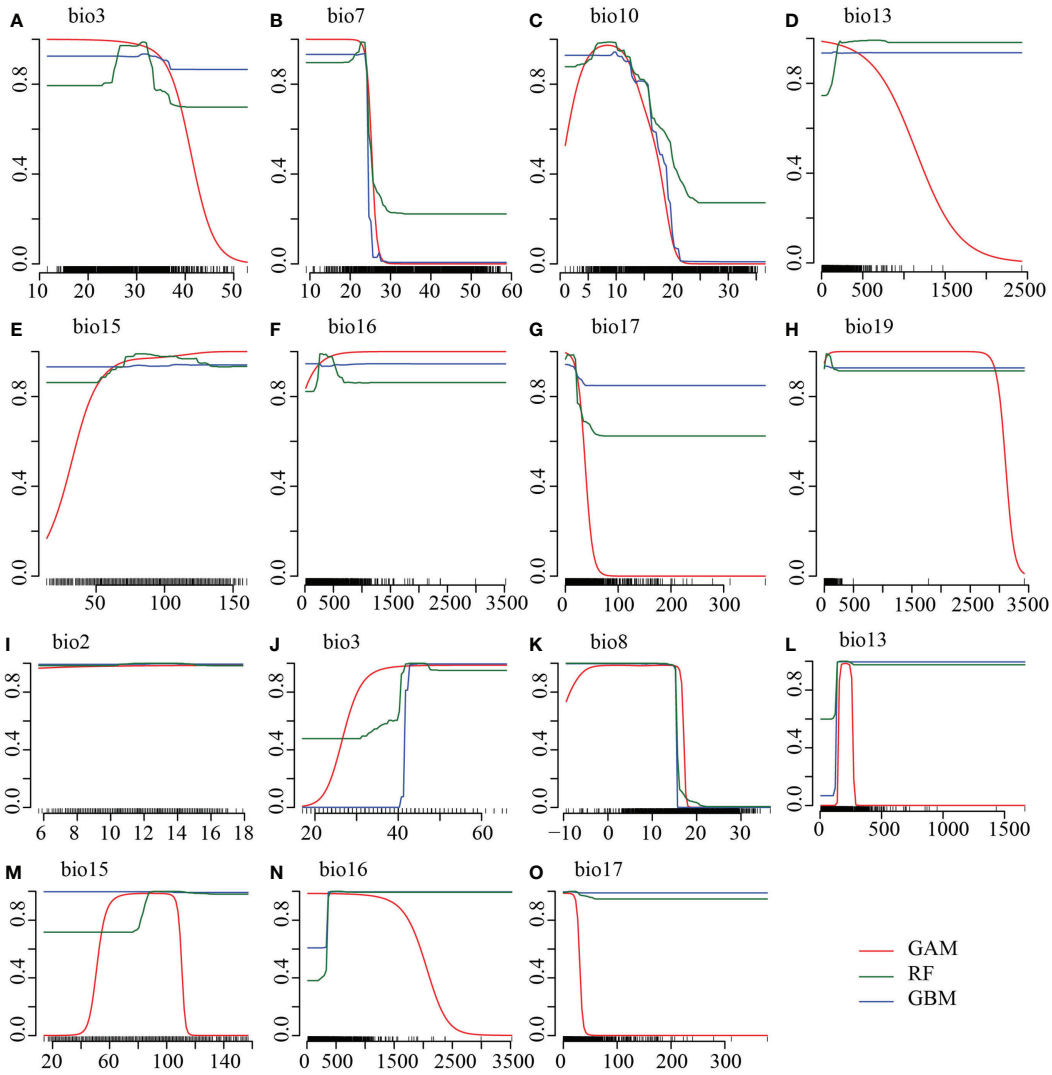

FIGURE 2
Response curves of the highly predictive top three algorithms showing the probability of presence (y-axis) under the **(A–C, I–K)** temperature-dependent and **(D–H, L–O)** precipitation-dependent variables (x-axis) for **(A–H)** *Rheum nobile* and **(I–O)** *Rheum alexandrae*. The predictive algorithms are the Generalised Additive Model (GAM; red line), Generalised Boosting Models (GBM; blue line), and Random Forest (RF; green line), with high model accuracy TSS > 0.9. Temperatures are expressed in °C (degree Celsius) and precipitation in mm (millimeter). Refer to Table 1 for the bioclimatic variables.

background tests is lower than expected under the null hypothesis, showing that the two species are more divergent depending on their habitat (Figures 3B, C). However, the predictive power of the niche assemblage differs significantly as a consequence of multiple algorithms. The lowest to average score on the identity test and background test through GAM indicates that the two species are ecologically apart (Supplementary Figures S3A, C, E). In contrast, RF algorithms with the highest identity and background tests imply that the two species' ecological niches are comparable and co-occur at the same locality (Supplementary Figures S3B, D, F).

Climate-induced range shifts of the two alpine 'glasshouse' *Rheum* species

The predicted suitable habitat under the initial bioclimatic modeling inferred the better suitability of *R. nobile* across the EH than the HM (Figure 4A). On the other hand, *R. alexandrae* has a robust distribution range in the eastern HM and is scattered across the EH (Figure 4B). The projected suitability using all environmental variables coupled with bioclimatic variables (second modeling) (Supplementary Figures S4A, G) or bioclimatic + each environmental variable (third modeling)

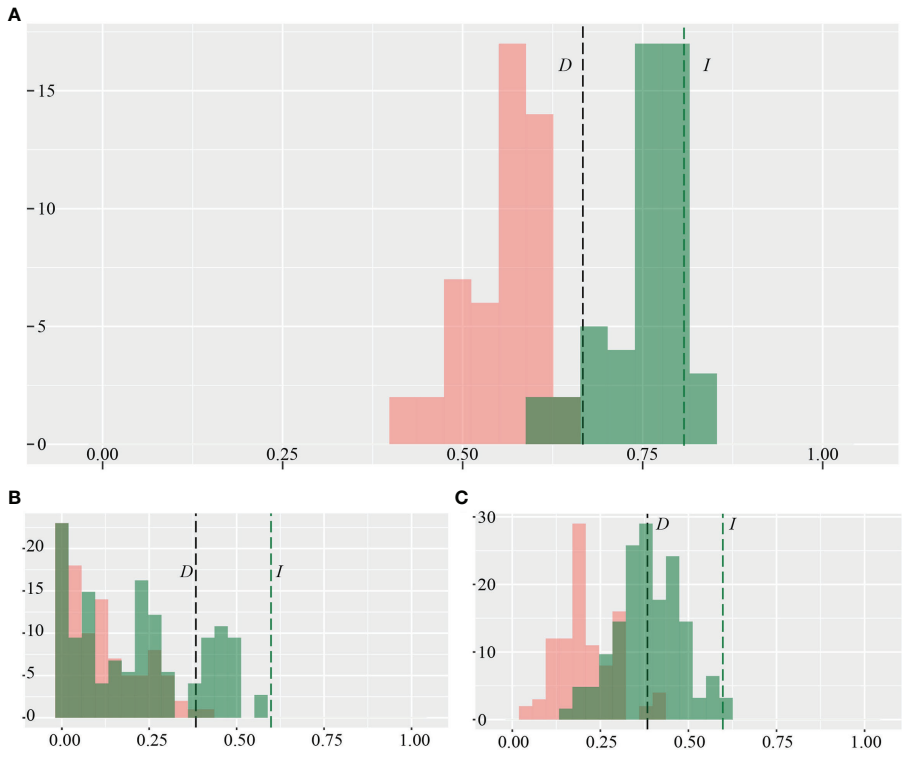

FIGURE 3
Pairwise niche **(A)** identity test and background test **(B)**, symmetric; **(C)**, asymmetric calculated between the two alpine 'glasshouse' herbs *Rheum nobile* and *Rheum alexandrae* as a function of *niche.overlap* ecospat test implemented in ENMtools. The niche equivalency test as species-wise pair comparisons was measured by Schoener's *D* (in black color) and Hellinger's-based *I* (in green color) indices.

(Supplementary Figures S4B–F, H–L) resulted in similar patterns for the distribution ranges. The continuous pattern of the distribution range of *R. nobile* runs from the EH to the HM (Supplementary Figures S4A–F). In contrast, all three modeling approaches revealed a narrower distribution range of *R. alexandrae* restricted in the HM (Supplementary Figures S4G–L). The conservative prediction of high suitability in the HM for both species represents the present-day distribution range of the species (Figures 1C, D and 4A, B; Supplementary Figure S4). Although they appear in distinct locations, their range comprises the same geographic region in the HM, namely Huluhai and Hongshan (field observation) (Figures 1B–D).

The prediction under four different climate scenarios (LIG, LGM, present-day, and future) are mainly observed across the Eastern Himalayas and the Hengduan Mountains (Figures 1C, D and 4; Supplementary Figure S4). From LIG to the present-day, *Rheum nobile* has a varied suitable distribution range, whereas a future range is comparable with the present-day (Figures 4A, C, E, G). Throughout LIG, the paleo-distribution model predicted refugial habitats in the southern HM (Figure 4C), which relocated east and west in distinct regions during the LGM (Figure 4E). Similarly, *R. alexandrae*'s suitable distribution expands from the LIG to the present-day and then to the future (Figures 4B, D, F, H). *R. alexandrae* was more common in the central HM during the LIG than *R. nobile*. Then, the distribution range shifts towards the eastern HM, with some patches towards the EH during the LGM. When projected to the future scenario, the suitable range in the northern HM moves even higher (Figure 4H). Both species were predicted to have suitable distribution ranges and a strong expansion towards the north (Figure 5). However, their distribution ranges were only slightly reduced from the paleo climatic scenario [LIG (Figures 5A, B) and LGM (Figures 5C, D)] to the present-day, and from the present-day to the future (Figures 5E, F). However, in comparison to the present-day situation, the expansion towards the north is accompanied by a habitat contraction in the south, notably in the HM. Conclusively, the ensemble forecasting for the two species shows different range shifts under different climatic scenarios.

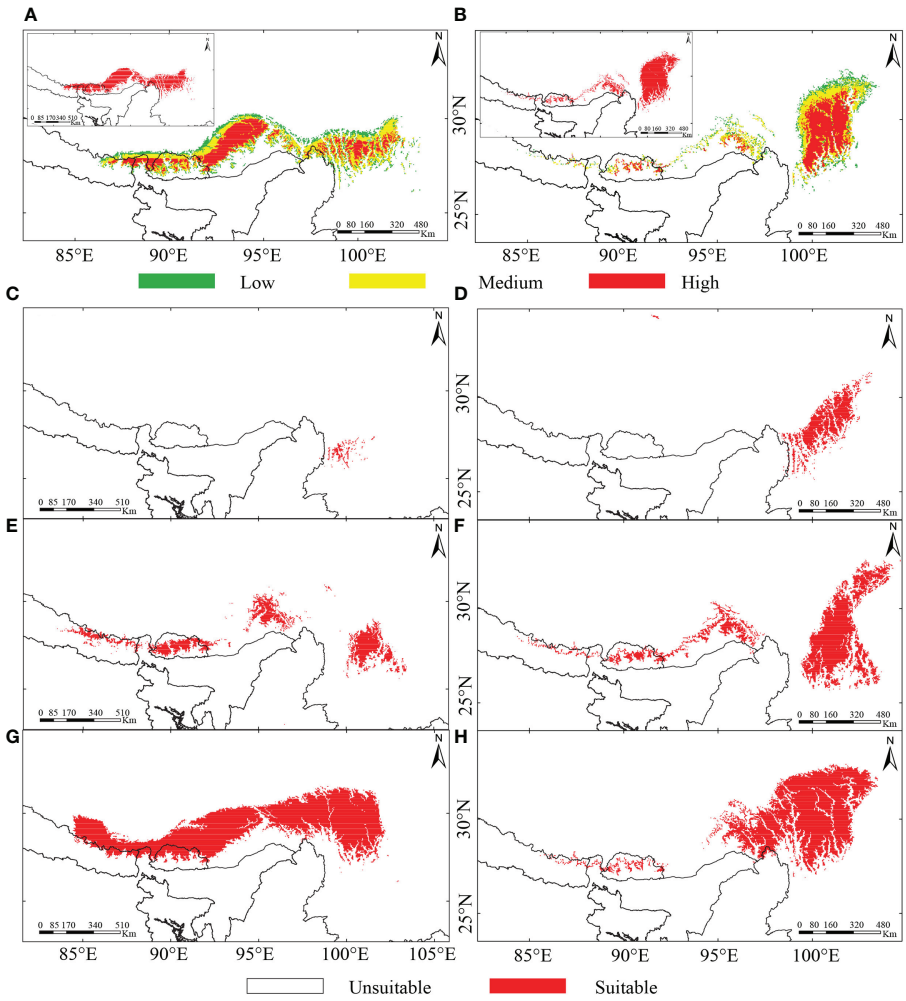

FIGURE 4
Predicted potentially suitable habitat of two alpine 'glasshouse' herbs, **(A, C, E, G)** *Rheum nobile* and **(B, D, F, H)** *Rheum alexandrae* under **(A, B)** present-day scenario of bioclimatic variables classifying their suitability level (suitable habitat in the left top corner of each map), **(C, D)** last-inter glacial (LIG), **(E, F)** last glacial maximum (LGM), and **(G, H)** future scenarios.

Discussion

Predictiveness of the multi-model median for eSDM

Climate change in mountainous regions is projected to shift plant distribution upwards, consequently, declining their populations in those areas where it is no longer suited for them. The capacity to model such alterations in plant distribution ranges is heavily reliant on the availability of sufficient environmental data and algorithms to analyze the temporal changes. Ensemble modeling has proven to be robust and predictive, overcoming the uncertainty and variability of single models across multiple GCMs (Murphy et al., 2004; Pierce et al., 2009; Rana et al., 2021). The use of ensemble modeling in conjunction with consensus projections not only reduces the predictive uncertainty of single models (Araujo and New, 2007; Ranjitkar et al., 2014) but also improves accuracy (Marmion et al., 2009) and addresses uncertainties inherent in SDM techniques (Barry and Elith, 2006). However, it is equally important to consider the selective nature of variables selected through a series of variable filtration used in the different modeling. Our study is the first to use an ensemble forecasting procedure in an assemblage of variables related to bioclimatic, geo-climatic, habitat heterogeneity, the number of growing days, landcover, and ultraviolet radiation to predict the range shift of plant species. It is anticipated to have a comparable predictive value when forecasting the range shift of montane plants based on only bioclimatic variables (Rana et al., 2021). Nonetheless, alpine plants must use bioclimatic variables with macro/micro-

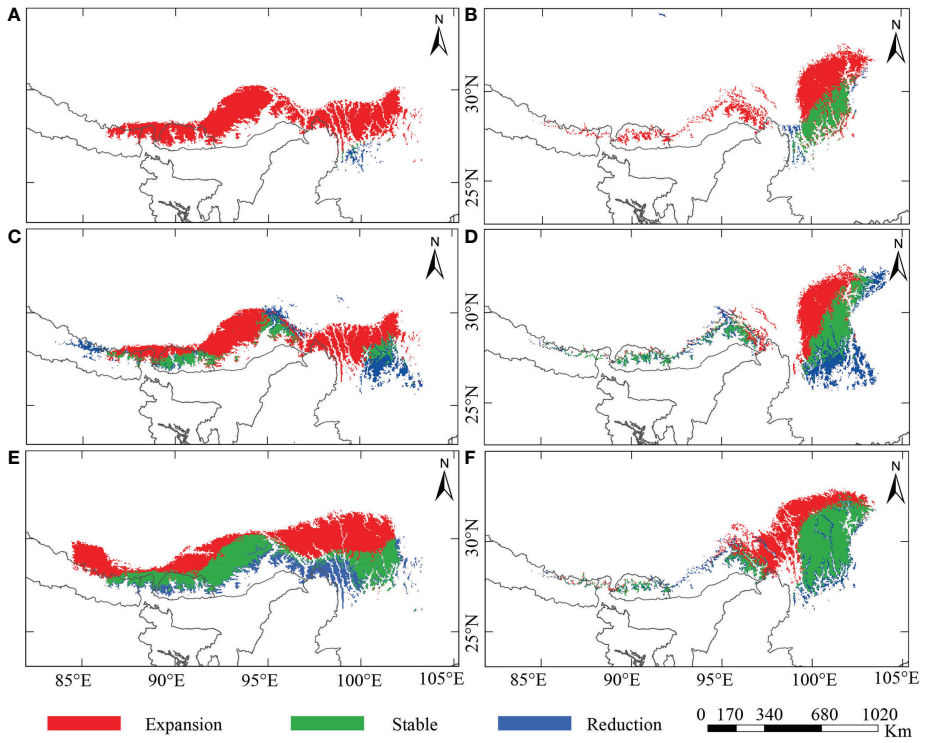

FIGURE 5
Potentially reduced, stable, and expanded range for the alpine 'glasshouse' herbs, **(A, C, E)** *Rheum nobile* and **(B, D, F)** *Rheum alexandrae* compared among different climate scenarios: **(A, B)** last interglacial (LIG) *versus* present-day; **(C, D)** last glacial maximum (LGM) *versus* present-day; and **(E, F)** present-day versus future [2070, Representative Concentration Pathway (RCP) 4.5].

climatic environmental variables, habitat heterogeneity, landcover, canopy cover, and UV radiation (Austin and van Niel, 2011; Robinson et al., 2018). As a result, model uncertainty is minimized, and the algorithm's accuracy is improved. We analyzed and evaluated the algorithms using threshold-independent (i.e., AUC) and threshold-dependent (i.e., TSS and Cohen's kappa) model performance measures and outlined the accuracy and predictiveness (matrices values >0.9) of algorithms in different eSDM for both species.

Ecological niche characterization of the two alpine 'glasshouse' *Rheum* species

Global warming will significantly impact the distribution and resilience of the earth's ecological communities (Mclaughlin and Zavaleta, 2012). These impacts will most likely be felt in mountainous regions, as many alpine plants' ranges are projected to migrate upwards/polewards (IPCC, 2014). Meanwhile, we found that the distribution of alpine plants, such as the two 'glasshouse' *Rheum* species, are characterized by precipitation-dependent variables more than temperature-dependent variables, thereby confirming Fu et al. (2018) and Sun et al. (2016). Along with that, the climatic niche for *R. nobile* is also characterized by a 'temperature annual range' with peak suitability at ca. 28°C, higher than Wang (2006) estimation (i.e., 15 °C). *Rheum alexandrae*, on the other hand, has a 'mean temperature of warmest quarter' of ca. 8 °C. Therefore, the temperature-induced shift in bioclimatic zones is the decisive factor responsible for the decline in the suitability range of the two alpine species. However, their local occurrence and ecological microhabitat are frequently associated with soil water conditions. *Rheum alexandrae* is found chiefly in alpine wetlands, including marsh, swampy meadows, and lakeshores (Chen, 1993); while *R. nobile*, usually occurs on alpine scree and rarely in open patches of alpine meadow, i.e., in well-drained habitats (Song et al., 2013a; Song et al., 2013b).

Specifically, climate regulates the distribution limitations of the two *Rheum* species. The species' cool range limits are governed directly by climatic factors, while the warm range limits are more impacted by biotic interactions, such as predation, mutualism, and resource competition (Paquette and Hargreaves, 2021). Furthermore, our model exemplifies the hypothesis of a combined latitudinal/upward range shift of species with cool range limitations. Despite their close relationship and similar morphology (Sun et al., 2012; Song

et al., 2020b), *R. alexandrae* and *R. nobile* exhibit distinct life histories, distribution limits, and ecological niches related to soil water conditions. Consequently, their specific local niches might underpin the biogeographic patterns of alpine 'glasshouse' species. Their specific areas of occurrence were barely apart from each other. They are in comparable geographical places. However, they had never existed together in the same microhabitat. Consequently, niche identity and background analyses for the two 'glasshouse' species revealed minimal evidence of comparable niche composition.

Global warming affects the distribution range of the two alpine 'glasshouse' *Rheum* species

Will species be able to adapt in the face of distribution range shift as a result of climate warming? Such topics have been hotly debated, but it is still poorly understood in science. Many researchers argue that species that have previously adapted to worsening climate conditions may be threatened more seriously. In contrast, others fear that the shift in species ranges caused by global warming may result in species extinction (Williams et al., 2007). For mountainous plant species, global warming is expected to act as an 'escalator to extinction' (Freeman et al., 2018). This is especially true for species living near mountaintops that cannot move higher. Our model illustrates the range shifts due to global warming for the two alpine 'glasshouse' *Rheum* species. The model identified their distinct niches, influencing their responses to predicted climate change and their shift across the Himalayas and the Hengduan Mountains (You et al., 2018). Further, our model suggested that the appropriate range for *Rheum* species has risen since the past LIG, as a result of climate change. The existence of suitable habitats in the HM for both the species during glacial-interglacial periods, especially for *R. alexandrae*, reflects that the HM was not completely glaciated and likely served as a refugium for many plants during glacial periods (Qiu et al., 2011; Zhang et al., 2018; Muellner-Riehl, 2019). The specific nature of the habitat niches for the two *Rheum* species led to an increased suitable range from LIG to LGM.

The southern HM provided a refugium for *R. nobile* and the southeast HM for *R. alexandrae*. As a result of global cooling, the eSDM suggested that both species were able to expand their geographic range from LIG to LGM in different magnitudes (Retallack, 2001; Meng et al., 2017). Possibly, glaciations during the LGM might have pushed the suitable range of *R. nobile* towards the EH and east of the HM. At the same time, *R. alexandrae*, during the LIG, slightly retreated its area of occurrence towards the southern HM. However, an occasional long-distance dispersal of the seed by wind (Song et al., 2013b) may have shaped the current HHM distribution for *R. nobile*. The present-day model of the suitable distribution range represents the actual distribution for both species, except for that of *R. alexandrae* in the EH. *Rheum nobile* is predicted to have a wide suitable range in the EH and the HM, but for *R. alexandrae* only in the HM. The HHM endemic *R. nobile* conjunctly occurs in the HM (especially in the Huluhai and Hongshan regions) but in the distinct areas from *R. alexandrae*.

The present-day similar distribution ranges of the two species in the EH and the HM will no longer exist under climate warming (Figures 4, 5). We speculate that super-competitor species that increase their range northward may benefit from identical niche requirements due to climate change (Liang et al., 2018; Rumpf et al., 2018). Species' ability to adapt genetically or modify their physiological tolerance will determine their local survival. The dramatic temperature fluctuation during the quaternary glacial cycles has led plant species to move downslope during the LGM and then return upslope with the Holocene warming (Flenley, 1998; Bush et al., 2004). Similarly, since glacial-interglacial periods, our model of warming scenarios predicted north- and upwards expansion of suitable habitats in the HHM and retreat of suitable habitats in the south. The complex topography in the high HM provides enough land surface, allowing upward relocation of suitable habitats and a northward expansion into adjacent areas with suitable habitats (Liang et al., 2018). Similar results were found in SDM studies for other Himalayan species (Song et al., 2004; Xiaodan et al., 2011; Zhao et al., 2011; Manish et al., 2016; Lamsal et al., 2017), which predicted a northward vegetation shift and re-shuffling of plant assemblages in the future due to global warming. Apart from that, comparable findings were observed for Australian plants (Auld et al., 2022), along with other mountain species in the European Alps (Thuiller et al., 2005; Benito et al., 2011; Dullinger et al., 2012), the Andes (Ruiz et al., 2008; Feeley and Silman, 2010), and in arctic regions of the northern hemisphere (Kaplan and New, 2006). However, such range shifts may not be sufficient to ensure population and species survival (Rana et al., 2017). Alpine species may need to change physiologically to cope with the specific climatic circumstances found at the higher elevations (Körner, 2003); seeds, in particular, must be viable for germination and resistant to the 'summit trap phenomena' (Pertoldi and Bach, 2007). A failure to adapt might cause mountaintop species to face the risk of 'mountaintop extinction' unless they have disjunct populations elsewhere on higher mountains or in colder latitudes (Williams et al., 2007; Lenoir et al., 2008).

Conservation implication in response to the rise in global temperature

Local extinction of mountain species is a significant driver altering ecosystem structure and misbalancing biodiversity in hotspots. The Himalayas and the Mountains of Southwest China (also known as the HM) are two crucial biodiversity hotspots

(Myers et al., 2000; Mittermeier et al., 2011) with a high proportion of endemic mountaintop species. Endemic high mountain species like *R. nobile* and *R. alexandrae* are more vulnerable to local extinction due to global warming as their distribution range is pushed higher and higher. The species' ability to survive in extreme conditions may be jeopardized if its distribution range expands towards mountaintops. Instead, despite having the adaptive capacity to endure challenging conditions at the mountaintops, the species must suffer local extinction due to increased elevational range contraction (Freeman et al., 2018). Therefore, a centerpiece of biodiversity conservation always warrants the conservation of remaining habitats from further loss.

Moreover, the quantification and mapping of the suitable range of the alpine 'glasshouse' *Rheum* in response to climate change have implications for conservation policies aimed at protecting their natural habitats. Our future-predicted map of suitable habitats can be used to identify critical habitat areas and prioritize conservation requirements, reducing biodiversity loss due to habitat degradation and loss. As a result, given the current period of biodiversity loss, there is a desperate need to understand the mechanisms driving the biodiversity dynamics in hotspots, as these findings will aid in the development of conservation policies to safeguard species threatened by environmental changes and human influences. We know that conservation efforts will be challenged by the severity of climate change and the different range shifts of certain species due to climate change (Williams et al., 2007). Furthermore, rising anthropogenic pressure from increased root harvesting for Tibetan medicinal purposes (Song et al., 2020b) has enhanced the need for conservation. Additionally, grazing pressure by yaks has dramatically increased in grassland during summer and autumn (Yang and Du, 1990). It is likely to pose a threat to the rare *R. nobile* even by moderate grazing and thus this flagship species could be endangered by intensified traditional pastoralism (Song et al., 2020b). The information presented here about future climate refugia should be utilized to drive the establishment of conservation areas and conservation initiatives.

Conclusions

Our research investigates the range shift pattern of two alpine 'glasshouse' species, *R. nobile* and *R. alexandrae*, under different climate change scenarios using different eSDM. We explored climatic variables in conjunction with environmental variables to forecast the species' geographical distribution range. This research demonstrated the importance of applying eSDM and multi-matrices model evaluation methodologies for robust alpine plant range shift projections. Our model predicted the two *Rheum* species' northward and upward migration from the last glacial period to a future climate change scenario. We not only predicted a shift in the two focus species' distribution ranges but also exemplified the sympatric coexistence of two *Rheum* species, albeit in distinct ecological niches. Despite having evolved to deal with extreme alpine climatic conditions, the predicted distribution range north- and upwards of the two *Rheum* species may not ensure their survival in the future. Our findings highlight the necessity of combining mechanistic research with knowledge of the physiological and molecular mechanisms that underpin distribution range and current biodiversity patterns. In this era of accelerating biodiversity loss, it is critical to understand the mechanism that drives biodiversity dynamics in hotspots. Through eSDM, we argue for a better understanding of alpine plants' species range shifts and better biogeographer insight into adaptations and biodiversity conservation objectives.

Data availability statement

The datasets presented in this study can be found in online repositories. The names of the repository/repositories and accession number(s) can be found below: Dryad depository (https://doi.org/10.5061/dryad.jq2bvq8b3).

Author contributions

HS, SKR and BS conceived the ideas. SKR, BS and HKR collected the data. SKR and HKR analyzed the data with the support of JS, SR; and SKR wrote the manuscript with the support of HS, BS, JS, HKR, and SR. All authors contributed to the article and approved the submitted version.

Funding

The first author is supported by the 'CAS President's International Fellowship Initiative' (PIFI) postdoctoral fellowship (2021PB0034). This study was funded by the Second Tibetan Plateau Scientific Expedition and Research (STEP) program (2019QZKK0502), the Strategic Priority Research Program of the Chinese Academy of Sciences (XDA20050203), the National Natural Science Foundation of China (31770249, 32071669 and 32150410356), the Key Projects of the Joint Fund of the National Natural Science Foundation of China (U1802232).

Acknowledgments

The authors thank numerous collaborators for their contribution to gathering the occurrence of the *Rheum* species, especially curators of the Herbarium of the Kunming Institute of Botany, CAS (KUN) and the National Herbarium and Plant Laboratories, Nepal (KATH).

Conflict of interest

The authors declare that the research was conducted in the absence of any commercial or financial relationships that could be construed as a potential conflict of interest.

Publisher's note

Supplementary material

The Supplementary Material for this article can be found online at: https://www.frontiersin.org/articles/10.3389/fpls.2022.925296/full#supplementary-material

SUPPLEMENTARY METHODS

_ODMAP Protocol.

SUPPLEMENTARY FIGURE 1

Response curves of the highly predictive top two algorithms showing the probability of presence and suitability (y-axis) under the **(A–C, I–K)** temperature-dependent and **(D–H, L–O)** precipitation-dependent variables (x-axis) for **(A–H)** *Rheum nobile* and **(I–O)** *Rheum alexandrae* under the function of ENMTools. The predictive algorithms are the Generalised Additive Model (GAM; red line) and Random Forest (RF; green line). Temperatures are expressed in °C (degree Celsius) and precipitation in mm (millimeter). Refer to for the bioclimatic variables.

SUPPLEMENTARY FIGURE 2

(A) The scree plot representing the variance explained by the first ten principal components of predictive environmental variables. **(B, C)** The contribution of top predictive environmental variables under the PC1 **(B)** and PC2 **(C)** scores. The Red dashed line indicates the expected average contribution if variable contributions were uniform. Refer to for abbreviated environmental variables.

SUPPLEMENTARY FIGURE 3

Pairwise niche **(A, B)** identity test and background test **(C, D**, symmetric; **E**, **F**, asymmetric test**)** for the highly predictive top two algorithms **(A, C, E)** Generalized additive model (GAM) and **(B, D, F)** Random forest (RF) model, between the two alpine 'glasshouse' herbs *Rheum nobile* and *Rheum alexandrae*, calculated as a function of *niche.overlap* ecospat test using ENMtools. The niche equivalency test as species-wise pair comparisons was measured by Schoener's *D* (in black color) and Hellinger's-based *I* (in green color) indices.

SUPPLEMENTARY FIGURE 4

Predicted potentially suitable habitat of two alpine 'glasshouse' herbs, **(A–F)** *Rheum nobile* and **(G–L)** *Rheum alexandrae*, under the present-day scenario of predictive **(A, G)** environmental variables, **(B, H)** geo-climatic, **(C, I)** habitat heterogeneity, **(D, J)** growing days, **(E, K)** ultra-violet radiations, and **(F, L)** consensus landcover.

References

Allouche, O., Tsoar, A., and Kadmon, R. (2006). Assessing the accuracy of species distribution models: prevalence, kappa and the true skill statistic (TSS). *J. Appl. Ecol.* 43, 1223–1232. doi: 10.1111/j.1365-2664.2006.01214.x

Araujo, M. B., and New, M. (2007). Ensemble forecasting of species distributions. *Trends Ecol. Evol.* 22, 42–47. doi: 10.1016/j.tree.2006.09.010

Araujo, M. B., Pearson, R. G., Thuiller, W., and Erhard, M. (2005). Validation of species-climate impact models under climate change. *Glob. Change Biol.* 11, 1504–1513. doi: 10.1111/j.1365-2486.2005.01000.x

Auld, J., Everingham, S. E., Hemmings, F. A., and Moles, A. T. (2022). Apline plants are on the move: Quantifying distribution shifts of Australian alpine plants through time. *Divers. Distrib.* 28, 943–955. doi: 10.1111/ddi.13494

Austin, M. P., and van Niel, K. P. (2011). Improving species distribution models for climate change studies: variable selection and scale. *J. Biogeogr.* 38, 1–8. doi: 10.1111/j.1365-2699.2010.02416.x

Baker, B. B., and Moseley, R. K. (2007). Advancing treeline and retreating glaciers: Implications for conservation in yunnan, PR China. *Arct. Antarct. Alp. Res.* 39, 200–209. doi: 10.1657/1523-0430(2007)39[200:ATARGI]2.0.CO;2

Barbet-Massin, M., Jiguet, F., Albert, C. H., and Thuiller, W. (2012). Selecting pseudo-absences for species distribution models: how, where and how many? *Methods Ecol. Evol.* 3, 327–338. doi: 10.1111/j.2041-210X.2011.00172.x

Barry, S., and Elith, J. (2006). Error and uncertainty in habitat models. *J. Appl. Ecol.* 43, 413–423. doi: 10.1111/j.1365-2664.2006.01136.x

Beckmann, M., Václavík, T., Manceur, A. M., Šprtová, L., von Wehrden, H., Welk, E., et al. (2014). glUV: a global UV-b radiation data set for macroecological studies. *Methods Ecol. Evol.* 5, 372–383. doi: 10.1111/2041-210X.12168

Benito, B., Lorite, J., and Peñas, J. (2011). Simulating potential effects of climatic warming on altitudinal patterns of key species in Mediterranean-alpine ecosystems. *Clim. Change* 108, 471–483. doi: 10.1007/s10584-010-0015-3

Boria, R. A., Olson, L. E., Goodman, S. M., and Anderson, R. P. (2014). Spatial filtering to reduce sampling bias can improve the performance of ecological niche models. *Ecol. Model.* 275, 73–77. doi: 10.1016/j.ecolmodel.2013.12.012

Bucklin, D. N., Basille, M., Benscoter, A. M., Brandt, L. A., Mazzotti, F. J., Romanach, S. S., et al. (2015). Comparing species distribution models constructed with different subsets of environmental predictors. *Divers. Distrib.* 21, 23–35. doi: 10.1111/ddi.12247

Bush, M. B., Silman, M. R., and Urrego, D. H. (2004). 48,000 years of climate and forest change in a biodiversity hotspot. *Science* 303, 827–829. doi: 10.1126/science.1090795

Chen, S. (1993). "Polygonaceae" in *Vascular plants of the hengduan mountains*. Eds. W. Wang, S. Wu, K. Lang, P. Li, F. Pu and S. Chen (Beijing, China: Science Press), 349–369.

Chen, I., Hill, J. K., Ohlemüller, R., Roy, D. B., and Thomas, C. D. (2011). Rapid range shifts of species associated with high levels of climate warming. *Science* 333, 1024–1026. doi: 10.1126/science.1206432

Chen, T., Yang, X., Wang, N., Li, H., Zhao, J., and Li, Y. (2018). Separation of six compounds including two n-butyrophenone isomers and two stibene isomers from *Rheum tanguticum* maxim by recycling high speed counter-current chromatography and preparative high-performance liquid chromatography. *J. Sep. Sci.* 41, 3660–3668. doi: 10.1002/jssc.201800411

Chowdhery, H. J., and Agrawala, D. K. (2009). *Rheum nobile* hook. f. and thoms. (Polygonaceae)-a rare and highly specialized plant of Himalayan region. *Indian J. Bot.* 32, 145–148.

Cleland, E. E., Chuine, I., Menzel, A., Mooney, H. A., and Schwartz, M. D. (2007). Shifting plant phenology in response to global change. *Trends Ecol. Evol.* 22, 357–365. doi: 10.1016/j.tree.2007.04.003

Colwell, R. K., Brehm, G., Cardelús, C. L., Gilman, A. C., and Longino, J. T. (2008). Global warming, elevational range shifts, and lowland biotic attrition in the wet tropics. *Science* 322, 258–261. doi: 10.1126/science.1162547

Doiron, M., Gauthier, G., and Levesque, E. (2014). Effects of experimental warming on nitrogen concentration and biomass of forage plants for an arctic herbivore. *J. Ecol.* 102, 508–517. doi: 10.1111/1365-2745.12213

Dullinger, S., Gattringer, A., Thuiller, W., Moser, D., Zimmermann, N. E., Guisan, A., et al. (2012). Extinction debt of high-mountain plants under twenty-first-century climate change. *Nat. Clim. Change* 2, 619–622. doi: 10.1038/nclimate1514

Environmental Systems Resource Institute (ESRI) (2016). *ArcMap 10.4.1* (Redlands, CA: ESRI).

Feeley, K. J., and Silman, M. R. (2010). Land-use and climate change effects on population size and extinction risk of Andean plants. *Glob. Change Biol.* 16, 3215–3222. doi: 10.1111/j.1365-2486.2010.02197.x

Flenley, J. R. (1998). Tropical forests under the climates of the last 30,000 years. *Clim. Change* 39, 177–197. doi: 10.1023/A:1005367822750

Forester, B. R., DeChaine, E. G., and Bunn, A. G. (2013). Integrating ensemble species distribution modelling and statistical phylogeography to inform projections of climate change impacts on species distributions. *Divers. Distrib.* 19, 1480–1495. doi: 10.1111/ddi.12098

Fox, J., and Weisberg, S. (2011). *An r companion to applied regression. 2nd ed.* (Thousand Oaks: Sage).

Freeman, B. G., Scholer, M. N., Ruiz-Gutierrez, V., and Fitzpatrick, J. W. (2018). Climate change causes upslope shifts and mountaintop extirpations in a tropical bird community. *Proc. Natl. Acad. Sci. U.S.A.* 115, 11982–11987. doi: 10.1073/pnas.1804224115

Fu, G., Shen, Z., and Zhang, X. (2018). Increased precipitation has stronger effects on plant production of an alpine meadow than does experimental warming in the northern Tibetan plateau. *Agric. Forest. Meteorol.* 249, 11–21. doi: 10.1016/j.agrformet.2017.11.017

GBIF.org (2021) *GBIF home page*. Available at: https://www.gbif.org (Accessed 10 August 2021).

Giménez-Benavides, L., Albert, M. J., Iriondo, J. M., and Escudero, A. (2011). Demographic processes of upward range contraction in a long-lived Mediterranean high mountain plant. *Ecography* 34, 85–93. doi: 10.1111/j.1600-0587.2010.06250.x

Guisan, A., and Thuiller, W. (2005). Predicting species distributions: Offering more than simple habitat models. *Ecol. Lett.* 8, 993–1009. doi: 10.1111/j.1461-0248.2005.00792.x

He, Y. P., Duan, Y. W., Liu., J. Q., and Smith, W. K. (2006). Floral closure in response to temperature and pollination in *Gentiana straminea* maxim. (Gentianaceae), an alpine perennial in the qinghai-Tibetan plateau. *Plant Syst. Evol.* 256, 17–33. doi: 10.1007/s00606-005-0345-1

Hijmans, R. J. (2012). Cross-validation of species distribution models: removing spatial sorting bias and calibration with a null model. *Ecology* 93, 679–688. doi: 10.1890/11-0826.1

Hijmans, R. J., Cameron, S. E., Parra, J. L., Jones, P. G., and Jarvis, A. (2005). Very high resolution interpolated climate surfaces for global land areas. *Int. J. Climatol.* 25, 1965–1978. doi: 10.1002/joc.1276

IPCC and Core Writing Team (2014). "Climate change 2014: Synthesis report", in *Contribution of working groups I, II and III to the fifth assessment report of the intergovernmental panel on climate change*. Eds. R. K. Pachauri and L. A. Meyer (Switzerland: IPCC Geneva), 151.

Jackson, L. S., Carslaw, N., Carslaw, D. C., and Emmerson, K. M. (2009). Modelling trends in OH radical concentrations using generalized additive models. *Atmos. Chem. Phys.* 9, 2021–2033. doi: 10.5194/acp-9-2021-2009

Kao, T. C., and Cheng, C. Y. (1975). Synopsis of the Chinese *Rheum*. *Acta Phytotaxon. Sin.* 13, 69–82.

Kaplan, J. O., and New, M. (2006). Arctic Climate change with a 2 °C global warming: timing, climate patterns and vegetation change. *Clim. Change* 79, 213–241. doi: 10.1007/s10584-006-9113-7

Kassambara, A., and Mundt, F. (2020) *Factoextra: Extract and visualize the results of multivariate data analyses (R package version 1.0.7)*. Available at: https://cran.r-project.org/web/packages/factoextra/index.html (Accessed January 3, 2021).

Kelly, A. E., and Goulden, M. L. (2008). Rapid shifts in plant distribution with recent climate change. *Proc. Natl. Acad. Sci. U.S.A.* 105 (33), 11823–11826. doi: 10.1073/pnas.0802891105

Körner, C. (2003). *Alpine plant life, second ed* (Berlin: Springer).

Lamsal, P., Kumar, L., Shabani, F., and Atreya, K. (2017). The greening of the Himalayas and Tibetan plateau under climate change. *Glob. Planet. Change* 159, 77–92. doi: 10.1016/j.gloplacha.2017.09.010

Lenoir, J., Gegout, J., Marquet, P., de Ruffray, P., and Brisse, H. (2008). A significant upward shift in plant species optimum elevation during the 20th century. *Science* 320, 1768–1771. doi: 10.1126/science.1156831

Lenoir, J., and Svenning, J. C. (2013). "Latitudinal and elevational range shifts under contemporary climate change", in *Encyclopedia biodiversity*. Ed. S. Levin (Waltham, MA: Academic Press), 599–611. doi: 10.1016/B978-0-12-384719-5.00375-0

Liang, Q., Xu, X., Mao, K., Wang, M., Wang, K., Xi, Z, et al. (2018). Shift in plant distributions in response to climate warming in a biodiversity hotspot, the hengduan mountains. *J. Biogeogr.* 45, 1334–1444. doi: 10.1111/jbi.13229

Li, A. R., and Gao, Z. J. (1998). *Flora of China* (Beijing: Science Press).

Losina-Losinskaya, A. S. (1936). The genus *Rheum* and its species. *Acta Inst. Bot. Acad. Sci. Union. Rerum. Public. Sovet. Soc Ser.* 1, 5–141.

Manish, K., Telwala, Y., Nautiyal, D. C., and Pandit, M. K. (2016). Modelling the impacts of future climate change on plant communities in the himalaya: a case study from Eastern himalaya, India. *Model. Earth Syst. Environ.* 2, 1–12. doi: 10.1007/s40808-016-0163-1

Manne, L. L., Brooks, T. M., and Pimm, S. L. (1999). Relative risk of extinction of passerine birds on continents and islands. *Nature* 399, 258–261. doi: 10.1038/20436

Marmion, M., Parviainen, M., Luoto, M., Heikkinen, R. K., and Thuiller, W. (2009). Evaluation of consensus methods in predictive species distribution modelling. *Divers. Distrib.* 15, 59–69. doi: 10.1111/j.1472-4642.2008.00491.x

Mclaughlin, B. C., and Zavaleta, E. S. (2012). Predicting species responses to climate change: demography and climate microrefugia in California valley oak (*Quercus lobata*). *Glob. Change Biol.* 18, 2301–2312. doi: 10.1111/j.1365-2486.2011.02630.x

Meng, H., Su, T., Gao, X., Li, J., Jiang, X., Sun, H., et al. (2017). Warm-cold colonization: response of oaks to uplift of the himalaya–hengduan mountains. *Mol. Ecol.* 26, 3276–3294. doi: 10.1111/mec.14092

Miller, J. (2010). Species distribution modeling. *Geogr. Compass* 4, 490–509. doi: 10.1111/j.1749-8198.2010.00351.x

Mittermeier, R. A., Turner, W. A., Larsen, F. W., Brooks, T. M., and Gascon, C. (2011). "Global biodiversity conservation: the critical role of hotspots", in *Biodiversity hotspots*. Eds. F. Zachos and J. Habel (Heidelberg, Berlin: Springer), 3–22.

Morueta-Holme, N., Engemann, K., Sandoval-Acuna, P., Jonas, J. D., Segnitz, R. M., Svenning, J., et al. (2015). Strong upslope shifts in chimborazo's vegetation over two centuries since Humboldt. *Proc. Natl. Acad. Sci. USA.* 112, 12741–12745. doi: 10.1073/pnas.1509938112

Muellner-Riehl, A. N. (2019). Mountains as evolutionary arenas: Patterns, emerging approaches, paradigm shifts, and their implications for plant phylogeographic research in the tibeto-Himalayan region. *Front. Plant Sci.* 10. doi: 10.3389/fpls.2019.00195

Muellner-Riehl, A. N., Schnitzler, J., Kissling, W. D., Moosbrugger, V., Rijsdijk, K. F., Seijmonsbergen, A. C, et al. (2019). Origins of global mountain plant biodiversity: Testing the 'mountain geobiodiversity hypothesis'. *J. Biogeogr.* 46, 2826–2838. doi: 10.1111/jbi.13715

Murphy, J. M., Sexton, D. M., Barnett, D. N., Jones, G. S., Webb, M. J., Collins, M, et al. (2004). Quantification of modelling uncertainties in a large ensemble of climate change simulations. *Nature* 430, 768–772. doi: 10.1038/nature02771

Myers, N., Mittermeier, R. A., Mittermeier, C. G., da Fonseca, G. A., and Kent, J. (2000). Biodiversity hotspots for conservation priorities. *Nature* 403, 853–858. doi: 10.1038/35002501

Ohba, H. (1988). "The alpine flora of the Nepal Himalayas: an introductory note", in *The Himalayan plants*, vol. vol. 1 . Eds. H. Ohba and S. B. Malla (Tokyo: University of Tokyo Press), 19–46.

Paquette, A., and Hargreaves, A. L. (2021). Biotic interactions are more often important at species' warm versus cool range edges. *Ecol. Lett.* 24, 2427–2438. doi: 10.1111/ele.13864

Parmesan, C., and Yohe, G. (2003). A globally coherent fingerprint of climate change impacts across natural systems. *Nature* 421, 37–42. doi: 10.1038/nature01286

Pearson, R. G., Raxworthy, C. J., Nakamura, M., and Peterson, A. T. (2007). Predicting species distributions from small numbers of occurrence records: A test case using cryptic geckos in Madagascar. *J. Biogeogr.* 34, 102–117. doi: 10.1111/j.1365-2699.2006.01594.x

Pertoldi, C., and Bach, L. (2007). Evolutionary aspects of climate-induced changes and the need for multidisciplinarity. *J. Therm. Biol.* 32, 118–124. doi: 10.1016/j.jtherbio.2007.01.011

Phillips, S. J., Anderson, R. P., and Schapire, R. E. (2006). Maximum entropy modeling of species geographic distributions. *Ecol. Model.* 190, 231–259. doi: 10.1016/j.ecolmodel.2005.03.026

Pierce, D. W., Barnett, T. P., Santer, B. D., and Gleckler, P. J. (2009). Selecting global climate models for regional climate change studies. *Proc. Natl. Acad. Sci. U.S.A.* 106, 8441–8446. doi: 10.1073/pnas.0900094106

Qiu, J. (2008). The third pole. *Nature* 454, 393–396. doi: 10.1038/454393a

Qiu, Y., Fu, C., and Comes, H. P. (2011). Plant molecular phylogeography in China and adjacent regions: Tracing the genetic imprints of quaternary climate and

environmental change in the world's most diverse temperate flora. *Mol. Phylogenet. Evol.* 59, 225–244. doi: 10.1016/j.ympev.2011.01.012

Quinn, G. P., and Keough, M. J. (2002). *Experimental design and data analysis for biologists* (Cambridge: Cambridge University Press), 111–154.

Quintero, I., and Wiens, J. J. (2013). Rates of projected climate change dramatically exceed past rates of climatic niche evolution among vertebrate species. *Ecol. Lett.* 16, 1095–1103. doi: 10.1111/ele.12144

Rahbek, C., Borregaard, M. K., Antonelli, A., Colwell, R. K., Holt, B. G., Nogues-Bravo, D, et al. (2019). Building mountain biodiversity: Geological and evolutionary processes. *Science* 365, 1114–1119. doi: 10.1126/science.aax0151

Rana, H. K., Luo, D., Rana, S. K., and Sun, H. (2020a). Geological and climatic factors affect the population genetic connectivity in *Mirabilis himalaica* (Nyctaginaceae): Insight from phylogeography and dispersal corridors in the himalaya-hengduan biodiversity hotspot. *Front. Plant Sci.* 10, 1721. doi: 10.3389/fpls.2019.01721

Rana, S. K., Rana, H. K., Ghimire, S. K., Shrestha, K. K., and Ranjitkar, S. (2017). Predicting the impact of climate change on the distribution of two threatened Himalayan medicinal plants of liliaceae in Nepal. *J. Mt. Sci.* 14, 558–570. doi: 10.1007/s11629-015-3822-1

Rana, S. K., Rana, H. K., Luo, D., and Sun, H. (2021). Estimating climate-induced 'Nowhere to go' range shifts of the Himalayan incarvillea juss. using multi-model median ensemble species distribution models. *Ecol. Indic.* 121, 107127. doi: 10.1016/j.ecolind.2020.107127

Rana, S. K., Rana, H. K., Ranjitkar, S., Ghimire, S. K., Gurmachhan, C. M., O'Neill, A. R, et al. (2020b). Climate-change threats to distribution, habitats, sustainability and conservation of highly traded medicinal and aromatic plants in Nepal. *Ecol. Indic.* 115, 106435. doi: 10.1016/j.ecolind.2020.106435

Ranjitkar, S., Xu, J., Shrestha, K. K., and Kindt, R. (2014). Ensemble forecast of climate suitability for the trans-Himalayan nyctaginaceae species. *Ecol. Model.* 282, 18–24. doi: 10.1016/j.ecolmodel.2014.03.003

Retallack, G. J. (2001). Cenozoic Expansion of grasslands and climatic cooling. *J. Geol.* 109, 407–426. doi: 10.1086/320791

Robinson, T. P., Di Virgilio, G., Temple-Smith, D., Hesford, J., and Wardell-Johnson, G. W. (2018). Characterisation of range restriction amongst the rare flora of banded ironstone formation ranges in semiarid south-western Australia. *Aust. J. Bot.* 67, 234–247. doi: 10.1071/BT18111

Ruiz, D., Moreno, H. A., Gutiérrez, M. E., and Zapata, P. A. (2008). Changing climate and endangered high mountain ecosystems in Colombia. *Sci. Total Environ.* 398, 122–132. doi: 10.1016/j.scitotenv.2008.02.038

Rumpf, S. B., Hülber, K., Klonner, G., Moser, D., Schütz, M., Wessely, J, et al. (2018). Range dynamics of mountain plants decrease with elevation. *Proc. Natl. Acad. Sci. U.S.A.* 115, 1848–1853. doi: 10.1073/pnas.1713936115

Salick, J., Fang, Z. D., and Hart, R. (2019). Rapid changes in eastern Himalayan alpine flora with climate change. *Am. J. Bot.* 106, 520–530. doi: 10.1002/ajb2.1263

Sandel, B., Arge, L., Dalsgaard, B., Davies, R. G., Gaston, K. J., Sutherland, W. J., et al. (2011). The influence of late quaternary climate-change velocity on species endemism. *Science* 334, 660–664. doi: 10.1126/science.1210173

Schickhoff, U., Bobrowski, M., Böhner, J., Bürzle, B., Chaudhary, R. P., Gerlitz, L., et al. (2014). Do Himalayan treelines respond to recent climate change? An evaluation of sensitivity indicators. *Earth Syst. Dynam. Discuss.*, 5, 1407–1461. doi: 10.5194/esdd-5-1407-2014

Song, B., Gao, Y., Stöcklin, J., Song, M., Sun, L., Sun, H., et al. (2020a). Ultraviolet screening increases with elevation in translucent bracts of *Rheum nobile* (Polygonaceae), an alpine 'glasshouse' plant from the high Himalayas. *Bot. J. Linn. Soc* 193, 276–286. doi: 10.1093/botlinnean/boaa005

Song, B., Stöcklin, J., Gao, Y., Zhang, Z., Yang, Y., Li, Z., et al. (2013a). Habitat-specific responses of seed germination and seedling establishment to soil water condition in two *Rheum* species in the high sino-Himalayas. *Ecol. Res.* 28, 643–651. doi: 10.1007/s11284-013-1057-6

Song, B., Stöcklin, J., Peng, D., Gao, Y., and Sun, H. (2015). The bracts of the alpine 'glasshouse' plant *Rheum alexandrae* (Polygonaceae) enhance reproductive fitness of its pollinating seed-consuming mutualist. *Bot. J. Linn. Soc* 179, 349–359. doi: 10.1111/boj.12312

Song, B., Stöcklin, J., Zhang, Z., Yang, Y., and Sun, H. (2013b). Seed and microsite limitation in *Rheum nobile*, a rare and endemic plant from the subnival zone of sino-himalaya. *Plant Ecol. Divers.* 6 (3–4), 503–509. doi: 10.1080/17550874.2013.788568

Song, B., Stoll, P., Peng, D., Sun, H., and Stöcklin, J. (2020b). Demography of the giant monocarpic herb *Rheum nobile* in the Himalayas and the effect of disturbances by grazing. *Ann. Bot.* 125, 447–458. doi: 10.1093/aob/mcz178

Song, B., Zhang, Z., Stocklin, J., Yang, Y., Niu, Y., Chen, J, et al. (2013c). Multifunctional bracts enhance plant fitness during flowering and seed development in *Rheum nobile* (Polygonaceae), a giant herb endemic to the high Himalayas. *Oecologia* 172, 359–370. doi: 10.1007/s00442-012-2518-2

Song, M., Zhou, C., and Ouyang, H. (2004). Distributions of dominant tree species on the Tibetan plateau under current and future climate scenarios. *Mt. Res. Dev.* 24, 166–173. doi: 10.1659/0276-4741(2004)024[0166:DODTSO]2.0.CO;2

Sun, J., Qin, X., and Yang, J. (2016). The response of vegetation dynamics of the different alpine grassland types to temperature and precipitation on the Tibetan plateau. *Environ. Monit. Assess.* 188, 20. doi: 10.1007/s10661-015-5014-4

Sun, Y., Wang, A., Wan, D., Wang, Q., and Liu, J. (2012). Rapid radiation of *Rheum* (Polygonaceae) and parallel evolution of morphological traits. *Mol. Phylogenet. Evol.* 63, 150–158. doi: 10.1016/j.ympev.2012.01.002

Sun, H., Zhang, J., Deng, T., and Boufford, D. E. (2017). Origins and evolution of plant diversity in the hengduan mountains, China. *Plant Divers.* 39, 161–166. doi: 10.1016/j.pld.2017.09.004

Thuiller, W., Georges, D., Engler, R., and Breiner, F. (2020) *Biomod2: Ensemble platform for species distribution modeling (R package version 3.4.12)*. Available at: https://cran.r-project.org/web/packages/biomod2/index.html (Accessed November 3, 2020).

Thuiller, W., Lavorel, S., Araujo, M. B., Sykes, M. T., and Prentice, I. C. (2005). Climate change threats to plant diversity in Europe. *Proc. Natl. Acad. Sci. U.S.A.* 102, 8245–8250. doi: 10.1073/pnas.0409902102

Tsukaya, H. (2002). Optical and anatomical characteristics of bracts from the Chinese 'glasshouse' plant, *Rheum alexandrae* batalin (Polygonaceae), in yunnan, China. *J. Plant Res.* 115, 59–63. doi: 10.1007/s102650200009

Tsukaya, H., and Tsuge, T. (2001). Morphological adaptation of inflorescences in plants that develop at low temperatures in early spring: the convergent evolution of "downy plants". *Plant Biol.* 3, 536–543. doi: 10.1055/s-2001-17727

Tuanmu, M. N., and Jetz, W. (2014). A global 1-km consensus land-cover product for biodiversity and ecosystem modelling. *Glob. Ecol. Biogeogr.* 23, 1031–1045. doi: 10.1111/geb.12182

Tuanmu, M. N., and Jetz, W. (2015). A global, remote sensing-based characterization of terrestrial habitat heterogeneity for biodiversity and ecosystem modelling. *Glob. Ecol. Biogeogr.* 24, 1329–1339. doi: 10.1111/geb.12365

Veloz, S. D. (2009). Spatially autocorrelated sampling falsely inflates measures of accuracy for presence-only niche models. *J. Biogeogr.* 36, 2290–2299. doi: 10.1111/j.1365-2699.2009.02174.x

Wang, Y. (2006). *Yunnan mountain climate (Chinese) Science and technology publisher* (Kunming, China:Science and Technology Publisher).

Wang, X., Yao, Y., Wortley, A. H., Qiao, H., Blackmore, S., Wang, Y., et al. (2018). Vegetation responses to the warming at the younger dryas-Holocene transition in the hengduan mountains, southwestern China. *Quat. Sci. Rev.* 192, 236–248. doi: 10.1016/j.quascirev.2018.06.007

Warren, D. L., and Dinnage, R. (2021) *ENMTools: Analysis of niche evolution using niche and distribution models (R package version 1.0.3)*. Available at: https://cran.r-project.org/web/packages/ENMTools/index.html (Accessed June 2, 2021).

Warren, D. L., Glor, R. E., and Turelli, M. (2008). Environmental niche equivalency versus conservatism: quantitative approaches to niche evolution. *Evolution* 62, 2868–2883. doi: 10.1111/j.1558-5646.2008.00482.x

Warren, D. L., Glor, R. E., and Turelli, M. (2010). ENMTools: a toolbox for comparative studies of environmental niche models. *Ecography* 33, 607–611. doi: 10.1111/j.1600-0587.2009.06142.x

Warren, D. L., Matzke, N. J., Cardillo, M., Baumgartner, J. B., Beaumont, L. J., Turelli, M., et al. (2021). ENMTools 1.0: an r package for comparative ecological biogeography. *Ecography* 44, 504–511. doi: 10.1111/ecog.05485

Warren, D. L., and Seifert, S. N. (2011). Ecological niche modeling in maxent: the importance of model complexity and the performance of model selection criteria. *Ecol. Appl.* 21, 335–342. doi: 10.1890/10-1171.1

Wiens, J. J. (2016). Climate-related local extinctions are already widespread among plant and animal species. *PloS Biol.* 14, e2001104. doi: 10.1371/journal.pbio.2001104

Williams, J. W., Jackson, S. T., and Kutzbach, J. E. (2007). Projected distributions of novel and disappearing climates by 2100AD. *Proc. Natl. Acad. Sci. U.S.A.* 104, 5738–5742. doi: 10.1073/pnas.0606292104

Xiaodan, W., Genwei, C., and Xianghao, Z. (2011). Assessing potential impacts of climatic change on subalpine forests on the eastern Tibetan plateau. *Clim. Change* 108, 225–241. doi: 10.1007/s10584-010-0008-2

Yang, Q. Y., and Du, Z. (1990). On altitudinal land use zonation of the hengduan mountain region in southwestern China. *GeoJournal* 20, 69–374. doi: 10.1007/bf00174977

Yao, Y., Wang, X., Qin, F., Wortley, A. H., Li, S., Blackmore, S, et al. (2020). Evidence for climate instability during the younger dryas interval in the hengduan mountains, yunnan, southwestern China. *Paleogeogr. Paleoclimatol. Paleoecol.* 554, 109798. doi: 10.1016/j.palaeo.2020.109798

Yoshida, T. (2002). "Adaptive strategies of alpine plants in nepal", in *Himalayan Botany in the twentieth and twenty-first centuries*. Eds. S. Noshiro and K. R. Rajbhandari (Tokyo: The Society of Himalayan Botany), 105–111.

You, J., Qin, X., Ranjitkar, S., Lougheed, S. C., Wang, M., Zhou, W., et al. (2018). Response to climate change of montane herbaceous plants in the genus *Rhodiola* predicted by ecological niche modelling. *Sci. Rep.* 8, 5879. doi: 10.1038/s41598-018-24360-9

Zhang, J., Zhong, D., Song, W., Zhu, R., and Sun, W. (2018). Climate is not all: Evidence from phylogeography of *Rhodiola fastigiate* (Crassulaceae) and comparison to its closest relatives. *Front. Plant Sci.* 9. doi: 10.3389/fpls.2018.00462

Zhao, D., Wu, S., Yin, Y., and Yin, Z. (2011). Vegetation distribution on Tibetan plateau under climate change scenario. *Reg. Environ. Change* 11, 905–915. doi: 10.1007/s10113-011-0228-7

Zurell, D., Franklin, J., König, C., Bouchet, P. J., Dormann, C. F., Elith, J., et al. (2020). A standard protocol for reporting species distribution models. *Ecography* 43, 1261–1277. doi: 10.1111/ecog.04960

Zu, K., Wang, Z., Zhu, X., Lenoir, J., Shrestha, N., Lyu, T., et al. (2021). Upward shift and elevational range contractions of subtropical mountain plants in response to climate change. *Sci. Total Environ.* 783, 146896. doi: 10.1016/j.scitotenv.2021.146896

frontiers | Frontiers in Plant Science

TYPE Original Research
PUBLISHED 11 October 2022
DOI 10.3389/fpls.2022.976646

OPEN ACCESS

EDITED BY
Boris Rewald,
University of Natural Resources and Life Sciences Vienna, Austria

REVIEWED BY
Hossein Afzalimehr,
Iran University of Science and Technology, Iran
Bimlesh Kumar,
Indian Institute of Technology Guwahati, India
Marcel Gabriel Clerc,
University of Chile, Chile

*CORRESPONDENCE
Shengtang Zhang
zst0077@163.com

SPECIALTY SECTION
This article was submitted to Functional Plant Ecology, a section of the journal Frontiers in Plant Science

RECEIVED 23 June 2022
ACCEPTED 15 September 2022
PUBLISHED 11 October 2022

CITATION
Zhang J, Zhang S, Wang C, Wang W and Ma L (2022) Flow characteristics of open channels based on patch distribution of partially discontinuous rigid combined vegetation. *Front. Plant Sci.* 13:976646. doi: 10.3389/fpls.2022.976646

Flow characteristics of open channels based on patch distribution of partially discontinuous rigid combined vegetation

Jingzhou Zhang, Shengtang Zhang*, Chuantao Wang, Wenjun Wang and Lijun Ma

College of Earth Science and Engineering, Shandong University of Science and Technology, Qingdao, China

To clarify the flow characteristics of open channels under the combined distribution of vegetation in a patch, this study used the computational fluid dynamics tool FLUENT and the Reynolds stress model to design four combined and four discrete distribution modes under two different inundation states (submerged and non-submerged). The flow characteristics of longitudinally discontinuous rigid vegetation patches occupying half the width of the channel were numerically simulated. The numerical model is verified by indoor open channel flume experiments, and the obtained model data is in good agreement with the measured data. The results showed that: 1) The diameter of vegetation is an important factor affecting the wake structure. Under the submerged condition. 2)The submerged state, distribution pattern and combination form of vegetation are important factors that affect the distribution of flow velocity and change the structure of water flow. That is, the influence of vegetation distribution pattern on flow velocity and turbulence intensity under submerged condition is significantly weaker than that under non-submerged condition, and the flow velocity in non-vegetation area is significantly higher than that in vegetation area. The increase in the combined vegetation comprehensive stem thickness and the discrete degree resulted in an increase in the difference in flow velocity and turbulence intensity. 3) As the water flowed downstream, the flow velocity along the vegetated area continuously decreased, while it increased continuously along the non-vegetated area, and the difference in flow velocity between the two areas became more apparent. 4) The inundation state and combination characteristics of vegetation were important factors affecting the Reynolds stress of the channel location in the patch area.

KEYWORDS

open channel flow, combined distribution, discrete distribution, patch vegetation, numerical simulation

1 Introduction

In recent years, the construction of ecological river courses has been vigorously promoted around the world and the coverage of vegetation in floodplains, and even the main channel, has been greatly improved. Vegetation is not only an important part of the river ecosystem, but also an important factor to consider during ecological river construction (Schulz et al., 2003; Cotton et al., 2006; Fathi-Moghadam et al., 2011; Curran and Hession, 2013; Zdankus et al., 2016). Vegetation can inhibit sediment suspension, purify the water environment, prevent water flow from eroding riverbanks, and have great practical value in maintaining the ecological function stability of river systems (Kemp et al., 2000; Wu et al., 2007; Nept, 2012; Aberle and Järvelä, 2013; Boothroyd et al., 2017). However, the existence of vegetation changes the flow characteristics of the channel, affects the flow velocity and turbulence characteristics, and changes the relationship between the storage and discharge of the channel, thereby changing the process of river confluence (Zhang and Su, 2008; Rominger and Nepf, 2011; Velísková et al., 2017), which has a non-negligible impact on the advancement of river flow, especially flood runoff in flood season (Mulahasan and Stoesser, 2017; Nosrati et al., 2022).

To date, there have been many achievements and advancements in research on the hydrodynamics of river vegetation. The distribution forms of vegetation in river channels are varied. In previous studies on river flow covered by vegetation, vegetation was mainly distributed uniformly or regularly throughout the whole test area. Nadaoka and Yagi (1998) used a Large Eddy Simulation (LES) model to study the turbulent flow characteristics of open channels with vegetation. Liu et al. (2021) studied the potential mechanism of morphological resistance of emergent vegetation under different vegetation densities and patterns by combining experimental and numerical simulation and concluded that the morphological resistance of vegetation is closely related to eddy current structure near vegetation. Tang et al. (2020) studied the velocity and turbulence characteristics of two kinds of flexible vegetation with different densities using an open channel test and concluded that the maximum velocity gradient and shear stress gradient appeared near the top of canopy. Using uniform grass cover, Yang et al. (2017) found that the resistance coefficient increased significantly with the increase of vegetation diameter, which effectively extended the retention time of concentrated flow on the slope, thus reducing soil erosion. This kind of model setup is relatively simple and is mainly used to study the influence of overall vegetation distribution on the hydraulic characteristics of open channels (Tanino and Nepf, 2008; Cheng et al., 2019), however, the flow characteristics caused by local vegetation distribution in river channels cannot be simply obtained from the overall vegetation flow characteristics.

In recent years, the water flow with partial vegetation distribution in open channels has received increasing attention because wetlands and floodplains have partial vegetation distribution, and the distribution of vegetation along riverbanks is a common feature of natural rivers and artificial ecological channels (Tooth and Nanson, 2000; Jang and Shimizu, 2007; White and Nepf, 2008; Truong and Uijttewaal, 2019). White and Nepf (2007) studied the flow structure and energy exchange in open channels distributed along riverbanks by some vegetation, and found that the shear layer at the junction between vegetated and non-vegetated domains has a double-layered structure. Tang et al. (2021) arranged two kinds of rigid vegetation with different heights on the side of the open channel to conduct an experimental study on the turbulent characteristics of river flow. The experimental results showed that the flow velocity and Reynolds stress increased sharply at the top of the vegetation, and that there was a strong mixed layer near the top of the vegetation. In addition, there was a strong shear layer between the non-vegetated area and the vegetated area, indicating that vegetation reduces flow velocity. Huai et al. (2019) laid continuous artificial vegetation on one side of an open channel to study the energy exchange and water turbulence characteristics between the vegetated and non-vegetated areas to determine whether artificial vegetation could be used to increase the water depth of natural rivers and improve navigation. Caroppi et al. (2022) focused on the effects of the flexible-induced reconfiguration of vegetation leaves on the wake and flow around the vegetation zone, on one side of a river channel, through experiments. They found that leaves increased vegetation resistance by 3.0–4.4 times, and the streamlined and reconstructed leaves reduced vegetation resistance by 60%.

However, for natural river channels, vegetation tends to be distributed in longitudinal discontinuous along riverbanks due to seasonal and temporal changes (Tanaka et al., 2008; Tanaka and Ohmoto, 2015; Yang et al., 2015). In addition, under the resource limitation of oxygen and other nutrients, aquatic vegetation can spontaneously develop spatial inhomogeneity and self-organize to form vegetation patches (Bordeu et al., 2016; Ruiz-Reynés et al., 2017), so that riparian vegetation presents the spatial configuration of vegetation landscape with longitudinal discontinuous patches distribution. Previous studies have mostly focused on the overall and continuous vegetation distribution, and even experimental and numerical simulation studies of patch vegetation have primarily focused on a single vegetation patch (Takemura and Tanaka, 2007; Nicolle and Eames, 2011; Chang et al., 2017; Li et al., 2018; Tny et al., 2019) or the interaction between two patches (Vandenbruwaene et al., 2011; Meire et al., 2014; Ghani et al., 2019a). For example, Kazem et al. (2021a); Kazem et al. (2021b) studied the vortex structure in the channel of vegetation patch and the characteristics of turbulence gradually subsiding in the undeveloped area downstream of the patch by changing the

patch size, and its research results showed that the presence of patches has a great influence on the flow structure inside and around the patches, and there are three different flow layers downstream of vegetation patches: wake layer, mixed layer and shear layer. However, studies on the patch distribution of partially discontinuous vegetation on open channel flow is not systematic enough, although this vegetation distribution pattern is more common in natural channels (Anjum and Tanaka, 2020; Li et al., 2020). In addition, most current studies use the uniform size of vegetation for generalized simulation processing, which does not conform to the natural situation of river vegetation (Sand Jensen and Madsen, 1992). Owing to the different vegetation species, growth cycles, and planting methods, the stem thickness and morphology of vegetation in river channels differ, resulting in a variety of river flow characteristics with different effects to that of uniform vegetation. At present, there are few studies on the influence of combined vegetation on open channel flow. Järvelä (2002) studied the flow-resistance coefficient using a combination of willow and sedge and concluded that the main vegetation biological characteristics that affect flow resistance include vegetation density, water-facing area of individual plants, vegetation stem thickness, and vegetation flexibility. However, the two types of vegetation belong to completely different species, and the research is mainly focused on qualitative research, and it is difficult to carry out quantitative research. Zhang et al. (2020) conducted overland flow scour experiments on vegetation with combinations of two different stem diameters, and found that the diameter of a plant has a power function relationship with the Darcy–Weisbach resistance coefficient. Under the same water depth, when the stem diameter of one plant remained constant, the flow resistance coefficient increased with the increase in the stem diameter of the other plant. Because the distribution characteristics of vegetation and the structure of overland flow are quite different from those of open channels, the research results cannot be completely applied to open channel flow. Therefore, the research on combined vegetation patches in open channels is very limited. Therefore, it is necessary to comprehensively consider the influence of partial discontinuous patch combination vegetation on river flow characteristics in order to properly replicate the riparian environment and provide an effective scientific basis for ecological river management and river restoration engineering design.

The purpose of this study is to simulate the three-dimensional flow structure of longitudinal discontinuous patch combination vegetation in a rectangular open channel. the aims are to: (1) determine the longitudinal distribution of streamwise velocity before and after the introduction of a single vegetation type with different stem thicknesses in the combined vegetation patches under different submerged states, (2) measure the effects of the combination forms and partial discontinuous distribution patterns of vegetation patches on the changes of streamwise and lateral flow velocity under different submergence conditions using a specific cross-section, (3) use the spatial distribution of transverse, longitudinal, and vertical velocity contours to analyze the distribution characteristics of flow velocity and energy exchange of open channels with partial discontinuous combined vegetation patches, (4) identify the influence of vegetation combination and discrete distribution characteristics on the vertical distribution of Reynolds stress under different submerged states using the specific position of the channel in the patch area, and to elucidate the spatial distribution inhomogeneity of the flow field under different vegetation distribution conditions, and (5) clarify the influence of vegetation combination and discrete distribution on water flow turbulence characteristics using the variation law of turbulent kinetic energy (TKE) in vegetated and non-vegetated areas under different submerged states in relation to the longitudinal distribution of TKE in a specific longitudinal section.

2 Materials and methods

2.1 Modelling setup and boundary conditions

The fluid mechanics simulation of the open channel was carried out using the software FLUENT, and the Reynolds Stress Turbulence Model (RSM) was used to model the computational domain with a length of 1.72 m and a width of 0.4 m. The area was composed of rigid combined vegetation patches with a longitudinal discontinuous distribution. For the simulated vegetation, since the object of this study is the combined vegetation patches of different stem thicknesses, and the vegetation stems are usually cylindrical, so this study uses cylinders with different diameters to simulate vegetation. In addition, in order to enhance the simulation and experimental effects and improve the efficiency, most of the current studies also generalize the whole plant to an effective water blocking cylinder (Zhao and Huai, 2016; Anjum and Tanaka, 2020; Wang et al., 2021). In this study, a cylinder with a height of h_v of 0.08 m was used to simulate open channel vegetation. It should be noted that this study focuses on the influence of the combined and discrete distribution of stem of patch vegetation on the channel flow structure, and the factors related to vegetation flexibility are not included in the numerical model of this study. Instead, the simulated vegetation is set as rigid and non-deformable. However, since vegetation is usually distributed vertically at the bottom of the channel, its unique morphological distribution has a different impact on the water flow than the stone particles at the bottom of the channel. The influence on the water flow structure of the open channel partly comes from the distribution characteristics of stone particles at the bottom of the channel, and the other part comes from the morphological characteristics

of the vegetation. The unique vertical morphological characteristics of vegetation is the main factor causing the significant change of vertical flow structure of open channel, that is, the presence of vegetation changes the mixing and energy dissipation effect of open channel flow. This study considered the vegetation layout of two different combinations of stem thickness under different states, non-submerged and submerged (Figure 1). The x, y, and z axes represent the longitudinal, transverse, and vertical directions, respectively. The vegetation layout in the numerical calculation area is shown in Figure 2.

The calculation model adopts the boundary conditions of the velocity inlet (0.3 $m{\cdot}s^{-1}$) and the pressure outlet, the upper surface uses the slip edge to replace the water-air interface, and the vegetation surface and the wall both use the standard wall function, which was a non-slip boundary. Simulation and post-processing were performed in FLUENT. The pressure-velocity coupling was determined using the SIMPLE algorithm, whereby the relaxation factors of kinetic energy and pressure were 0.7 and 0.3 respectively, the flow velocity was 0.7, the Reynolds stress was 0.5, and the turbulent kinetic energy and turbulent dissipation rate were both 0.8. The minimum residual value of each equation was set to 1×10^{-5}, that is, the iteration ended when the calculated residual value was less than the minimum residual value. Therefore, using the above criteria, it was assumed that the solution had reached a steady state.

In order to further study the effect of the combined vegetation comprehensive stem thickness change on the flow characteristics of the open channel, the model was setup with four vegetation combination distributions with different comprehensive stem thicknesses (*d* & *D)* which were 0.012 m & 0.012 m, 0.012 m & 0.015 m, 0.012 m & 0.018 m, and 0.012 m & 0.021 m. Under the premise that the comprehensive stem thickness of vegetation remains unchanged, the discrete degree of stem thickness of adjacent plants will inevitably become an inducing factor for the change of water flow characteristics. To study the influence of vegetation stem dispersion degree on the flow characteristics of an open channel, the model was set up with four different discrete stem diameter distributions, 0.012 m & 0.012 m, 0.009 m & 0.015 m, 0.006 m & 0.018 m, and 0.003 m & 0.021 m. In this study, both vegetation combination and discrete distribution belong to two types of combined distribution of different stem diameter vegetation, but there are essential differences between them from the perspective of research emphasis. The combined distribution study is based on the premise that the comprehensive stem thickness is constantly changing to explore the effect of the vegetation comprehensive stem thickness on the flow characteristics of the open channel, the so-called comprehensive stem thickness is the average diameter of two kinds of combined vegetation (Figure 3A). The discrete distribution study is based on the premise that the comprehensive stalk thickness of the vegetation is constant, to explore the influence of the degree of stem thickness differentiation between the two types of vegetation on the water flow characteristics of the open channel (Figure 3B).

2.2 Validation of numerical simulation methods

Based on the open channel flume experiment, a hydraulic model was established indoors. The length (*x*-axis), width (*y*-axis), and height (*z*-axis) of the open channel flume were 5m, 0.4m, and 0.3m, respectively, and the experimental slope was 0.0%.The flow discharges under vegetation non-submerged and submerged conditions were 0.0072 $m^3{\cdot}s^{-1}$ and 0.012 $m^3{\cdot}s^{-1}$, respectively. By adjusting the tailgate at the downstream end of the flume, the water depth in the flume was adjusted so that the water depth at 1.64 m of the flume length was consistent with that at the corresponding inlet of the model, so that the inlet velocity of the model should be 0.3 $m{\cdot}s^{-1}$. In order to homogenize the flow discharge, measurements were made every ten minutes in the experiment. Cover the entire bottom of the flume with a PVC baseboard. Rigid cylinders (diameter *d* & *D* is 0.012 m & 0.012 m, 0.012 m & 0.015m, 0.012m & 0.018m, 0.012m & 0.021 m, 0.009 m

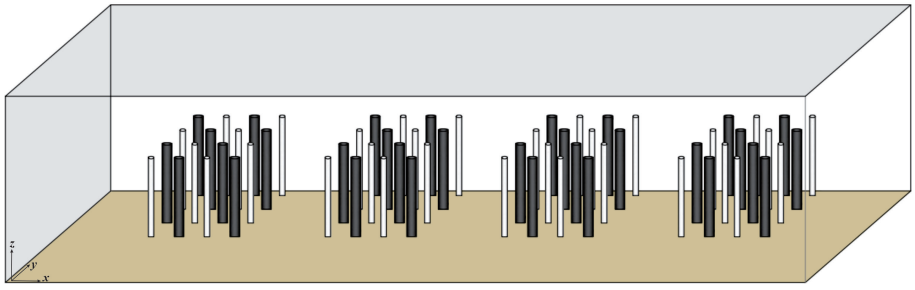

FIGURE 1
Three-dimensional view of numerical calculation area.

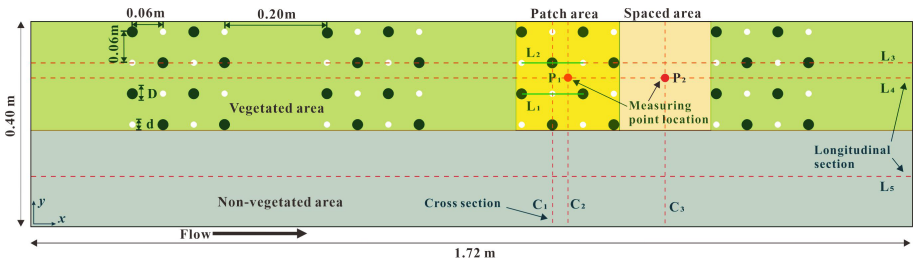

FIGURE 2
Schematic diagram of floor layout in numerical calculation area.

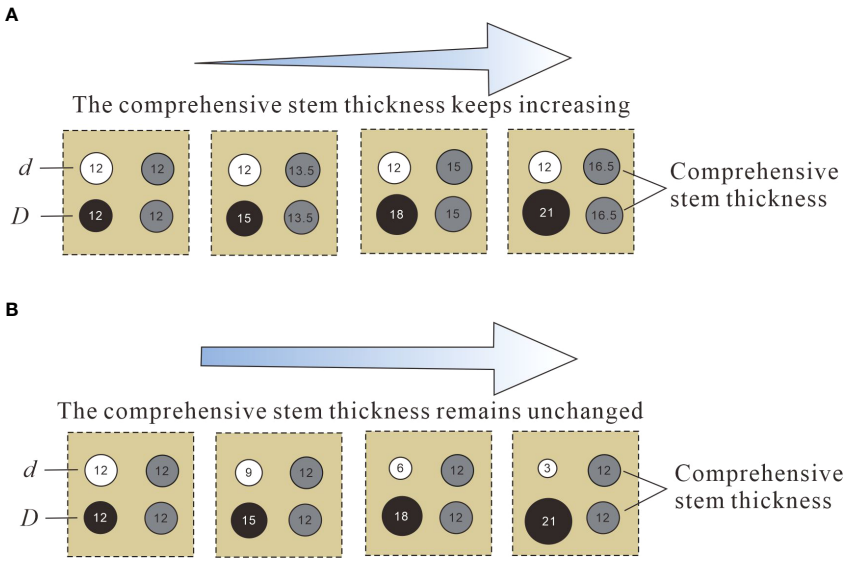

FIGURE 3
Creative diagram of the distributions of two different vegetation combinations. **(A)** Vegetation combination distribution, **(B)** Vegetation discrete distribution.

& 0.015 m, 0.006 m & 0.018 m, 0.003 m & 0.021 m) were used to simulate rigid vegetation and were intermittently fixed on the experimental floor in the form of patches. Additionally, 3D acoustic doppler velocimeter (3D ADV) is used to measure the velocity at specific positions P_1 and P_2 in Figure 2.

Under the conditions of different combinations and discrete distribution of vegetation, the average velocity calculation results obtained at the specified location were compared with the experimental results (Figure 4). The results showed that the experimental and simulated data were similar, which verifies the accuracy of the numerical simulation method, and further revealed that the numerical model could simulate the flow of open channels with discontinuous vegetation patches.

3 Results and discussion

3.1 Longitudinal distribution of streamwise velocity before and after a single vegetation

Figure 5 shows the longitudinal distribution of the streamwise velocity before and after a single vegetation in patches with h of 0.06m (non-submerged condition) and 0.10m (submerged condition), that is, at the L_1 and L_2 positions, the lengths of L_1 and L_2 were 0.12 m. For this study, the central position of L_1 represented the smaller diameter plant d (the combined vegetation was 0.012 m, and the discrete

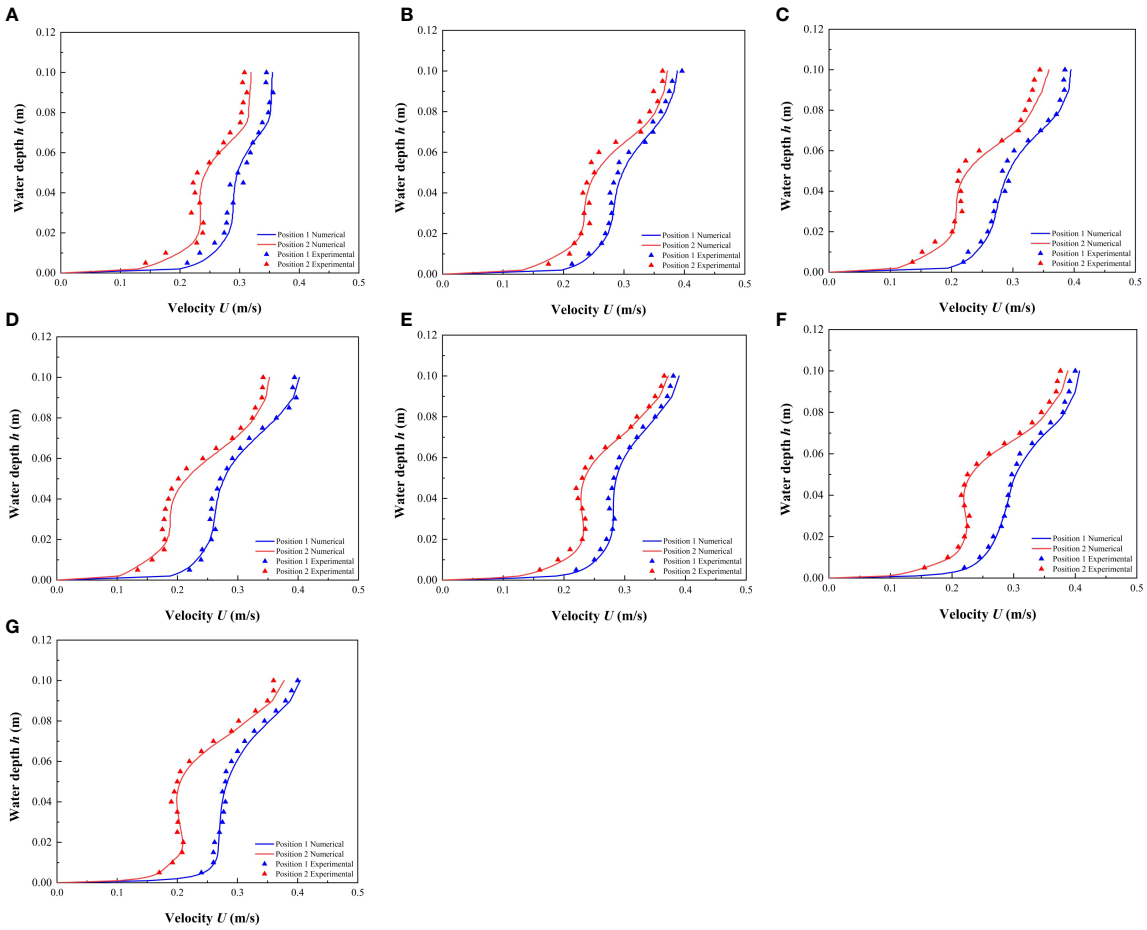

FIGURE 4
Comparison between the experimental results and the numerical results of the modeling method used in this study. **(A)** 0.012 m & 0.012 m, **(B)** 0.012 m & 0.015 m, **(C)** 0.012 m & 0.018 m, **(D)** 0.012 m & 0.021 m, **(E)** 0.009 m & 0.015 m, **(F)** 0.006 m & 0.018 m, **(G)** 0.003 m & 0.021 m.

vegetation sizes were 0.012 m, 0.009 m, 0.006 m, and 0.003 m), and the central position of L_2 represented the larger diameter plant D (the combined vegetation corresponds to 0.012 m, 0.015 m, 0.018 m, and 0.021 m, and the discrete vegetation corresponds to 0.012 m, 0.015 m, 0.018 m, 0.021 m). This setup was used to study the influence of combination and discrete characteristics of longitudinal discontinuous patches on streamwise velocity.

It can be seen from Figure 5 that under non-submerged conditions ($h<h_v$), upstream streamwise velocity decreased when approaching the front edge of vegetation, and the streamwise velocity rapidly decreased to a minimum value behind (trailing edge) the vegetation, and then gradually increased until the water reached the next plant for velocity circulation. The flow velocity shows the typical characteristics of the wake downstream of the cylindrical obstacle, and the distance from the trailing edge of the vegetation to the longitudinal position where the streamwise velocity decreased to a minimum value represents the length of the stable wake zone. The formation of the stable wake zone is primarily due to the shear layer originating from the shoulders on both sides of the cylinder, which isolates the high-speed water flowing around from both sides of the cylinder outside the wake zone, therefore the momentum in the stable wake zone was relatively low. When the shear layers on both sides are wide enough to intersect, the wake flow velocity begins to recover and the stable wake zone ends, that is, the end point of the stable wake zone corresponds to the position where the shear layers intersect. It can be concluded from Figure 5 that the length of the stable wake zone is closely related to the stem thickness of vegetation. For the combined vegetation patches, when the stem diameter of vegetation remained unchanged at 0.012 m, the length of the stable wake zone was unchanged at approximately 0.0015 m (Figure 5A). When the stem diameter of vegetation increased from 0.012 m to 0.021 m, the length of the stable wake zone also increased from 0.0015 m to 0.0030 m

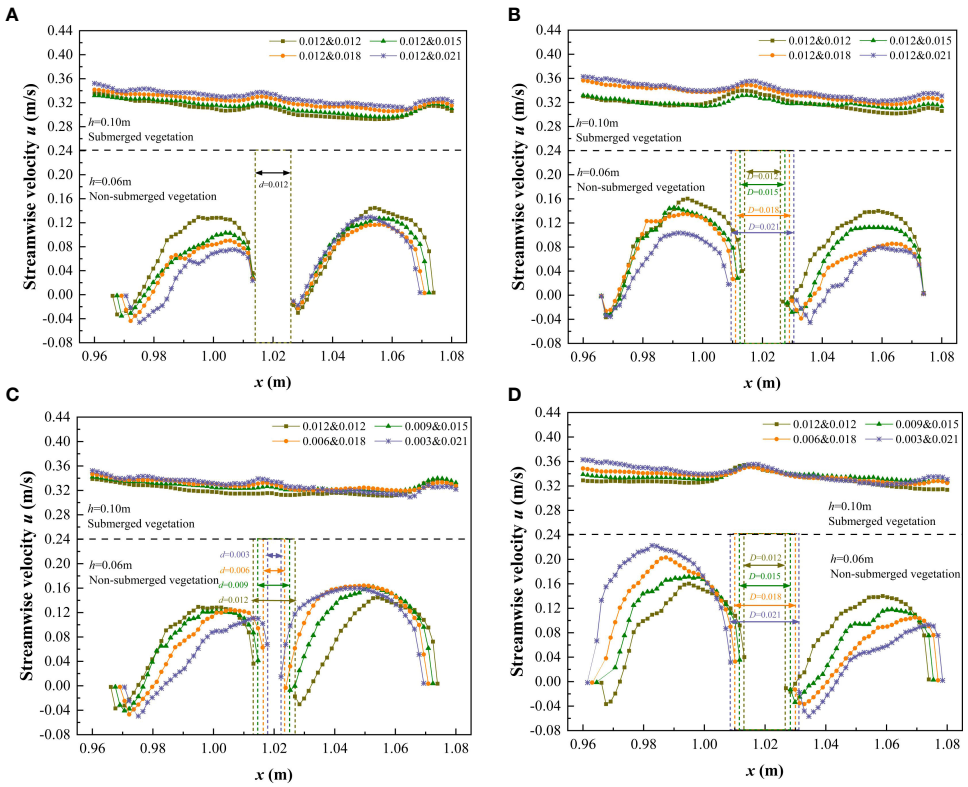

FIGURE 5
Variation streamwise velocity before and after a single vegetation (h = 0.06 m and 0.10 m) under different submerged conditions. **(A)** L_1, vegetation combination distribution, **(B)** L_2, vegetation combination distribution, **(C)** L_1, vegetation discrete distribution, **(D)** L_2, vegetation discrete distribution.

(Figures 5B, D). When the stem diameter of vegetation was < 0.012 m, the length of the wake zone at the trailing edge of vegetation was very small (Figure 5C). Therefore, we concluded that the diameter of vegetation is an important factor affecting the wake structure.The research results are of great significance for understanding the flow structure around the flow field in the vegetation unit area.

Under the non-submerged condition, for the distribution of four different combinations of vegetation in the patch, the difference in streamwise velocity behind the vegetation was low when the stem thickness of vegetation was constant. Further, the streamwise velocity behind the vegetation decreased as the stem thickness of vegetation increased. Regarding the distribution of the four different discrete vegetation types in the patch, the streamwise velocity behind the vegetation was negatively correlated with the thickness of the vegetation stem, that is, the larger the stem thickness, the smaller the streamwise velocity. Additionally, as the vegetation dispersion increased so did the difference in streamwise velocity front and behind the vegetation, indicating that the discrete distribution of vegetation somewhat interferes with the longitudinal continuity of the velocity, and destroys the uniformity of velocity in the longitudinal flow field.

Under the complete submersion ($h>h_v$) condition, the higher the comprehensive stem thickness of the combined vegetation, the higher the streamwise velocity corresponding to the free layer, that is, $u_{0.012\&0.012}<u_{0.012\&0.015}<u_{0.012\&0.018}<u_{0.012\&0.021}$. For the discrete distribution of vegetation, the greater the degree of vegetation dispersion, the greater the streamwise velocity corresponding to the free layer, that is, $u_{0.012\&0.012}<u_{0.009\&0.015}<u_{0.006\&0.018}<u_{0.003\&0.021}$. This occurred because as the comprehensive stem thickness and degree of vegetation dispersion increases, the density of vegetation coverage also increases, which hinders the water flow in the vegetation layer and produces a strong lateral divergent flow in the free layer leading to an elevated streamwise velocity in the free layer. Of note, in the submerged state, because the free layer is less affected by the water blocking effect of vegetation, the difference in streamwise velocity under different combinations and discrete forms is not clear, which further indicates that in the submerged state, the influence of vegetation distribution patterns on the flow characteristics of the free layer is weakened. It also shows that the influence of vegetation heterogeneity on the difference of water flow characteristics is closely related to the submerged state.

3.2 Velocity distribution in specific cross-sections

3.2.1 Streamwise velocity distribution in specific cross-sections

The cross-sections C_2 and C_3 at the middle of the third patch area and the middle of the spaced area behind the patch, respectively, were selected to measure the change of flow velocity distribution. The streamwise velocity of a specific water depth on the cross-section under different submerged conditions is shown in Figures 6, 7. Under the non-submerged vegetation condition, the streamwise velocity in the non-vegetated area was significantly higher than that in the vegetated area (Figure 6). Table 1 also shows that the average streamwise velocity in the non-vegetated area was significantly higher than that in the vegetated area, indicating a strong energy exchange between vegetated and non-vegetated areas in an open channel with patchy distributions of partially discontinuous combined vegetation, similar to the findings of Huai et al. (2019) and Tang et al. (2021). In addition, when the water flow encountered cylindrical obstacles, there was strong lateral divergence with high streamwise velocity at narrow channels between the vegetation (Figures 6A, C). When water flow was not blocked by cylindrical obstacles, the amplitude of streamwise velocity in the C_3 spaced area decreased more than when compared with that in the C_2 patch area, but it was still uneven (Figures 6B, D), indicating that the patch influence still existed in a certain distance beyond the downstream edge.

In the non-submerged state, the combination and discrete distribution of patch vegetation were the important factors affecting the change of streamwise velocity in the cross-section. The streamwise velocity at C_2 and C_3 in the vegetated area showed the same change rule, that is, the streamwise velocity at the vegetated channel in the patch area decreased continuously as the comprehensive stem thickness of the combined vegetation and the degree of vegetation dispersion increased. It can also be concluded from Figures 6A, C that the flow velocity behind the large-diameter vegetation in the non-submerged state was lower than that behind the small-diameter vegetation (at C_2). This demonstrates that the trailing edge of thicker vegetation is more conducive to the accumulation of sediment and provides a good environment for vegetation growth (Shi et al., 2016). In addition, the streamwise velocity in the non-vegetated area was also somewhat affected by the vegetation distribution form in the

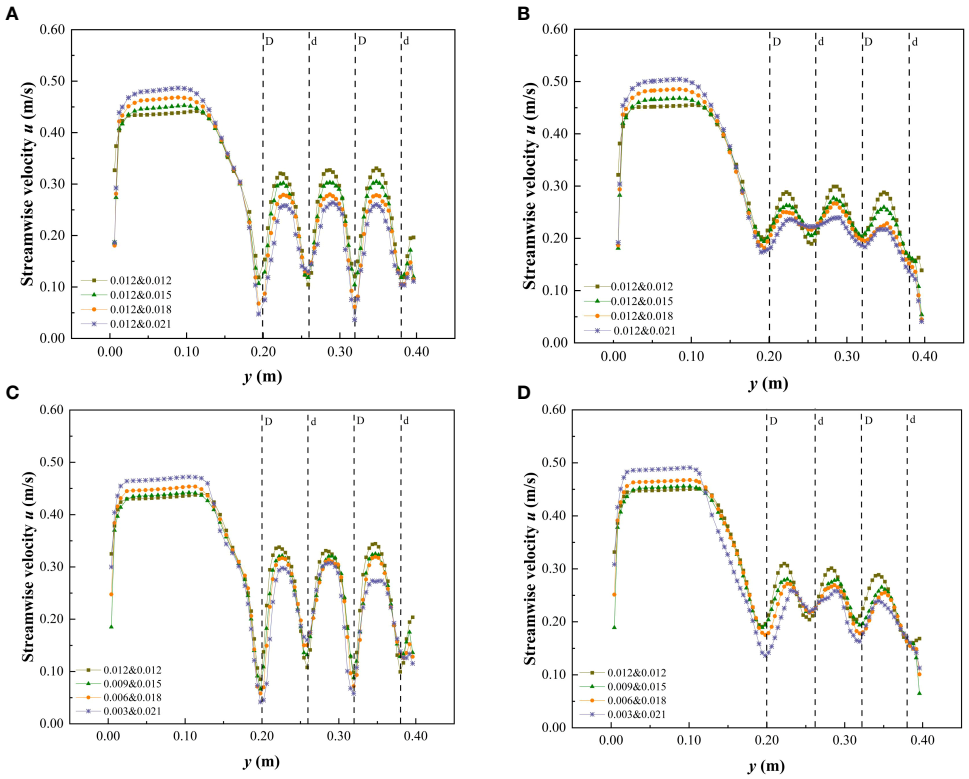

FIGURE 6
Variation of streamwise velocity in cross-section when *h* is 0.06 m under the non-submerged condition. **(A)** C_2, vegetation combination distribution, **(B)** C_3, vegetation combination distribution, **(C)** C_2, vegetation discrete distribution, **(D)** C_3, vegetation discrete distribution.

10.3389/fpls.2022.976646

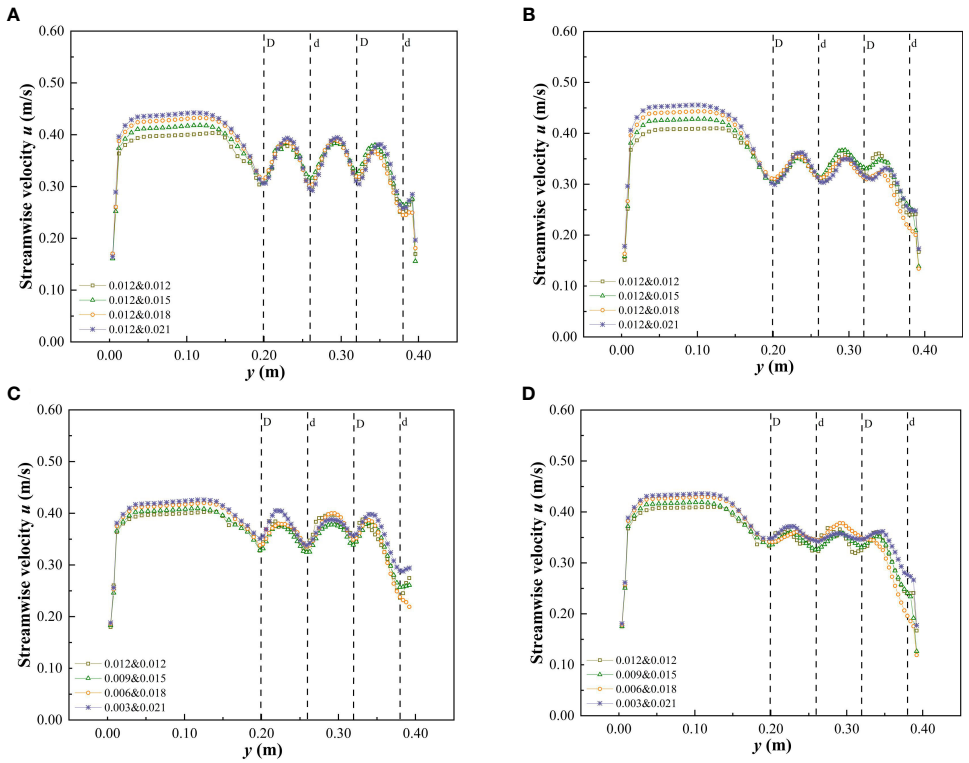

FIGURE 7
Variation of streamwise velocity in cross-section when h is 0.10 m under the submerged condition. **(A)** C_2, vegetation combination distribution, **(B)** C_3, vegetation combination distribution, **(C)** C_2, vegetation discrete distribution, **(D)** C_3, vegetation discrete distribution.

TABLE 1 The average streamwise velocity $\bar{u}$ value and its rate of change between C_1 and C_2 cross-sections under different distribution patterns when the non-submerged condition h is 0.06 m.

Vegetation non-submerged state (h=0.06m)

C_2	Combined distribution (d&D)	$\bar{u}_{\text{vegetation area}}$	Growth rate of $\bar{u}_{\text{vegetation area}}$ relative 0.012&0.012 (%)	$\bar{u}_{\text{non-vegetated area}}$	$\bar{u}_{\text{non-vegetated area}}/\bar{u}_{\text{vegetated area}}$
	0.012&0.012	0.2415	–	0.4371	1.8102
	0.012&0.015	0.2243	-7.12%	0.4468	1.9924
	0.012&0.018	0.2050	-15.08%	0.4623	2.2544
	0.012&0.021	0.1854	-23.20%	0.4792	2.5843
C_3	Combined distribution (d&D)	$\bar{u}_{\text{vegetation area}}$	Growth rate of $\bar{u}_{\text{vegetation area}}$ relative 0.012&0.012 (%)	$\bar{u}_{\text{non-vegetated area}}$	$\bar{u}_{\text{non-vegetated area}}/\bar{u}_{\text{vegetated area}}$
	0.012&0.012	0.2368	–	0.4525	1.9104
	0.012&0.015	0.2254	-4.84%	0.4627	2.0530
	0.012&0.018	0.2132	-9.97%	0.4791	2.2468
	0.012&0.021	0.2010	-15.13%	0.4969	2.4723
C_2	Discrete distribution (d&D)	$\bar{u}_{\text{vegetation area}}$	Growth rate of $\bar{u}_{\text{vegetation area}}$ relative 0.012&0.012 (%)	$\bar{u}_{\text{non-vegetated area}}$	$\bar{u}_{\text{non-vegetated area}}/\bar{u}_{\text{vegetated area}}$
	0.012&0.012	0.2491	–	0.4336	1.7409
	0.009&0.015	0.2362	-5.15%	0.4376	1.8524
	0.006&0.018	0.2295	-7.85%	0.4492	1.9574
	0.003&0.021	0.2136	-14.25%	0.4682	2.1924
C_3	Discrete distribution (d&D)	$\bar{u}_{\text{vegetation area}}$	Growth rate of $\bar{u}_{\text{vegetation area}}$ relative 0.012&0.012 (%)	$\bar{u}_{\text{non-vegetated area}}$	$\bar{u}_{\text{non-vegetated area}}/\bar{u}_{\text{vegetated area}}$
	0.012&0.012	0.2419	–	0.4487	1.8550
	0.009&0.015	0.2296	-5.10%	0.4520	1.9693
	0.006&0.018	0.2219	-8.27%	0.4646	2.0939
	0.003&0.021	0.2096	-13.35%	0.4872	2.3243

vegetated area, that is, with the increase of the comprehensive stem thickness and discrete degree of the combined vegetation, the streamwise velocity in the non-vegetated area showed an increasing trend. Table 1 shows that as the comprehensive stem thickness of the combined vegetation and the degree of dispersion increase, the average streamwise velocity of the cross-sections C_2 and C_3 in the vegetated area decreased, while the average streamwise velocity in the non-vegetated area showed an increasing trend.

When compared with the non-submerged state, the difference in flow velocity between the non-vegetated and vegetated areas was reduced in the submerged state (Figure 7 and Table 2), indicating that the energy exchange between the two areas was reduced in the submerged state. In addition, the combination and discrete vegetation distributions showed no clear effect on the streamwise velocity differences in the vegetated area, while in the non-vegetated area the streamwise velocity retained the variation law that it would increase as the comprehensive stem thickness and discrete degree of the combined vegetation increased.

This study can understand the overall change of the flow field velocity in the vegetated area and the non-vegetation area under different combinations of vegetation, and provide a certain scientific basis for the research on the mechanism of riverbank sediment erosion and deposition and the growth and evolution trend of vegetation communities, which can be applied to the restoration and management of actual river channels.

3.2.2 Lateral velocity distribution in specific cross-sections

For open channels with partial discontinuous combined vegetation patches, the unique distribution was expected to have a different impact on the lateral velocity of water flow. Figure 8 shows the variation in lateral velocity of cross-sections C_2 and C_3 in specific water depths under different submerged conditions. The lateral velocity at C_2 under the vegetated non-submerged state is shown in Figure 8A. When the vegetation stem thickness was uniform, the lateral velocity variation in the patch area was low. As the comprehensive vegetation stem thickness and the discrete degree of the vegetation stem increased, the lateral velocity variation in the patch area also increased, while the vegetation combination and discrete distribution form at C_3 of the spaced area had minimal effect on the transverse velocity of the y-section (Figure 8C). In addition, in the non-submerged state, the lateral flow velocity of the y-section was primarily negative (Figures 8A, C), indicating that the direction of the overall lateral velocity was towards the non-vegetated area. In the submerged state, the lateral velocity of the free layer was minimally affected by the vegetation combination and discrete distribution form of the vegetation layer, and the lateral velocity was predominantly positive

TABLE 2 The average streamwise velocity $\bar{u}$ value and its rate of change between C_1 and C_2 cross-sections under different distribution patterns when the submerged condition h is 0.10 m.

Vegetation submerged state (h=0.10m)

C_2	**Combined distribution (d&D)**	$\bar{u}_{\text{vegetation area}}$	**Growth rate of $\bar{u}_{\text{vegetation area}}$ relative 0.012&0.012 (%)**	$\bar{u}_{\text{non-vegetated area}}$	$\bar{u}_{\text{non-vegetated area}}/\bar{u}_{\text{vegetated area}}$
	0.012&0.012	0.3356	–	0.3978	1.1852
	0.012&0.015	0.3407	1.52%	0.4138	1.2145
	0.012&0.018	0.3349	-2.24%	0.4278	1.2775
	0.012&0.021	0.3396	11.93%	0.4381	1.2899
C_3	**Combined distribution (d&D)**	$\bar{u}_{\text{vegetation area}}$	**Growth rate of $\bar{u}_{\text{vegetation area}}$ relative 0.012&0.012 (%)**	$\bar{u}_{\text{non-vegetated area}}$	$\bar{u}_{\text{non-vegetated area}}/\bar{u}_{\text{vegetated area}}$
	0.012&0.012	0.3201	–	0.4073	1.2723
	0.012&0.015	0.3221	0.62%	0.4255	1.3210
	0.012&0.018	0.3084	-3.67%	0.4404	1.4283
	0.012&0.021	0.3162	-1.22%	0.4526	1.4314
C_2	**Discrete distribution (d&D)**	$\bar{u}_{\text{vegetation area}}$	**Growth rate of $\bar{u}_{\text{vegetation area}}$ relative 0.012&0.012 (%)**	$\bar{u}_{\text{non-vegetated area}}$	$\bar{u}_{\text{non-vegetated area}}/\bar{u}_{\text{vegetated area}}$
	0.012&0.012	0.3482	–	0.3978	1.1425
	0.009&0.015	0.3408	-2.11%	0.4053	1.1892
	0.006&0.018	0.3450	-0.90%	0.4145	1.2012
	0.003&0.021	0.3607	3.59%	0.4208	1.1667
C_3	**Discrete distribution (d&D)**	$\bar{u}_{\text{vegetation area}}$	**Growth rate of $\bar{u}_{\text{vegetation area}}$ relative 0.012&0.012 (%)**	$\bar{u}_{\text{non-vegetated area}}$	$\bar{u}_{\text{non-vegetated area}}/\bar{u}_{\text{vegetated area}}$
	0.012&0.012	0.3272	–	0.4073	1.2450
	0.009&0.015	0.3239	-14.62%	0.4162	1.2847
	0.006&0.018	0.3239	-21.04%	0.4267	1.3172
	0.003&0.021	0.3410	6.84%	0.4330	1.2697

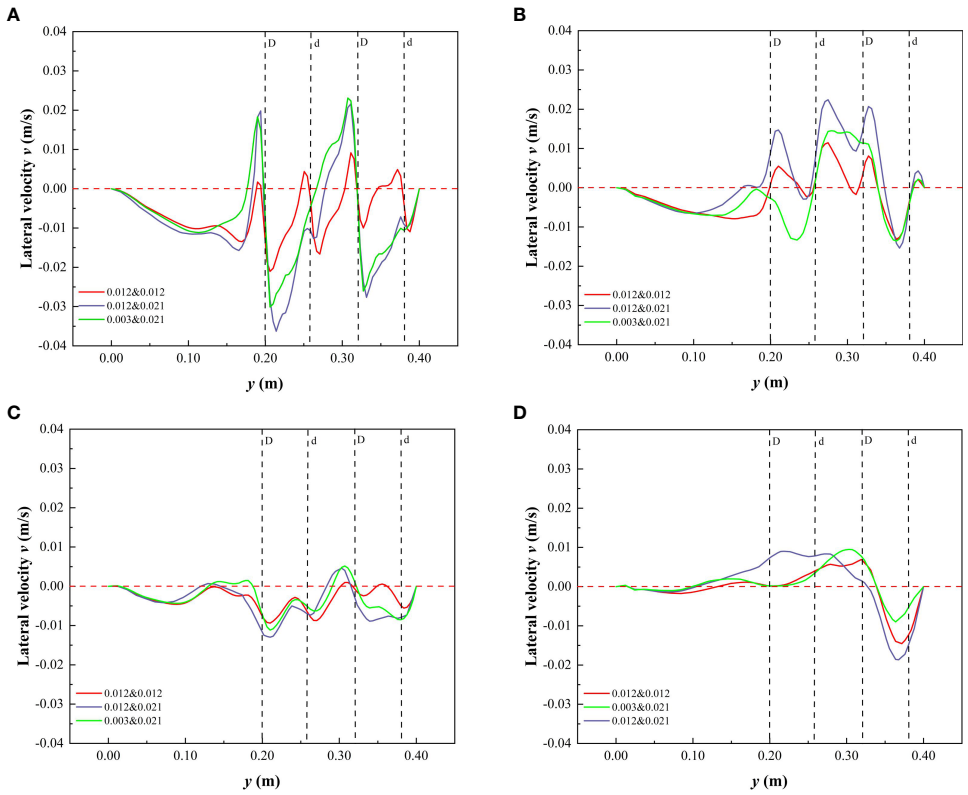

FIGURE 8
Variation of lateral velocity in cross-section at h of 0.06 m and 0.10 m under different submerged conditions. **(A)** C_2, h = 0.06 m, non-submerged vegetation, **(B)** C_2, h = 0.10 m, submerged vegetation, **(C)** C_3, h = 0.06 m, non-submerged vegetation, **(D)** C_3, h = 0.10 m, submerged vegetation.

(Figures 8B, D), indicating that the direction of the overall lateral velocity was towards the side of the vegetated area. The distribution of vegetation along the riverbank is a common feature of natural rivers and artificial ecological rivers. The study of lateral flow velocity in the flow field is helpful to understand the lateral transport of sediment and to improve the navigation of the river.

3.3 Spatial distribution of velocity contours in different sections

The spatial distribution of the velocity contours of the xy and yz profiles (C_1 and C_2) under two different submerged states are shown in Figures 9, 10. From the figures, it can be deduced that the submerged state and distribution pattern of vegetation are important factors that affect the velocity change and energy exchange of the two water passages in the vegetated and the non-vegetated areas. In the non-submerged state, the velocity in the vegetated area was significantly lower than that in the non-vegetated area and the velocity difference was high. In the submerged state, the velocity difference was significantly reduced, indicating that there was a strong energy exchange at the interface between the vegetated and the non-vegetated areas, while in the submerged state, the energy exchange was weakened. In addition, the increases in the comprehensive stem thickness of the combined vegetation and the dispersion degree were also important factors causing the increased velocity difference between the vegetated and the non-vegetated areas. Figure 9 also reflects the difference in flow velocity along the xy profile. In the non-submerged state, the overall flow velocity in the vegetated area gradually decreased as the downstream distance increased, while the overall flow velocity in the non-vegetated area showed the opposite trend. Under the submerged state, the overall flow velocity in the non-vegetated area was similar to that of the non-submerged state, while the overall flow velocity in the vegetated area had no clear regularity.

The spatial distribution of the velocity contours of the xz profile under two different submerged states is shown in Figure 11, which shows the velocity distribution changes along the longitudinal profile of the vegetation array (L_3), and the longitudinal profile of the vegetation passage (L_4)

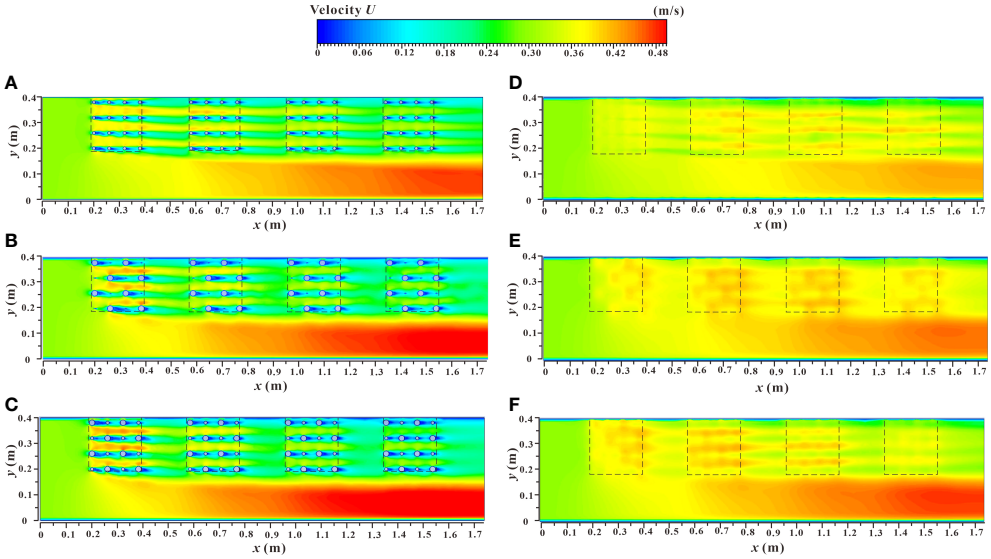

FIGURE 9
Spatial distribution of velocity contours of xy sections under different submerged states. **(A)** h = 0.06 m, d & D = 0.012 m & 0.012 m, non-submerged vegetation, **(B)** h = 0.06 m, d & D = 0.003 m & 0.021 m, non-submerged vegetation, **(C)** h = 0.06 m, d & D = 0.012 m & 0.021 m, non-submerged vegetation, **(D)** h = 0.10 m, d & D = 0.012 m & 0.012 m, submerged vegetation, **(E)** h = 0.10 m, d & D = 0.003 m & 0.021 m, submerged vegetation, **(F)** h = 0.10 m, d & D = 0.012 m & 0.021 m, submerged vegetation.

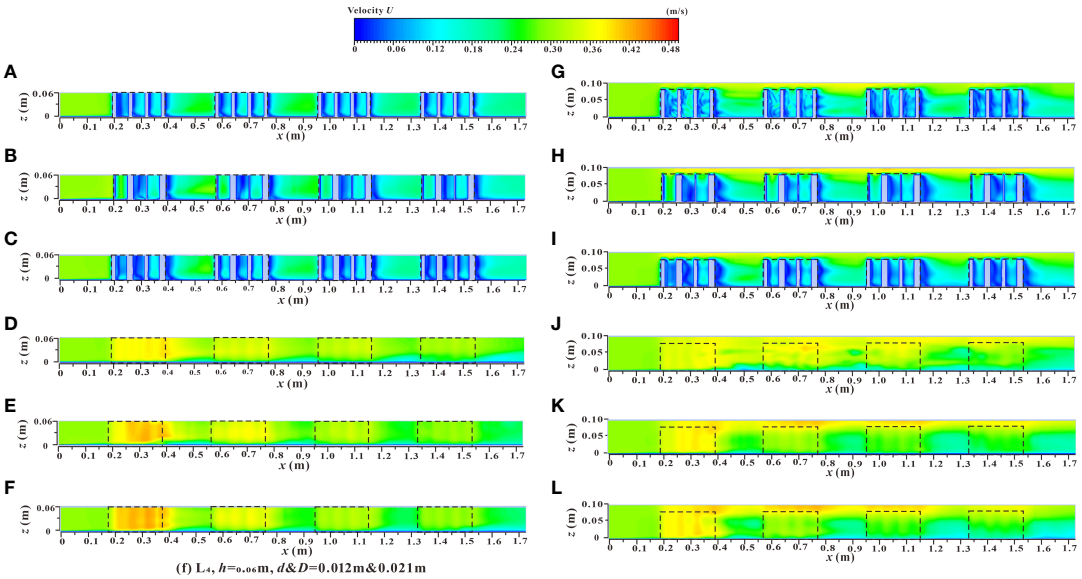

FIGURE 10
Spatial distribution of velocity contours of yz sections under different submerged states. **(A)** L_3, h = 0.06 m, d & D = 0.012 m & 0.012 m, non-submerged vegetation, **(B)** L_3, h = 0.06 m, d & D = 0.003 m & 0.021 m, non-submerged vegetation, **(C)** L_3, h = 0.06 m, d & D = 0.012 m & 0.021 m, non-submerged vegetation, **(D)** L_4, h= 0.06 m, d & D = 0.012 m & 0.012 m, non-submerged vegetation, **(E)** L_4, h = 0.06 m, d & D = 0.003 m & 0.021 m, non-submerged vegetation, **(F)** L_4, h = 0.06 m, d & D = 0.012 m & 0.021 m, non-submerged vegetation, **(G)** L_3, h = 0.10 m, d & D = 0.012 m & 0.012 m, submerged vegetation, **(H)** L_3, h = 0.10 m, d & D = 0.003 m & 0.021 m, submerged vegetation, **(I)** L_3, h = 0.10 m, d & D = 0.012 m & 0.021 m, submerged vegetation, **(J)** L_4, h = 0.10 m, d & D = 0.012 m & 0.012 m, submerged vegetation, **(K)** L_4, h = 0.10 m, d & D = 0.003 m & 0.021 m, submerged vegetation, **(L)** L_4, h = 0.10 m, d & D = 0.012 m & 0.021 m, submerged vegetation.

10.3389/fpls.2022.976646

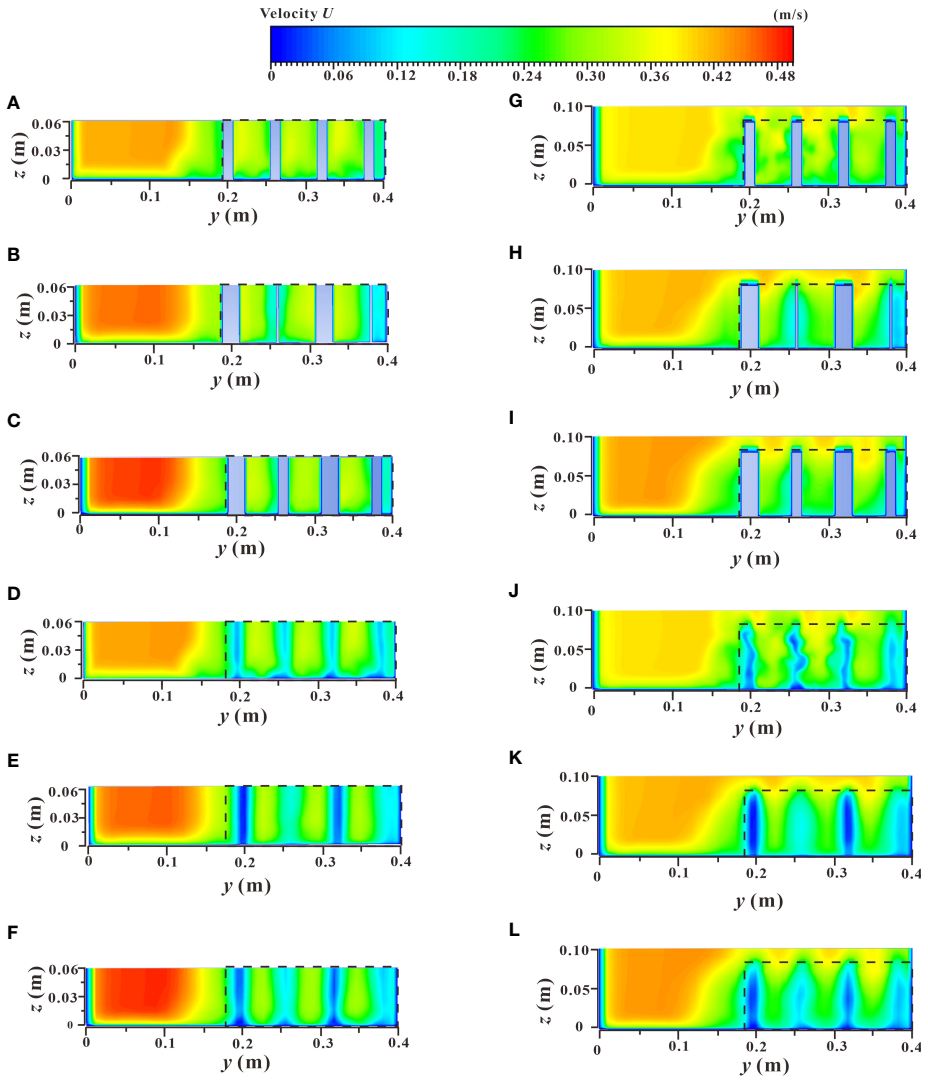

FIGURE 11
Spatial distribution of velocity contours of xz sections under different submerged states. **(A)** C_1, h = 0.06 m, d & D = 0.012 m & 0.012 m, non-submerged vegetation, **(B)** C_1, h = 0.06 m, d & D = 0.003 m & 0.021 m, non-submerged vegetation, **(C)** C_1, h = 0.06 m, d & D = 0.012 m & 0.021 m, non-submerged vegetation, **(D)** C_2, h = 0.06 m, d & D = 0.012 m & 0.012 m, non-submerged vegetation, **(E)** C_2, h = 0.06 m, d & D = 0.003 m & 0.021 m, non-submerged vegetation, **(F)** C_2, h = 0.06 m, d & D = 0.012 m & 0.021 m, non-submerged vegetation, **(G)** C_1, h = 0.10 m, d & D = 0.012 m & 0.012 m, submerged vegetation, **(H)** C_1, h = 0.10 m, d & D = 0.003 m & 0.021 m, submerged vegetation, **(I)** C_1, h = 0.10 m, d & D = 0.012 m & 0.021 m, submerged vegetation, **(J)** C_2, h = 0.10 m, d & D = 0.012 m & 0.012 m, submerged vegetation, **(K)** C_2, h = 0.10 m, d & D = 0.003 m & 0.021 m, submerged vegetation, **(L)** C_2, h = 0.10 m, d & D = 0.012 m & 0.021 m, submerged vegetation.

under different vegetation distribution modes. In the non-submerged state, when water flowed through the vegetation array (L_3), the influence of the wake area behind the cylinder caused the velocity to decline to a minimum value. This resulted in a significantly lower flow velocity in the vegetation patch than in the spaced area between adjacent patches (Figures 11A–C), which led to sediment deposition and increased availability of soil nutrients and ultimately a suitable environment for the growth and reproduction of vegetation.

When the water flow passed through the vegetation passage (L_4), the influence of vegetation shear force caused a narrowing of the passage which resulted in a higher flow velocity in the vegetation patch than that in the spaced area (Figures 11D–F). From an ecological perspective, the low flow velocity area was more suitable for the survival of aquatic organisms (Widdows & Navarro, 2007; Folkard & Gascoigne, 2009), concluded from the Figures 11A–F, in the process of water flow downstream, the velocity of the vegetation array (L_3) and the vegetation passage (L_4) in the patch area and the

spaced area showed a trend of decreasing gradually with the increase of the downstream distance, and the flow velocity was more moderate in the downstream parts of the river. In terms of the vegetation distribution of partial discontinuous patches in the river, the velocity distribution areas of specific patches and the rear spaced area from high to low were as follows: L_4 patch area > L_4 spaced area > L_3 spaced area > L_3 patch area. In addition, the increased comprehensive stalk thickness and discrete degree of the combined vegetation resulted in a greater obstruction to water flow by the vegetation. This led to a stronger sedimentation effect and increased the water carrying capacity of the river channel. The velocity distribution of the xz longitudinal profile under the submerged condition (Figures 11G–L) was consistent with that under the non-submerged condition. As shown in Figures 11G–L and Figures 10G–L, there was a significant difference in flow velocity between the upper and lower layers (vegetation layer and free layer), bounded by the top of the vegetation in the submerged state, indicating a strong mixed layer near the top of the vegetation and a strong energy exchange occurs.

3.4 Turbulence characteristics

3.4.1 Vertical distribution of Reynolds stress at specific locations of vegetation patch channels

Reynolds stress is the additional shear stress caused by the mixing of turbulent liquid particles, which is closely related to the flow structure and distribution of vegetation in the river channel (Liu et al., 2010; Li et al., 2020; Caroppi et al., 2022). Reynolds stress can also be caused by the uneven distribution of the flow field in space and is the statistical average value of the momentum per unit time and unit area caused by turbulent flow pulsation (Afzalimehr et al., 2010). Therefore, Reynolds stress is an indispensable factor in the study of the characteristics of channel flow.

Figure 12 shows the vertical distribution of Reynolds stress at the vegetation patch channel P_1 under different submerged states. For the unsubmerged vegetation (Figures 12A, B), the Reynolds stress is higher near the bottom of the channel and the bottom of the vegetation where h is approximately 0.015 m (1/4 of the overall water depth), and further decreases at the bottom

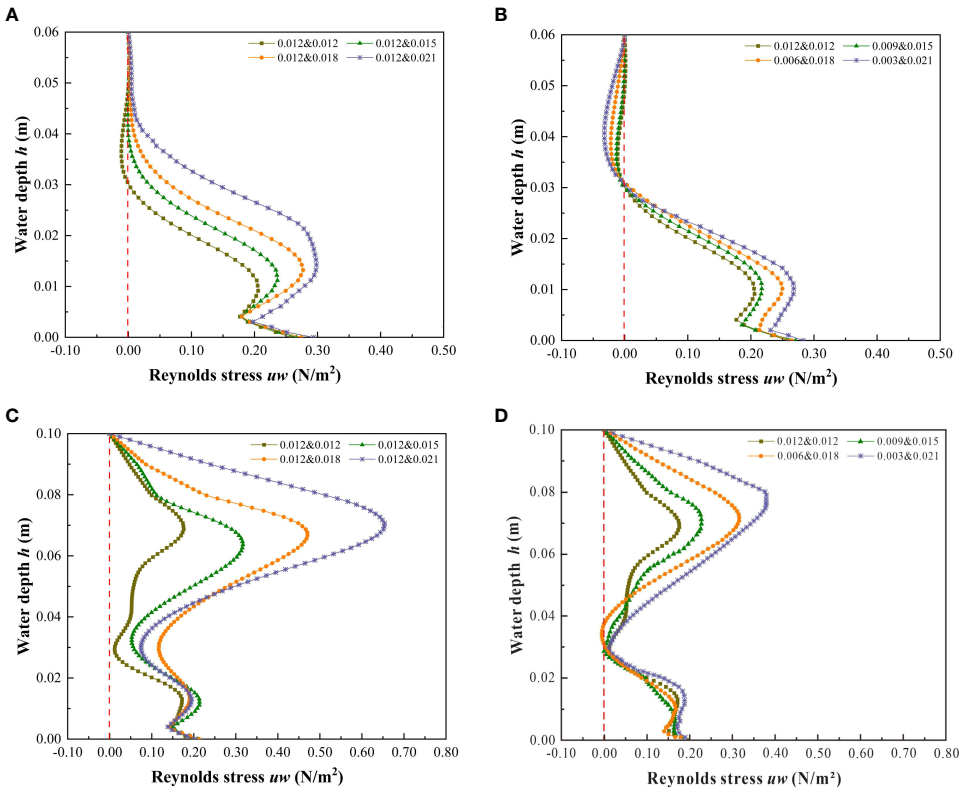

FIGURE 12
Vertical distribution of Reynolds stress at the location of vegetation patch channel P_1 under different submerged states. **(A)** h = 0.06 m, vegetation combination distribution, non-submerged vegetation, **(B)** h = 0.06 m, vegetation discrete distribution, non-submerged vegetation, **(C)** h = 0.10 m, vegetation combination distribution, submerged vegetation, **(D)** h = 0.10 m, vegetation discrete distribution, submerged vegetation.

TABLE 3 The Reynolds stress *uw* value and its rate of change in specific water depths at P_1 position under different submerging states and distribution modes.

Vegetation non-submerged state (*h*=0.06m)					
Combined distribution *d*&*D* (m)	***uw* (*h*=0.015m)**	**Growth rate of *uw* relative 0.012&0.012 (%)**	**Discrete distribution *d*&*D* (m)**	***uw* (*h*=0.015m)**	**Growth rate of *uw* relative 0.012&0.012 (%)**
0.012&0.012	0.2057	–	0.012&0.012	0.2057	–
0.012&0.015	0.2364	14.90%	0.009&0.015	0.2173	5.60%
0.012&0.018	0.2770	34.61%	0.006&0.018	0.2499	21.45%
0.012&0.021	0.2982	44.92%	0.003&0.021	0.2680	30.28%
Vegetation submerged state (*h*=0.10m)					
Combined distribution *d*&*D* (m)	***uw* (*h*=0.015m)**	**Growth rate of *uw* relative 0.012&0.012 (%)**	**Discrete distribution *d*&*D* (m)**	***uw* (*h*=0.015m)**	**Growth rate of *uw* relative 0.012&0.012 (%)**
0.012&0.012	0.1759	–	0.012&0.012	0.1758	–
0.012&0.015	0.3169	80.13%	0.009&0.015	0.2280	29.67%
0.012&0.018	0.4705	167.41%	0.006&0.018	0.3161	79.79%
0.012&0.021	0.6537	271.56%	0.003&0.021	0.3795	115.87%

of the channel (*h* is from 0 to 0.005 m) due to the large resistive shear force caused by the riverbed (Dey, 2014). When *h* > 0.005 m, the Reynolds stress first increases then decreases, reaching the lowest point when *h* is approximately 0.015 m. For the vegetation combination distribution (Figure 12A), when *h* was 0.015 m, *d*&*D* were 0.012 m & 0.015 m, 0.012 m & 0.018 m, and 0.012 m & 0.021 m, and the Reynolds stress growth rate was 14.90%, 34.61%, and 44.92%, respectively, compared to 0.012 m & 0.012 m (Table 3). When the water depth is approximately 0.05 m to the water surface, the vegetation combination distribution has almost no effect on the change of Reynolds stress, which is effectively 0. For the discrete distribution of vegetation (Figure 12B), *h* is at 0.015 m, *d*&*D* is 0.009 m & 0.015 m, 0.006 m & 0.018 m, and 0.003 m & 0.021 m, and the Reynolds stress growth rate is 5.60%, 21.45%, and 30.28%, respectively, compared to 0.012 m & 0.012 m (Table 3), when the water depth is approximately 0.03 m to the water surface, the discrete vegetation distribution has almost no effect on the change of Reynolds stress, which is effectively 0.

The submerged state of vegetation is also an important factor affecting Reynolds stress distribution. For submerged vegetation (Figures 12C, D), the Reynolds stress reaches a maximum value near the top of the vegetation canopy, indicating that the shear stress inside the water flow near the top of the vegetation reaches a maximum value, and there is a strong shear between the top of the vegetation and the water body. This is consistent with the findings of Anjum et al. (2018) and Ghani et al. (2019b) on discontinuous bilayer patch vegetation. The Reynolds stress decreases rapidly from the top of vegetation to the water surface and is almost zero near the water surface. It also decreases rapidly from the top of the vegetation down to the inner area of the vegetation, indicating that the shear velocity of the water flow from the top to the bottom is decreasing, conducive with the deposition of sediment particles, thereby achieving the evolution of water quality, improving the water ecological environment, and weakening the sediment in the riverbed. This law is the theoretical basis explaining the dynamics of vegetation sediment deposition, and a critical factor for vegetation bank protection. Additionally, Figure 12C, D show that the maximum value of Reynolds stress in the submerged state increases continuously with the increase of the comprehensive stalk thickness and discrete degree of the combined vegetation. For the vegetation combination distribution (Figure 12C), *h* is at 0.070 m, *d*&*D* are 0.012 m & 0.015 m, 0.012 m & 0.018 m, 0.012 m & 0.021 m, and the Reynolds stress growth rates at 0.012 m & 0.012 m are 80.13%, 167.41%, and 271.56%, respectively (Table 3).

For the vegetation discrete distribution (Figure 12D), *h* is at 0.070 m, *d*&*D* are 0.009 m & 0.015 m, 0.006 m & 0.018 m, 0.003 m & 0.021 m, and the Reynolds stress growth rates at 0.012 m & 0.012 m are 80.13%, 167.41%, and 271.56%, respectively (Table 3). A common feature of increasing combined vegetation comprehensive stem thickness and dispersion degree is an increase of vegetation coverage. Therefore, with an increase of vegetation coverage, the maximum value of Reynolds stress also increases. This result is similar to that of Zeng and Li (2014) , who found that vegetation coverage is the key factor affecting the increase of Reynolds stress.

3.4.2 Longitudinal distribution of turbulent kinetic energy in a specific longitudinal section

Turbulent kinetic energy (TKE) is a basic parameter used to characterize the turbulent flow in natural river channels, which can directly reflect the overall turbulent flow condition. It is the average kinetic energy per unit mass related to eddy currents,

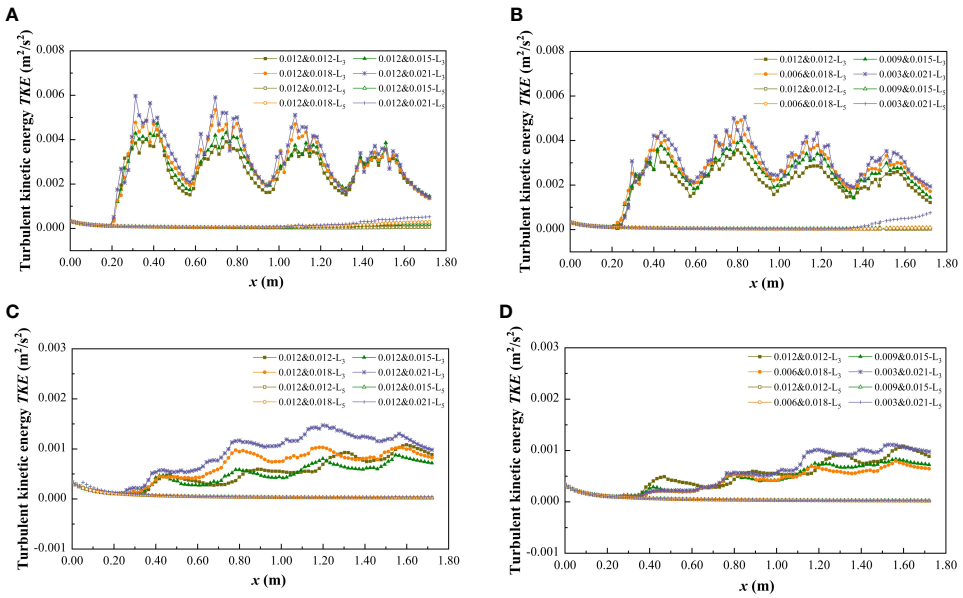

FIGURE 13
Turbulent kinetic energy distribution of longitudinal sections L_3 and L_5 at h = 0.06 m and 0.10 m under different submerged conditions. **(A)** h = 0.06 m, vegetation combination distribution, non-submerged vegetation, **(B)** h = 0.06 m, vegetation discrete distribution, non-submerged vegetation, **(C)** h = 0.10 m, vegetation combination distribution, submerged vegetation, **(D)** h = 0.10 m, vegetation discrete distribution, submerged vegetation.

and TKE is characterized by the fluctuation of root mean square velocity, which plays an important role in energy conversion and transfer. In order to clarify the influence of vegetation combination and discrete characteristics on the flow turbulence structure, the longitudinal distribution of TKE in specific longitudinal sections (L_3 and L_5) under different submerged conditions (h =0.06 m, h =0.10 m) is shown in Figure 13.

In the non-submerged state (Figures 13A, B), owing to the discontinuity in patch vegetation distribution, when the water flows through the patch area, the morphological resistance of the vegetation exerts a certain degree of interference, which causes the

TABLE 4 The average turbulent kinetic energy $\overline{TKE}$ value and its rate of change at longitudinal section L3 under different submerged states and different distribution modes.

Vegetation non-submerged state (h=0.06m)					
Combined distribution d&D (m)	$\overline{TKE}$	**Growth rate of $\overline{TKE}$ relative 0.012&0.012 (%)**	**Discrete distribution d&D (m)**	$\overline{TKE}$	**Growth rate of $\overline{TKE}$ relative 0.012&0.012 (%)**
0.012&0.012	0.00239	–	0.012&0.012	0.00239	–
0.012&0.015	0.00258	7.97%	0.009&0.015	0.00245	2.50%
0.012&0.018	0.00273	13.93%	0.006&0.018	0.00252	5.47%
0.012&0.021	0.00294	22.73%	0.003&0.021	0.00264	10.31%
Vegetation submerged state (h=0.10m)					
Combined distribution$d$&D (m)	$\overline{TKE}$	**Growth rate of $\overline{TKE}$ relative 0.012&0.012 (%)**	**Discrete distribution d&D (m)**	$\overline{TKE}$	**Growth rate of $\overline{TKE}$ relative 0.012&0.012 (%)**
0.012&0.012	0.00052	–	0.012&0.012	0.00052	–
0.012&0.015	0.00047	-10.25%	0.009&0.015	0.00045	-14.62%
0.012&0.018	0.00064	22.84%	0.006&0.018	0.00041	-21.04%
0.012&0.021	0.00086	64.90%	0.003&0.021	0.00056	6.84%

TKE in the patch area (L_3) to be non-uniform and significantly higher than that in the non-vegetated area (L_5). This is because the TKE value in the non-vegetated area is low and shows good uniformity due to the absence of vegetation interference. For the vegetated area (L_3), when the water flow passes through the patch area, the TKE increases significantly and shows a zigzag distribution, and when the water flow enters the interval area, the TKE decreases significantly. This kind of patch interval distribution causes the vertical section of the vegetated area to form a turbulent region with alternating high and low. In addition, the combination form and discrete degree of vegetation are also important factors affecting the degree of water turbulence under non-submerged conditions. For the combined vegetation, the TKE increases with the increase of the comprehensive stem thickness and discrete degree of the vegetation, that is, $TKE_{0.012\&0.012}<TKE_{0.012\&0.015}<TKE_{0.012\&0.018}<TKE_{0.021\&0.021}$, $TKE_{0.012\&0.012}<TKE_{0.009\&0.015}<TKE_{0.006\&0.018}<TKE_{0.003\&0.021}$. This can be explained by the increase in the comprehensive stem thickness and the discrete degree of the combined vegetation leading to an increased vegetation coverage density. Dense vegetation provides greater resistance than sparse vegetation, causing the flow through vegetation to produce a greater turbulence intensity. The average turbulent intensity growth rate relative to a *d*&*D* of 0.012&0.012 under different combined and discrete distribution conditions is shown in Table 4.

In the submerged state (Figures 13C, D), the variation law of the TKE value in the non-vegetated area (L_5) was similar to that in the non-submerged state, while the TKE in the vegetated area (L_3) no longer followed the trend of continuous increases and decreases. Instead, it gradually increased as the length of the ordinate increased, and compared with the non-submerged vegetation state, the overall TKE value in the submerged state decreased. In addition, the TKE in the vegetated area (L_3) no longer followed the change rule that increased with the increases in comprehensive stem thickness and vegetation dispersion degree (Table 4), indicating that the influence of vegetation distribution pattern on flow turbulence in the free layer is weakened in the submerged state.

4 Conclusion

In this study, the influence of patch distribution of partial discontinuous combination vegetation on the flow characteristics of open channels was investigated using a three-dimensional Reynolds stress model. The results show that the combination and discrete distribution have significant influences on flow structure. The main conclusions are as follows:

1) For the streamwise velocity before and after introduction of a single vegetation, the diameter of the vegetation under non-submerged conditions is an important factor affecting wake structure, that is, the length of the stable wake area increases as the stem thickness increases. With the increase in stem thickness, the streamwise velocity at the trailing edge of vegetation decreased, and the difference in streamwise velocity before and after the introduction of vegetation increased with the increase in vegetation discrete degree. Under the submerged condition, the influence of vegetation distribution pattern on the streamwise velocity in the free layer is weakened.
2) For the cross-section velocity distribution, in the non-submerged state, the streamwise velocity in the non-vegetated area is significantly greater than that in the vegetated area, resulting in a strong energy exchange at the interface between the two areas. With the increase in the comprehensive stem thickness and dispersion degree of the combined vegetation, the average streamwise velocity in the vegetated area showed a decreasing trend, while that in the non-vegetated area showed an increasing trend. In the submerged state, the difference in streamwise velocity between the non-vegetated and vegetated areas decreased, and the vegetation combination and discrete distribution had no apparent effect on the difference in the streamwise velocity. In addition, the submerged state of vegetation is an important factor affecting the change in lateral velocity. In the non-submerged state, the direction of the overall lateral velocity is towards the side of the non-vegetated area, while in the submerged state, it is towards the vegetated area.
3) For the change in overall velocity along the route, as the water flows downstream, the velocity along the route in the vegetated area decreases continuously, while in the non-vegetated area it increases continuously, and the difference in velocity between the two areas becomes increasingly apparent. In addition, with the increase in comprehensive stem thickness and dispersion degree of the combined vegetation, the obstructing effect of vegetation on water flow and sediment deposition is stronger, and the water carrying capacity of the channel is also increased.
4) For the variation in Reynolds stress at the channel location of the patch area, in the non-submerged state, the Reynolds stress is highest at 1/4 of the overall water depth. In the submerged state, the Reynolds stress is highest near the top of the vegetation and there is a strong shearing effect between the top of the vegetation and the water body. With the increase in comprehensive stem thickness and the degree of dispersion of the combined vegetation, the Reynolds stress shows an increasing trend.
5) For the longitudinal turbulent kinetic energy, in the vegetated area TKE is significantly higher than that in the non-vegetated area. In the non-submerged state, the

turbulence intensity in the patch area is significantly greater than that in the spaced area, forming a jagged distribution and indicating that the presence of vegetation in the patch area leads to a significant increase in the turbulent intensity of water flow. When the water flow passes through the spaced area, the turbulent kinetic energy decreases, indicating that the spaced area is a low-turbulence area, which is more suitable for the survival of aquatic organisms. The turbulent intensity of the water flow in the vegetated area increased as the comprehensive stem thickness and the discrete degree of the combined vegetation increase. In the submerged state, the turbulent kinetic energy in the vegetated area increases as the longitudinal length increases, and the influence of vegetation combination and discrete distribution on the flow turbulence in the free layer is weakened.

This study verifies that the effect of combined vegetation on the flow characteristics of open channels is different to that of uniform vegetation distribution. Therefore, it is necessary to comprehensively consider the influence of patch distribution of partial discontinuous combined vegetation on the flow characteristics of open channels, which is of great significance to the ecological application of aquatic vegetation in river channels and provides guidance for the restoration and management of eco-river systems. It should be noted that in this paper, a numerical simulation study was carried out on the flow characteristics of the longitudinally discontinuous rigid combined vegetation patches occupying one side of the river bank, and the rigid simulated vegetation was selected to focus on the study of the combined distribution and discrete distribution of the patch vegetation on the water flow structure of the river, vegetation flexibility does not take into account the effects on the flow structure,that is, it is assumed that the vegetation under the action of water flow does not deform and oscillate. However, vegetation with greater flexibility in real river courses will have a certain degree of deformation and swing under the action of water flow, which makes the water flow structure more complex. At present, the numerical model of this study does not include factors related to vegetation flexibility, so this is also the focus of our future research and the direction of our efforts.

Data availability statement

The original contributions presented in the study are included in the article/supplementary materials. Further inquiries can be directed to the corresponding author.

Author contributions

JZ: Conceptualization, Methodology, Writing original draft, Formal analysis, SZ: Resources, Project administration, Funding acquisition. CW: Data curation, Visualization. WW: Data curation, Visualization. LM: Supervision, Investigation. All authors contributed to the article and approved the submitted version.

Funding

The authors acknowledge the support from the following projects: The Natural Science Foundation of Shandong Province (ZR2020ME248); Postgraduate Science and Technology Innovation Project of Shandong University of Science and Technology (YC20210826).

Conflict of interest

The authors declare that the research was conducted in the absence of any commercial or financial relationships that could be construed as a potential conflict of interest.

Publisher's note

References

Aberle, J., and Järvelä, J. (2013). Flow resistance of emergent rigid and flexible floodplain vegetation. *J. Hydraul. Res.* 51, 33–45. doi: 10.1080/00221686.2012.754795

Afzalimehr, H., Fazel Najfabadi, E., and Singh, V. P. (2010). Effect of vegetation on banks on distributions of velocity and reynolds stress under accelerating flow. *J. Hydrol. Eng.* 15, 708–713. doi: 10.1061/(ASCE)HE.1943-5584.0000229

Anjum, N., Ghani, U., Ahmed Pasha, G., Latif, A., Sultan, T., and Ali, S. (2018). To investigate the flow structure of discontinuous vegetation patches of two vertically different layers in an open channel. *Water.* 10, 75. doi: 10.3390/w10010075

Anjum, N., and Tanaka, N. (2020). Investigating the turbulent flow behaviour through partially distributed discontinuous rigid vegetation in an open channel. *River. Res. Appl.* 36, 1701–1716. doi: 10.1002/rra.3671

Boothroyd, R. J., Hardy, R. J., Warburton, J., and Marjoribanks, T. I. (2017). Modeling complex flow structures and drag around a submerged plant of varied posture. *Water. Resour. Res.* 53, 2877–2901. doi: 10.1002/2016WR020186

Bordeu, I., Clerc, M. G., Couteron, P., Lefever, R., and Tlidi, M. (2016). Self-replication of localized vegetation patches in scarce environments. *Sci. Rep-UK.* 6, 1–11. doi: 10.1038/srep33703

Caroppi, G., Västilä, K., Järvelä, J., Lee, C., Ji, U., Kim, H. S., et al. (2022). Flow and wake characteristics associated with riparian vegetation patches: Results from field-scale experiments. *Hydrol. Process.* 36, e14506. doi: 10.1002/hyp.14506

Chang, W. Y., Constantinescu, G., and Tsai, W. F. (2017). On the flow and coherent structures generated by a circular array of rigid emerged cylinders placed in an open channel with flat and deformed bed. *J. Fluid. Mech.* 831, 1–40. doi: 10.1017/jfm.2017.558

Cheng, N. S., Hui, C. L., Wang, X., and Tan, S. K. (2019). Laboratory study of porosity effect on drag induced by circular vegetative patch. *J. Eng. Mech.* 145, 04019046. doi: 10.1061/(ASCE)EM.1943-7889.0001626

Cotton, J. A., Wharton, G., Bass, J. A. B., Heppell, C. M., and Wotton, R. S. (2006). The effects of seasonal changes to in-stream vegetation cover on patterns of flow and accumulation of sediment. *Geomorphology.* 77, 320–334. doi: 10.1016/j.geomorph.2006.01.010

Curran, J. C., and Hession, W. C. (2013). Vegetative impacts on hydraulics and sediment processes across the fluvial system. *J. Hydrol.* 505, 364–376. doi: 10.1016/j.jhydrol.2013.10.013

Dey, S. (2014). "Turbulence in open-channel flows," in *Fluvial hydrodynamics* (Berlin, Heidelberg: Springer), 95–187.

Fathi-Moghadam, M., Kashefipour, M., Ebrahimi, N., and Emamgholizadeh, S. (2011). Physical and numerical modeling of submerged vegetation roughness in rivers and flood plains. *J. Hydrol. Eng.* 16, 858–864. doi: 10.1061/(ASCE)HE.1943-5584.0000381

Folkard, A. M., and Gascoigne, J. C. (2009). Hydrodynamics of discontinuous mussel beds: Laboratory flume simulations. *J. Sea. Res.* 62, 250–257. doi: 10.1016/j.seares.2009.06.001

Ghani, U., Anijum, N., Pasha, G. A., and Ahmad, M. (2019a). Investigating the turbulent flow characteristics in an open channel with staggered vegetation patches. *River. Res. Appl.* 35, 966–978. doi: 10.1002/rra.3460

Ghani, U., Anjum, N., Pasha, G. A., and Ahmad, M. (2019b). Numerical investigation of the flow characteristics through discontinuous and layered vegetation patches of finite width in an open channel. *Environ. Fluid. Mech.* 19, 1469–1495. doi: 10.1007/s10652-019-09669-x

Huai, W. X., Zhang, J., Wang, W. J., and Katul, G. G. (2019). Turbulence structure in open channel flow with partially covered artificial emergent vegetation. *J. Hydrol.* 573, 180–193. doi: 10.1016/j.jhydrol.2019.03.071

Jang, C. L., and Shimizu, Y. (2007). Vegetation effects on the morphological behavior of alluvial channels. *J. Hydraul. Res.* 45, 763–772. doi: 10.1080/00221686.2007.9521814

Järvelä, J. (2002). Flow resistance of flexible and stiff vegetation: A flume study with natural plants. *J. Hydrol.* 269, 44–54. doi: 10.1016/S0022-1694(02)00193-2

Kazem, M., Afzalimehr, H., and Sui, J. (2021a). Formation of coherent flow structures beyond vegetation patches in channel. *Water.* 13, 2812–2827. doi: 10.3390/w13202812

Kazem, M., Afzalimehr, H., and Sui, J. (2021b). Characteristics of turbulence in the downstream region of a vegetation patch. *Water.* 13, 3468–3488. doi: 10.3390/w13233468

Kemp, J. L., Harper, D. M., and Crosa, G. A. (2000). The habitat-scale ecohydraulics of rivers. *Ecol. Eng.* 16, 17–29. doi: 10.1016/S0925-8574(00)00073-2

Li, W. Q., Dan, W., Jiao, J. L., and Yang, K. J. (2018). Effects of vegetation patch density on flow velocity characteristics in an open channel. *J. Hydrodyn.* 31, 1052–1059. doi: 10.1007/s42241-018-0086-6

Li, D., Huai, W. X., and Liu, M. Y. (2020). Investigation of the flow characteristics with one-line emergent canopy patches in open channel. *J. Hydrol.* 590, 125248. doi: 10.1016/j.jhydrol.2020.125248

Liu, D., Diplas, P., Hodges, C. C., and Fairbanks, J. D. (2010). Hydrodynamics of flow through double layer rigid vegetation. *Geomorphology* 116, 286–296. doi: 10.1016/j.geomorph.2009.11.024

Liu, X. D., Liu, Z. Q., Tang, L. C., Han, Y., and Yang, S. Q. (2021). Analysis of vegetation resistance based on two typical distribution types in ecological channel. *Ecol. Eng.* 169, 106325. doi: 10.1016/j.ecoleng.2021.106325

Meire, D., Kondziolka, J., and Nepf, H. (2014). Interaction between neighboring vegetation patches: impact on flow and deposition. *Water. Resour. Res.* 50, 3809–3825. doi: 10.1002/2013WR015070

Mulahasan, S., and Stoesser, T. (2017). Flow resistance of in-line vegetation in open channel flow. *Int. J. River. Basin Manage.* 15, 329–334. doi: 10.1080/15715124.2017.1307847

Nadaoka, K., and Yagi, H. (1998). Shallow-water turbulence modelling and horizontal large-eddy computation of river fow. *ASCE. J. Hydraul. Eng.* 124, 493–500. doi: 10.1061/(ASCE)0733-9429(1998)124:5(493

Nept, H. M. (2012). Hydrodynamics of vegetated channels. *J. Hydraul. Res.* 50, 262–279. doi: 10.10.80/00221686.2012.696559

Nicolle, A., and Eames, I. (2011). Numerical study of flow through and around a circular array of cylinders. *J. Fluid. Mech.* 679, 1–31. doi: 10.1017/jfm.2011.77

Nosrati, K., Afzalimehr, H., and Sui, J. (2022). Drag coefficient of submerged flexible vegetation patches in gravel bed rivers. *Water.* 14, 743. doi: 10.3390/w14050743

Rominger, J. T., and Nepf, H. M. (2011). Flow adjustment and interior flow associated with a rectangular porous obstruction. *J. Fluid. Mech.* 680, 636–659. doi: 10.1017/jfm.2011.199

Ruiz-Reynés, D., Gomila, D., Sintes, T., Hernández-García, E., Marbà, N., and Duarte, C. M. (2017). Fairy circle landscapes under the sea. *Sci. Adv.* 3, e1603262. doi: 10.1126/sciadv.1603262

Sand Jensen, K., and Madsen, T. V. (1992). Patch dynamics of the stream macrophyte, callitriche cophocarpa. *Freshw. Biol.* 27, 277–282. doi: 10.1111/j.1365-2427.1992.tb00539.x

Schulz, M., Kozerski, H. P., Pluntke, T., and Rinke, K. (2003). The influence of macrophytes on sedimentation and nutrient retention in the lower river spree (germany). *Water. Res.* 37, 569–578. doi: 10.1016/S0043-1354(02)00276-2

Shi, Y., Jiang, B., and Nepf, H. M. (2016). Influence of particle size and density, and channel velocity on the deposition patterns around a circular patch of model emergent vegetation. *Water. Resou. Res.* 52, 1044–1055. doi: 10.1002/2015WR018278

Takemura, T., and Tanaka, N. (2007). Flow structures and drag characteristics of a colony-type emergent roughness model mounted on a flat plate in uniform flow. *Fluid. Dyn. Res.* 39, 694–710. doi: 10.1016/j.fluiddyn.2007.06.001

Tanaka, T., and Ohmoto, T. (2015). Turbulent structure in open channel with permeable and impermeable side cavities. *J. Appl. Water. Eng. Res.* 4, 44–53. doi: 10.2208/jscejhe.68.I_805

Tanaka, T., Ohmoto, T., and Tanaka, T. (2008). Flow resistance and momentum transport in open channel with longitudinaly discontinuous vegetation. *Proceed. Hydraul. Eng.* 52, 763–768. doi: 10.2208/prohe.52.763

Tang, X., Rahimi, H., Guan, Y., and Wang, Y. (2021). Hydraulic characteristics of open-channel flow with partially-placed double layer rigid vegetation. *Environ. Fluid. Mech.* 21, 317–342. doi: 10.1007/s10652-020-09775-1

Tang, C., Yi, Y., Jia, W., and Zhang, S. (2020). Velocity and turbulence evolution in a flexible vegetation canopy in open channel flows. *J. Clean. Prod.* 270, 122543. doi: 10.1016/j.jclepro.2020.122543

Tanino, Y., and Nepf, H. M. (2008). Laboratory investigation of mean drag in a random array of rigid, emergent cylinders. *J. Hydraul. Eng.* 134, 34–41. doi: 10.1061/(ASCE)0733-9429(2008)134:1(34

Tny, A., Phsdl, A., Dfs, A., Cgdap, A., Jgja, B., and Hmn, B. (2019). From patch to channel scale: the evolution of emergent vegetation in a channel. *Adv. Water. Resour.* 129, 131–145. doi: 10.1016/j.advwatres.2019.05.009

Tooth, S., and Nanson, G. C. (2000). The role of vegetation in the formation of anabranching channels in an ephemeral river, northern plains, arid central Australia. *Hydrol. Process.* 14, 3099–3117. doi: 10.1002/1099-1085(200011/12)14:16/17<3099::AID-HYP136>3.0.CO;2-4

Truong, S. H., and Uijttewaal, W. S. J. (2019). Transverse momentum exchange induced by large coherent structures in a vegetated compound channel. *Water Resour. Res.* 55, 589–612. doi: 10.1029/2018WR023273

Vandenbruwaene, W., Temmerman, S., Bouma, T. J., Klaassen, P. C., de Vries, M. B., Callaghan, D. P., et al. (2011). Flow interaction with dynamic vegetation patches: implications for biogeomorphic evolution of a tidal landscape. *J. Geophys. Res.-Earth Surf.* 116, F01008. doi: 10.1029/2010JF001788

Velísková, Y., Dulovičová, R., and Schügerl, R. (2017). Impact of vegetation on flow in a lowland stream during the growing season. *Biologia.* 72, 840–846. doi: 10.1515/biolog-2017-0095

Wang, M., Avital, E., Chen, Q., Williams, J., and Xie, Q. (2021). A numerical study on suspended sediment transport in a partially vegetated channel flow. *J. Hydro.* 599, 126335. doi: 10.1016/j.jhydrol.2021.126335

White, B. L., and Nepf, H. M. (2007). Shear instability and coherent structures in shallow flow adjacent to a porous layer. *J. Fluid. Mech.* 593, 1–32. doi: 10.1017/S0022112007008415

White, B. L., and Nepf, H. M. (2008). A vortex-based model of velocity and shear stress in a partially vegetated shallow channel. *Water. Resou. Res.* 44, W01412. doi: 10.1029/2006WR005651

Widdows, J., and Navarro, J. M. (2007). Influence of current speed on clearance rate, algal cell depletion in the water column and resuspension of biodeposits of cockles (Cerastoderma edule). *J. Exp. Mar. Biol. Ecol.* 343, 44–51. doi: 10.1016/j.jembe.2006.11.011

Wu, F. S., Wang, W. Y., and Jiang, S. H. (2007). Development of hydrodynamics in vegetated open channel. *Adv. Water. Sci.* 18, 456–461. doi: 10.14042/j.cnki.32.1309.2007.03.024

Yang, Y., Irish, J. L., and Socolofsky, S. A. (2015). Numerical investigation of wave-induced flow in mound-channel wetland systems. *Coast. Eng.* 102, 1–12. doi: 10.1016/j.coastaleng.2015.05.002

Yang, D., Xiong, D., Zhang, B., Guo, M., Su, Z., Dong, Y., et al. (2017). Effect of grass basal diameter on hydraulic properties and sediment yield processes in gully beds in the dry-hot valley region of southwest China. *Catena.* 152, 299–310. doi: 10.1016/j.catena.2017.01.023

Zdankus, N., Punys, P., Martinaitis, E., and Zdankus, T. (2016). Lowland river flow control by an artificial water plant system. *River. Res. Appl.* 32, 1382–1391. doi: 10.1002/rra.2973

Zeng, C., and Li, C. W. (2014). Measurements and modeling of open-channel flows with finite semi-rigid vegetation patches. *Environ. Fluid. Mech.* 14, 113–134. doi: 10.1007/s10652-013-9298-z

Zhang, J., and Su, X. (2008). Numerical model for flow motion with vegetation. *J. Hydrodyn.* 20, 172–178. doi: 10.1016/S1001-6058(08)60043-8

Zhang, S. T., Wang, Z. K., Liu, Y., Li, G. B., Chen, S., and Liu, M. (2020). The influence of combined vegetation stalk thickness on water flow resistance. *Water. Environ. J.* 34, 455–463. doi: 10.1111/wej.12480

Zhao, F., and Huai, W. (2016). Hydrodynamics of discontinuous rigid submerged vegetation patches in open-channel flow. *J. Hydro-environ. Res.* 12, 148–160. doi: 10.1016/j.jher.2016.05.004

frontiers | Frontiers in Plant Science

TYPE Original Research
PUBLISHED 06 January 2023
DOI 10.3389/fpls.2022.1074191

OPEN ACCESS

EDITED BY
Antonio (Antonello) Montagnoli,
University of Insubria, Italy

REVIEWED BY
Péter Török,
University of Debrecen, Hungary
Teresa Navarro,
University of Malaga, Spain

*CORRESPONDENCE
Yong Jiang
yongjiang226@126.com

†These authors have contributed equally to this work and share first authorship

SPECIALTY SECTION
This article was submitted to Functional Plant Ecology, a section of the journal Frontiers in Plant Science

RECEIVED 19 October 2022
ACCEPTED 13 December 2022
PUBLISHED 06 January 2023

CITATION
Chen KQ, Pan YF, Li YQ, Cheng JY, Lin HH, Zhuo WH, He Y, Fang YC and Jiang Y (2023) Slope position- mediated soil environmental filtering drives plant community assembly processes in hilly shrublands of Guilin, China. *Front. Plant Sci.* 13:1074191. doi: 10.3389/fpls.2022.1074191

Slope position- mediated soil environmental filtering drives plant community assembly processes in hilly shrublands of Guilin, China

Kunquan Chen[1†], Yuanfang Pan[1,2†], Yeqi Li[1], Jiaying Cheng[1], Haili Lin[1], Wenhua Zhuo[1], Yan He[1], Yaocheng Fang[1] and Yong Jiang[1*]

[1]Key Laboratory of Ecology of Rare and Endangered Species and Environmental Protection (Guangxi Normal University), Ministry of Education, Guili, China, [2]Guangxi Mangrove Research Center, Guangxi Academy of Sciences, Beihai, Guangxi, China

Background and aims: A major goal of community ecology focuses on trying to understand how environmental filter on plant functional traits drive plant community assembly. However, slopes positions- mediated soil environmental factors on community-weighted mean (CWM) plant traits in shrub community has not been extensively explored to analyze and distinguish assembly processes.

Methods: Here, we surveyed woody shrub plant communities from three slope positions (foot, middle, and upper) in a low hilly area of Guilin, China to assess differences in functional trait CWMs and environmental factors across these positions. We also measured the CWMs of four plant functional traits including specific leaf area, leaf dry matter content, leaf chlorophyll content, and leaf thickness and nine abiotic environmental factors, including soil water content, soil organic content, soil pH, soil total nitrogen, soil total phosphorus, soil total potassium, soil available nitrogen, soil available phosphorus, and soil available potassium. We used ANOVA and Tukey HSD multiple comparisons to assess differences in functional trait CWMs and environmental factors across the three slope positions. We used redundancy analysis (RDA) to compare the relationships between CWMs trait and environmental factors along three slope positions, and also quantified slope position-mediated soil environmental filtering on these traits with a three-step trait-based null model approach.

Results: The CWMs of three leaf functional traits and all soil environmental factors except soil pH showed significant differences across the three slope positions. Soil total nitrogen, available nitrogen, available potassium, and soil organic matter were positively correlated with the CWM specific leaf area and leaf chlorophyll content along the first RDA axis and soil total potassium, total phosphorous, and soil water content were positively correlated with the CWM

leaf dry matter content along the second RDA axis. Environmental filtering was detected for the CWM specific leaf area, leaf dry matter content, and leaf chlorophyll content but not leaf thickness at all three slope positions.

Conclusions: Ultimately, we found that soil environmental factors vary along slope positions and can cause variability in plant functional traits in shrub communities. Deciduous shrub species with high specific leaf area, low leaf dry matter content, and moderate leaf chlorophyll content dominated at the middle slope position, whereas evergreen species with low specific leaf area and high leaf dry matter content dominated in slope positions with infertile soils, steeper slopes, and more extreme soil water contents. Altogether, our null model approach allowed us to detect patterns of environmental filtering, which differed between traits and can be applied in the future to understand community assembly changes in Chinese hilly forest ecosystems.

KEYWORDS

community assembly, plant functional traits, soil poperties, slope positions, environmental filtering

Introduction

Plant functional traits are defined as the morpho-physio-phenological plant features that indirectly affect fitness within a given environmental context that also provide insights into how environmental factors shape species distributions at regional and local scales (Violle et al., 2007; de Bello et al., 2013). Functional traits can improve biodiversity predictions with environmental change because they represent a species' strategy use under different resources (de Bello et al., 2013; Bruelheide et al., 2018; Maes et al., 2020). For example, specific leaf area and leaf dry matter content are core traits in leaf economic spectrum and nutrient resources (Hodgson et al., 2011; Gao et al., 2022; Ren et al., 2022). Specially, nutrient-poor soils are often associated with leaf economic spectrum of "slow-growing" plants with older, smaller specific leaf area with high leaf dry matter content (Ordoñez et al., 2009). In contrast, "fast-growing" plants that are often associated with nutrient-rich soils possess the opposite sets of traits (i.e. younger leaves, larger specific leaf area, higher leaf nitrogen; Wright et al., 2001; Wright et al., 2004). With these traits, specific leaf area and leaf dry matter content are mainly affected by soil nutrient factors, such as pH and soil nitrogen and phosphorus content (Wang et al., 2022). Generally, soil total nitrogen content and the ratio of carbon to nitrogen are positively correlated with specific leaf area and negatively correlated with leaf dry matter content (Hodgson et al., 2011). Additionally, leaf chlorophyll content provides information about the physiological state of the plant (Lu et al., 2018), where any shortage of soil water or nitrogen significantly reduces its chlorophyll and photosynthetic rate (Qiu et al., 2018). Leaf thickness also demonstrateds the physical resistance of the leaf blade to adverse environmental condititons (Afzal et al., 2017; Pinho et al., 2018), and has been shown to be positively correlated with soil fertility and soil water availability (Schmitt et al., 2022).

Understanding the deterministic processes that underly the functional structure of ecological communities is one of the central goals of community ecology (Cornwell and Ackerly, 2009; de Bello et al., 2013). In theory, the environmental filtering hypothesis proposed that abiotic environment factors act as "filters" to select species from the regional pool with similar trait values into communities to adapt to the local environment conditions (Kraft et al., 2015; Le Bagousse-Pinguet et al., 2017). A substantial number of studies have shown that community composition is often influenced by environment-driven factors that results in trait convergence—particularly at local scales (Alice et al., 2018; Báez et al., 2022; Da et al., 2022). Habitats in the slope foot tend to be more moist than at higher, steeper positions, which are often more dry and exposed, where furthermore, these temperature and moisture differences may alter nutrient mineralization along the slope position. Altogether, these environmental differences can cause flexible responses in plant functional traits, with the most researched being tree height, specific leaf area, and leaf dry matter content (Niinemets et al., 2006; Mitchell et al., 2016; Guo et al., 2018). For instance, Lim et al. (2017) demonstrated that the community-weighted mean (CWM) height decreased down a slope into frost hollows while the CWM the leaf area was

greater toward the top of the slope position. Additionally, Méndez-Toribio et al. (2017) found that wood density and leaf dry matter content were greater at lower slope positions. Although several previous studies have shown links between topography and soil resource availability, soil environmental factors along different slope positions have not been extensively investigated to understand how differences in plant functional traits affect shrub communities (Punchi-Manage et al., 2012; Liu et al. (2014).

Shrubs act as an essential component of global and regional vegetation and have rich characteristic such as wide distributions, high germination rates, and high morphological and physiological plasticity, which is an ideal natural experimental model to facilitate adaptation for diverse environments (Xu et al., 2020; Venn et al., 2021). Generally, shrubs are an important component of forest ecosystems and play a vital role in natural forest dynamics, especially during the first stages of tree development. Moreover, shrubs have gained importance since they are more tolerant to drought and aridity than tree species, which has become significant under the current context of global warming (Bateman et al., 2018). Despite the importance of shrubs on the global scale, they are often understudied studied compared to other plants, like trees. Because of these issues, it is necessary to identify the response of shrubs to environmental conditions based on the perspective of functional traits at the local community level. Currently, there are many studies that have focused on trying to understand changes in communities level plant features over natural gradients to assess community assembly processes, such as trait convergence, trait divergence, and stochastic process. Pinho et al., 2018 found soil fertility operates as a key filter causing functional convergence towards more conservative resource-use strategies in tropical forest regeneration. Da et al. (2022) demonstrated that soil and topography factors were the main environment driver of trait convergence in temperate forest communities at local scale. However, very few have focused on trait convergence by habitat filtering for shrub plants in different environments, or how these traits could be affected by harsh conditions due to complex abiotic filters (e.g., soil and slope positions factors; Asefa et al., 2017; Molina-Venegas et al., 2018).

In this study, we measured functional traits of shrubs along a slope gradient in the Jiangjiaba hilly area of Guilin, China to assess relationships between community-level trait values and environmental factors. Initially, we expected slope position to interact with environmental factors to filter trait values and ultimately affect community assembly. Specifically, our goals were to: (1) the major plant functional traits at the community level to understand if they are significantly different with slope position, and if soil nutrients act as important dominant factors, and (2) to quantify the impact of slope position-mediated soil environmental filtering on the functional composition of shrub communities across three slope positions at hilly area. We anticipated that soil environmental factors vary along slope positions and can cause variability in plant functional traits in shrub communities. And environmental filtering became the major mechanism that maintained in this typical subtropical shrub community and would be helpful in the future to understand community assembly changes in Chinese hilly forest ecosystems.

Materials and methods

Study area

The study area was located on Jiangjiaba Hill, Guilin City, Southwest China (25°05′23″N, 110°17′32″E). The region belongs to the non-karst hill in Guilin, possesses laterite soil and ranges in altitudes from 100 to 500 m above sea level. Topography and altitude strongly influence microclimate and soil environmental factors, and therefore affect the distribution of plant species (Mantilla-Contreras et al., 2012). To measure such effects, we surveyed three slope positions (foot, middle, and upper) along an altitudinal transect. Based on our research, the upper slope had strong wind and shallow soils with little capacity for moisture retention that causes poor soil nutrients, while the slope foot had thick soil with a high soil water storage that was cooler, more humid, and had lower solar radiation. By comparison, the middle slope position had a relatively flat terrain with rich soil nutrients and moderate temperature, moisture, and light conditions (Liu et al., 2020). This region has a typical humid subtropical monsoon climate with noticeably dry and less rainy autumns and winters. Its annual temperature ranges from 17.8-19.1 °C with a frost-free period of 309 d and a mean annual sunshine duration of 1670 h (Data from the China Meteorogical Data Service Center; http://data.cma.cn). The coldest month (January) averages 8 °C and the hottest (August) averages 28 °C. The mean annual precipitation varies from 1814 to 1941 mm, with a distinct wet season from May to October (more than 80% of precipitation occurs during the wet season) and a dry season from November to April. The annual average evaporative capacity ranges from 1490 to 1905 mm, and the natural vegetation of this hilly region is dominated by shrub communities.

Sampling design and field investigation

Data his study were collected in a typical hilly shrub community at the study site. Based on an initial field survey of woody shrubs, we established 108 10 m × 10 m plots with 36 plots each at the foot slope, middle slope, and upper slope from July to September 2016. The three positions are located at different points on a single slope (see Figure 1 for details), and the plots in each slope are distributed continuously. In each

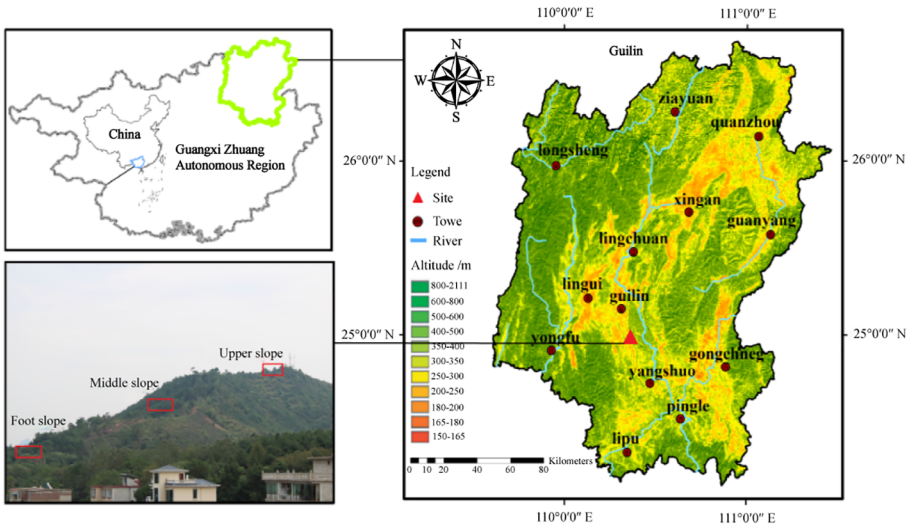

FIGURE 1
The geographical location of the study area and sampling sites in the hilly region, Guilin, Southwest China.

sampling plot, all the woody individuals with basal diameter (BD) ≥ 1 cm were mapped, marked, and identified as species. We also reported topography (slope degree and position), dominant species, and abundance of evergreen and deciduous species at each slope position (Table 1). The nomenclature of each species were identified using the *Flora of China* (English edition; http://foc.iplant.cn).

Our initial investigation documented 2966 live individuals of 75 tree species from 57 genera and 34 families. With each slope position, *Rhodomyrtus tomentosa* (Ait.) Hassk, *Quercus fabri* Hance, *Ficus hirta Vahl*, and *Mallotus apelta* (Lour.) Muell. Arg were the dominant species at the slope foot; *Quercus fabri* Hance, *Rhodomyrtus tomentosa* (Ait.) Hassk, *Rhododendron molle* (Blum) G. Don, and *Melastoma malabathricum* Linnaeus were dominant at the middle slope. The upper slope was mainly composed of *Schima superba* Gardn. et Champ, *Quercus fabri* Hance, *Melastoma malabathricum* Linnaeus, *and Rhodomyrtus tomentosa* (Ait.) Hassk. *Rhodomyrtus tomentosa*, *Ficus hirta*, *Mallotus apelta* and *Schima superba* are evergreen species, while *Quercus fabric*, *Rhododendron molle*, and *Melastoma malabathricum* are deciduous species that are among the most dominant species in each position.

Measurement of functional traits

Four major functional traits were selected to characterize the ecological strategies of the plants at each different slope gradient: specific leaf area, leaf dry matter content, leaf chlorophyll content, and leaf thickness (Pérez-Harguindeguy et al., 2013;

TABLE 1 Topographic and ecological features of the three slope positions.

Slope Position	Number of Plots	Evergreen species	Deciduous species	Evergreen individuals	Deciduous individuals	Slope Degree Range (°)	Dominant Species
Foot	36	35	27	660	485	13–18	*Rhodomyrtus tomentosa* *Quercus fabri* *Ficus hirta* *Mallotus apelta*
Middle	36	26	23	463	561	7–12	*Quercus fabri* *Rhodomyrtus tomentosa* *Rhododendron molle* *Melastoma malabathricum*
Upper	36	21	17	387	410	17–21	*Schima superba* *Quercus fabri* *Melastoma malabathricum* *Rhodomyrtus tomentosa*

Jiang et al., 2015). For each individual, we collected three newly mature leaves from canopy branches that were completely exposed to sunlight, and avoided senescent or damaged leaves. The collected leaves were stored in sealed plastic bags with moistened paper towels and transported to the Key Laboratory of Ecology of Rare and Endangered Species and Environmental Protection at the Guangxi Normal University, Guilin, China, for further experiments. The leaf area was first measured by scanning fresh leaves using a Yaxin-1241 (Yaxin, Beijing, China). The mass of dried (72 h at 70 °C) leaf samples was then estimated with a precision of 0.1 mg and specific leaf area was calculated as leaf area divided by leaf dry mass. Leaf dry matter content was calculated from the oven-dry mass divided by fresh mass (Cornelissen et al., 2003; Pérez-Harguindeguy et al., 2013). Leaf thickness was measured by an electronic digital display caliper (SF2000, Guanglu, Guilin, China) with an accuracy of 0.01 mm and calculated as the mean thickness of three equally distanced points in the direction of the main veins. Leaf chlorophyll content was estimated using three values per lamina from a SPAD 502Plus meter (KONICA Minolta, Osaka, Japan).

Measurement of soil environmental factors

Soil samples were collected between July and September 2016. According to the "S" type, we removed the leaf litter and humus layer, and five topsoil (0-15 cm depth) samples were collected from each 10 m × 10 m plot that were mixed to one 1000g sample for further analysis. We used the agricultural and chemical methods described by Bao (2000) to determine soil properties. Soil water content (SWC) was calculated as: SWC = (Massf - Massd)/Massd; where, Massf is the soil fresh mass and Massd is the soil dry mass. A digital pH meter (FE20K, Mettler-Toledo, Zurich, Switzerland) was used to measure soil pH using with a soil: to water ratio of 1:2.5. The soil organic content was measured using potassium dichromate oxidation method. Additionally, the total nitrogen was also determined by using automatic Kjeldahl analysis (KJELTEC^{TM} 8400, FOSS Quality Assurance Co., Ltd., HillerØd, Denmark). The total phosphorus content of the soil was analyzed by acid digestion with an H_2SO_4 + $HClO_4$ solution, and the total potassium was digested with an HF-$HClO_4$-HNO_3 acid mixture and determined by flame photometry. Additionally, the soil available nitrogen was quantified using the alkaline hydrolysis diffusion method, and the available phosphorus was measured using a molybdenum blue colorimeter after the sample had been extracted with 0.5 M Na_2CO_3. To measure soil available potassium, samples were shaken for 30 min with a 1 M ammonium acetate solution (1:10 *w/v*) and then analyzed by flame photometry. For each soil sample, the measurements were repeated three times and the average values were used for all subsequent soil physical and chemical analyses.

Statistical analysis

The three slope positions (foot, middle, and upper) were used as groups for a One-way ANOVA comparison of the environmental factors, and Tukey's HSD post-hoc comparisons were made to test for significant differences (family-wise error rate< 0.05) between groups. We coupled the individual traits to each individuals' plot and then calculated CWM trait values. CWM values are proportional to species abundance and are more appropriate than unweighted means to characterize trait variation at the community level (Garnier et al., 2004; Lavorel et al., 2008). Here, we calculated CWMs with the "dbFD" function in the "*FD*" package of R software (Laliberté and Legendre, 2010; R Core Team, 2021), which is based on the Fdvar index:

$$CWM = \sum_{i=1}^{S} p_i \times trait_i$$

where S is the total number of species, p_i is the relative abundance of the ith species and $trait_i$ is the trait value of the ith species.

To improve data normality and homoscedasticity, we rank-transformed the CWM values of the functional traits and environmental factors. We then used the One-way ANOVA and Tukey's HSD post-hoc comparisons again to test how the CWM trait values varied among the three slope positions. We then performed redundancy analysis (RDA) to assess the correlations between plant functional traits and environmental variables across the three slope positions. From the trait and abundance data, we built a plot by trait matrix by averaging the trait values of each species weighted by their abundance in each plot. We then applied a forward selection that included the environmental variables and a Monte Carlo test with 999 unrestricted permutations to detect environmental factors that have a significant effect on trait variation.

To test the effects of modification of non-random assembly processes across the three slope positions, we adopted a trait-based null model approach. Here, the plant species found in each plot were treated as the local species pool, while all species observed across the 108 plots along the different slope positions were defined as the regional species pool. Following, the null distributions were built from a three-step procedure: 1) each species was randomly drawn without replacement from the species pool and repeated 999 times, 2) one species mean trait value derived from the regional functional species pool was randomly allocated to each previously selected species, and 3) the range of trait values in each plot (max-min) was calculated to generally predict the trait value distributions. By comparing the observed values of each plot with the expectation of the respective null model (Cornwell and Ackerly, 2009), we

inferred random dispersion among local species trait values if the observed trait values were close to the expected distribution, while trait convergence was inferred if the range of the observed trait values was lower than expected, which would result from stronger environmental filtering. Trait divergence was also inferred if the range of the observed trait values was higher than expected, which would result from greater niche complementarity (greater niche complementarity; Lhotsky et al., 2016). We calculated the standardized effect size (SES; Gotelli and McCabe, 2002), implemented in the R package "*picante*" (Kembel et al., 2010) as:

$$SES = (Iobs - Inull)/SD_{null}$$

Where I_{obs} is the observed value, I_{null} is the mean of the null distributionand SD_{null} is the standard deviation of null distribution in the plot. Positive and negative SES values indicate that the observed values are above and below the average expected value, respectively. The Wilcoxon signed rank test was then used to assess whether there were significant differences in random variation of functional trait values between plots at different slope positions.

Results

Changes in environmental factors across slope positions

All soil environmental factors except soil pH differed significantly between at least two slope positions (Figure 2). Soil water content significantly decreased from slope foot to middle slope and from middle slope to upper slope (Figure 2A). The middle slope had significantly higher soil organic content, total nitrogen, available nitrogen, available phosphorus, and available potassium of than the slope foot and upper slope (Figures 2B, F–I, respectively). The slope foot had significantly higher total phosphorus and total potassium of soil than the middle and upper slopes (Figures 2D, E, respectively). The soil pH was slightly acidic to strongly acidic, and its soil organic matter, total nitrogen and available nitrogen were relatively rich, while soil total phosphorus, available phosphorus, total potassium and available potassium were relatively deficient, according to China's second national soil census nutrient classification standard.

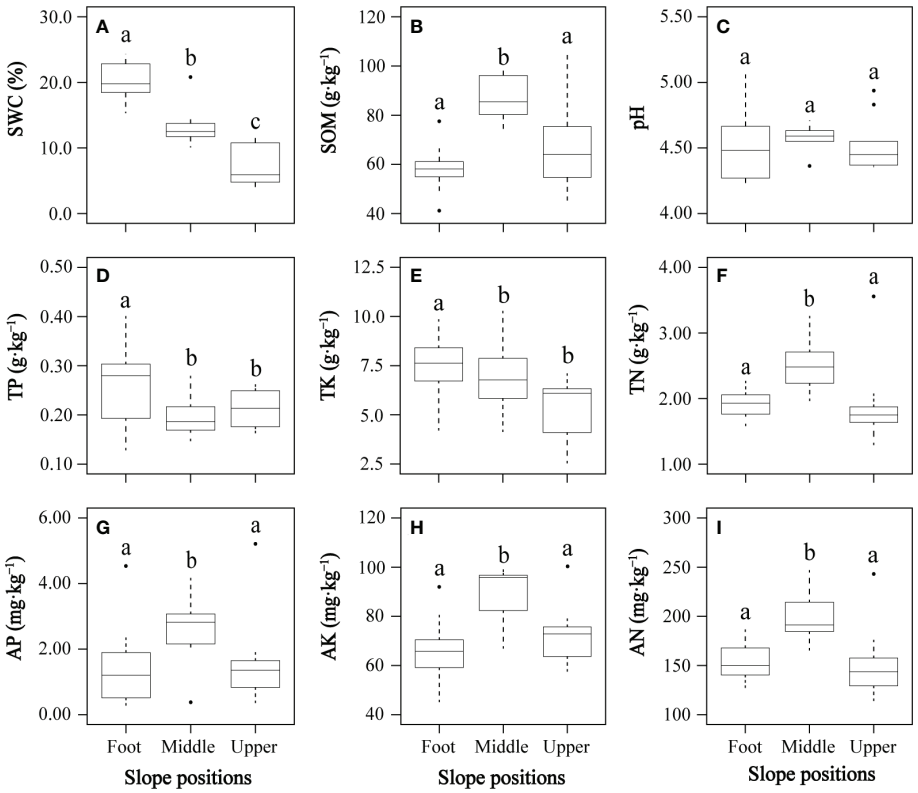

FIGURE 2
Changes of soil environmental factors **(A–I)** at three slope positions. AK, soil available potassium; AN, soil available nitrogen; AP, soil available phosphorus; pH, soil pH; SOM, soil organic content; SWC, soil water content; TK, soil total potassium; TN, soil total nitrogen; TP, soil total phosphorus. In each panel, boxes with different letters on top of the bars represent a significant difference at $P < 0.05$.

Changes in community-level plant functional traits across slope positions

All CWMs of leaf functional traits except leaf thickness differed significantly between at least two slope positions (Figure 3). The CWM specific leaf area at the middle slope was significantly higher than both the slope foot and upper slope positions, and the slope foot CWM specific leaf area was significantly higher than the upper slope (Figure 3A). The CWM leaf dry matter content showed an inverted pattern; the middle slope was significantly lower than the slope foot, which was significantly lower than the upper slope (Figure 3B). The CWM leaf chlorophyll content significantly decreased from slope foot to middle slope and again from middle to upper slope (Figure 3C). There were no significant differences in CWM leaf thickness (Figure 3D).

Relationships between community level plant functional traits and environmental factors across slope positions

Redundancy analysis found significant relationships between community level plant functional traits and the environmental factors across the three slope positions (Figure 4). Soil environmental factors (available nitrogen, total nitrogen, available potassium, and organic content) significantly influenced the CWM specific leaf area and CWM leaf chlorophyll content, whereas soil total potassium, total phosphorus, and water content had significant effects on the CWM leaf dry matter content.

Environmental filtering of traits across slope positions

By comparing to our null model expectations, we detected significant reductions in the community ranges of specific leaf area, leaf dry matter content, and leaf chlorophyll content (Figure 5)—indicating that environmental filtering had significant effects on plant functional trait values. We found no significant difference between the expected and observed distributions of leaf thickness, which suggested no environmental filtering of this trait (Figure 5).

Discussion

Relationships between community level plant functional traits and environment factors variation across slope positions

Slope position is an important topographic factor that encompasses substantial variation in micro-habitat conditions and which affects community-level plant functional traits (Méndez-Toribio et al., 2017). Consistent with a growing body of studies (e.g., Wang et al., 2016; Chelli et al., 2022), we found that SLA was negatively correlated with LDMC and observed the highest CWM specific leaf area with the lowest CWM leaf dry matter content. This fit our expectations for resource-rich environments, as the middle slope had high soil SOM, TN, AN, and AK, intermediate SWC, and a flatter terrain. In contrast, we found communities adapted to slope foot and upper slope conditions—generally resource poor environments—with low CWM specific leaf area and high CWM leaf dry matter content. Several studies have demonstrated that specific leaf area and leaf dry matter content can be useful proxies for resource capture and utilization (Fernanda et al., 2002; Shipley, 2006; Grotkopp and Rejmánek, 2007; Hodgson et al., 2011). The CWM leaf chlorophyll content significantly decreased from slope foot to middle slope to upper slope (Figure 3C), which may result, in part, from differences in species composition across slope positions. Most species found at the slope foot were evergreen and highly abundant (Table 1), indicating that evergreen species allocated greater resources to photosynthesis in this habitat with lower soil nutrients and weaker light (Liu et al., 2020). The middle slope position had intermediate CWM leaf chlorophyll content and more evergreen than deciduous species, but these evergreen species were less abundant. We had

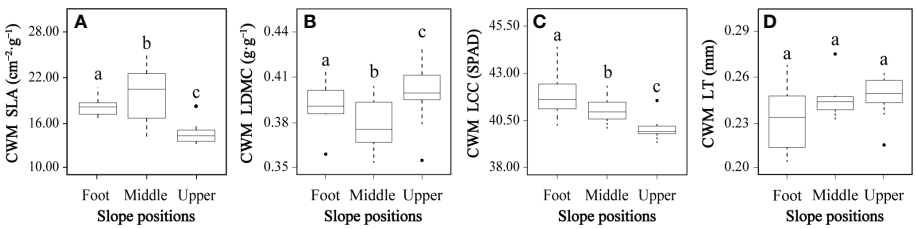

FIGURE 3
Community-weighted means (CMWs) of plant functional traits **(A–D)** at three slope positions. CWM SLA, CWM specific leaf area; CWM LDMC, CWM leaf dry matter content; CWM LCC, CWM leaf chlorophyll content; CWM LT, CWM leaf thickness. In each panel, boxes with different letters on top of the bars represent a significant difference at $P< 0.05$.

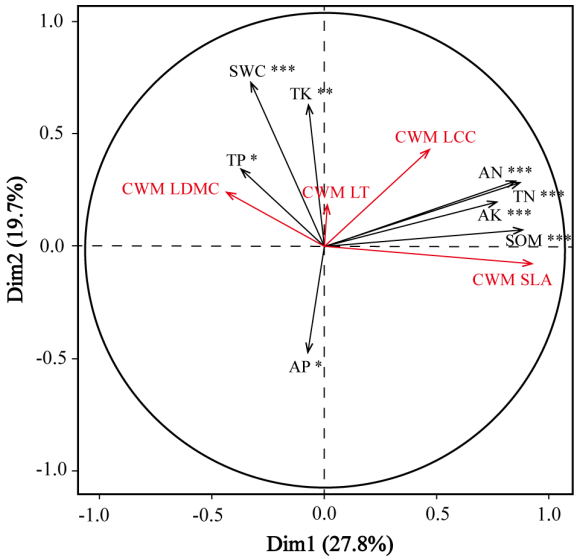

FIGURE 4
Redundancy analysis ordination diagram of the relationships between the four community-weighted means of functional traits (red) and eight selected soil environmental factors (black) across three slope positions. AK, soil available potassium; AN, soil available nitrogen; AP, soil available phosphorus; pH, soil pH; SOM, soil organic content; SWC, soil water content; TK, soil total potassium; TN, soil total nitrogen; TP, soil total phosphorus; CWM SLA, CWM specific leaf area; CWM LDMC, CWM leaf dry matter content; CWM LCC, CWM leaf chlorophyll content; CWM LT, CWM leaf thickness. *, **, and *** indicate significant correlation at $P< 0.05$, $P< 0.01$, and $P< 0.001$, respectively.

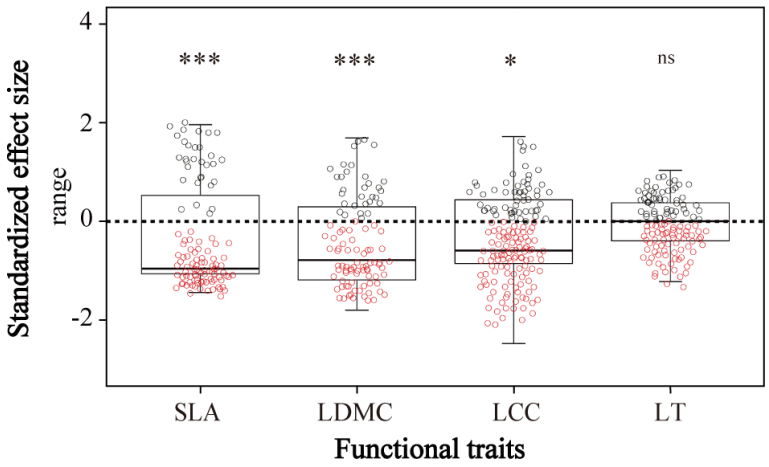

FIGURE 5
The standardized effect size of community-weighted means (CWMs) of plant functional traits between observed and randomly created communities. SLA, specific leaf area; LDMC, leaf dry matter content; LCC, leaf chlorophyll content; LT, leaf thickness. ns means no significant difference, * and *** indicate significant correlation at $P< 0.05$ and $P< 0.001$, respectively, by the Wilcoxon signed rank test.

predicted the CWM leaf chlorophyll content of the middle slope to be highest because of its high nutrient richness. The unexpected result that it was intermediate may be due to two reasons: first, a decrease in soil water content could inhibit chlorophyll biosynthesis leading to relatively low of leaf chlorophyll content (He et al., 2022); second, high available potassium, total nitrogen, and available nitrogen of soil may increase net photosynthetic rate (Hu et al., 2017).

Environmental filtering for plants with different functional traits

The observed ranges of specific leaf area, leaf dry matter content, and leaf chlorophyll content (but not leaf thickness) were significantly smaller than expected based on our null models, suggesting that environmental factors significantly filter the CWM specific leaf area, leaf dry matter content, and leaf chlorophyll content (Figure 5). We showed that soil nutrients and water availability strongly restricted these CWM trait values across the three slope positions, as evidenced by the collinearity of these features with CWMs in the RDA ordination (Figure 4). Local topography (i.e., slope position) can therefore drive functional trait values, mostly through indirect effects of soil nutrients and soil water content. At our study site, the upper slopes were steep and the soils infertile; the upper slope had less developed soil, less soil water, and fewer soil nutrients, while the slope foot had relatively thick soil with higher soil water storage, lower solar radiation, and was cooler and more humid. The middle slope position was relatively flat with fertile soil and mild temperature, moisture, and light conditions. The species composition changed from mostly evergreen, shade-intolerant species with relatively low nutrient demand at the slope foot and upper slope positions to deciduous species with high nutrient demands at the middle slope position. Fertile soils and mild climatic conditions had strong filtering effects; deciduous shrub species with high specific leaf area, low leaf dry matter content, and moderate leaf chlorophyll content dominated at the middle slope position, whereas evergreen species with low specific leaf area and high leaf dry matter content dominated in slope positions with infertile soils, steeper slopes, and more extreme soil water contents. Our null model approach allowed us to detect patterns of habitat filtering, which differed between traits.

Conclusion

Our results showed that multiple environmental factors and the CWMs of specific leaf area, leaf dry matter content, and leaf chlorophyll content were significantly different between slope positions and that most environmental factors examined had significant effects on plant functional traits. Together, these findings indicate that slope position gradients—with varying soil nutrient and climatic conditions—have significant effects on plant functional trait variation. In summary, the detection of habitat filtering depends critically on the type of trait considered: different traits, which reflects different aspects of plant physiology, may be differentially filtered by the environment.

Data availability statement

The original contributions presented in the study are included in the article/supplementary materials, further inquiries can be directed to the corresponding author/s.

Author contributions

YJ designed and oversaw the study. KC, YP, Y.L, YH, WZ, HL, JC, and YF collected the field and laboratory data. KC, YP and YJ conducted the statistical analyses and wrote the first draft of the manuscript. All authors contributed to the article and approved the submitted version.

Funding

This research was funded by the Key Laboratory of Ecology of Rare and Endangered Species and Environmental Protection (Guangxi Normal University), Ministry of Education, China (ERESEP2021Z07), National Natural Science Foundation of China (31860124 and 32260283), Guangxi Natural Science Foundation (2022GXNSFAA035600), 2021 Guangxi Postgraduate Innovation Project (YCSW2021104), and College Students' Innovation and Entrepreneurship Training Program (202110602067 and S202210602027).

Acknowledgments

We are grateful to numerous students from the Chinese Guangxi Normal University for their support with field sampling and providing assistance in processing soil samples. We are also indebted to the editor and reviewers for insightful and constructive suggestions for improving the manuscript.

Conflict of interest

The authors declare that they have no known competing financial interests or personal relationships that could have appeared to influence the work reported in this paper.

Publisher's note

References

Afzal, A., Duiker, S. W., and Watson, J. E. (2017). Leaf thickness to predict plant water status. *Biosyst. Engin.* 156, 148–156. doi: 10.1016/j.biosystemseng.2017.01.011

Alice, N., Melanie, K., Pedro, P., Paula, M., Edoardo, A. C. C., Cristina, S., et al. (2018). Local topographic and edaphic factors largely predict shrub encroachment in Mediterranean drylands. *Sci. Total Environ.* 657, 310–318. doi: 10.1016/j.scitotenv.2018.11.475

Asefa, M., Cao, M., Zhang, G. C., Ci, X. Q., Li, J., and Yang, J. (2017). Environmental filtering structures tree functional traits combination and lineages across space in tropical tree assemblages. *Sci. Rep.* 7, 132. doi: 10.1038/s41598-017-00166-z

Báez, S., Fadrique, B., Feeley, K., and Homeier, J. (2022). Changes in tree functional composition across topographic gradients and through time in a tropical montane forest. *PloS One* 17, e0263508. doi: 10.1371/journal.pone.0263508

Bao, S. D. (2000). *Soil agrochemical analysis* (China. Beijing: China agriculture press).

Bateman, A., Lewandrowski, W., Stevens, J. C., and Munoz-Rojas, M. (2018). Ecophysiological indicators to assess drought responses of arid zone native seedlings in reconstructed soils. *Land Degrad. Dev.* 29, 984–993. doi: 10.1002/ldr.2660

Bruelheide, H., Dengler, J., Purschke, O., Lenoir, J., Jiménez-Alfaro, B., Hennekens, S. M., et al. (2018). Global trait-environment relationships of plant communities. *Nat. Ecol. Evol.* 2, 1906–1917. doi: 10.1016/j.foreco.2021.119977

Chelli, S., Ottaviani, G., Tsakalos, J. L., Campetella, G., Simonetti, E., Wellstein, C., et al (2022). Intra- and inter-specific leaf trait responses of understorey species to changes in forest maturity. *FOREST ECOL. MANAG.* 506, 119977. doi: 10.1016/j.foreco.2021.119977

Cornelissen, J. H. C., Lavorel, S., Garnier, E., Díaz, S., Buchmann, N., Gurvich, D. E., et al. (2003). A handbook of protocols for standardized and easy measurement of plant functional traits worldwide. *Aust. J. Bot.* 51, 335–380. doi: 10.1071/BT02124

Cornwell, W. K., and Ackerly, D. D. (2009). Community assembly and shifts in plant trait distributions across an environmental gradient in coastal California. *Ecol. Monog.* 79, 109–126. doi: 10.1890/07-1134.1

Da, R., Hao, M. H., Qiao, X. T., Zhang, C. Y., and Zhao, X. H. (2022). Unravelling trait-environment relationships at local and regional scales in temperate forests. *Front. Plant Sci.* 13. doi: 10.3389/fpls.2022.907839

de Bello, F., Lavorel, S., Lavergne, S., Albert, C. H., Boulangeat, I., Mazel, F., et al. (2013). Hierarchical effects of environmental filters on the functional structure of plant communities: a case study in the French Alps. *Ecography* 36, 393–402. doi: 10.1111/j.1600-0587.2012.07438.x

Fernanda, V., Sandra, D., Diego, E. G., Peter, J. W., Ken, T., and John, G. H. (2002). Leaf traits as indicators of resource-use strategy in floras with succulent species. *New Phytol.* 154, 147–157. doi: 10.2307/1513940

Gao, J., Wang, K. Q., and Zhang, X. (2022). Patterns and drivers of community specific leaf area in China. *Glob. Ecol. Conser.* 33, e01971. doi: 10.1016/j.gecco.2021.e01971

Garnier, E., Cortez, J., Billès, G., Navas, M.-L., Roumet, C., Debussche, M., et al. (2004). Plant functional markers capture ecosystem properties during secondary succession. *Ecology* 85, 2630–2637. doi: 10.1890/03-0799

Gotelli, N. J., and McCabe, D. (2002). Species co-occurrence: a meta-analysis of j. m. diamond's assembly rules model. *Ecology* 83, 2091–2096. doi: 10.2307/3072040

Grotkopp, E., and Rejmánek, M. (2007). High seedling relative growth rate and specific leaf area are traits of invasive species: phylogenetically independent contrasts of woody angiosperms. *Ameri. J. Bot.* 94, 526–532. doi: 10.3732/ajb.94.4.526

Guo, Z. W., Lin, H., Chen, S. L., and Yang, Q. P. (2018). Altitudinal patterns of leaf traits and leaf allometry in bamboo pleioblastus amarus. *Front. Plant Sci.* 9. doi: 10.3389/fpls.2018.01110

He, Y. C., Li, T. T., Zhang, R. Y., Wang, J. S., Zhu, J. T., Li, Y., et al. (2022). Plant evolution history overwhelms current environment gradients in affecting leaf chlorophyll across the Tibetan plateau. *Fronti. Plant Sci.* 13. doi: 10.3389/FPLS.2022.941983

Hodgson, J. G., Montserrat-Martí, G., Charles, M., Jones, G., Wilson, P., Shipley, B., et al. (2011). Is leaf dry matter content a better predictor of soil fertility than specific leaf area? *Ann. Bot.* 108, 1337–1345. doi: 10.1093/aob/mcr225

Hu, W., Coomer, T. D., Loka, D. A., Oosterhuis, D. M., and Zhou, Z. (2017). Potassium deficiency affects the carbon-nitrogen balance in cotton leave. *Plant Physiol. Bioche.* 115, 408–417. doi: 10.1016/j.plaphy.2017.04.005

Jiang, Y., Zang, R. G., Lu, X. H., Huang, Y. F., Ding, Y., Liu, W. D., et al. (2015). Effects of soil and microclimatic conditions on the community-level plant functional traits across different tropical forest types. *Plant Soil* 390, 351–367. doi: 10.1007/s11104-015-2411-y

Kembel, S. W., Cowan, P. D., Helmus, M. R., Cornwell, W. K., Morlon, H., Ackerly, D. D., et al. (2010). Picante: R tools for integrating phylogenies and ecology. *Bioinformatics.* 26, 1463–1464. doi: 10.1093/bioinformatics/btq166

Kraft, N. J. B., Adler, P. B., Godoy, O., James, E. C., Fuller, S., and Levine, J. M. (2015). Community assembly, coexistence and the environmental filtering metaphor. *Funct. Ecol.* 29, 592–599. doi: 10.1111/1365-2435.12345

Laliberté, E., and Legendre, P. (2010). A distance-based framework for measuring functional diversity from multiple traits. *Ecology* 91, 299–305. doi: 10.1890/08-2244.1

Lavorel, S., Grigulis, K., McIntyre, S., Williams, N. S., Garden, D., Dorrough, J., et al. (2008). Assessing functional diversity in the field-methodology matters! *Funct. Ecol.* 22, 134–147. doi: 10.1111/j.1365-2435.2007.01339.x

Le Bagousse-Pinguet, Y., Gross, N., Maestre, F. T., Maire, V., de Bello, F., Fonseca, C. R., et al. (2017). Testing the environmental filtering concept in global drylands. *J. Ecol.* 105, 1058–1069. doi: 10.1111/1365-2745.12735

Lhotsky, B., Kovács, B., Ónodi, G., Csecserits, A., Rédei, T., Lengyel, A., et al. (2016). Changes in assembly rules along a stress gradient from open dry grasslands to wetlands. *J. Ecol.* 104, 507–517. doi: 10.1111/1365-2745.12532

Lim, F. K. S., Pollock, L. J., and Vesk, P. A. (2017). The role of plant functional traits in shrub distribution around alpine frost hollows. *J. Veg. Sci.* 28, 585–594. doi: 10.1111/jvs.12517

Liu, R. H., Pan, Y. F., Bao, H., Liang, S. C., Jiang, Y., Tu, H. R., et al. (2020). Variations in soil physico-chemical properties along slope position gradient in secondary vegetation of the hilly region, guilin, southwest China. *Sustainability.* 12, 1303. doi: 10.3390/su12041303

Liu, J., Tan, Y. H., and Slik, J. W. F. (2014). Topography related habitat associations of tree species traits, composition and diversity in a Chinese tropical forest. *For. Ecol. Manage.* 330, 75–81. doi: 10.1016/j.foreco.2014.06.045

Lu, S., Lu, F., You, W. Q., Wang, Z. Y., Liu, Y., and Omasa, K. (2018). A robust vegetation index for remotely assessing chlorophyll content of dorsiventral leaves across several species in different seasons. *Plant Methods* 14, 15. doi: 10.1186/s13007-018-0281-z

Maes, S. L., Perring, M. P., Depauw, L., Bernhardt-Römermann, M., Blondeel, H., Brūmelis, G., et al. (2020). Plant functional trait response to environmental drivers across European temperate forest understorey communities. *Plant Biol.* 22, 410–424. doi: 10.1111/plb.13082

Mantilla-Contreras, J., Schirmel, J., and Zerbe, S. (2012). Influence of soil and microclimate on species composition and grass encroachment in heath succession. *J. Plant Ecol.* 5, 249–259. doi: 10.1093/jpe/rtr031

Méndez-Toribio, M., Ibarra-Manríquez, G., Navarrete-Segueda, A., and Paz, H. (2017). Topographic position, but not slope aspect, drives the dominance of functional strategies of tropical dry forest trees. *Environ. Res. Lett.* 12, 085002. doi: 10.1088/1748-9326/aa717b

Mitchell, R. M., Wright, J. P., and Ames, G. M. (2016). Intraspecific variability improves environmental matching, but does not increase ecological breadth along a wet-to-dry ecotone. *Oikos* 126, 988–995. doi: 10.1111/oik.04001

Molina-Venegas, R., Aparicio, A., Lavergne, S., and Arroyo, J. (2018). Soil conditions drive changes in a key leaf functional trait through environmental

filtering and facilitative interactions. *Acta Oecol.* 86, 1–8. doi: 10.1016/j.actao.2017.11.008

Niinemets, U., Portsmuth, A., and Tobias, M. (2006). Leaf size modifies support biomass distribution among stems, petioles and mid-ribs in temperate plants. *New Phytol.* 171, 91–104. doi: 10.1111/j.1469-8137.2006.01741.x

Ordoñez, J. C., van Bodegom, P. M., Witte, J.-P. M., Wright, I. J., Reich, P. B., and Aerts, R. (2009). A global study of relationships between leaf traits, climate and soil measures of nutrient fertility. *Global Ecol. Biogeogr.* 18, 137–149. doi: 10.1111/j.1466-8238.2008.00441.x

Pérez-Harguindeguy, N., Diaz, S., Garnier, E., Lavorel, S., Poorter, H., Jaureguiberry, P., et al. (2013). New handbook for standardised measurement of plant functional traits worldwide. *Aust. J. Bot.* 61, 167–234. doi: 10.1071/BT12225

Pinho, B. X., de Melo, F. P. L., Arroyo-Rodriguez, V., Pierce, S., Lohbeck, M., and Tabarelli, M. (2018). Soil-mediated filtering organizes tree assemblages in regenerating tropical forests. *Plant Biol.* 106, 458–463. doi: 10.1111/1365-2745.12843

Punchi-Manage, R., Getzin, S., Wiegand, T., Kanagaraj, R., Gunatilleke, C. V. S., Nimal Gunatilleke, I. A. U., et al. (2012). Effects of topography on structuring local species assemblages in a Sri Lankan mixed dipterocarp forest. *J. Ecol.* 101, 149–160. doi: 10.1111/1365-2745.12017

Qiu, K. Y., Xie, Y. Z., Xu, D. M., Qi, T. Y., and Pott, R. (2018). Photosynthesis-related properties are affected by desertification reversal and associated with soil n and p availability. *Braz. J.Bot.* 41, 329–336. doi: 10.1007/s40415-018-0461-0

R Core Team (2021). *R: A language and environment for statistical computing* (Vienna: R Foundation for Statistical Computing). Available at: https://www.R-project.org/.

Ren, L., Huang, Y. M., Pan, Y. P., Xiang, X., Huo, J. X., Meng, D. H., et al. (2022). Differential investment strategies in leaf economic traits across climate regions worldwide. *Front. Plant Sci.* 13. doi: 10.3389/FPLS.2022.798035

Schmitt, S., Trueba, S., Coste, S., Ducouret, E., Tysklind, N., and Heuertz, M. (2022). Seasonal variation of leaf thickness: An overlooked component of functional trait variability. *Plant Biol.* 24, 458–463. doi: 10.1111/PLB.13395

Shipley, B. (2006). Net assimilation rate specific leaf area and leaf mass ratio: Which is most closely correlated with relative growth rate? a meta-analysis. *Funct. Ecol.* 20, 565–574. doi: 10.2307/3806604

Venn, S. E., Gallagher, R. V., and Nicotra, A. B. (2021). Germination at extreme temperatures: Implications for alpine shrub encroachment. *Plants-Basel.* 10, 327–327. doi: 10.3390/plants10020327

Violle, C., Navas, M. L., Vile, D., Kazakou, E., Fortunel, C., Hummel, I., et al. (2007). Let the concept of trait be functional! *Oikos* 116, 882–892. doi: 10.1111/j.0030-1299.2007.15559.x

Wang, J., Wang, X., Ji, Y., and Gao, J. (2022). Climate factors determine the utilization strategy of forest plant resources at large scales. *Front. Plant Sci.* 2022 (13). doi: 10.3389/fpls.2022.990441

Wang, R. L., Yu, G. R., He, N. P., Wang, Q. F., Zhao, N., and Xu, Z. ,. W. (2016). Latitudinal variation of leaf morphological traits from species to communities along a forest transect in eastern China. *J. Geog. Sci.* 26, 15–26. doi: 10.1007/s11442-016-1251-x

Wright, I. J., Reich, P. B., and Westoby, M. (2001). Strategy shifts in leaf physiology, structure and nutrient content between species of high- and low-rainfall and high- and low-nutrient habitats. *Funct. Ecol.* 15, 423–434. doi: 10.1046/j.0269-8463.2001.00542.x

Wright, I. J., Reich, P. B., Westoby, M., Ackerly, D. D., Baruch, Z., Bongers, F., et al. (2004). The worldwide leaf economics spectrum. *Nature* 428, 821–827. doi: 10.1038/nature02403

Xu, G. Q., Arndt, S. K., and Farrell, C. (2020). Leaf traits of drought tolerance for 37 shrub species originating from a moisture gradient. *Water* 12, 1626. doi: 10.3390/w12061626

frontiers | Frontiers in Plant Science

TYPE Original Research
PUBLISHED 06 January 2023
DOI 10.3389/fpls.2022.1052791

OPEN ACCESS

EDITED BY
Antonio (Antonello) Montagnoli,
University of Insubria, Italy

REVIEWED BY
Lorenzo Rossi,
University of Florida, United States
Fabio Gomes,
Universidade Estadual de Santa Cruz, Brazil

*CORRESPONDENCE
Youjun Chen
chenyoujun2005@163.com

SPECIALTY SECTION
This article was submitted to Functional Plant Ecology, a section of the journal Frontiers in Plant Science

RECEIVED 24 September 2022
ACCEPTED 05 December 2022
PUBLISHED 06 January 2023

CITATION
Chen X, Chen Y, Zhang W, Zhang W, Wang H and Zhou Q (2023) Response characteristics of root to moisture change at seedling stage of *Kengyilia hirsuta*.
Front. Plant Sci. 13:1052791.
doi: 10.3389/fpls.2022.1052791

Response characteristics of root to moisture change at seedling stage of *Kengyilia hirsuta*

Xueyao Chen[1], Youjun Chen[1,2]*, Wei Zhang[1,2], Wenlu Zhang[1,2], Hui Wang[1,2] and Qingping Zhou[1,2]

[1]Sichuan Zoige Alpine Wetland Ecosystem National Observation and Research Station, Southwest Minzu University, Chengdu, China, [2]Institute of the Qinghai-Tibetan Plateau, Southwest Minzu University, Chengdu, China

Kengyilia hirsuta is an important pioneer plant distributed on the desertified grassland of the Qinghai-Tibet Plateau. It has strong adaptability to alpine desert habitats, so it can be used as a sand-fixing plant on sandy alpine land. To study the response mechanisms of root morphological and physiological characteristics of *K. hirsuta* to sandy soil moisture, 10%, 25% and 40% moisture levels were set up through potted weighing water control method. The biomass, root-shoot ratio, root architecture parameters, and biochemical parameters malondialdehyde, free proline, soluble protein, indole-3-acetic acid, abscisic acid, cytokinin, gibberellin, relative conductivity and antioxidant enzyme activities were measured in the trefoil stage, and the response mechanisms of roots at different moisture levels were analyzed. The results showed that with the increase of soil moisture, root morphological indexes such as root biomass, total root length, total root volume and total root surface increased, while the root topological index decreased continuously. The malondialdehyde content, relative conductivity, superoxide dismutase activity, peroxidase activity, catalase activity, free proline content, soluble protein content, abscisic acid content and cytokinin content at the 25% and 40% moisture levels were significantly decreased compared with the 10% level ($P< 0.05$). Thus, the root growth of *K. hirsuta* was restricted by the 10% moisture level, but supported by the 25% and 40% moisture levels. An artificial neural network revealed that total root length, total root surface area, root link average length, relative conductivity, soluble protein, free proline and moisture level were the key factors affecting root development. These research results could contribute to future agricultural sustainability.

KEYWORDS

***Kengyilia hirsuta*, seedling stage, soil moisture, root architecture, root physiological**

1 Introduction

The alpine grassland of northwest Sichuan located in the southeastern margin of the Qinghai-Tibet Plateau has an important ecological function and is a major water source, which is of great significance to the ecological security of the lower reaches of the Yangtze and Yellow Rivers (Lu et al., 2004; Yu et al., 2011). In recent years, with the increasing population and the demands of social development, which have exerted great pressure on desertified areas, the ecological system has been disturbed and natural resources have been depleted in Northwest China. Since the 1960s, the average annual growth rate of the dune area in the northwest of Sichuan has reached 3.44% (Wei et al., 2010), affecting the development of animal husbandry and leading to the deterioration of the ecological environment (Gou et al., 2019). Against the background of the severe expansion of grassland desertification, choosing suitable herbage species as sand-fixing materials is the main way to achieve good results in artificial restoration of desertified grassland (Chen et al., 2019). Therefore, the selection of pioneer plants with poor-soil and drought tolerance is important to maintain a stable ecosystem.

Kengyilia hirsuta is one of the main pioneer grass species distributed on the desertified grassland of the Qinghai-Tibet Plateau, and has strong adaptability to alpine desert habitats, with drought and wind erosion resistance characteristics (Ren, 2016), so it can be used as a forage resource and sand-fixing plant on sandy alpine land. The adaptability of *K. hirsuta* to sandy land mainly depends on the growth and development of its root system, and this trait is co-regulated by internal genetic factors and external environmental factors (Chen et al., 2020).

Soil moisture is the key factor restricting plant growth and development, and the most important factor affecting vegetation restoration in desertified grassland (Knapp et al., 2015). When the soil moisture changes, the root system is the first part affected in desert species (Schiefelbein and Benfey, 1991). Morphological and physical characteristics are the main factors that respond to the complicated environment of desertified grassland, and the biomass, root-shoot ratio, root architecture and root physiology of a plant change under different soil moisture levels (Merchan et al., 2010).

Previous studies have shown that the biomass of plants is the cumulative product of photosynthesis and determined by their photosynthetic capacity (Hester et al., 2001). Under drought stress conditions, aboveground biomass accumulation moves to underground parts, which adapt to the variable environment by changing the root-shoot ratio, enhancing the plant's ability to resist drought stress (Wang et al., 2016). Root architecture determines the distribution of the root system in the soil space, including root morphology, fractal characteristics and topological structure (Su et al., 2018), and the root system can respond to changes in the external environment through changes of root architecture; for example, total root length, root surface area and root volume are basic indexes closely related to soil moisture (Zeng et al., 2013). Besides, average root diameter, root link average length, number of root tips and number of forks are also closely related to the development of roots in different moisture environments. Where, root link average length is the average length between all two branches of the root system (Tang et al., 2020). Fractal abundance and the fractal dimension are important characteristics of root fractal structure, and the root fractal dimension can be used to study the degree of branching and development, while the fractal abundance is closely related to the extension range and resource competitiveness of roots (Yang and Luo, 1994; Yang et al., 2009). As part of the root system architecture, the topological structure determines the spatial distribution of roots in the soil and affects the nutrient absorption and fixation capacity of roots (Berntson, 1997). The closer the topology index (TI) is to 0.5, the closer the root branching habit is to dichotomous branching, while the closer TI is to 1, the more the root branching habit is similar to herringbone branching (Shan et al., 2012). Under drought stress conditions, root development will be affected to some extent, the fractal dimension and fractal abundance of roots will change, and the root branching mode will tend toward herringbone branching, which is an adaptive strategy for plant roots to expand their space and effectively utilize water and nutrients (Yang et al., 2018).

Root physiology changes with the change of soil moisture, which ultimately affects the root morphological structure (Li et al., 2001). Under conditions of soil moisture deficit, the number of free radicals in plant cells rises, which aggravates membrane lipid peroxidation and affects membrane permeability, resulting in the accumulation of malondialdehyde (MDA) (Lorenz et al., 2011; Zhao et al., 2011), which is a harmful peroxidation product that increases of relative conductivity (RC) (Harfouche et al., 2014). When subjected to drought stress, to protect cell membranes from oxidative damage, the enzyme defense system, namely antioxidant enzymes including catalase (CAT), superoxide dismutase (SOD) and peroxidase (POD), removes excess reactive oxygen species, protects cells from free radical damage and reduces the degree of membrane lipid peroxidation (Pauls and Thompson, 1980; Gao and Zhang, 1998; Kholová et al., 2011). At the same time, under conditions of insufficient or excessive soil moisture, some osmotic regulatory substances including proline (Pro), soluble protein (SP), and soluble sugar (SS), are accumulated to maintain osmotic potential so that plants can obtain the water needed, ensure normal growth and improve their resilience to adversity (Manivannan et al., 2008). Plant endogenous hormones, chemical signaling substances produced in some cells or tissues (Tiwari et al., 2017), can regulate the physiological processes of other cells by interacting with specific protein receptors. Among these hormones, abscisic acid (ABA), indole-3-acetic acid (IAA), gibberellin (GA) and cytokinin (CTK) play important roles in regulating plant root development under water stress (Tiwari

et al., 2017).

In this experiment, we selected *K. hirsuta* as the experimental material and measured the biomass, root-shoot ratio, root architecture parameters and physiological indexes to reveal changes of root architecture and root physiology at 10%, 25% and 40% moisture levels. To quantify root morphological and physiological indicators of root system development under different moisture levels, artificial neural network (ANN) model analysis was used to evaluate the importance of root architecture, physiological indexes and field water capacity in determining root biomass. This analysis revealed the regulatory mechanism of root adaptation to soil moisture changes at the seedling stage and explored the sand-growing characteristics of *K. hirsuta* to lay a foundation for resource development and variety breeding of pioneer grass species.

2 Materials and methods

2.1 Materials

Kengyilia hirsuta which grows in high altitude and alpine desert areas has developed a 'rhizosheath-root system' as a xerophytic adaptive-trait. It is a plant species of genus *Kengyilia* Yen et J. L. Yang, and no other varieties have been found or cultivated at present. The seeds and sandy soil for the test were collected by the forage grass team of Qinghai-Tibet Plateau Research Institute of Southwest Minzu University in the sandy grassland in Waqie Town, Hongyuan County, Tibetan Qiang Autonomous Prefecture of Ngawa, Sichuan Province. The temperature difference between day and night in the sandy land in this area is large in summer. The sand surface is directly exposed to the sun during the day, and its temperature can reach more than 50°C, while can be as low as about 5°C at night and it has been enclosed in the past five years.

2.2 Experimental design

Three soil moisture gradients were set up by potted water control method, which were 10%, 25% and 40% field capacity, respectively. These soil moisture gradients are set for research, because the soil moisture of sandy grassland in Hongyuan county is about 3% ~ 8% and through pre-test screening, the phenotypes of *K. hirsuta* under these three water gradients are quite different.

Based on our experiment design, the completely randomized block design method has been chosen. The seedlings with identical growth were randomly divided into three groups. There were 48 replicates in each group and one seedling in each replicate. Meanwhile, each group was treated with 10%, 25% and 40% field capacity respectively, and other conditions were kept consistent. The specific steps were as follows:

The seeds were sterilized with 75% ethanol for 1min, washed for 3 times with distilled water, soaked in distilled water for 8h, and then washed for 3 times. Then, seeds of the same size and full size were spread in the Petri dish and were cultivated in an artificial climate box at a day/night temperature of 24/20°C with a photoperiod of 14/10 h light/dark, illumination of 30000 lx, and relative humidity ranging from 50 to 60%. After growing for 3 cm, seedings with the same growth were selected and transplanted into the PS nutrient bowl filled with the tested sandy soil. Each pot with one plant is poured with soil moisture (100% FC) and placed in the artificial climate box with the same culture condition as above. The seedling pot position was randomly changed every two days during the seedling culture period. Irrigate thoroughly on the 5th day after transplanting, and stop watering afterwards. When the soil moisture in all nutrient pots has dropped to 10% field capacity, seedlings were randomly divided into three groups, then weighed and watered according to the three designed moisture levels. The balance was used to weigh and then water was added to the set value at the same time every morning (10:00). Samples were taken when the plants grew to the three leaf stage.

2.3 Determination and measurement

After being loaded into the centrifugal tube, the roots were quickly put into the liquid nitrogen barrel, and then stored at -80°C to measure activity of antioxidant enzymes, MDA content, free Pro content, SP content and hormones content.

2.3.1 Measurement of biomass

The whole plants were taken out from the nutrition bowl, then the roots were washed with distilled water and packed in envelopes. Afterward, samples were put into the oven at 110°C for 10 min and dried at 75°C until constant weight to measure abovground and root dry weight. Root-root shoot ratio was calculated as the ratio of underground dry weight to overground dry weight (Agathokleous et al., 2019).

2.3.2 Measurement of root morphology

Root morphology was determined according to Liu et al. (2019). The roots in the transparent tray were scanned using a root scanner (EPSON Expression 12000XL) at a pixel of 600 dpi. Then the root analysis software (Win RHIZO Pro 2017A) was used to calculate and analyze the morphological indexes of the scanned original image, and the morphological indexes such as total root length, total root surface area, total root volume, average root diameter, root link average length, number of root tips and number of forks were obtained.

2.3.3 Calculation of root fractal dimension and fractal abundance

Root analysis software (Win RHIZO Pro 2017A) was used to analyze the original image scanned by the digital scanner (EPSON Expression 12000XL), and the small square with side length r on the root distribution map and the number of small squares cut by the root, Nr, were obtained. The graph was drawn with logr and logNr as horizontal and vertical coordinates respectively. The equation of the regression line was as follows (Ketipearachchi and Tatsumi, 2000):

$$\log Nr = -FD\log r + \log K$$

In this formula, K is the constant value. The negative number of the slope of the regression line is the fractal dimension FD and logK is the fractal abundance.

2.3.4 Calculation of root topological index

The root topological index (TI) was calculated as follows (Ma and Wang, 2020):

$$TI = \lg A / \lg M$$

In the above formula, A is the total number of internal connections of the longest root channel; M is the total number of all external connections of the root system. Both A and M values could be calculated in the root analysis software (Win RHIZO Pro 2017A).

2.3.5 Determination of malondialdehyde (MDA) content and relative conductivity (RC)

MDA content was assayed using Thiobarbituric acid reaction according to Draper and Hadley (1990). The 0.2 g sample and 1.6 ml 10% trichloroacetic acid solution were mixed and ground into pulp, centrifuged at 8000 g at 4°C for 10 min, and placed on ice for testing. After mixing 1.5 ml supernatant and 1.5 ml thiobarbituric acid solution, the mixture was placed in a 95°C water bath for 30 min, cooled in an ice bath, and centrifuged at 10000g for 10 min. The absorption (OD) values at 532 nm and 600 nm were measured. MDA content was determined according to fresh weight.

RC was measured by electrolyte extravasation volume method according to Luo et al. (2014). 0.2 g of fresh root was taken from each treatment and 4 ml of deionized water was added. After 24 h at room temperature, the conductivity of the solution R1 was measured. Then, the solution was boiled in a constant temperature water bath at 100°C for 20 min, and the solution conductivity R2 was measured after cooling to room temperature with cold water. The RC was calculated as follows:

$$RC\,(\%) = R1/R2 \times 100\,\%$$

2.3.6 Determination of free proline (Pro) content and soluble protein content (SP)

Free Pro contwas determined by sulfosalicylic acid method reported by Zhang and Nie (2008). The 0.2g sample was mixed with 5mL 3% sulfosalicylic acid solution, extracted in a boiling water bath for 10 min, and then filtered after cooling. After being added 2 ml of filtrate, 2 ml of glacial acetic acid, and 2 ml of ninhydrin acid, the mixture was heated in a boiling water bath. After cooling, 4 ml toluene was added to the sample, shaken for 30 s, left for a while, 10 ml of the upper solution was taken and centrifuged at 3000g for 5 min. After that, the upper Pro red toluene solution was absorbed into the colorimetric cup, toluene was used as the blank control, OD value was measured at 520nm wavelength on the spectrophotometer, and Pro standard curve was made. SP content was estimated following the method of Coomassie Brilliant Blue according to Bradford (1976). 0.1 g sample was added with 1 ml PBS buffer solution, ground and homogenized, centrifuged at 8000g for 10 min. 1 ml supernatant was placed in a centrifuge tube, then 5ml Coomash bright blue solution was add. After mixing, the OD value at 620 nm was determined. The SP content was determined by the standard curve.

2.3.7 Determination of antioxidant enzymes

Before the enzyme activity was measured, 0.2 g sample was added with 1.6 ml phosphate buffered saline (PBS), ground and homogenized, centrifuged at 8000g for 10 min, and the supernatant was taken and placed on ice for testing.

Referring to the study of Giannopolitis and Ries (1977), the activity of superoxide dismutase (SOD) was measured by nitroblue tetrazolium (NBT) photochemical reduction. One unit of SOD was defined as the amount of enzyme that inhibited the photochemical reduction of nitroblue tetrazole by 50%, and the OD value was measured at 560 nm. The activity of peroxidase (POD) was assessed using guaiacol method, and the OD value was measured at 470 nm (Nahid and Abdollah, 2018). Catalase (CAT) activity was determined by the method of UV absorption method, and the initial OD values and 1 min later OD values were determined at 240 nm (Zhang et al., 2018). When CAT was added into the reaction system, the absorbance of the reaction solution would decrease with the reaction time. Therefore, the activity of CAT could be calculated according to the change rate of the absorbance of the reaction solution.

2.3.8 Determination of hormones contents

0.1 g sample was added to 0.9 mL PBS with pH=7.2~7.4, and then ground into homogenate. The supernatant was collected from homogenate separated by centrifugation at 4°C at 3000g for 20 min. The contents of abscisic acid (ABA), indole-3-acetic

acid(IAA), gibberellin (GA) and cytokinin (CTK) in roots of *K. hirsuta* were determined using the Enzyme-Linked ImmunoSorbent Assay (ELISA) kit following the instructions from the manufacturer (Jiangsu Meimian industrial Co., Ltd. Jiangsu, China). The OD value of each hormone were detected *via* enzyme-labeled instrument (Varioskan LUX, Thermo Fisher Scientific). Linear regression equations of ABA, IAA, GA and CTK standard curves were calculated by using the concentration and OD value of the standard material.

2.4 Data analysis

2.4.1 Artificial neural network analysis

Artificial neural network, an algorithm-based mathematical model that repeatedly adjusts the network connected between a large number of internal nodes by imitating the information processing capacity of biological neurons (Bagheri et al., 2017), can identify the complex nonlinear relationship between input and output variables (Rahimikhoob, 2010; Rossi et al., 2019). Multilayer perceptron ANN (MLPANN) normally has three layers, including an input layer, a hidden layer with multiple neurons, and an output layer, and is capable of Clarifying the most cluttered information (Mateo et al., 2011; Biglarijoo et al., 2017). Therefore, this paper chose MLPANN to build a neural network model, and used three-layer network to describe the mapping between the input and the output. After training and comparative analysis, the effects of root structure, physiology and field capacity on root biomass were explored.

P_i was the input layer, which was the root architecture and physiological indexes of *K. hirsuta* at seedling stage.

The output of the hidden layer is:

$$Y_i = F_j\left(\sum_{i=1}^{M} w_{ij} x_i\right)$$

Where Y_i is the hidden layer, w_{ij} is the connection weight between input layer i and hidden layer j, and x_i is the input value. F_j, the nonlinear activation function which is developed to calculate the output value of the hidden layer, is the hyperbolic tangent function (tanh). The formula is as follows:

$$F_j(u) = \frac{\sinh u}{\cosh u} = \frac{e^u - e^{-u}}{e^u + e^{-u}}$$

The value of the output layer is the root biomass. Then the output of the output layer unit is:

$$T_k = F_k\left(\sum_{i=1}^{M} w_{jk} x_j\right)$$

Where T_k is the output layer, w_{jk} is the connection weight between hidden layer j and output layer k, and x_i is the input value. F_k, the linear activation function which is developed to calculate the output value of the output layer, is the identity function. The output value is calculated as follow:

$$F_k(u) = u$$

In order to eliminate the influence caused by the large difference in the order of magnitude of index values, the measured data are normalized. After normalization, the values of each factor are distributed between [-1, 1]. In this paper, the data normalization and the inverse normalization of the simulated values output by the neural network are completed by using SPSS 26.0 software. The formula for data standardization is:

$$I_i = \frac{x_{i-u}}{x_{max} - x_{min}}$$

In this formula, I_i is the standardized value; x_i is the measured value of index i; x_{min} and x_{max} are the minimum and maximum values of index i samples. u is the average of all samples of this indicator.

2.4.2 Result processing

Results were analyzed by one-way ANOVA and tested for significance of difference by Duncan multiple-range method, the statistical significance level was below 0.05. Bivariate Pearson correlation analysis was used to analyze the relationship between physiological and morphological indexes. The neural network model of the influence of root architecture indexes, physiological indexes and field capacity on biomass was established by Multilayer perceptron. The data in the figures and tables represented as the mean ± standard error of 4 repetitions in the test. Excel 2016 was employed for summarizing all statistics, SPSS 26.0 was used for data analysis and Origin 2018 was assigned to plotting.

3 Results

3.1 Biomass and root-shoot ratio characteristics of *K. hirsuta* at the seedling stage under different soil moisture conditions

With the increasing soil moisture gradient, the biomass of *K. hirsuta* at the seedling stage showed an upward trend (Figure 1). The total biomass and aboveground biomass of plants grown in soil under 25% and 40% field capacity were greater than those under 10% field capacity ($P< 0.05$) (Figures 1A, C), but no significant difference between 25% and 40% field capacity was observed in these data ($P > 0.05$). There were significant differences in root biomass among the 10%, 25% and 40% field capacity treatments ($P< 0.05$). Moreover, as field capacity increased, root biomass increased. The root biomasses in the 25% and 40% field capacity treatments were 1.3 and 1.6 times higher than that of the 10% field capacity treatment, respectively (Figure 1B). However, the root-shoot ratio showed

10.3389/fpls.2022.1052791

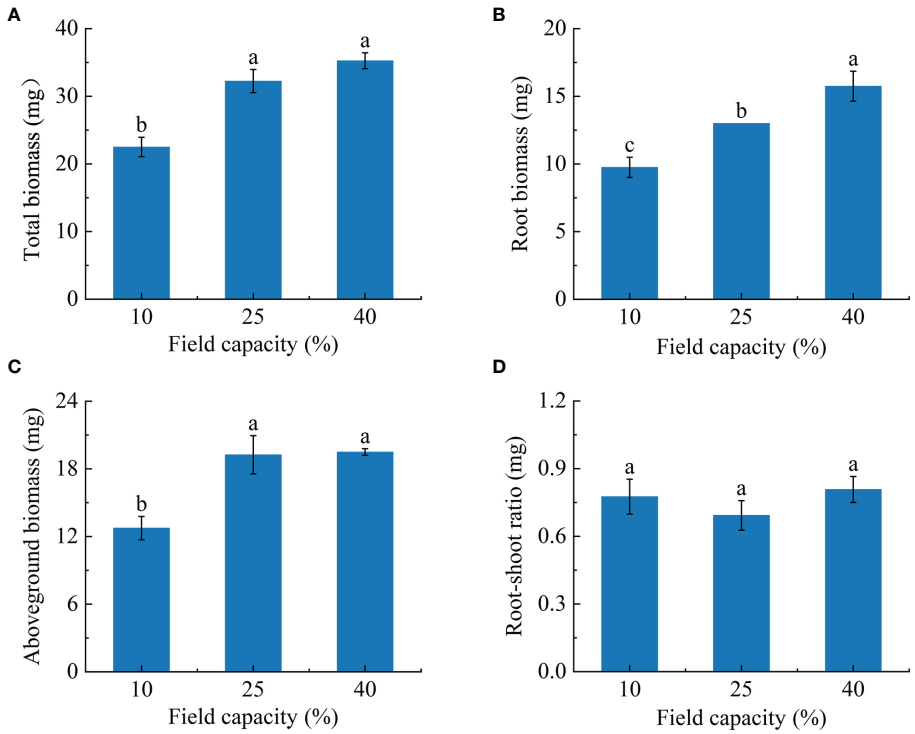

FIGURE 1
Effects of different soil moisture on total biomass **(A)**, root biomass **(B)**, aboveground biomass **(C)** and root-shoot ratio **(D)** of *K hirsuta*. Results were analyzed by one-way ANOVA and tested for significance of difference by Duncan multiple-range method. Each value represents the mean ± standard error. Each experiment was repeated four times. Different letters indicate that the differences between treatments were significant ($P< 0.05$).

no significant changes under different field capacities ($P > 0.05$) (Figure 1D).

3.2 Root morphology characteristics of *K. hirsuta* at the seedling stage under different soil moisture conditions

Most root morphological indexes were sensitive to the different soil moisture conditions. The total root length, total root volume and total root surface area of plants grown in soil under the three field capacity treatments showed remarkable differences ($P< 0.05$). The total root length, total root volume and total root surface area increased with increasing soil moisture. Total root length in the 25% and 40% field capacity treatments was 1.3 and 1.7 times than that in the 10% field capacity treatment, respectively (Figure 2A), total root surface area was 1.5 and 1.9 times greater, respectively (Figure 2B), and total root volume was 1.3 and 1.9 times greater, respectively (Figure 2C). However, no notable differences were observed for average root diameter ($P > 0.05$) (Figure 2D).

As the soil moisture rose, the number of root tips and forks first increased and then decreased. The numbers of root tips and forks under 10% field capacity were significantly lower than those under 25% and 40% field capacity ($P< 0.05$). The numbers of root tips and forks under 25% field capacity were 2.4 and 2.3 times those under 10% field capacity, and 1.3 and 1.2 times those under 40% field capacity, respectively (Figures 3A, B). The root link average length under 40% field capacity was significantly longer than those under 25% and 10% ($P< 0.05$) (Figure 3C).

3.3 Root fractal dimension, fractal abundance and root topological index characteristics of *K. hirsuta* at the seedling stage under different soil moisture conditions

There were no marked differences in the root fractal dimension ($P >0.05$) (Table 1). As can be seen from the table, the root fractal abundances of the 25% and 40% field capacity

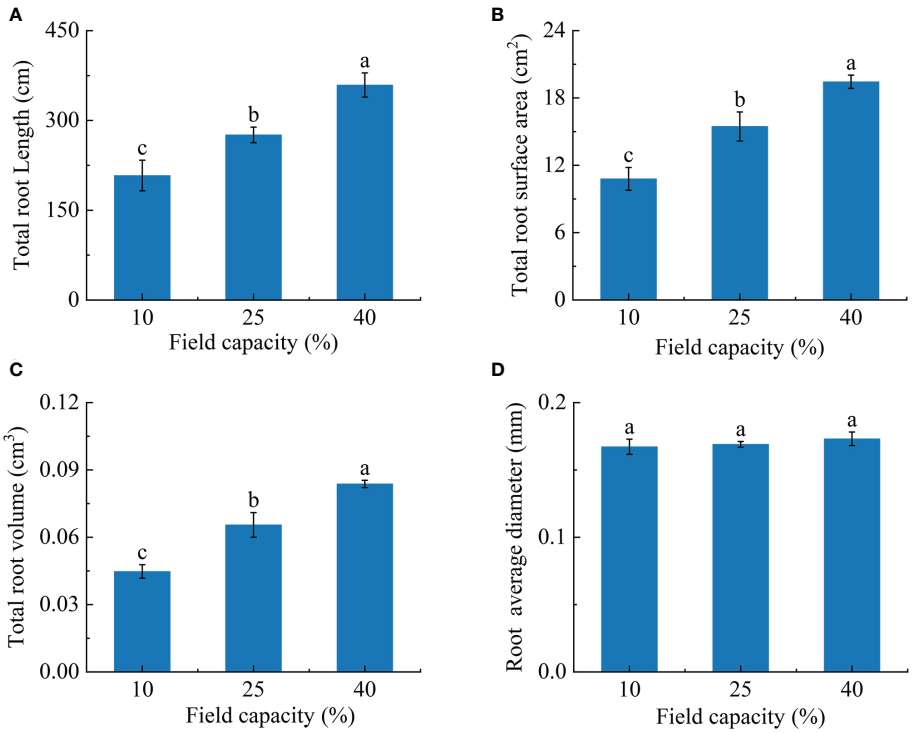

FIGURE 2
Effects of different soil moisture on total root length **(A)**, total root surface area **(B)**, total root volume **(C)** and average root diameter **(D)** of *K hirsuta*. Results were analyzed by one-way ANOVA and tested for significance of difference by Duncan multiple-range method. Each value represents the mean ± standard error. Each experiment was repeated four times. Different letters indicate that the differences between treatments were significant ($P< 0.05$).

treatments were greater than that of the 10% field capacity treatment ($P<0.05$), but there were no significant differences between the 25% and 40% field capacity treatments ($P >0.05$).

As the soil moisture rose, the root topological index of *K. hirsuta* decreased continuously (Table 1). The topological index under 10% field capacity was significantly higher than those under 25% and 40%, which were closer to 1 ($P<0.05$). This result indicated that the root branching pattern changed from dichotomous branching to herringbone branching with the decrease of soil moisture.

3.4 Membrane permeability and osmotic regulatory substances characteristics in *K. hirsuta* roots at the seedling stage under different soil moisture conditions

The investigation showed that the MDA content and RC of roots varied with different soil moisture treatments (Figure 4). The MDA content of roots under 10% field capacity was significantly higher than those under 25% and 40% ($P< 0.05$), at 1.7 and 1.5 times, respectively. Additionally, there were significant differences in RC among the three field capacity treatments ($P< 0.05$). The RC displayed a declining trend with the increase of soil moisture, being lowest in the 40% field capacity treatment (Figure 4B).

With the increase of soil moisture, the free Pro and SP contents decreased (Figure 4). The free Pro and SP contents of roots under 10% field capacity were notably higher than those under 25% and 40% field capacity ($P< 0.05$), but no significant differences were found between the 25% and 40% field capacity treatments ($P >0.05$).

3.5 Antioxidant enzyme activities characteristics in *K. hirsuta* roots at the seedling stage under different soil moisture conditions

With the increasing soil moisture, the activities of root antioxidant enzymes first decreased and then increased slightly (Figure 5). The SOD and POD activities at 10% field capacity were significantly higher than those at 25% and 40% field capacity ($P< 0.05$). Compared with 25% and 40% field

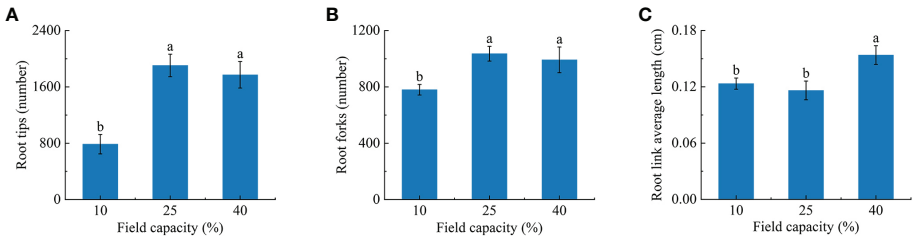

FIGURE 3
Effects of different soil moisture on root tips **(A)**, root forks **(B)**, root link average length **(C)** of *K hirsuta*. Results were analyzed by one-way ANOVA and tested for significance of difference by Duncan multiple-range method. Each value represents the mean ± standard error. Each experiment was repeated four times. Different letters indicate that the differences between treatments were significant ($P< 0.05$).

capacity, SOD activity was increased by 165.0% and 126.6% (Figure 5A), and POD activity was increased by 186.0% and 145.1% (Figure 5B), respectively, under 10% field capacity. Notable differences were observed for CAT activity among the three field capacity treatments ($P< 0.05$) and CAT activity under 10% field capacity was increased by 218.8% and 92.1% compared with 25% and 40% field capacity, respectively (Figure 5C).

3.6 Hormones contents in *K. hirsuta* roots at the seedling stage under different soil moisture conditions

Root hormone contents varied under the different soil moisture treatments (Figure 6). With the increase of soil moisture, the ABA content showed a significant trend of an initial decrease followed by an increase ($P< 0.05$), and was lowest

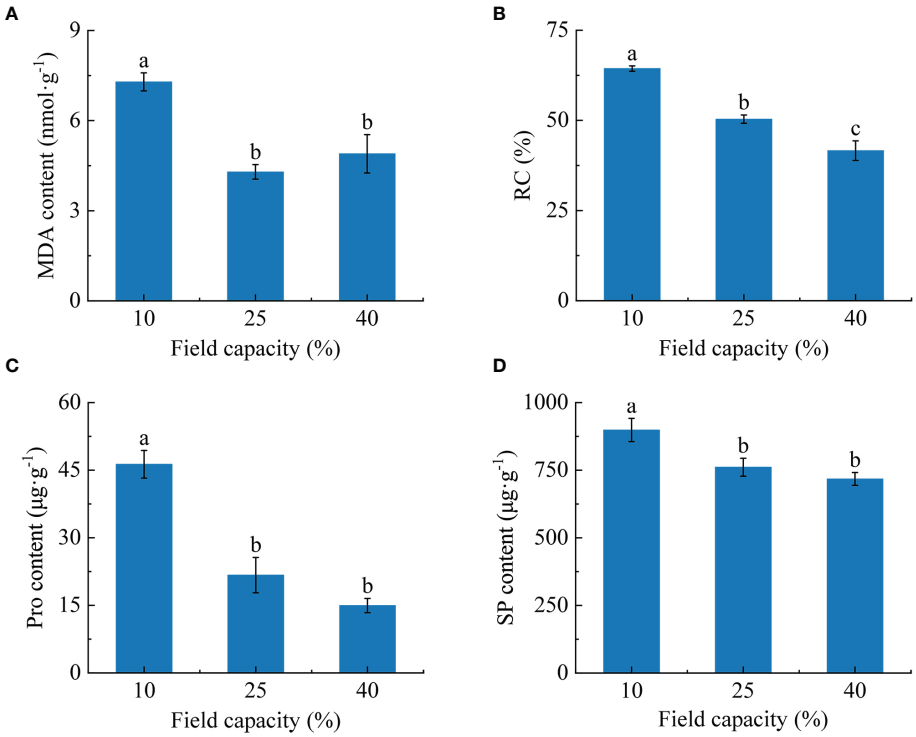

FIGURE 4
Effects of different soil moisture on malondialdehyde (MDA) content **(A)**, relative conductivity (RC) **(B)**, proline (Pro) content **(C)** and soluble protein (SP) content **(D)** of *K hirsuta*. Results were analyzed by one-way ANOVA and tested for significance of difference by Duncan multiple-range method. Each value represents the mean ± standard error. Each experiment was repeated four times. Different letters indicate that the differences between treatments were significant ($P< 0.05$).

TABLE 1 Effects of different soil moisture on root fractal dimension, root fractal abundance and root topological index of *K. hirsuta*.

Field capacity (%)	Root fractal dimension	Root fractal abundance	Root topological index
10%	1.263 ± 0.045a	3.323 ± 0.110b	0.819 ± 0.053a
25%	1.229 ± 0.019a	3.557 ± 0.050a	0.762 ± 0.019b
40%	1.2495 ± 0.015a	3.638 ± 0.051a	0.755 ± 0.013b

Results were analyzed by one-way ANOVA and tested for significance of difference by Duncan multiple-range method. Each value represents the mean ± standard error. Each experiment was repeated four times. Different letters indicate that the differences between treatments were significant (P< 0.05).

under 25% field capacity (Figure 6A). The IAA content in roots was not obviously affected by the different soil moisture treatments (Figure 6B), and the differences between treatments did not reach a significant level ($P > 0.05$). With the increase of soil moisture, the GA content showed a trend of a significant increase at first and then a slight decline (Figure 6C). The GA content was highest under 25% field capacity and was significantly higher than under 10% ($P< 0.05$). The CTK content was at its maximum under 10% field capacity and was significantly higher than under 25% and 40% ($P< 0.05$) (Figure 6D).

3.7 Correlation analysis of root physiology and root architecture in *K. hirsuta* at the seedling stage under different soil moisture conditions

Correlation analysis was performed on root physiology and root architecture (Figure 7). The results showed that ABA and CTK had significant positive correlation with fractal dimension ($P< 0.05$), and significant negative correlation with root tips and forks ($P< 0.05$). Pro showed a significant positive correlation with topological index ($P< 0.05$), and very significant negative correlation with root biomass, root fractal abundance, total root length, total root volume, root tips and root forks ($P< 0.05$). There was a very significant positive correlation between SP and topological index ($P< 0.01$), significant negative correlation with root biomass, fractal abundance, total root length and forks ($P< 0.05$), and very significant negative correlation with total root surface area and total root volume ($P< 0.01$). MDA had a significant positive correlation with topological index ($P< 0.05$), significant negative correlation with total root length, total root surface area and root forks ($P< 0.05$), and extremely significant negative correlation with fractal abundance and root tips ($P< 0.01$). RC was positively correlated with topological index ($P< 0.05$), negatively correlated with root forks ($P< 0.05$), and extremely significant negatively correlated with fractal abundance, total root length, total root surface area, total root volume and root tips ($P< 0.01$). There were only weak correlations between root morphological indexes and GA or IAA ($P > 0.05$).

3.8 Artificial neural network analysis

The artificial neural network model we established included an input layer, hidden layer and output layer, in which root architecture indexes (including root fractal dimension, root fractal abundance, root topological index, total root length, total root surface area, total root volume, root average diameter, root tips, root forks, and root link average length), root physiology indexes (including MDA, RC, SOD, POD, CAT, Pro, SP, ABA, IAA, GA and CTK) and the three field capacity treatments (10%, 25% and 40%) were used as input variables (a total of 24 values), and the hidden layer was set as 1 layer. After several network tests and adjustments, seven nodes in the hidden layer were determined to give the best estimation. Subsequently,

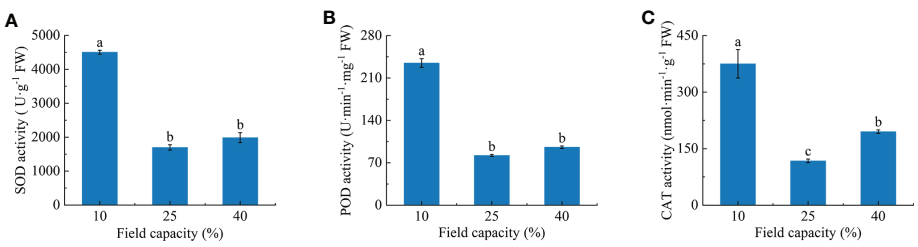

FIGURE 5
Effects of different soil moisture on superoxide dismutase (SOD) **(A)**, peroxidase (POD) **(B)** and catalase (CAT) **(C)** activities of *K hirsuta*. Results were analyzed by one-way ANOVA and tested for significance of difference by Duncan multiple-range method. Each value represents the mean ± standard error. Each experiment was repeated four times. Different letters indicate that the differences between treatments were significant (*P*< 0.05).

10.3389/fpls.2022.1052791

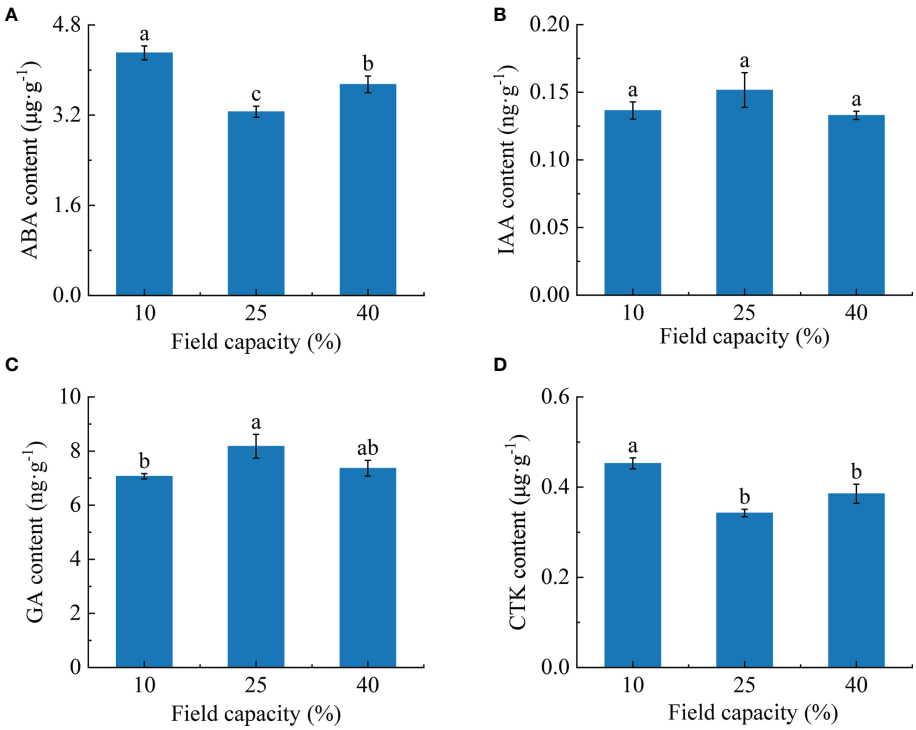

FIGURE 6
Effects of different soil moisture on abscisic acid (ABA) **(A)**, indole-3-acetic acid (IAA) **(B)**, gibberellin (GA) **(C)** and cytokinin (CTK) **(D)** contents of *K hirsuta*. Results were analyzed by one-way ANOVA and tested for significance of difference by Duncan multiple-range method. Each value represents the mean ± standard error. Each experiment was repeated four times. Different letters indicate that the differences between treatments were significant ($P< 0.05$).

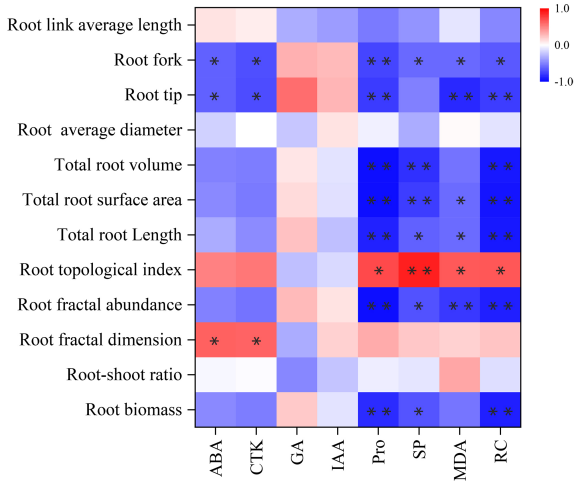

FIGURE 7
Correlation between root physiology and architecture. Each experiment was repeated four times. Significant correlation between root physiology and architecture are indicated by one asterisk (* $P<0.05$) or two asterisk (** $P<0.01$), as determined by Bivariate Pearson correlation analysis.

root biomass was used as the output layer. Finally, the predictive value, relative error and importance of independent variables of the neural network were determined.

The predicted data versus the observed data were plotted for the testing data set, and the coefficients of determination (R^2) were determined (Figure 8). The validation analysis showed that the ANN models gave a high R^2 and low relative error, which were 0.9435 and 0.4%, respectively, indicating that the network model fitted the original data well and had high simulation accuracy, and could be used to analyze the factor importance of other indexes on root biomass.

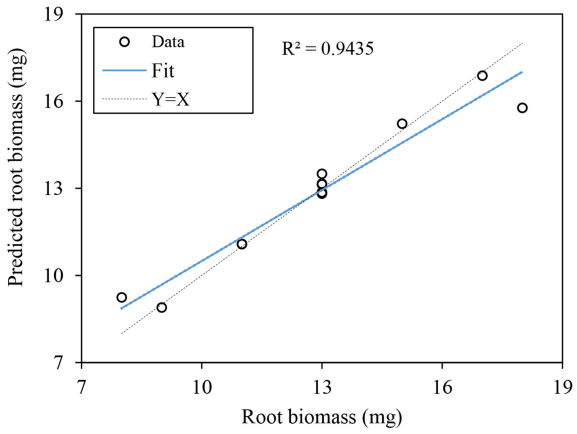

FIGURE 8
Relationship between values of root biomass as measured and predicted by the ANN model.

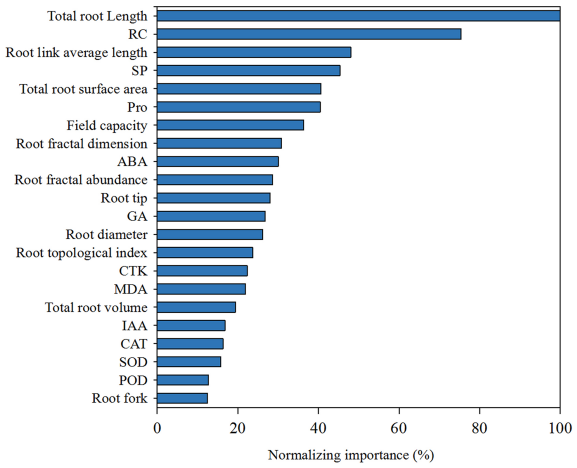

FIGURE 9
The factor importance of root architecture indexes, physiological indexes and Field capacity to root biomass at seedling stage of *K. hirsuta*.

In the results, the indices with higher normalized importance values could explain the variation of the overall development components of *K. hirsuta*. As can be seen from Figure 9, total root length was identified as the most important factor affecting overall root development and showed the greatest normalized importance (100%). Other important factors included RC, root link average length, SP, total root surface area, field capacity and Pro, with normalized importance values in ranked order of 75.4%, 48%, 45.3%, 40.6%, 40.4%, 36.3%, respectively.

4 Discussion

4.1 Effects of different soil moisture conditions on biomass and root-shoot ratio

The biomass of plants is the product of photosynthesis and thus reflects the ability of plants to utilize external nutrients, so it is an important indicator of plant adaptation to water change Hester et al. (2001); Guo et al. (2016) found a significant correlation between biomass and soil moisture in various plants, among which *Tamarix ramosissima* showed a significant positive correlation and *Haloxylon ammodendron* displayed a significant negative correlation with soil moisture. Dalal et al. (2018) reported that the root biomass of wheat increased in response to drought stress, while Sofi et al. (2018) reported that root biomass showed a downward trend when *Phaseolus vulgaris* L. was subjected to drought stress. Consistent with the results of Sofi, our research revealed that total biomass, root biomass and aboveground biomass were significantly lower under 10% field capacity than under 25% and 40%. These results suggested that the growth and development of *K. hirsuta* was restricted under the 10% field capacity condition, which represents an arid environment, and the photosynthetic capacity of seedlings was weakened, resulting in a decrease of photosynthetic product, while field capacities of 25% and 40% were beneficial to the survival of *K. hirsuta*, and thus increased biomass accumulation (Rahman et al., 2020).

The root-shoot ratio directly reflects the distribution of aboveground and root biomass (Enquist and Niklas, 2002). According to many studies, when a plant encounters drought stress, the substance distribution changes and the amount of assimilates transported from aboveground parts to the roots increases, which makes the root-shoot ratio rise as the plant seeks more water (Smucker and Aiken, 1992). It was reported that the root-shoot ratio of maize at different growth stages increased with increasing degrees of drought (Benjamin et al., 2014). Nevertheless, there were no obvious changes in our study when *K. hirsuta* was exposed to different soil moisture contents. This might have been because *K. hirsuta* is a drought-tolerant species, and the root-shoot ratio is controlled by its own genetic

mechanism to adapt to a wider range of soil moisture levels, such that changes of field capacity in the range of 10%–40% had no significant effect on the root-shoot ratio (Tang et al., 2020).

4.2 Changes of root architecture under different soil moisture conditions

Root morphology plays an important role in root absorption and utilization of water and nutrients (Lynch, 1995), and can respond to changes of soil moisture to a certain extent (Comas et al., 2013). Some previous studies suggested that when soil moisture was insufficient, the total root length, total root surface area and root diameter of plants increased, which was conducive to the large-scale absorption of soil water and nutrients (Mu et al., 2005), while others had found that drought stress inhibits root growth and development (David, 1991). This discrepancy may be related to plant growth stages and tolerance to water stress. In this study, the total root length, total root volume, total root surface area and root link average length increased as the field capacity rose from 10% to 40%. This is consistent with the finding of Liu et al. (2019), who showed that when soil moisture reduced, root length, root surface area, root volume and other indicators of switchgrass decreased significantly. Our experimental results also showed that root tips and root forks were increased under 25% and 40% field capacity compared with 10%. Scholars have shown that root length and root link average length reflect root elongation and water absorption efficiency (Mu et al., 2005; Tang et al., 2020), as the root tips is one of the main channels for water and nutrients to enter the plant (Ma et al., 2011), root forks reflect the complexity of root architecture (Tang et al., 2020). Therefore, considering the observations reported above, when field capacity was too low, at 10%, which was beyond the adaptive range of *K. hirsuta*, root growth was inhibited, while an increase of soil moisture could promote the root development of *K. hirsuta* at the seedling stage.

Root fractal characteristics and the topological index respond to changes of soil moisture. A higher fractal dimension represents a higher degree of root development (Oppelt et al., 2001), larger fractal abundance indicates a wider distribution range of roots in the soil and better resource absorption efficiency (Shan et al., 2012), and the topological index determines the root spatial distribution state and affects the acquisition of resources in the soil environment (Berntson, 1997). Chen et al. (2006) found that the fractal dimension of *Tilia tomentosa* decreased under waterlogging or drought conditions and increased under suitable moisture conditions, but there was no significant change in the fractal dimension of *K. hirsuta* under the three soil moisture conditions in our research, which may be because the fractal dimension of different plants responds differently to soil moisture. Shan et al. (2012) reported that with an increase in the degree of drought, the fractal abundance of *Reaumuria soongorica* became smaller. Similarly, the root fractal abundance of *K. hirsuta* under 10% field capacity conditions was remarkably lower than under the 25% and 40% field capacity treatments and suggested that *K. hirsuta* at the seedling stage adapted to drought stress by reducing the root expansion range. In previous research, wheat roots were deeply rooted under limited water conditions with a herringbone branching pattern, but were shallow rooted under waterlogging conditions with a dichotomous branching mode (Miao et al., 2019). Our results were similar to those of the above research that the root topological index of *K. hirsuta* under 10% field capacity conditions was significantly larger than those under 25% and 40%, which were closer to herringbone branching. This indicated that the root branching habit becomes closer to herringbone branching by reducing overlapping roots and increasing link length, so as to reduce the competition for nutrients within the root system and ensure effective nutrient distribution for *K. hirsuta* to adapt to an arid environment (Shan et al., 2012).

4.3 Responses of physiological parameters to different soil moisture conditions

Differences of soil moisture lead to a series of physiological metabolism changes in roots, including changes of membrane structure and function, the activation of the protective enzyme system, osmotic regulation, and hormone contents (Farooq et al., 2009).

The MDA content and RC can indicate the degree of stress injury to plants under water stress (Zhao et al., 2011). We found that the MDA content and RC in *K. hirsuta* roots were highest under 10% field capacity conditions, and were significantly higher than under 25% and 40%, consistent with the results of previous studies. Additionally, MDA and RC were negatively correlated with fractal abundance, total root length, total root surface area, root tips and forks. This suggested that root cell membranes were damaged and their permeability increased when *K. hirsuta* was grown in soil with 10% field capacity, which inhibited the growth and development of the root system and was not conducive to its establishment.

Pro and SP are key osmotic regulatory substances in plants that can maintain osmotic pressure and alleviate the threat of oxidative stress during drought stress (Babita et al., 2010; Ben et al., 2014). It was demonstrated that Pro and SP contents in *P. cornutum* roots at the seedling stage increased with the severity of drought under mild and moderate water stress Zhang et al. (2016). Thus, it was shown that under mild and moderate water stress, plants could maintain low intracellular osmotic potential by increasing their Pro and SP contents, improve the ability of cells to retain water, and reduce the damage caused by drought in *P. cornutum*, but severe stress damages root cells and makes plants unable to effectively maintain osmotic pressure. In our study, the Pro and SP

contents increased as soil moisture declined at the seedling stage in *K. hirsuta* and reached their highest values at 25% field capacity. The Pro and SP contents were positively correlated with the root topological index, and negatively correlated with root biomass, fractal abundance, total root length, total root surface area, total root volume, root tips and root forks. In general, this was because the root Pro and SP contents of *K. hirsuta* at the seedling stage were sensitive to water deficit and under drought conditions the root system maintained cell turgor by increasing the contents of free Pro and SP, which restricted the development of root morphology, so as to maintain the original physiological activities and adapt to water change.

Lack of soil moisture can lead to the accumulation of reactive oxygen species in plants, but plants can remove excess reactive oxygen species by increasing the activities of SOD, POD and CAT in the enzyme antioxidant defense system (Mittler, 2002). In a study by Zhang et al. (2016), the root antioxidant enzyme activity of *Pugionium cornutum* at the seedling stage increased with an increasing degree of drought, and the activities of SOD, POD and CAT in roots showed an upward trend. Differing from the above study, the SOD, POD and CAT activities here showed a trend of first decreasing and then increasing with an increasing moisture gradient, and were significantly higher at 10% field capacity than at 25% and 40%, with the lowest activities at 25% field capacity. Therefore, under the stress of 10% field capacity, the degree of membrane peroxidation in *K. hirsuta* roots was more serious, which triggered the antioxidant system in roots and improved the activity of antioxidant enzymes, while under the 25% field capacity condition, the antioxidant enzyme activity in *K. hirsuta* roots was lowest, and the metabolism of reactive oxygen species was in equilibrium (Kholová et al., 2011).

The root development of plants is closely related to their resistance to environmental drought stress, and root growth depends on hormone regulation (Guo et al., 2018; Ye et al., 2018). Among the many plant hormones, growth regulators such as ABA, IAA, GA and CTK play important regulatory roles in plant root responses to soil water changes (Tiwari et al., 2017).

ABA is produced in roots and an increase of ABA content can promote the expression and activity of aquaporins, and enhance the elongation of the root cell wall to promote root water absorption under water deficit (Lutz and Wolfgang, 2005; Guo et al., 2018). Ye et al. (2018) found that in an arid environment, the ABA content of maize increased by large quantities to enhance the drought resistance of plants, which was similar to the results of Ding et al. (2016) who reported that PEG treatment for 24 h induced ABA accumulation in the roots of rice seedlings. In our experiment, the ABA content first decreased and then increased with the rise of soil moisture, and was the highest under 10% field capacity conditions. We also found ABA in *K. hirsuta* roots was significantly positively correlated with the fractal dimension and notably negatively correlated with root tips and forks. The above results showed that the root system of *K. hirsuta* synthesized a large amount of ABA to promote water absorption and reduce root tip and fork numbers to adjust the root architecture to adapt to water shortage conditions, while under suitable soil moisture conditions, ABA was present at a normal level.

IAA regulates the processes of principal growth, lateral root formation and elongation, and adventitious root and root hair development (Guo et al., 2018). In the absence of soil moisture, the IAA concentration and mode of transport change the root morphology and improve the adaptability of plants to adversity (Krome et al., 2010; Guo et al., 2018). Wang et al. (2019) reported that the synthesis of endogenous IAA in sweet potato roots was significantly inhibited by 10 days of drought stress, resulting in a decrease of IAA content. Unlike the above research results, Mahouachi et al. (2007) found that the IAA content in roots of papaya seedlings did not change under drought stress. Consistent with the results of Mahouachi, the IAA content in *K. hirsuta* roots was not sensitive to different water conditions, indicating that IAA in the roots of different plants has different responses to water.

GA is related to the growth of the plant root structure and the formation of lateral roots, and its content changes under water deficit stress (Fonouni-Farde et al., 2019). Studies have found that gene expression related to GA biosynthesis was upregulated in soybean (Bashir et al., 2019), but the endogenous GA content in pea roots decreased (Yan et al., 2009) under drought stress. The two different results above may be due to changes of GA content related to plant species. In this study, as the soil moisture rose, the GA content of *K. hirsuta* first increased and then declined, reaching its highest value under 25% field capacity conditions, which was significantly higher than that under 10% field capacity conditions. These results suggested that *K. hirsuta* roots coped with water deficiency conditions by reducing GA metabolism but maintained a high GA content under moderate and moist soil moisture conditions to promote root development.

CTK, mainly synthesized in roots, regulates root microtubule tissue development, root cell extension, root geotropism, adventitious root differentiation and lateral root development (Aloni et al., 2004; Wei et al., 2012; Guo et al., 2018). It was reported that the CTK content in sorghum roots and leaves decreased significantly under drought stress (Zhou et al., 2014). However, Gong et al. (2018) found that the CTK content in seedling roots of two wheat varieties increased significantly under water-limited conditions, and was significantly negatively correlated with total root length and total root surface area, which was consistent with the results of our experiment. The CTK contents in *K. hirsuta* roots growing in soil under 25% and 40% field capacity conditions were remarkably lower than in those growing at 10% field capacity, and were significantly negatively correlated with root tips and root forks. This may be because under conditions of moderate and sufficient water, the CTK content in *K. hirsuta* roots decreased, which promotes better root development.

4.4 Based on the actual demand for soil moisture of *K. hirsuta*, the optimal growth conditions of *K. hirsuta* were explored from the perspective of water economy

Water, the source and the foundation of life, is important part of life on the earth. With the global climate change and the interference of human activities, water resources are being affected and gradually scarce, which will bring many adverse effects, threatening human health and living environment (Falkenmark, 2013). At the same time, water is the most important natural resource in agricultural production, and irrigation is a common way of water demand for crop cultivation. Improper use of water and fertilizer will cause water waste and land salinization, which will harm agricultural production (Wege, 2022). Therefore, exploring the minimum optimum water demand of plants is beneficial to plant growth and water use. It was reported that plant varieties with strong stress resistance can help save water resources and cope with climate change (Hanjra and Qureshi, 2010). In our study, *K. hirsuta*, the wind proof and sand fixing plant, could be grown and cultured normally under 25% and 40% field capacity, and some indicators were developed better under 25% field capacity. Thus, in the actual cultivation, 25% field capacity conditions can be selected to *K. hirsuta*, which not only ensure the normal growth of plants, but also reduce the consumption of water resources, providing reference for the cultivation of other desertification plants.

4.5 Analysis of the importance of root architecture indexes, physiological indexes and field capacity for root biomass of *K. hirsuta* at the seedling stage

In previous studies, root biomass has been considered an important index to evaluate plant development, reflect the distribution of the root system and measure the overall growth and development of plant roots (Lv et al., 2019; Wu and Sheng, 2020; Su et al., 2021). The root architecture and physiological indexes of *K. hirsuta* we measured were numerous and complex, and it was difficult to show a linear relationship with root biomass. Therefore, we used artificial neural network analysis to explore and quantify the influence of various root system architecture indexes, physiological indexes and the field capacity gradient on root biomass variation under different soil moisture conditions. The neural network model we constructed showed high R^2 and low relative error, indicating that it had high simulation accuracy and was suitable to analyze the importance of factors affecting root biomass.

Among all the root architecture indexes of *K. hirsuta*, total root length was the most obvious factor causing variation of root biomass, and its normalized importance was 100%. However, root link average length and total root surface area also had an important impact on root biomass. Lv et al. (2019) established a root biomass model with high simulation accuracy using the least squares method and found that root length played the most important role in influencing maize root architecture and root biomass. In a study by Rong et al. (2020), the root biomass of *Fokienia hodginsii* seedlings was significantly positively correlated with total root length, total root surface area and root average diameter. The above results were consistent with our experiment. Among all root physiological indexes, RC, SP and Pro had significant effects on root biomass and combined with correlation analysis, our results suggested that these physiological indexes negatively regulated root development. The results of Du et al. (2017) showing that physiological indexes such as Pro and SP in barley negative regulated root development were similar to ours. Furthermore, the results of factor importance analysis and one-way ANOVA showed that different field capacities had a significant effect on root biomass. In the results discussed above, although the plant species, root types and habitats (water, climate, soil conditions) varied, the main factors affecting root development were similar, but whether there are differences in other plants remains to be determined.

5 Conclusion

We found that 25% and 40% field capacity conditions were beneficial to the growth and acquisition of nutrients and water of *K. hirsuta* roots at the seedling stage, with better development of root morphology and a smaller variation range of physiological indexes.

However, the root growth and development of *K. hirsuta* was inhibited under the 10% field capacity condition, which was reflected in the reduction of biomass accumulation and the obstruction of root morphological development. This suggested *K. hirsuta* adapts to an arid environment by simplifying its root configuration and reducing its root branches to make the root topology closer to herringbone branching. Additionally, the activity of antioxidant enzymes in roots was high to slow down the degree of membrane lipid peroxidation and membrane permeability, free Pro and SP contents were high, and more ABA and CTK were synthesized to resist drought stress.

We found that three root architecture indexes including total root length, root link average length and total root surface, three root physiological indexes including RC, SP and Pro, and the field capacity were key factors affecting root biomass and had an important impact on the growth and development of *K. hirsuta* roots at the seedling stage.

Data availability statement

The raw data supporting the conclusions of this article will be made available by the authors, without undue reservation.

Author contributions

XC, YC contributed to the study design; XC, YC, WZ, WLZ, HW, QZ, were involved in drafting the manuscript and agree to be accountable for the work. All authors read and approved the final manuscript.

Funding

This research was funded by the National Natural Science Foundation of China (Grant No. 31802123). The Survey of Forage Resources in southern China (2017FY100602). The Fundamental Research Funds for the Central Universities Southwest Minzu University (ZYN2022036 and 2021PTJS30).

Conflict of interest

The authors declare that the research was conducted in the absence of any commercial or financial relationships that could be construed as a potential conflict of interest.

Publisher's note

All claims expressed in this article are solely those of the authors and do not necessarily represent those of their affiliated organizations, or those of the publisher, the editors and the reviewers. Any product that may be evaluated in this article, or claim that may be made by its manufacturer, is not guaranteed or endorsed by the publisher.

References

Aloni, R., Langhans, M., Aloni, E., and Ullrich, C. I. (2004). Role of cytokinin in the regulation of root gravitropism. *Planta.* 220, 177–182. doi: 10.1007/s00425-004-1381-8

Agathokleous, E., Belz, R. G., Kitao, M., Koike, T., and Calabrese, E. J. (2019). Does the root to shoot ratio show a hormetic response to stress? An ecological and environmental perspective. *J. For. Res.* 30, 1569–1580. doi: 10.1007/s11676-018-0863-7

Babita, M., Maheswari, M., Rao, L. M., Shanker, A. K., and Rao, D. G. (2010). Osmotic adjustment, drought tolerance and yield in castor (*Ricinus communis* l.) hybrids. *Environ. Exp. Bot.* 69, 243–224. doi: 10.1016/j.envexpbot.2010.05.006

Bagheri, M., Bazvand, A., and Ehteshami, M. (2017). Application of artificial intelligence for the management of landfill leachate penetration into groundwater, and assessment of its environmental impacts. *J. Clean. Prod.* 149, 784–796. doi: 10.1016/j.jclepro.2017.02.157

Bashir, W., Anwar, S., Zhao, Q., Hussain, I., and Xie, F. (2019). Interactive effect of drought and cadmium stress on soybean root morphology and gene expression. *Ecotoxicol Environ. Saf.* 15, 90–101. doi: 10.1016/j.ecoenv.2019.03.042

Ben, R. K., Abdelly, C., and Savouré, A. (2014). How reactive oxygen species and proline face stress together. *Plant Physiol. Biochem.* 80, 278–284. doi: 10.1016/j.plaphy.2014.04.007

Benjamin, J. G., Nielsen, D. C., Vigil, M. F., Mikha, M. M., and Calderon, F. (2014). Water deficit stress effects on corn (*Zea mays*, l.) root: Shoot ratio. *Open J. Soil Science.* 4, 151–160. doi: 10.4236/ojss.2014.44018

Berntson, G. M. (1997). Topological scaling and plant root system architecture: developmental and functional hierarchies. *New Phytologist.* 135, 621–634. doi: 10.1046/j.1469-8137.1997.00687.x

Biglarijoo, N., Mirbagheri, S. A., Bagheri, M., and Ehteshami, M. (2017). Assessment of effective parameters in landfill leachate treatment and optimization of the process using neural network, genetic algorithm and response surface methodology. *Process Saf. Environ. Prot.* 106, 89–103. doi: 10.1016/j.psep.2016.12.006

Bradford, M. M. (1976). A rapid and sensitive method for the quantitation of microgram quantities of protein utilizing the principle of protein-dye binding. *Anal. Biochem.* 72, 248–254. doi: 10.1016/0003-2697(76)90527-3

Chen, Y. J., Dong, Q. M., and Zhou, Q. P. (2020). The impact of different soil moisture and sterilization treatments on root architecture and rhizosheath formation of *Kengyilia hirsuta* at seedling stage. *Acta Prataculturae Sinica.* 29, 60–69. doi: 10.11686/cyxb2019278

Chen, Y. J., Gou, X. L., Sun, J., Dong, Q. M., and Zhou, Q. P. (2019). Root morphology patterns of three grasses used to restore the desert on the southeast tibetan plateau. *Pratacultural Science.* 36, 1137–1147. doi: 10.11829/j.issn.1001-0629.2019-0018

Chen, J. H., Yu, X. X., You, X. L., Liu, P., Zhang, C. D., and Xie, G. (2006). Fractal characteristics of *tilia tomentosa*'s root system under different water conditions. *Sci. Soil Water Conserv.* 4, 71–74. doi: 10.16843/j.sswc.2006.02.015

Comas, L. H., Becker, S. R., Cruz, V. M., Byrne, P. F., and Dierig, D. A. (2013). Root traits contributing to plant productivity under drought. *Front. Plant Sci.* 4. doi: 10.3389/fpls.2013.00442

Dalal, M., Sahu, S., Tiwari, S., Rao, A. R., and Gaikwad, K. (2018). Transcriptome analysis reveals interplay between hormones, ROS metabolism and cell wall biosynthesis for drought-induced root growth in wheat. *Plant Physiol. Biochem.* 130, 482–492. doi: 10.1016/j.plaphy.2018.07.035

David, M. E. (1991). On the relationship between specific root length and the rate of root proliferation: A field study using citrus rootstocks. *New Phytol.* 118, 63–68. doi: 10.1111/j.1469-8137.1991.tb00565.x

Ding, L., Li, Y., Wang, Y., Gao, L. M., Wang, M., Chaumont, F., et al. (2016). Root ABA accumulation enhances rice seedling drought tolerance under ammonium supply: Interaction with aquaporins. *Front. Plant Sci.* 7. doi: 10.3389/fpls.2016.01206

Draper, H. H., and Hadley, M. (1990). Malondialdehyde determination as index of lipid peroxidation. *Methods Enzymol.* 186, 421–431. doi: 10.1016/0076-6879(90)86135-i

Du, H., Ma, T. T., Guo, S., Zhang, Y., and Bai, Z. Y. (2017). Response of root morphology and leaf osmoregulation substances of seedling in barley genotypes with different heights to PEG stress. *Scientia Agricultura Sinica.* 50, 2423–2432. doi: 10.3864/j.issn.0578-1752.2017.13.002

Enquist, B. J., and Niklas, K. J. (2002). Global allocation rules for patterns of biomass partitioning in seed plants. *Science.* 295, 1517–1520. doi: 10.1126/science.1066360

Falkenmark, M. (2013). Growing water scarcity in agriculture: future challenge to global water security. *Philos. Trans. A Math Phys. Eng. Sci.* 371, 20120410. doi: 10.1098/rsta.2012.0410

Farooq, M., Wahid, A., Kobayashi, N., Fujita, D., and Basra, S. M. A. (2009). Plant drought stress: Effects, mechanisms and management. *Agron. Sustain Dev.* 29, 185–212. doi: 10.1007/978-90-481-2666-8_12

Fonouni-Farde, C., Miassod, A., Laffont, C., Morin, H., Bendahmane, A., Diet, A., et al. (2019). Gibberellins negatively regulate the development of medicago truncatula root system. *Sci. Rep.* 9. doi: 10.1038/s41598-019-38876-1

Gao, Z. Q., and Zhang, S. X. (1998). Continuous cropping obstacle and rhizospheric microecology i. root exudates and their ecological effects. *Chin. J. Appl. Ecology.* 5, 102–107. Avialable at: https://kns.cnki.net/kcms/detail/detail.a

spx?dbcode=CJFD&dbname=CJFD9899&filename=YYSB805.021&uniplatform=NZKPT&v=_TE34P2S2YEd3mBFAW5nSax7FZs_llAvyeCNwhptcWuaLEt_jQm9GnTUZrZtWyQ6

Giannopolitis, C. N., and Ries, S. K. (1977). Superoxide dismutase: I. occurrence in higher plants. *Plant Physiol.* 59, 309–314. doi: 10.1104/pp.59.2.309

Gong, P., Li, Z. Z., Yue, H. F., Ren, Y. Z., Xin, Z. L., Lin, T. B., et al. (2018). Study on the relationship between root system characters and the content of main hormones in germination of drought-resistant winter wheat. *J. Henan Agric. University.* 52, 16–21. doi: 10.16445/j.cnki.1000-2340.2018.01.004

Gou, X. L., Liu, W. H., Chen, Y. J., Zhoum, R., and Zhou, Q. P. (2019). Effect of different vegetation planting patterns in restoration of degraded sandy land in northwest sichuan. *Acta Prataculturae Sinica.* 28, 33–44. doi: 10.11686/cyxb2018398

Guo, B. H., Dai, Y., and Song, L. (2018). Research progress on the effects of phytohormones on crop root system development under drought condition. *Biotechnol. Bulletin.* 34, 48–56. doi: 10.13560/j.cnki.biotech.bull.1985.2018-0425

Guo, J. H., Li, C. J., Zeng, F. J., Zhang, B., Liu, B., and Guo, Z. C. (2016). Relationship between root biomass distribution and soil moisture, nutrient for two desert plant species. *Arid Zone Res.* 33, 166–171. doi: 10.13866/j.azr.2016.01.21

Hanjra, M. A., and Qureshi, M.E. (2010). Global water crisis and future food security in an era of climate change. *Food Policy.* 35, 365–377. doi: 10.1016/j.foodpol.2010.05.006

Harfouche, A., Meilan, R., and Altman, A. (2014). Molecular and physiological responses to abiotic stress in forest trees and their relevance to tree improvement. *Tree Physiol.* 34, 1181–1198. doi: 10.1093/treephys/tpu012

Hester, M. W., Mendelssohn, I. A., and Mckee, K. L. (2001). Species and population variation to salinity stress in *Panicum hemitomon*, *Spartina patens*, and *Spartina alterniflora*: morphological and physiological constraints. *Environ.Exp.Bot.* 46, 277–297. doi: 10.1016/S0098-8472(01)00100-9

Ketipearachchi, K. W., and Tatsumi, J. (2000). Local fractal dimensions and multifractal analysis of the root system of legumes. *Plant Prod Sci.* 3, 289-295. doi: 10.1626/pps.S3.289

Kholová., J., Hash, C. T., Kočová, M., and Vadez, V. (2011). Does a terminal drought tolerance QTL contribute to differences in ROS scavenging enzymes and photosynthetic pigments in pearl millet exposed to drought? *Environ.Exp.Bot.* 71, 99–106. doi: 10.1016/j.envexpbot.2010.11.001

Knapp, A. K., Hoover, D. L., Wilcox, K. R., Avolio, M. L., Koerner, S. E., La Pierre, K. J., et al. (2015). Characterizing differences in precipitation regimes of extreme wet and dry years: implications for climate change experiments. *Glob Chang Biol.* 21, 2624–2633. doi: 10.1111/gcb.12888

Krome, K., Rosenberg, K., Dickler, C., Kreuzer, K., Ludwig-Müller, J., Ullrich-Eberius, C., et al. (2010). Soil bacteria and protozoa affect root branching *via* effects on the auxin and cytokinin balance in plants. *Plant Soil.* 328, 191–201. doi: 10.1007/s11104-009-0101-3

Li, L. H., Li, S. Q., Zai, J. H., and Shi, J. T. (2001). Review of the relationship between wheat roots and water stress. *Acta Botanica Boreali-Occidentalia Sinica.* 1, 1–7. doi: 10.3321/j.issn:1000-4025.2001.01.001

Liu, T. Y., Chen, M. X., Zhang, Y., Zhu, F. Y., Liu, Y. G., Tian, Y., et al. (2019). Comparative metabolite profiling of two switchgrass ecotypes reveals differences in drought stress responses and rhizosheath weight. *Planta.* 250, 1355–1369. doi: 10.1007/s00425-019-03228-w

Lorenz, W. W., Alba, R., Yu, Y. S., Bordeaux, J. M., Simões, M., and Dean, J. F. (2011). Microarray analysis and scale-free gene networks identify candidate regulators in drought-stressed roots of loblolly pine (*P. taeda* l.). *BMC Genomics* 12, 264–280. doi: 10.1186/1471-2164-12-264

Lutz, W., and Wolfgang, M. (2005). Plant responses to drought and phosphorus deficiency: contribution of phytohormones in root-related processes. *J. Plant Nutr. Soil Science.* 168, 531–540. doi: 10.1002/jpln.200520507

Lu, C. X., Xie, G. D., Xiao, Y., and Yu, Y. J. (2004). Ecosystem diversity and economic valuation of qinghai-Tibet plateau. *Acta Ecologica Sinica.* 24, 2749–2755 +3011. doi: 10.3321/j.issn:1000-0933.2004.12.011

Luo, N., Wei, S., Li, J., Gu, W. R., He, D., Qu, T. M., et al. (2014). Effects of low-temperature stress on root system characteristics and electric conductivity of maize seedlings. *Chinese J. Ecol.* 33, 2694–2699. doi: 10.13292/j.1000-4890.2014.0232

Lv, G. H., Xie, Y. B., Wen, R. H., Wang, X. Y., and Jia, Q. Y. (2019). Modeling root biomass of maize in northeast China. *Chin. J. Eco-Agriculture.* 27, 572–580. doi: 10.13930/j.cnki.cjea.180115

Lynch, J. (1995). Root architecture and plant productivity. *Plant Physiol.* 109, 7–13. doi: 10.1104/pp.109.1.7

Mahouachi, J., Arbona, V., and Gómez-Cadenas, A. (2007). Hormonal changes in papaya seedlings subjected to progressive water stress and re-watering. *Plant Growth Regul.* 53, 43–51. doi: 10.1007/s10725-007-9202-2

Manivannan, P., Jaleel, C. A., Somasundaram, R., and Panneerselvam, R. (2008). Osmoregulation and antioxidant metabolism in drought-stressed *Helianthus annuus* under triadimefon drenching. *C R Biol.* 331, 418–425. doi: 10.1016/j.crvi.2008.03.003

Ma, X. F., Song, F. B., and Zhang, J. Z. (2011). Advances of research of roots responses to environmental stress on soil. *Chin. Agric. Sci. Bulletin.* 27, 44–48. doi: 10.1093/mp/ssq070

Mateo, F., Gadea, R., Mateo, E. M., and Jimenez, M. (2011). Multilayer perceptron neural networks and radial-basis function networks as tools to forecast accumulation of deoxynivalenol in barley seeds contaminated with fusarium culmorum. *Food Control.* 22, 88–95. doi: 10.1016/j.foodcont.2010.05.013

Ma, X. Z., and Wang, X. P. (2020). Root architecture and adaptive strategy of two desert plants in the alxa plateau. *Acta Ecologica Sinica.* 40, 6001–6008. doi: 10.5846/stxb201905030894

Merchan, F., Lorenzo, L. D., Rizzo, S. G., Niebel, A., Manyani, H., Frugier, F., et al. (2010). Identification of regulatory pathways involved in the reacquisition of root growth after salt stress in medicago truncatula. *Plant J.* 51, 1–17. doi: 10.1111/j.1365-313X.2007.03117.x

Miao, Q. X., Fang, Y., and Chen, Y. L. (2019). Studies in the responses of wheat root traits to drought stress. *Chin. Bull. Botany.* 54, 652–661. doi: 10.11983/CBB19089

Mittler, R. (2002). Oxidative stress, antioxidants and stress tolerance. *Trends Plant Sci.* 7, 405–410. doi: 10.1016/s1360-1385(02)02312-9

Mu, Z. X., Zhang, S. Q., Hao, W. F., Liang, A. H., and Liang, Z. S. (2005). The effect of root morphological traits and spatial distribution on WUE in maize. *Acta Ecologica Sinica.* 25, 2895–2900. doi: 10.3321/j.issn:1000-0933.2005.11.015

Nahid, N. K., and Abdollah, N. (2018). Physiological and biochemical responses of durum wheat under mild terminal drought stress. *Cell Mol. Biol. (Noisy-le-grand).* 64, 59–63. doi: 10.14715/cmb/2018.64.4.10

Oppelt, A. L., Kurth, W., and Godbold, D. L. (2001). Topology, scaling relations and leonardo's rule in root systems from African tree species. *Tree Physiol.* 21, 117–128. doi: 10.1093/treephys/21.2-3.117

Pauls, K. P., and Thompson, J. E. (1980). *In vitro* simulation of senescence-related membrane damage by ozone- induced lipid peroxidation. *Nature.* 283, 504–506. doi: 10.1038/283504a0

Rahimikhoob, A. (2010). Estimation of evapotranspiration based on only air temperature data using artificial neural networks for a subtropical climate in Iran. *Theor. Appl. Climatol.* 101, 83–91. doi: 10.1007/s00704-009-0204-z

Rahman, M. N., Hangs, R., and Schoenau, J. (2020). Influence of soil temperature and moisture on micronutrient supply, plant uptake, and biomass yield of wheat, pea, and canola. *J. Plant Nutr.* 43, 1–11. doi: 10.1080/01904167.2020.1711941s

Ren, J. D. (2016). *Diversity evaluation of the major varieties of KengyiliaYen in Qing hai plateau* (Qinghai University). Available at: https://kns.cnki.net/KCMS/detail/detail.aspx?dbname=CMFD201602&filename=1016722447.nh.

Rong, J. D., Fan, L. L., Chen, L. G., Zhang, Y. H., He, T. Y., Chen, L. Y., et al. (2020). Impacts on biomass allocation and root growth of fokienia hodginsii seedlings of different patterns and quantities of nitrogen application. *Scientia Silvae Sinicae.* 56, 175–184. doi: 10.11707/j.1001-7488.20200718

Rossi, L., Bagheri, M., Zhang, W., Chen, Z. H., Burken, J. G., and Ma, X. M. (2019). Using artificial neural network to investigate physiological changes and cerium oxide nanoparticles and cadmium uptake by brassica napus plants. *Environ. pollut.* 246, 381–389. doi: 10.1016/j.envpol.2018.12.029

Schiefelbein, J. W., and Benfey, P. N. (1991). The development of plant roots: new approaches to underground problems. *Plant Cell.* 3, 1147–1154. doi: 10.1105/tpc.3.11.1147

Shan, L. S., Yi, L. I., Dong, Q. L., and Geng, D. M. (2012). Ecological adaptation of *Reaumuria soongorica* root system architecture to arid environment. *J. Desert Res.* 32, 1293–1290.Available at: https://kns.cnki.net/kcms/detail/detail.aspx?dbcode=CJFD&dbname=CJFD2012&filename=ZGSS201205016&uniplatform=NZKPT&v=vnpfvngbeYdRJJDYgdGj2eEziMWkvsM2nK-ebib2xeBln5LLFi9PRm9-ItpNS8iv.

Smucker, A., and Aiken, R. M. (1992). Dynamic root responses to water deficits. *Soil Science.* 154, 281–289. doi: 10.1097/00010694-199210000-00004

Sofi, P. A., Djanaguiraman, M., Siddique, K. H. M., and Prasad, P. V. V. (2018). Reproductive fitness in common bean (*Phaseolus vulgaris* l.) under drought stress is associated with root length and volume. Indian j. plant. *Physiol.* 23, 796–809. doi: 10.1007/s40502-018-0429-x

Su, L., Du, H., Wang, H., Zeng, F. P., Song, T. Q., Peng, W. X., et al. (2018). Root architecture of the dominant species in various vegetation restoration processes in karst peak-cluster depression. *Acta Botanica Boreali-Occidentalia Sinica.* 38, 150–157. doi: 10.7606/j.issn.1000-4025.2018.01.0150

Su, T. Y., Jia, B. Y., Hu, Y. L., Yang, Q., and Mao, W. (2021). Effects of groundwater depth on soil environmental factors and root biomass of typical plant communities in sandy grassland. *Pratacultural Science.* 38, 1694–1705. doi: 10.11829/j.issn.1001-0629.2021-0721

Tang, Z. Q., Chen, Y. J., Hu, J., Wang, H., Lei, Y. X., Shua, i., et al. (2020). Analysis of root architecture and rhizosheath characteristics of seven forage speciesin desertified grassland of Northwest sichuan. *Chin. J. Grassland.* 42, 22–31. doi: 10.16742/j.zgcdxb.20190315

Tiwari, S., Lata, C., Chauhan, P. S., Prasad, V., and Prasad, M. (2017). A functional genomic perspective on drought signalling and its crosstalk with phytohormone-mediated signalling pathways in plants. *Curr. Genomics* 18, 469–482. doi: 10.2174/1389202918666170605083319

Wang, J. Q., Li, H., Liu, Q., and Xiang, D. (2019). Effects of drought stress on root development and physiological characteristics of sweet potato at seedling stage. *Chin. J. Appl. Ecology.* 30, 3155–3163. doi: 10.13287/j.1001-9332.201909.026

Wang, J. J., Wang, Z. G., An-Wei, M. A., Lin, W. H., Kuang, Y., Tian, P., et al. (2016). Effect of different temperature and moisture conditions on seedling growth of Festuca sinensis. *Acta Prataculturae Sinica* 25, 65–73. doi: 10.11686/cyxb2015492

Wege, S. (2022). The flow of water: Critical factors of root axial water transport determined. *Plant Physiol.* 190, 1083–1084. doi: 10.1093/plphys/kiac349

Wei, Z. H., Dong, Z. B., Hu, G. Y., and Lu, J. F. (2010). Spatial and temporal patterns of sand dunes in zoige basin in last 40 years. *J. Desert Res.* 30, 26–32. Available at: https://kns.cnki.net/kcms/detail/detail.aspx?dbcode=CJFD&dbname=CJFD2010&filename=ZGSS201001005&uniplatform=NZKPT&v=R5p2RlirXk6KtSCpIoMobG0qV0GnqMB39ux3OfD0I2e4X6TPGwQ0mzG6zunCODLb

Wei, X. W., Lv, J., Wu, H., Gou, C., Xu, H. W., and Zhou, X. F. (2012). Research advances on plant roots. *Northern Horticulture.* 18, 206–209. Available at: https://kns.cnki.net/kcms/detail/detail.aspx?dbcode=CJFD&dbname=CJFD2012&filename=BFYY201218075&uniplatform=NZKPT&v=VtZ9_0bOZWwIK49lUeDBc23Y6C0by1uxCbMcWRB-Gm5RfY-vEfqGcg4-khnwcUEl

Wu, J., and Sheng, M. Y. (2020). Research progress in root ecology of karst vegetation in China. *Plant Sci. J.* 38, 565–573. doi: 10.11913/PSJ.2095-0837.2020.40565

Yang, P. L., and Luo, Y. P. (1994). Fractal characteristics of root morphology in *Triticum aestivum l. Chin. J. Eco-Agriculture.* 20, 1911–1913. Available at: https://kns.cnki.net/kcms/detail/detail.aspx?dbcode=CJFD&dbname=CJFD9495&filename=KXTB199420024&uniplatform=NZKPT&v=yuW0Zk530cdW_MkMaZA_EmaPi4jeOktlSrhDQYp4x9PMz-6qUmU1wbDFiJ-z8dFO

Yang, X. L., Zhang, X. M., Li, Y. L., Xie, T. T., and Wang, W. H. (2009). Root fractal characteristics at the hinterland of taklimakan desert. *Arid Land Geography.* 32, 249–254. doi: 10.13826/j.cnki.cn65-1103/x.2009.02.013

Yang, Z. Y., Zhou, B. Z., Chen, Q. B., Ge, X. G., Wang, X. M., Cao, Y. H., et al. (2018). Effects of drought on root architecture and non-structural carbohydrate of *cunninghamia lanceolate*. *Acta Ecologica Sinica.* 38, 6729–6740. doi: 10.5846/stxb201803260604

Yan, Z. L., Xuan, C. X., Niu, J. Y., Ling-Ling, X. I., and Zhao, T. W. (2009). Effect of drought stress and water recovery on endogenous hormone content in roots of pea. *Chin. J. Eco-Agriculture.* 17, 297–301. doi: 10.3724/SP.J.1011.2009.00297

Ye, H., Roorkiwal, M., Valliyodan, B., Zhou, L., Chen, P., Varshney, R. K., et al. (2018). Genetic diversity of root system architecture in response to drought stress in grain legumes. *J. Exp. Bot.* 69, 3267–3277. doi: 10.1093/jxb/ery082

Yu, F. L., Yang, M. Y., Gan, Y. M., Yang, S. J., Xiao, B. X., Zheng, Q. Y., et al. (2011). Drought resistance evaluation of three grass species at germination stage from the Northwest plateau of sichuan province. *Pratacultural Science.* 28, 993–997. doi: 10.3969/j.issn.1001-0629.2011.06.023

Zeng, F. J., Song, C., Guo, H. F., Liu, B., and Luo, W. C. (2013). Responses of root growth of *Alhagi sparsifolia* shap. (Fabaceae) to different simulated groundwater depths in the southern fringe of the taklimakan desert, China. *J. Arid Land.* 5, 220-232. doi: 10.1007/s40333-013-0154-2

Zhang, G. L., and Nie, R. B. (2008). Study on judgement of maturity degree by free proline content in flue-cured tobacco leaves. *Crop Res.* 1, 31–32. doi: 10.3969/j.issn.1001-5280.2008.01.010

Zhang, C., Shi, S., Wang, B., and Zhao, J. (2018). Physiological and biochemical changes in different drought-tolerant alfalfa (Medicago sativa l.) varieties under PEG-induced drought stress. *Acta Physiologiae Plantarum.* 40, 1–15. doi: 10.1007/s11738-017-2597-0

Zhang, X. L., Wang, P., Shi, L., and Yang, J. (2016). Root morphology and antioxidant enzyme activity of *Pugionium cornutum* (l.) gaertn under drought stress. *Agric. Res. Arid Areas.* 34, 160–164. doi: 10.7606/j.issn.1000-7601.2016.03.25

Zhao, Y., Du, H. M., Wang, Z. L., and Huang, B. R. (2011). Identification of proteins associated with water-deficit tolerance in C4 perennial grass species, *Cynodon dactylon* × *Cynodon transvaalensis* and *Cynodon dactylon*. *Physiol. Plant* 141, 40–55. doi: 10.1111/j.1399-3054.2010.01419.x

Zhou, Y. F., Wang, D. Q., Lu, Z. B., Wang, N., Wang, Y. T., Li, F. X., et al. (2014). Effects of drought stress on photosynthetic characteristics and endogenous hormone ABA and CTK contents in green-stayed sorghum. *Scientia Agricultura Sinica.* 47, 655–663. doi: 10.3864/j.issn.0578-1752.2014.04.005

frontiers | Frontiers in Plant Science

TYPE Original Research
PUBLISHED 11 January 2023
DOI 10.3389/fpls.2022.1060686

OPEN ACCESS

EDITED BY
Boris Rewald,
University of Natural Resources and Life Sciences Vienna, Austria

REVIEWED BY
Xiliang Song,
Shandong Agricultural University, China
Huakun Zhou,
Key Laboratory of Restoration Ecology in Cold Regions (CAS), China
Xiaojun Yu,
Gansu Agricultural University, China

*CORRESPONDENCE
Yushou Ma
mayushou@sina.com
Yanlong Wang
wangyl506@163.com

SPECIALTY SECTION
This article was submitted to Functional Plant Ecology, a section of the journal Frontiers in Plant Science

RECEIVED 03 October 2022
ACCEPTED 20 December 2022
PUBLISHED 11 January 2023

CITATION
Dong R, Yang S, Wang X, Xie L, Ma Y, Wang Y, Zhang L, Zhang M and Qin J (2023) C:N:P stoichiometry in plant, soil and microbe in *Sophora moorcroftiana* shrubs across three sandy dune types in the middle reaches of the Yarlung Zangbo River. *Front. Plant Sci.* 13:1060686. doi: 10.3389/fpls.2022.1060686

C:N:P stoichiometry in plant, soil and microbe in *Sophora moorcroftiana* shrubs across three sandy dune types in the middle reaches of the Yarlung Zangbo River

Ruizhen Dong[1], Shihai Yang[2], Xiaoli Wang[1], Lele Xie[1], Yushou Ma[1]*, Yanlong Wang[1]*, Litian Zhang[1], Min Zhang[1] and Jinping Qin[1]

[1]Qinghai Provincial Key Laboratory of Adaptive Management on Alpine Grassland, Qinghai Academy of Animal and Veterinary Science, Qinghai University, Qinghai Province, Xining, Qinghai, China, [2]Tibet Yunwang Industrial Co., Ltd, R & D Department, Shigatse, Tibet, China

The alpine sandy dune ecosystem is highly vulnerable to global climate change. Ecological stoichiometry in plants and soils plays a crucial role in biogeochemical cycles, energy flow and functioning in ecosystems. The alpine sandy dune ecosystem is highly vulnerable to global climate change. However, the stoichiometric changes and correlations of plants and soils among different types of sandy dunes have not been fully explored. Three sandy dune types (moving dune, MD; semifixed dune, SFD; and fixed dune, FD) of the *Sophora moorcroftiana* shrub in the middle reaches of the Yarlung Zangbo River were used as the subjects in the current study. Plant community characteristics, soil physicochemical properties, carbon (C), nitrogen (N), and phosphorus (P) contents of leaves, understorey herbs, litter, and soil microbes were evaluated to explore the C:N:P stoichiometry and its driving factors. Sandy dune type significant affected on the C:N:P stoichiometry in plants and soils. High soil N:P ratio was observed in FD and high plant C:P and N:P ratios in SFD and MD. The C:N ratio decreased with sand dune stabilization compared with other stoichiometric ratios of soil resources. Leaf C:P and N:P ratios in *S. moorcroftiana* were higher than those in the understorey herb biomass, because of the low P concentrations in leaves. C, N and P contents and stoichiometry of leaves, understorey herbs, litter and microbe were significantly correlated with the soil C, N and P contents and stoichiometry, with a higher correlation for soil N:P ratio. P was the mainly limiting factor for the growth of *S. moorcroftiana* population in the study area and its demand became increasingly critical with the increase in shrub age. The variation in the C:N:P stoichiometry in plants and soils was mainly modulated by the soil

physicochemical properties, mainly for soil moisture, pH, available P and dissolved organic C. These findings provide key information on the nutrient stoichiometry patterns, element distribution and utilization strategies of C, N and P and as well as scrubland restoration and management in alpine valley sand ecosystems.

KEYWORDS

Sophora moorcroftiana population, sandy dune type, C:N:P ecological stoichiometry, nutrient limitation, plant-soil-microbe interaction

1 Introduction

Carbon (C), nitrogen (N), and phosphorus (P) are key elements in living organisms (Chen and Chen, 2021). Carbon provides the structural basis of plants and accounts for relatively 50% of dry plant biomass (Schade et al., 2003; Yang et al., 2018). Nitrogen is an essential component of proteins and plays an important role in plant production, photosynthesis and litter decomposition (Daufresne, 2004; Chen et al., 2016b; Yang et al., 2018). Phosphorus is the limiting element responsible for the structure of cells and the composition of DNA and RNA, and P promotes C/N transpiration and assimilation (Tilman, 1996; Xiao et al., 2009; Pii et al., 2015). Nutrient sources have differences in the elemental composition; however, living organisms maintain these elements around specific ratios for their growth and reproduction in a process known as homeostasis (Sterner and Elser, 2002).

C:N:P ecological stoichiometry comprises on the interaction and balance of chemical elements in ecological processes and is used to study feedback and relationships between above- and belowground components of ecosystems (Mooshammer et al., 2014; Ren et al., 2016; Zhang et al., 2019). Two major methods are used for analysis of C:N:P stoichiometry (Cross et al., 2005). The first method relies on the principle that release of major nutrients (C, N, and P) occurs in a predictable manner, depending on the limitation of the C:N:P ratio (Sterner and Elser, 2002; Yang et al., 2018). Leaf N:P ratio (mass ratio) is utilized as a key indicator for assessing N or P limitation (Güsewell, 2004; Cleveland and Liptzin, 2007). The second method is based on the theory that natural resources are in stoichiometric homeostasis (Sterner and Elser, 2002; Yang et al., 2018). At the organismal level, life stages characterized by high growth rates are associated with high RNA contents (C:N:P ratios ranging from 18:6:1 to 21:7:1), and thus organisms can alter their overall stoichiometry (McGroddy et al., 2004). Several studies have demonstrated that the C:N:P ratios in plants, soils and soil microorganisms affect primary production and nutrient cycling as well as indicate the nutrient limits in plants in terrestrial ecosystems (Sterner and Elser, 2002; Manzoni et al., 2008; Huang et al., 2013). The relative supplies of nutrients (soil N and P) are key modulators of C:N:P ratios in plants (Plum et al., 2015). Plant C:N:P ratios can be transformed through litter decomposition into soil inputs and microbes (Zechmeister-Boltenstern et al., 2015). Researchers have demonstrated that more diverse plant assemblages can increase the C:nutrient (N or P) ratios of plants and associated litter (Mooshammer et al., 2014). The high plant C:nutrient (N or P) ratios in turn increase the C:N and C:P ratios in soil microbial biomass because microorganisms adjust their biomass C:N:P ratios to match the litter substrate (Zechmeister-Boltenstern et al., 2015). Stoichiometric imbalances in the plant–soil–microbe system have not been fully elucidated (Mooshammer et al., 2014; Zhang et al., 2019). Studies should be conducted to explore how plant diversity, successional stage, and environmental factors affect redistribution of nutrients (C, N, and P) between plants and soils (Zhang et al., 2019), and how relationships between above- and belowground elemental stoichiometry modulate terrestrial ecosystem processes (Li et al., 2016; Liu et al., 2020). Evaluation of the C:N:P stoichiometry of plants, soils, and soil microbial biomass will provide insights into element cycling and promote ecosystem sustainability (Chen and Chen, 2021).

In semiarid ecosystems, nurse shrubs facilitate the establishment of other plant species under their canopies and induce changes in the understory plant communities as they grow (Hortal et al., 2013). Studies should be conducted to predict the feedback effects of shrub/understorey species interactions (Bai et al., 2018). Understorey herbaceous plants overall negative, neutral, and positive effects on shrub growth and reproductive output, exhibiting antagonistic, commensalistic, and facultative mutualistic relationships (Bai et al., 2019). Moreover, understorey herbaceous plants are crucial in increasing soil nutrient contents and promoting nutrient cycling among plants and soil systems (Zhang et al., 2019). Nurse shrubs mitigate the responses of understorey herbaceous species to N enrichment and increased precipitation (Bai et al., 2019). Therefore, it is imperative to explore the biochemical cycle of ecosystems using stoichiometry theory to evaluate the

internal relationship between understorey species and shrubs and their relationship with soil elements.

The Tibetan Plateau is characterized by excessive land desertification and is one of the most ecologically vulnerable regions (Shen et al., 2012). Degradation of alpine grasslands causes a reduction in ecosystem services, such as the loss of biodiversity, water erosion and reduced productivity (Du and Gao, 2021). Shrub species in dune habitats are the key elements in rehabilitating a degraded ecosystem (Liao et al., 2021). This is because shrubs have specific and significant "morphological, physiological or behaviour" effects in these extreme and harsh environmental conditions (Yu and Steinberger, 2012). These adaptations markedly affect the substrate stability and sand movement as well as the basal soil organic matter (SOM), nutrient contents, salinity and other conditions, and affect the activity, quantity and diversity of soil microorganisms (Wang et al., 2019). *Sophora moorcroftiana* (Benth.) Baker, a perennial leguminous shrub, is an endemic species in Tibet region. The species is limited to the hillsides, sandy gravel floodplains, sandy areas and alluvial fans of the wide valley in the middle reaches of the Yarlung Zangbo River (Cheng et al., 2017). It is one of the most important sand-fixing plant species characterized by high tolerances to drought, cold, barren land and sand burial, as well as acts as a key species for vegetation restoration and reconstruction in this region (Zhao et al., 2007; Guo et al., 2014). The species plays an essential role in water and soil conservation, fixation of sand dunes and prevention of shifting sands in the middle reaches of the Yarlung Zangbo River (Guo et al., 2009). However, the ecological effects of the interrelationships among this shrub, understorey species, litter, soil and microbes in the different sandy dune types have not been fully evaluated from the perspective of C:N:P stoichiometry.

In this study, we evaluated the dynamics of C, N, and P contents and stoichiometry in plants (including green leaves, understorey species, and litter), soils and microbial biomass from three different sandy dune types (mobile, semifixed, and fixed dunes) in an *S. moorcroftiana* population. We hypothesized that the C:N:P stoichiometry in the shrub, understorey species, litter, soils and microbes are affected by the sandy dune type, and the C, N, and P concentrations and their ratios in the soils, plants and microbes are highly coupled because they coevolved. In addition, we also presumed that soil properties are a key driver of C:N:P stoichiometry in plant-soil-microbe systems. Therefore, the objectives of the present study were to (1) evaluate the effect of sandy dune type on C:N:P stoichiometry in plants, soils, and microbes and determine the element limiting the growth of *S. moorcroftiana* shrubs and understorey plants; (2) explore the relationships of C:N:P stoichiometry between plants, soils, and microbes; and (3) determine the driving factors of the C:N:P stoichiometry.

2 Materials and methods

2.1 Study area

This study was conducted at the southern Tibetan Plateau in the middle reaches of the Yarlung Zangbo River (28°59′–29°26′ N, 88°04′–93°18′ E) (Table 1). The terrain of the catchment area is higher in the northwest and lower in the southeast, with an altitude ranging from 2,900–4,550 m. This terrain provides significant negative topographic conditions for the accumulation of eolian sediments, and eolian deposits (such as eolian sand and sandy loess), which are widely distributed in the basin. The river basin is characterized by strong winds during winter and spring. The average wind velocity is extremely high at 32.5 m/s, the monthly maximum wind velocity is 4.7 m/s, and the number of windy days is about 172 days per year (Shen et al., 2012). The region has a temperate semihumid and semiarid plateau monsoon climate. The average annual temperature is approximately 6–8°C, with summer temperatures above 15°C and winter temperatures below -2°C. The average annual precipitation is 300–600 mm, and the precipitation around the basin is unevenly distributed throughout the year, mainly occurring from June to September, which accounts for 86.6% of the annual precipitation. The soil type in this area is primarily mountainous shrub steppe soil and alpine meadow soil, and some areas have alpine cold desert soil, subalpine meadow soil, and subalpine steppe soil. The area has low and sparse vegetation, with grassland as the main vegetation type. The main vegetation in the middle reaches of the Yarlung Zangbo River are shrubs dominated by *S. moorcroftiana* (Table 1). *Pennisetum centrasiaticum*, an important companion species, is distributed in all three sandy dune types, but *Agriophyllum squarrosum* is only distributed in the semifixed dune type and moving dune types. *P. centrasiaticum* and *Artemisia wellbyi* were the main companion species in the semifixed dune type and moving dune types. Several new species, such as *Thermopsis fabacea*, *Setaria viridis*, *Erodium stephanianum*, and *Achnatherum splendens*, were observed in the fixed dune type, with *P. centrasiaticum*, *Arisaema flavum*, *A. wellbyi*, *Orinus thoroldii*, and *Artemisia stechmanniana* as the main companion species.

2.2 Experimental design

Field plant collection and soil sampling were conducted in August 2020. We selected three sandy dune types, including fixed dune (FD), semifixed dune (SFD), and moving dune (MD), in which *S. moorcroftiana* was the dominant species, according to the vegetation coverage and degree of soil surface fixation in the Yarlung Zangbo River basin (Shen et al., 2012; Table S1). Three independent replicate plots of 10 m × 10 m were randomly set up at each site, with five subplots (1 m × 1 m) at the centre and opposite

TABLE 1 Main geographic characteristics and floristic compositions of the *S.moorcroftiana* shrubs sampling sites among the middle reaches of the Yarlung Zangbo River basin.

Sites	Longitude (E)	Latitude (N)	Elevation (m)	Main companion species	Minor species
FD1	88°31'54.74"	29° 11'00.39"	3957	*Pennisetum centrasiaticum*	*Poaannua*, *Astragalus membranaceus*
FD2	88°38'04.54"	29° 09'11.07"	3964	–	–
FD3	89°20'30.35"	29° 05'17.94"	3886	*Pennisetum centrasiaticum*	*Astragalus membranaceus*
FD4	87°27'38.31"	29° 06'09.21"	3998	*Pennisetum centrasiaticum*	*Thermopsis fabacea*
FD5	88°09'27.16"	29° 21'14.97"	3886	*Pennisetum centrasiaticum*	*Astragalus membranaceus*, *Artemisia scoparia*
FD6	89°23'52.30"	29° 22'09.29"	3806	*Arisaema flavum*	*Pennisetum centrasiaticum*, *Dysphania schraderiana*, *Artemisia scoparia*, *Orinus thoroldii*
FD7	89°35'44.24"	28° 55'46.39"	4019	*Pennisetum centrasiaticum*	*Artemisia stechmanniana*, *Artemisia wellbyi*, *Astragalus membranaceus*
FD8	89°45'24.52"	29° 18'15.28"	3745	–	*Pennisetum centrasiaticum*, *Arisaema flavum*, *Artemisia scoparia*, *Setaria viridis*
FD9	90°10'39.67"	29° 26'16.11"	3785	*Pennisetum centrasiaticum*	*Artemisia wellbyi*
FD10	90°50'54.31"	29° 16'51.66"	3543	*Pennisetum centrasiaticum*	*Astragalus membranaceus*, *Tribulus terrestris*, *Erodium stephanianum*
FD11	90°54'15.75"	29° 20'00.87"	3539	*Pennisetum centrasiaticum*	*Artemisia wellbyi*, *Heteropappus gouldii*, *Oxytropis sericopetala*
FD12	91°21'19.16"	29° 18'24.35"	3534	*Artemisia wellbyi*	*Pennisetum centrasiaticum*, *Ceratostigma minus*, *Achnatherum splendens*
FD13	91°53'45.30"	29° 16'57.26"	3535	*Pennisetum centrasiaticum*, *Orinus thoroldii*	*Artemisia stechmanniana*, *Artemisia wellbyi*, *Artemisia demissa*, *Achnatherum splendens*
FD14	92°43'02.36"	29° 06'11.87"	3126	*Artemisia stechmanniana*	*Artemisia wellbyi*, *Arisaema flavum*
FD15	93°18'21.68"	28° 59'37.45"	3032	*Artemisia wellbyi*, *Artemisia stechmanniana*	*Pennisetum centrasiaticum*, *Poaannua*, *Astragalus membranaceus*
SFD1	91°05'06.60"	29° 20'15.46"	3543	–	*Oxytropis sericopetala*, *Artemisia wellbyi*
SFD2	91°09'09.82"	29° 19'35.75"	3543	*Orinus thoroldii*	*Pennisetum centrasiaticum*, *Astragalus membranaceus*, *Oxytropis sericopetala*, *Agriophyllum squarrosum*, *Trikeraia hookeri*
SFD3	91°30'03.92"	29° 19'58.66"	3530	*Pennisetum centrasiaticum*, *Artemisia wellbyi*	*Oxytropis sericopetala*, *Astragalus membranaceus*
SFD4	91°31'42.81"	29° 15'19.90"	3523	*Pennisetum centrasiaticum*	*Dysphania schraderiana*, *Artemisia wellbyi*, *Poaannua*
MD1	88°04'20.50"	29° 21'53.67"	3884	–	*Oxytropis sericopetala*, *Astragalus membranaceus*, *Artemisia scoparia*, *Pennisetum centrasiaticum*
MD2	89°30'27.56"	29° 21'40.85"	3750	*Pennisetum centrasiaticum*	*Oxytropis sericopetala*
MD3	91°21'05.25"	29° 18'45.76"	3553	*Pennisetum centrasiaticum*	*Agriophyllum squarrosum*, *Artemisia wellbyi*, *Oxytropis sericopetala*

(Continued)

TABLE 1 Continued

Sites	Longitude (E)	Latitude (N)	Elevation (m)	Main companion species	Minor species
MD4	91°31'42.81"	29° 15'19.90"	3523	*Artemisia wellbyi*	*Oxytropis sericopetala*, *Tribulus terrestris*, *Pennisetum centrasiaticum*, *Dysphania schraderiana*
MD5	91°35'20.60"	29° 15'14.44"	3548	*Agriophyllum squarrosum*	*Pennisetum centrasiaticum*, *Saussurea arenaria*, *Dysphania schraderiana*

FD, fixed dune; SFD, semifixed dune; MD, moving dune.

corners of each plot for the subsequent plant sample collection and soil sampling. All the selected sites had similar topographies (flat sandy land) to ensure comparability of the plant and soil samples. Basic information for each sandy dune type of *S. moorcroftiana* shrub is presented in Table 1.

2.3 Soil and plant sampling

Nine soil cores (5 cm diameter) were obtained from each plot (10 m × 10 m) at a depth of 20 cm along an "S" shape under the canopy of the shrub and then thoroughly mixed and pooled to form one soil sample. A total of 72 soil samples (twenty-four replicate sites × three replicate plots) were collected in this study. In addition, three cutting ring soil samples were collected from a 0–20 cm depths in each plot to determine the soil bulk density (BD). Each soil sample was sieved through a 2 mm mesh, and visible gravel and plant materials were removed and then divided into two parts: One portion of the fresh soil from the field was stored at 4°C for microbial biomass (carbon, nitrogen, and phosphorus), inorganic N (NH_4^+–N and NO_3^--N) and available phosphorus (AP) analyses, and the other portion was air-dried and stored at room temperature for subsequent analysis of soil physicochemical properties.

For *in situ* analysis of plants, five subplots (1 m × 1 m) were used to determine the name, height, coverage, and number of each species and to collect litter from the plants. We randomly chose 8–10 well-grown *S. moorcroftiana* shrubs in each plot after the basic vegetation survey. Samples of fully expanded leaves were collected, and the diameter at breast height (DBH), height (SH), and shrub crown size (SCS) were determined to characterize the shrub age class as reported previously (Pugnaire et al., 1996; Hortal et al., 2013). All the plant samples were oven-dried at 65°C to a constant mass. The plant samples were analyzed as previously described (Higgins et al., 2012).

2.4 Analysis of plant and soil physicochemical properties

Soil samples were collected in a steel ring (Volume 100 cm^3) for soil BD determination. The soil samples were then oven dried at 105°C (± 2°C) for 24 h, and the dry mass was weighed. Soil pH was determined in a 1:5 (soil:water) ratio after shaking the samples for 30 min at room temperature. The soil moisture (SM) content was determined by oven drying the soil samples at 105°C to constant mass. Organic carbon concentrations of soils and plant samples were assayed using $K_2Cr_2O_7$ oxidation and $FeSO_4$ titration methods (Huang et al., 2014). Total nitrogen (TN) was determined using Cleverchem 200+ (Chilehaus A, Fischertw iete2-20095 Hamburg, Germany) after digestion with H_2SO_4-H_2O_2. Total phosphorus (TP) concentration was determined using the molybdenum antimony colorimetric method following digestion with H_2SO_4-$HClO_4$. Soil dissolved organic carbon (DOC) was extracted with 0.5 M K_2SO_4 and analysed using vario TOC cube (Elementar, Germany). The soil inorganic N (IN) concentration was extracted with 1 M KCl for 30 min on a shaker at room temperature, and the filtrates were analysed using Cleverchem 200+ (Chilehaus A, Fischertw iete2-20095 Hamburg, Germany). Available P (AP) concentration was determined using the molybdenum blue method (Yang and Liu, 2019).

2.5 Determination of soil microbial biomass

Soil microbial biomass carbon (MBC), nitrogen (MBN) and phosphorus (MBP) were determined by the chloroform fumigation extraction method (Brookes et al., 1985; Vance et al., 1987; Wu et al., 2000). Three 30 g soil subsamples for each soil sample were fumigated with chloroform for 24 h at 25°C under dark conditions. Three replicates of the same amount of soil without fumigation were used to extract MBC and MBN using 0.5 M K_2SO_4 (of 1:2 soil to acid ratio) for 30 min on a shaker. The extracts were analysed for total organic C and total N using a TOC analyser (vario TOC, Elementar, Germany). MBP was extracted with 0.5 M $NaHCO_3$ (pH = 8.5, at a soil solution ratio of 1:20) for 30 min on a shaker. The $NaHCO_3$ filtrates (25 ml) were digested with 1 ml 33% H_2SO_4 and 4 ml 5% potassium persulfate at 120°C for 30 min (high temperature, high pressure, humid-heat treatment) then the extractions were analysed colorimetrically using a spectrophotometer (Analytikjena, SPECORD 210, Germany) at 880 mm. MBC, MBN and MBP were presented as

the difference between levels of fumigated and unfumigated soil samples and expressed as extraction efficiency (conversion coefficient k) (k_C = 0.45 for MBC, k_{EN} = 0.45 for MBN, k_P = 0.40 for MBP) (Brookes et al., 1985; Vance et al., 1987; Joergensen and Mueller, 1996).

2.6 Statistical analysis

Statistical analyses were performed using SPSS 20.0 (SPSS Inc., Chicago, IL, USA) software. A linear mixed model (LMM) in R was sued to evaluate the effect of sandy dune types on plant characteristics (including leaf, understorey herb biomass and litter C:N:P stoichiometry, DBH, SCS, H, SH, understorey grass coverage, and *S. moorcroftiana* coverage) and soil properties (BD, SM, DOC, AP, IN, and C:N:P stoichiometry) among different sampling sites, with "sandy dune type " as the fixed factor and "sampling site" as the random factor, and the result was expressed as the mean ± standard error (SE). Pearson's correlation analysis was performed to explore the stoichiometric relationships among plants, soils, and microbial biomass. Structural equation modeling (SEM) was used to determine the direct and indirect effects of soil physicochemical properties on the plant-soil-microbe C–N–P stoichiometry. Some variables (such as soil C:N and C:P ratios, leaf C:P ratio, understorey herb biomass C:P ratio, litter C:P and N:P ratios and microbial biomass C:N and C:P ratios) were excluded from SEM analysis due to insignificant effects or collinearity. The distributions of all data were evaluated and normality of data was determined using the Kolmogorov-Smirnov test, and the non-normal variables were log-transformed to improve normality, before conducting SEM analysis. We selected the best model based on overall goodness of fit parameters, including the χ^2/df< 3, chi-square test statistic (P > 0.05), whole-model P value greater than 0.05, goodness of fit index (GFI> 0.90), comparative fit index (CFI > 0.90), and root mean square error of approximation (RMSEA< 0.05) (Schermelleh-Engel et al., 2003; Eisenhauer et al., 2016). SEM analyses were performed using AMOS version 24.0 software (IBM SPSS Inc.) and redundancy analysis (RDA) was conducted using CANOCO 5.0 tool to evaluate the relationships between C, N, and P concentrations and soil and leaf, understorey herb biomass, litter, and soil microbes. Origin 2021 software (Origin Lab Inc., Northampton, USA) was used to generate. P< 0.05 was considered statistically significant.

3 Results

3.1 Plant and soil properties

The results showed that plant and soil properties were significantly affected by sandy dune type, but exhibited differential responses (Table 2). Analysis of plant characteristics indicated that SBC and SH were high in the FD type, whereas DBH and SCS were higher in the MD type than in the other types (P< 0.05). Analysis of soil characteristics showed that the content of DOC, IN and AP increased from the MD to FD type; however, no significant changes were observed among sites in several cases. Soil pH, BD and SM did not significantly differ among the different sandy dune types. These findings indicate that sand dune stabilization and revegetation improve the soil fertility level.

TABLE 2 Characteristics of the plant and soil under three sandy dune types.

Types	FD	SFD	MD	F	*P*
Shrub coverage (%)	52.11 ± 2.62a	17.21 ± 1.43b	5.72 ± 0.36b	18.615	**<0.001**
Shrub crown size (m^2)	1.19 ± 0.75c	1.78 ± 0.42b	1.96 ± 0.28a	33.236	**<0.001**
Diameter at breast height (cm)	9.88 ± 0.25c	9.93 ± 0.80b	12.55 ± 0.92a	13.843	**<0.001**
Shrub height (cm)	56.38 ± 2.50a	43.52 ± 5.32c	51.76 ± 3.13b	8.459	**0.001**
Soil moisture (%)	4.99 ± 0.54a	4.08 ± 0.29a	3.47 ± 0.29a	1.663	0.197
pH	9.93 ± 0.08a	9.60 ± 0.12a	9.58 ± 0.14a	1.918	0.154
BD (g cm^{-3})	1.52 ± 0.01a	1.55 ± 0.02a	1.56 ± 0.01a	1.074	0.347
DOC (mg kg^{-1})	93.34 ± 7.53a	37.79 ± 4.83a	30.84 ± 4.69a	1.275	0.286
Inorganic N (mg kg^{-1})	5.90 ± 0.39a	4.68 ± 0.76a	4.63 ± 0.49a	0.754	0.474
Available P (mg kg^{-1})	2.23 ± 0.16a	2.08 ± 0.15b	1.57 ± 0.11b	4.100	**0.021**

FD, fixed dune; SFD, semifixed dune; MD, moving dune; BD, soil bulk density; DOC, dissolved organic carbon. Different lowercase letters indicate significant difference among the sandy dune types at p< 0.05. P-values < 0.05 were marked in bold.

3.2 C:N:P stoichiometry in plants and soils

Carbon concentrations in leaves, understorey herb biomass and litter were not significantly different among the three sandy dune types ($P > 0.05$; Figure 1). Nitrogen concentration was higher in leaves than in understorey herb biomass, and was significantly higher in understorey herb biomass and litter of the FD type than that in the MD ($P< 0.05$). The P concentration in leaves was significantly higher in the FD than that in leaves in the SFD and MD types, whereas the P concentrations in the understorey herb biomass and litter were highest in FD type compared with the other sandy dune types; however, no significant changes were observed among sites in several cases. The C:N in leaves, understorey herb biomass and litter were not significantly different among the three sandy dune types ($P > 0.05$) (Figure 1). The C:P ratio in leaves, understorey herb biomass and litter were lowest in FD type in the order MD > SFD > FD ($P< 0.05$) (Figure 1). The N:P ratio in leaves and litter in MD type was significantly higher than that in FD type ($P< 0.05$). The N:P ratio in understorey herb biomass was not significantly different among the three sandy dune types (Figure 1).

The sandy dune type significantly affected C, N and P concentrations and their ratios in soil and microbial biomass. however, sandy dune type did not affect soil C:P and N:P ratios. The C, N and P concentrations in the soil and microbial biomass increase with the increase in sand dune stabilization, and were significantly higher in the FD type than in MD type (Figure 2B). The soil C:N ratios in SFD and MD types were significantly relative to those in FD type ($P< 0.05$). The soil N:P ratio was higher in FD type than in SFD and MD types ($P > 0.05$). Microbial biomass C:P and N:P ratios were significantly higher in FD type than in SFD and MD types ($P< 0.05$).

3.3 Relationships between plant and soil C:N:P ecological stoichiometry and the potential regulators

The C, N, and P concentrations of plant components and microbial biomass and their stoichiometries exhibited different responses to soil C, N, and P concentrations and their ratios (Figure S1). Soil C concentrations were positively correlated with the C, N, and P concentrations in understorey herb biomass, litter, and microbial biomass and C concentration in litter ($P< 0.05$). Soil TN concentrations were positively correlated with N and P concentrations in understorey herb biomass, litter, and microbial biomass and C concentrations in understorey herb biomass and microbial biomass and negatively correlated with C concentration in leaves ($P< 0.05$). Soil P concentrations were positively correlated with C concentrations in leaves and microbial biomass and N and P concentrations in understorey herb biomass ($P< 0.05$). MBC, MBN and MBP were positively

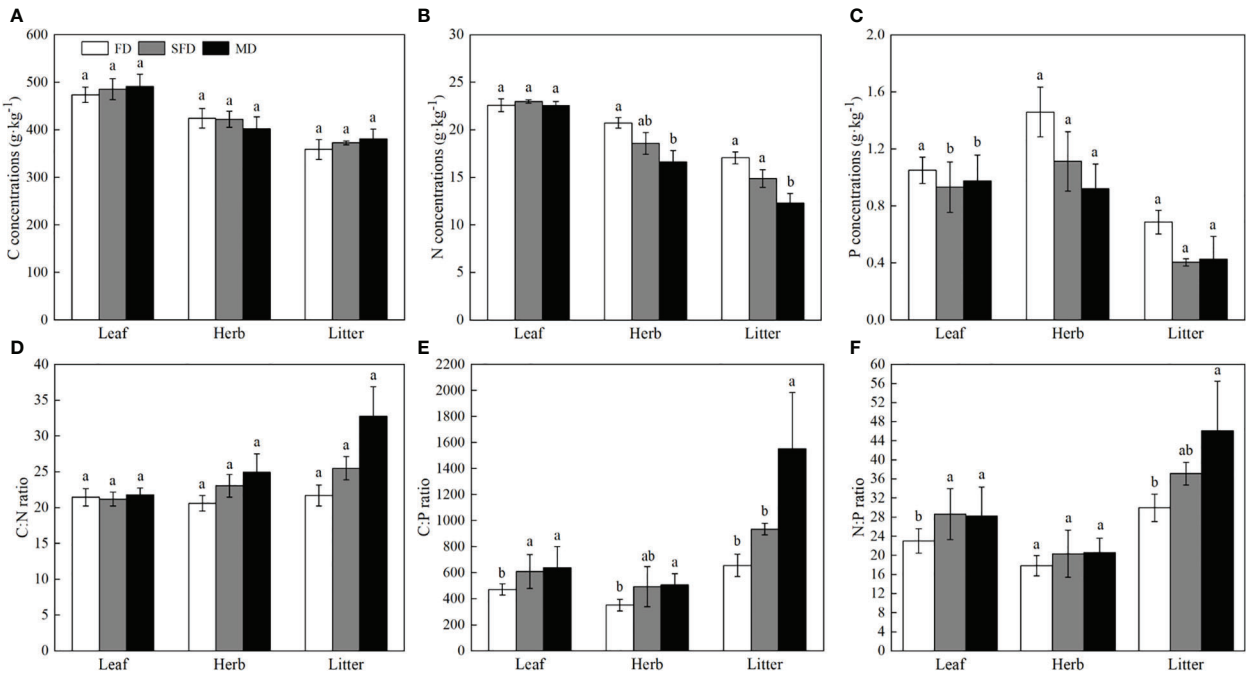

FIGURE 1
C, N, and P concentrations **(A–C)** and stoichiometry **(D–F)** in different components. *Sophora moorcroftiana* shrub under different sandy dune types. Different lowercase letters indicate significant difference under different sandy dune types based on analysis of variance and least significant difference tests (P< 0.05). FD, fixed dune; SFD, semifixed dune; MD, moving dune; Herb, understorey herb biomass.

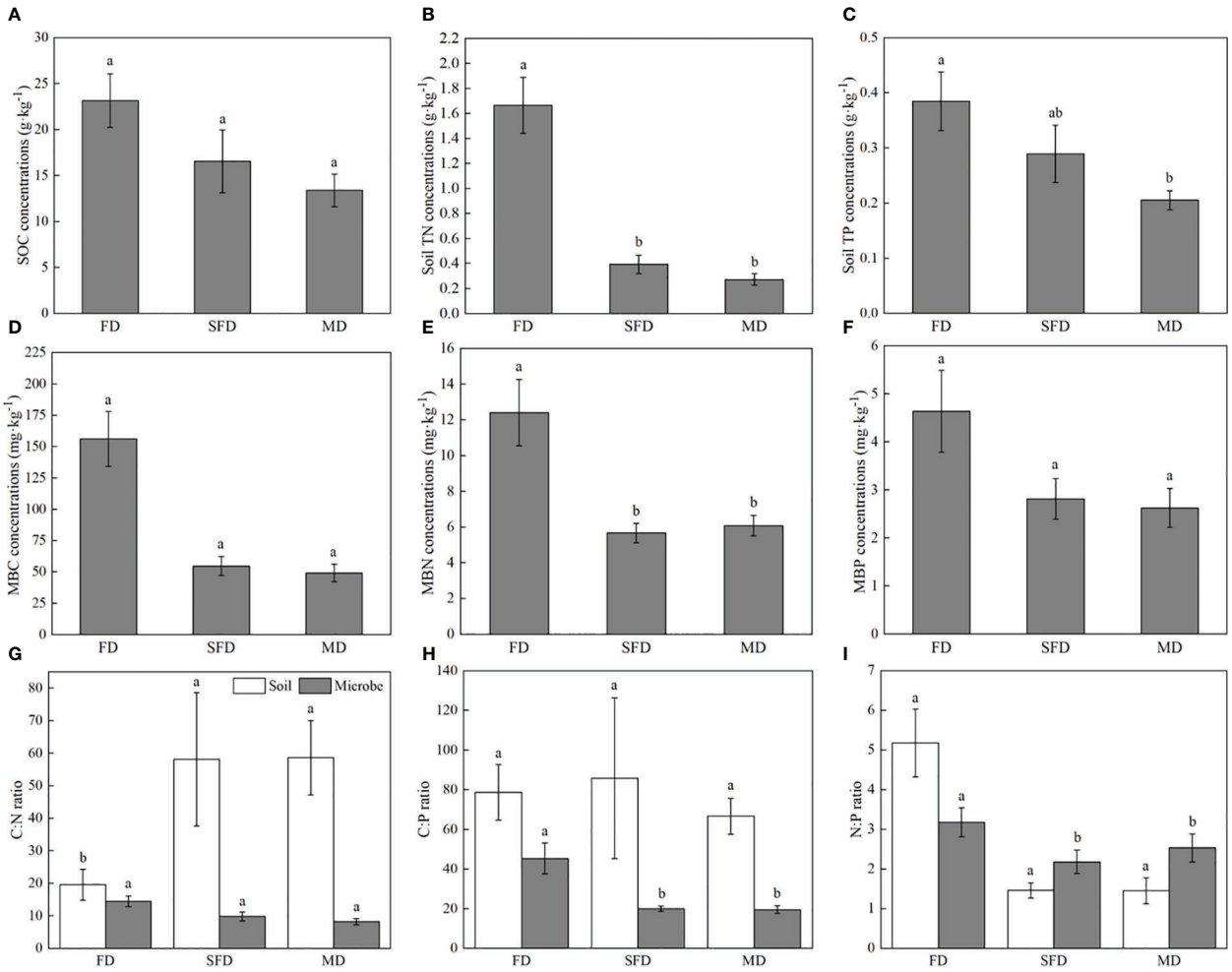

FIGURE 2
C, N, and P concentrations and stoichiometry in soils and microbes of Sophora moorcroftiana population in 0–20 cm soil layer under different sandy dune types. C, N, and P concentrations in soils **(A–C)** and microbes **(D–F)**. C, N, and P stoichiometry **(G–I)** in soils and microbes. Different lowercase letters indicate a significant difference under different sandy dune types ($P < 0.05$). FD, fixed dune; SGL, sandy gravel land; SFD, semifixed dune; MD, moving dune.

correlated with the C, N, and P concentrations in understorey herb biomass and litter. The findings showed no significant correlation between C, N, and P concentrations in leaves and C, N, and P concentrations in soil (Figure S1). Leaves C:N ratio was significantly correlated with soil C:N and N:P ratios. Understorey herb biomass C:P and N:P ratios were significantly correlated with soil C:P and N:P ratios. Litter C:N, C:P and N:P ratios were significantly correlated with soil C:N and N:P ratios. Microbial biomass C:N and C:P ratios were significantly correlated with soil C:N and N:P ratios (Table 3).

RDA showed that the soil physicochemical properties (SM, BD, pH, DOC, AP, and IN) explained 30.7% of the total variation in the data, with axes 1 and 2 explaining 18.8% and 7.6% of the total variation, respectively (Table 4). DOC, AP and pH variables accounted for a greater proportion of the variance of the C:N:P ecological stoichiometry in plants, soils and microbes than SM, IN and BD variables (Figure 3). DOC and AP significantly affected C:N:P ecological stoichiometry in plants, soils and microbes.

SEM exhibited a good fit according to the χ^2 test, GFI, AGFI, CFI and RMSEA metrics (Figure 4). SEM analysis showed that soil physicochemical properties directly affected microbe stoichiometry or indirectly through plant and soil stoichiometry. SM had the greatest negative direct effect on microbial biomass N:P ratio (path coefficient = −0.824) compared with the other five variables and was significantly positively correlated with understorey herb biomass N:P ratio (0.399). SM indirectly impacted on leaves C:N and N:P ratios. pH indirectly impacted on N:P ratios in leaves, soil and microbial biomass. The results showed that AP directly affected N:P ratios in understorey herb biomass and soil. DOC directly affected N:P ratios in understorey herb biomass and soil and C:N ratios in leaves and litter. The findings showed that IN indirectly affected

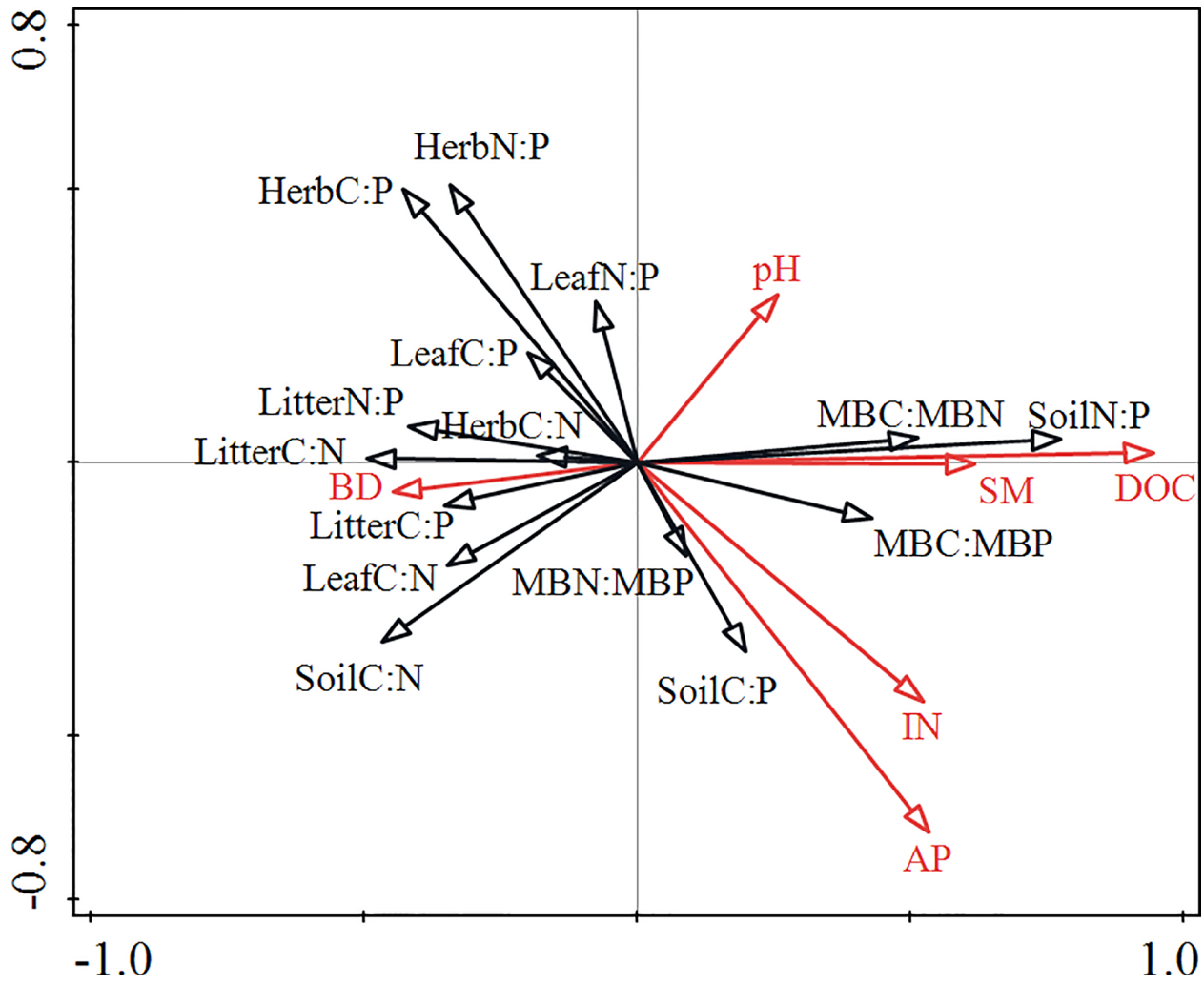

FIGURE 3
Redundancy analysis (RDA) showing the relationship between the plant-soil-microbe C:N:P ecological stoichiometry and soil physicochemical properties. SM, soil moisture content; IN, inorganic N (NH_4^+-N and NO_3^--N); AP, available phosphorus; BD, soil bulk density; DOC, dissolved organic carbon; Herb, understorey herb biomass.

plant and soil stoichiometry through DOC. Notably, BD was mainly modulated plant and soil stoichiometry through DOC. Soil N:P ratio directly affected microbial biomass C:N and N:P ratios. Leaf N:P ratio directly affected microbial biomass N:P ratio through C:N ratios in understorey herb biomass and litter as well as soil N:P ratio.

3.4 Effect of shrub age on plant and soil C:N:P ecological stoichiometry

Shrub age characteristics (including diameter at breast height, height and shrub crown size) exhibited varying responses to soil and leaf C:N:P stoichiometry (Figure 5). The height of *S. moorcroftiana* was significantly negatively correlated with C:N and C:P ratios of understorey herb biomass (Figure 5). On the contrary, height of *S. moorcroftiana* was significantly positively correlated with the C:N ratio of leaves (Figure 5) and exhibited a downward "unimodal" trend with litter N:P ratio (Figure 5). Soil N:P ratio decreased from 17 to 50 cm height and then increased, exhibiting an upward "unimodal" trend (Figure 5). Diameter at breast height and shrub crown size were positively correlated with C:N and C:P ratios of litter and N:P ratio of litter (Figures 5B, C, E). Conversely, diameter at breast height and shrub crown size were significantly negatively correlated with soil N:P (Figure 5), but significantly positively correlated with soil C:N ratio (Figures 5). Shrub crown size was significantly negatively correlated with microbial biomass C:N and C:P ratios (Figures 5). These findings indicate that the C:N:P ratio in soil was significantly correlated with the shrub crown size and diameter at breast height.

TABLE 3 Correlation coefficients between soil ecological stoichiometry and plant, soil microbial biomass ecological stoichiometry.

	Soil C:N	Soil C:P	Soil N:P
Leaf C:N	0.335**	0.190	-0.381**
Leaf C:P	0.178	-0.209	-0.268*
Leaf N:P	0.004	-0.170	-0.116
Herb C:N	0.273*	0.118	-0.082
Herb C:P	0.062	-0.258*	-0.315**
Herb N:P	-0.118	-0.393**	-0.294*
Litter C:N	0.456**	0.000	-0.413**
Litter C:P	0.464**	-0.009	-0.418*
Litter N:P	0.294*	-0.005	-0.354**
SMB C:N	-0.438**	0.137	0.534**
SMB C:P	-0.285*	0.149	0.318**
SMB N:P	-0.012	0.168	0.101

Herb, understorey herb biomass; SMB, soil microbial biomass. *P < 0.05, **P < 0.01.

4 Discussion

4.1 C:N:P stoichiometry in plants among the different sandy dune types

N and P are the main mineral elements that limit plant growth. The two mineral elements play important roles in modulating plant growth, reproduction and metabolism in most terrestrial ecosystems (Chapin, 1980; Reich et al., 1997; Han et al., 2005). Previous studies reported that leaf N:P ratio in plant biomass indicates the relative N or P limitation at the community level. Shifts in limitation cause changes in plant functional traits, vegetation composition and botanical diversity (Koerselman and Meuleman, 1996; Roem and Berendse, 2000; Güsewell, 2004). The "law of the minimum" states that there is a "critical N:P ratio" below which plant growth is limited only by N, and conversely above which growing plants are only limited by P (Güsewell, 2004). Previous findings indicate that N:P ratios > 16 indicate P limitation, whereas N:P ratios< 14 represent N limitation, and plant growth is co-limited by N and P under intermediate values (Aerts and Chapin, 2000; Reich, 2005; Fan et al., 2015). Güsewell (2004) observed that plant growth was relatively limited by nitrogen when the N:P ratio in leaves was< 10, whereas plant growth was relatively limited by phosphorus when the N:P ratio was > 20. Moreover, plant growth was limited by N or P when the N:P ratio was between 10 and 20, depending on plant-specific conditions.

In the current study, the leaf N:P ratio ranged from 18.5 to 28.3, and the mean foliar N:P ratio was 25.7, higher than the value reported by Han et al. (2005). The average N:P ratio of China's flora is 16.3 and the global averages are 12.7 and 13.8 (Elser et al., 2000; Reich and Oleksyn, 2004). Leaf N concentrations ranged between 22.5 to 23.0 $g{\cdot}kg^{-1}$, and the P concentrations were > 1.0 mg g^{-1}, ranging from 1.0 to 1.3 $g{\cdot}kg^{-1}$ (Figure 1). This finding indicates that P was the main limiting element for the *S. moorcroftiana* population in the study area. This finding is consistent with a report that Chinese vegetation exhibits a higher degree of P limitation, as indicated by analysis of 753 species (Han et al., 2005). The high leaf N:P ratios (low P content) can be attributed to the low P content of soils in China (Han et al., 2005). Plant and soil phosphorus are generally coupled at the ecosystem scale (Aerts and Chapin, 2000; Han et al., 2005). In addition, the P limitation may be caused by the ability of leguminous plants to fix N from the air resulting in a higher N:P ratio (Yang et al., 2018), whereas P is a 'rock-derived' element and cannot be obtained in high amounts from the soil (Walker and Syers, 1976). Recent studies report that understorey species have higher ability to obtain P from the soil than dominant tree species (Huang et al., 2013), resulting in P limitation in overstorey trees (Zhang et al., 2019). Roots of overstory trees are distributed deeper into the soil as they age (Jiao et al., 2016). Deep-rooted systems cannot preferentially access P and other resources supplied by plants (Chen et al., 2016a), resulting in lower P concentrations and higher N:P ratio in leaves (Figure 1), and which limits the growth of *S. moorcroftiana* (Table 2).

TABLE 4 Redundancy analysis (RDA) of the plant-soil-microbe ecological stoichiometry and soil physicochemical properties using forward selection with a Monte Carlo permutation test.

Variables	Explains (%)	Contribution (%)	F-ratio	*P*-Value	Axis	1	2
DOC	16.8	54.6	14.2	0.001	Eigenvalues	18.8	7.6
AP	5.9	19.2	5.3	0.001	Explained variation	18.8	26.37
pH	2.9	9.5	2.7	0.031	Pseudo-canonical correlation	0.756	0.527
SM	2.8	9.0	2.6	0.028	Explained fitted variation	60.97	85.53
IN	1.6	5.2	1.5	0.187			
BD	0.7	2.4	0.7	0.627			

SM, soil moisture content; IN, inorganic N ($NH4^+$-N and $NO3^-$-N); AP, available phosphorus; BD, soil bulk density; DOC, dissolved organic carbon.

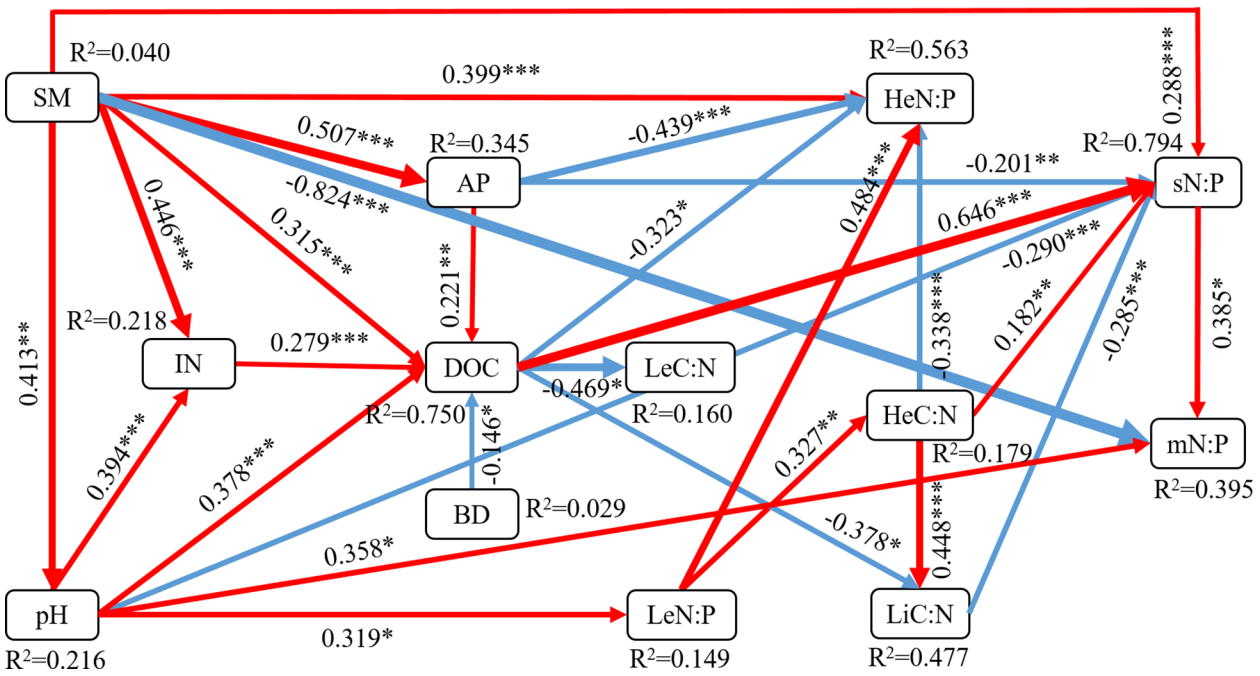

FIGURE 4
Structural equation modeling (SEM) analysis of the effects of soil physicochemical properties on the plant-soil-microbe C–N–P stoichiometry. Results of model fitting: $\chi 2$ = 0.004, df = 1, P = 0.953, GFI = 1.000, AGFI = 0.999, CFI = 1.000, RMSEA = 0.000. Numbers on arrows are standardized path coefficients. Red and blue arrows indicate positive and negative effects, respectively, with the thickness representing the extent of influence. R2 values represent the proportion of the variance explained for each endogenous variable. SM, soil moisture content; IN, inorganic N (NH4+-N and NO_3^--N); AP, available phosphorus; BD, soil bulk density; DOC, dissolved organic carbon; Le, Sophora moorcroftiana leaf; He, understorey herb biomass; Li, litter; s, soil; m, microbial biomass. Significance levels are as follows: *P < 0.05, **P < 0.01, and ***P < 0.001.

Litter is a nutrient pool (Xiao et al., 2015; Liu and Wang, 2021), and its C:N:P stoichiometry ratio modulates soil nutrient availability and quality in terrestrial ecosystems (Villalobos-Vega et al., 2011; Zhang et al., 2017). Previous studies reported that a litter C:N ratio< 40, promotes decomposition of the litter and net release of nitrogen, and lower ratios of C:N and C:P are associated with faster decomposition rate (Parton et al., 2007). In this study, the C:N ratio in litter was lower than 40, indicating a high rate of decomposition and faster release of nitrogen from litter. N:P ratio is a vital indicator for characterizing the decomposition rate of litter, and a lower ratio is associated with higher rate of litter decomposition (Sun et al., 2019). The present results showed that the N:P ratio in litter ranged from 29.9 to 46.1 and higher than the level of 25 reported previously (Güsewell and Verhoeven, 2006). This N:P ratio in litter indirectly indicated the nutrient limitations of *S. moorcroftiana* shrub community growth in the study area.

4.2 C:N:P stoichiometry in soils and microbes across the different sandy dune types

Vegetation restoration can affect plant diversity and composition (Zhao et al., 2019), increasing quantity and quality of litter and rhizodeposition (Zhang et al., 2019). These effects ultimately improve the soil pool and soil nutrients (Deng et al., 2013; Yang et al., 2018; Deng et al., 2018). Variations in environmental conditions of soil structure, pH, temperature and moisture can be modulated by vegetation restoration (Fernández-Calviño et al., 2011; Ahmed et al., 2019), which in turn increases soil microbial biomass and enzyme activities associated with nutrient decomposition and circulation (Zhang et al., 2019; Figure 2). Ultimately, these effects increase soil C, N, and P contents (Figure 2). An increase in C, N and P imbalance causes changes in soil C:N:P stoichiometry (Zhang et al., 2019). In the present study, the soil C:N ratios of the SFD and MD types were significantly higher than the rations in FD type. The N:P ratios varied in an opposite pattern among the three sandy dune types (Figure 2), because the increasing ratios of N was higher than that of C and P (Figure 2). Soil C:N ratio is an important indicator of microbial activity. Soil C:N ratio determines the mineralization rate of SOM and release of available N, and can directly modulate the competition between microorganisms and plants for N and indirectly affect plant photosynthesis (Brust, 2019; Qi et al., 2022). The average soil C:P ratio in this study was 77.3, which is higher than the average ratio reported in China (61.0), and the N:P ratio (3.8) was lower than the global average ratio (5.9) (Han et al., 2005; Yang et al., 2018). This finding indicates that the soil N (C:N = 36.8) and P (C:P = 62.5) (Han

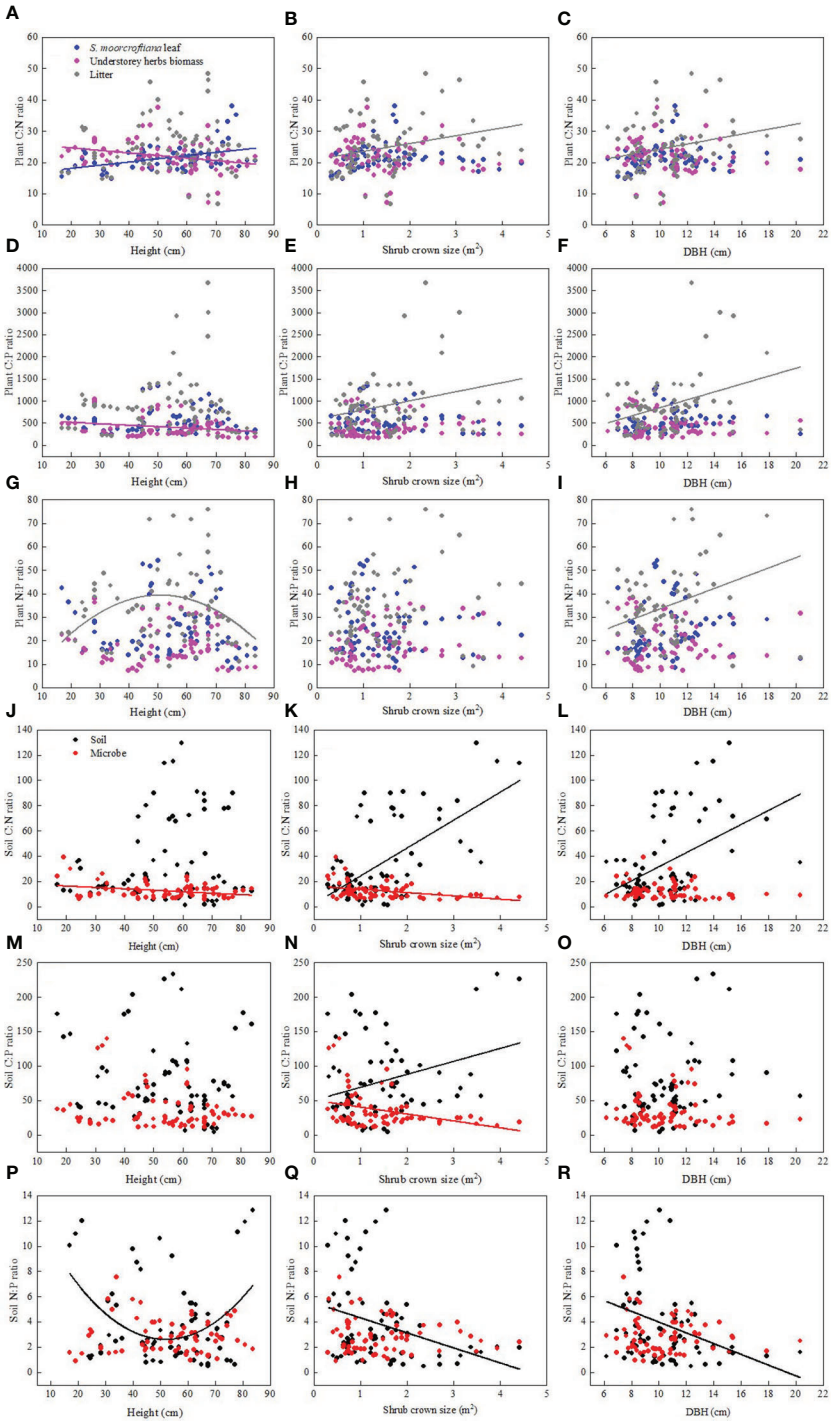

FIGURE 5
Relationships between Sophora moorcroftiana height and plant stoichiometry **(A–G)** , shrub crown size and plant stoichiometry **(B–H)** diameter at breast height (DBH) and plant stoichiometry **(C–I)**, Sophora moorcroftiana height and soil stoichiometry **(J–P)**, shrub crown size and soil stoichiometry **(K–Q)**, diameter at breast height (DBH) and soil stoichiometry **(L–R)**, respectively.

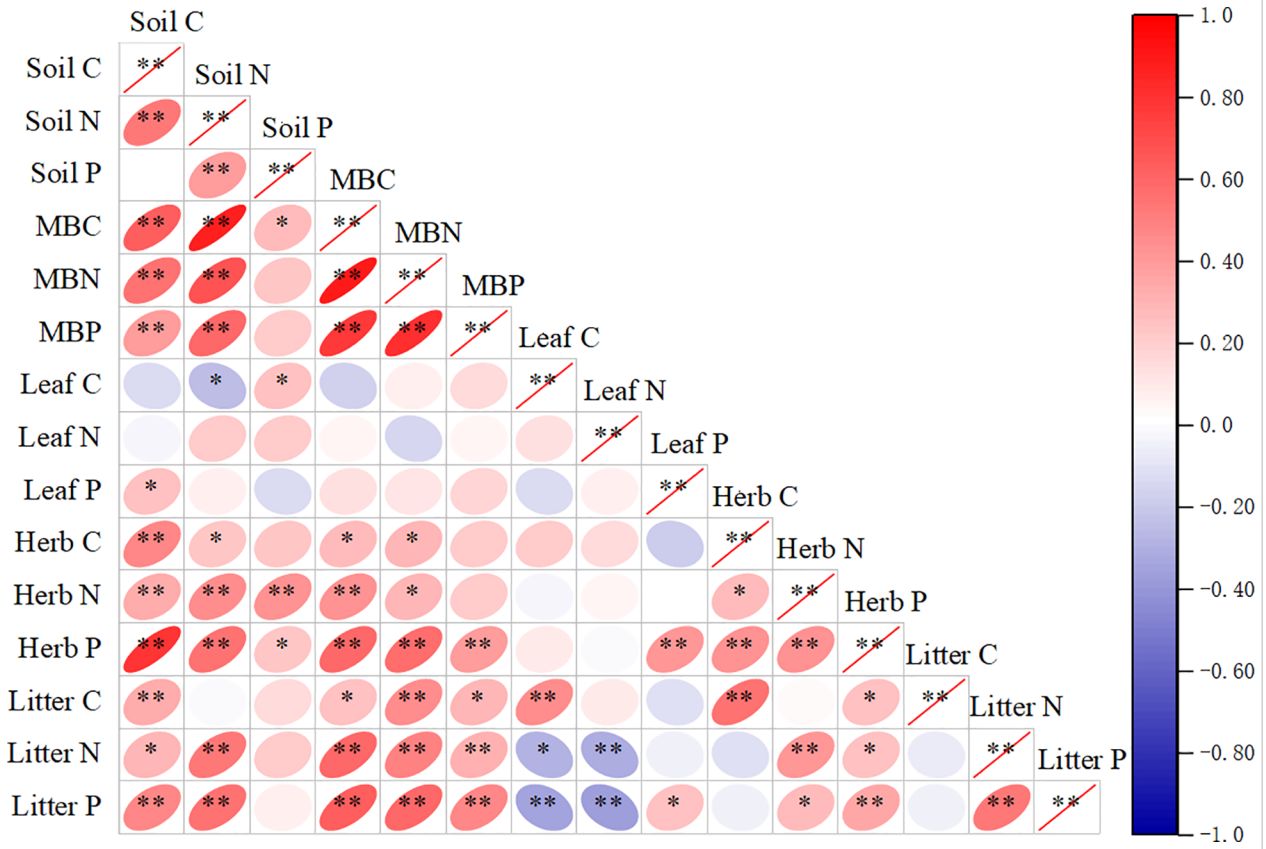

FIGURE 6
Correlations between soil, soil microbial biomass, Sophora moorcroftiana leaf, herb, and litter C, N, and P concentrations. Herb, understorey herb biomass. *P < 0.05, **P < 0.01.

et al., 2005) contents in the study sites were relatively low. This observation can be attributed to insufficient supply of P caused by the N fixation process (Bell et al., 2014).

Soil microbes act as the main nutrient reservoir, and their stoichiometry is highly correlated with the above-ground plant communities (Qi et al., 2022). Soil microbes can maintain stoichiometric homeostasis through compensatory regulation (Chen and Chen, 2021). The soil microbial biomass C:N:P stoichiometry in this study was 15:1.2:1, which was narrower than that of shrub-land (43:6:1), desert (31:4:1) and the global average (42:6:1) (Xu et al., 2013). This large discrepancy is mainly attributed to the lower SOC content in deserts (Wang et al., 2022b); The stoichiometric variability decreases with soil OM processing (Mooshammer et al., 2014). In this study, significantly positive correlations were observed between the microbial biomass C, N, and P and SOC (Figure S1). Soil microbial biomass C is mainly positively correlated with microbial biomass N (Figure 6), as higher microbial biomass leads to higher microbial N requirements (Deng et al., 2016). A meta-analysis by Xu et al. (2013) reported that the average microbial biomass C:N ratios was 7.6 and ranged from 4.5 to 12.5, and the average of microbial N:P ratios was 5.6, with a rang from 3.5 to 10.6. The soil samples at the present study site exhibited significantly higher microbial biomass C:N (13.4) and lower N:P (2.9) ratio (Figure 2), which can be attributed to relatively lower N availability to soil microbes. A greater microbial biomass C:N ratio indicates a lower level of N in the soil and poor mineralization rate due to a lack of enough detrital material and the desired type of microbial population (Arunachalam and Pandey, 2002).

4.3 Correlations with the C:N:P stoichiometry

In this study, plant C and N concentrations were significantly correlated with soil C and N concentrations but weakly correlated with soil P concentrations (Figure S1). This finding indicates that the C and N contents in understorey herb plants and litter have a significant relationship with soil nutrients. This type of interaction is observed mainly because

the soil C content is determined by the coefficient of humus and organic matter in the soil, whereas the N in decomposed litter is mainly absorbed to the soil, whereas P is mainly retained in the litter (Robbins et al., 2019). The soil C:N ratio was significantly correlated with the C:N ratios in leaves, litter and microbial biomass (Table 3). The litter in the surface layer can act as the main supply to the soil, leading to accumulation of C and N (Yang and Liu, 2019). Nitrogen-fixing plants effectively absorb N and SOC (Li et al., 2014). The effects of diversity on plant C:N:P ratios may modulate soil nutrient input levels and microorganisms through litter (Zechmeister-Boltenstern et al., 2015; Chen and Chen, 2021). RDA indicated that soil physicochemical properties explained the largest variance in the plant and soil C:N:P stoichiometry (Figure 3), with DOC, AP, pH and SM as the most important factors (Table 4). Water loss can lead to nutrient loss (Peng et al., 2020), which is consistent with the observed significant positive correlations between the SM and DOC, AP and IN in this study. Plant diversity positively affects soil microbial community through the regulation of water absorption (Wang et al., 2022a). The present results showed a positive correlation between SM and N:P ratios in the understorey herb biomass and soil, and a negative correlation between SM and MBN : MBP (Figure 4). Soil pH is a key indicator of soil nutrient availability and is correlated with soil microbial activity. Soil pH and litter elements ratios are the main factors that modulate surface soil N:P ratio (Yang et al., 2018; Qiao et al., 2020), which is consistent with the present findings. Soil C:N:P ratios represent stoichiometric ratios of their sources, including plant and microbial residues (Chen and Chen, 2021). Higher litter inputs increase soil nutrient retention, resulting in reduction of soil microbial C: nutrient ratio (Chen and Chen, 2021). A previous study reported that slow-growing shrubs in P-poor systems transfer P from deeper soil layers to shallow soils, which helps meet the high leaf P requirements of fast-growing understorey herbs (He et al., 2014; Luo et al., 2021). This explains why leaf P content was closely correlated with the understorey herb biomass P content and the C:P and N:P ratios in the present study. This finding indicates that a correlation between the P levels of plants and soil P levels. AP can indicate the degree of P limitation (Zhang et al., 2019). These results validated our second hypothesis that soil properties is a key driver of C:N:P stoichiometry in plant-soil-microbe systems.

5 Conclusion

The aim of this study was to explore the effects of sandy dune type on the C:N:P stoichiometry in “plant-soil-microbe” and evaluate the factors that modulate *S. moorcroftiana* shrub community. The findings showed that sandy dune type had significant effects on C, N, and P contents and stoichiometry in plants, soils and microbes, implying that the C:N:P stoichiometric ratios can form a complex network in this region. The results indicated that a significant correlation was observed between plants and soils C:N:P stoichiometry. This observation implies that the changes in C:N:P stoichiometry may be induced by shifts in soil physicochemical properties, especially DOC, AP, SM and pH. Furthermore, significant increases in plant and soil C:P ratios and decreases in soil N:P ratios were observed with an increase in shrub age, indicating that the demand for P increased with shrub age. In this study, C:N:P stoichiometry interactions among plants, soils, and soil microbes and their responses to the sandy dune type were evaluated. The findings highlight the importance of soil physicochemical properties in shaping the C:N:P stoichiometry and improve our understanding of the nutrient stoichiometry patterns and management strategies of plants and soils in alpine desert ecosystems on the Tibetan Plateau.

Data availability statement

The original contributions presented in the study are included in the article/Supplementary Material. Further inquiries can be directed to the corresponding authors.

Author contributions

RD: Formal analysis, Writing-original draft, Writing-review and editing, SY: Resources, Funding acquisition, XW: Funding acquisition, LX: Resources, YM: Conceptualization, Resources, YW: Resources, LZ: Investigation, MZ: Investigation, JQ: Investigation. All authors contributed to the article and approved the submitted version.

Funding

This work was supported by the "A Demonstration Study on Domestication and Application of Native Ecological Grass Species in Alpine Region", Scientific Research Project of "Qinghai Scholars" in Qinghai Province, the Joint Grant from Chinese Academy of Sciences-People's Government of Qinghai Province on Sanjiangyuan National Park (2020-LHZX-08), the Comprehensive Research Base for Utilization and Innovation of Native Plant Germplasm Resources of Shigatse City, and the Regional Science and Technology Collaborative Innovation Project of Shigatse Bureau of Science and Technology (QYXTZX-RKZ2022-01).

Acknowledgments

The authors especially thank Shigatse Baiyacheng Agricultural Products Processing Co., Ltd, Shigatse, China and Tibet Yunwang Industrial Co., Ltd, Shigatse, China for their help with the fieldwork.

Conflict of interest

Author SY was employed by Tibet Yunwang Industrial Co., Ltd.

The remaining authors declare that the research was conducted in the absence of any commercial or financial relationships that could be construed as a potential conflict of interest.

Publisher's note

Supplementary material

The Supplementary Material for this article can be found online at: https://www.frontiersin.org/articles/10.3389/fpls.2022.1060686/full#supplementary-material

References

Aerts, R., and Chapin, F. S. (2000). The mineral nutrition of wild plants revisited: a re-evaluation of processes and patterns. *Adv. Ecol. Res.* 30, 1–67.

Ahmed, I. U., Mengistie, H. K., Godbold, D. L., and Sanden, H. (2019). Soil moisture integrates the influence of land-use and season on soil microbial community composition in the Ethiopian highlands. *Appl. Soil Ecol.* 135, 85–90.

Arunachalam, A., and Pandey, H. N. (2003). Ecosystem restoration of jhum fallows in northeast India: Microbial c and n along altitudinal and successional gradients. *Restor. Ecol.* 11, 168–173.

Bai, Y. X., She, W. W., Michalet, R., Zheng, J., Qin, S., and Zhang, Y. Q. (2018). Benefactor facilitation and beneficiary feedback effects drive shrub-dominated community succession in a semi-arid dune ecosystem. *Appl. Veg. Sci.* 21, 595–606.

Bai, Y. X., She, W. W., Zhang, Y. Q., Qiao, Y. G., Fu, J., and Qin, S. G. (2019). N enrichment, increased precipitation, and the effect of shrubs collectively shape the plant community in a desert ecosystem in northern China. *Sci. Total Environ.* 716, 135379.

Bell, C., Carrillo, Y., Boot, C. M., Rocca, J. D., Pendall, E., and Wallenstein, M. D. (2014). Rhizosphere stoichiometry: are C:N:P ratios of plants, soils, and enzymes conserved at the plant species-level? *New Phytol.* 201, 505–517.

Brookes, P. C., Landman, A., Pruden, G., and Jenkinson, D. S. (1985). Chloroform fumigation and the release of soil nitrogen: a rapid direct extraction method to measure microbial biomass nitrogen in soil. *Soil Biol. Biochem.* 17, 837–842.

Brust, G. E. (2019). "Chapter 9-management strategies for organic vegetable fertility," in *Safety and practice for organic food*. Eds. D. Biswas and S. A. Micallef (Academic Press), 193–212.

Chapin, F. S. (1980). The mineral nutrition of wild plants. *Ann. Rev. Ecol. Syst.* 11, 233–260.

Chen, X. L., and Chen, H. Y. H. (2021). Plant mixture balances terrestrial ecosystem C:N:P stoichiometry. *Nat. Commu.* 12, 4562.

Chen, Y., Chen, L., Peng, Y., Ding, J., Li, F., and Yang, G. (2016b). Linking microbial C:N:P stoichiometry to microbial community and abiotic factors along a 3500-km grassland transect on the Tibetan plateau. *Glob. Ecol. Biogeogr.* 25, 1416–1427.

Cheng, S. M., Qiong, L., Lu, F., Yonezawa, T., Yin, G. Q., Song, Z. P., et al. (2017). Phylogeography of *Sophora moorcroftiana* supports wu's hypothesis on the origin of Tibetan alpine flora. *J. Hered.* 108, 405–414.

Chen, L., Mu, X., Yuan, Z., Deng, Q., Chen, Y., and Yuan, L. Y. (2016a). Soil nutrients and water affect the age-related fine root biomass but not production in two plantation forests on the loess plateau, China. *J. Arid Environ.* 135, 173–180.

Cleveland, C. C., and Liptzin, D. (2007). C:N:P stoichiometry in soil: is there a 'Redfield ratio'for the microbial biomass? *Biogeochemistry* 85, 235–252.

Cross, W. F., Benstead, J. P., Frost, P. C., and Thomas, S. A. (2005). Ecological stoichiometry in freshwater benthic systems: recent progress and perspectives. *Freshw. Biol.* 50, 1895–1912.

Daufresne, T. (2004). Optimal nitrogen-to-phosphorus stoichiometry of phytoplankton. *Nature* 429, 171–174.

Deng, Q., Cheng, X. L., Hui, D. F., Zhang, Q., Li, M., and Zhang, Q. F. (2016). Soil microbial community and its interaction with soil carbon and nitrogen dynamics following afforestation in central China. *Sci. Total Environ.* 541, 230–237.

Deng, L., Kim, D. G., Peng, C. H., and Shangguan, Z. P. (2018). Controls of soil and aggregate-associated organic carbon variations following natural vegetation restoration on the loess plateau in China. *Land Degrad. Dev.* 29, 3974–3984.

Deng, L., Shangguan, Z. P., and Sweeney, S. (2013). Changes in soil carbon and nitrogen following land abandonment of farmland on the loess plateau, China. *PloS One* 8, e71923.

Du, C. J., and Gao, Y. H. (2021). Grazing exclusion alters ecological stoichiometry of plant and soil in degraded alpine grassland. *Agric. Ecosyst. Environ.* 308, 107256.

Eisenhauer, N., Bowkerc, M. A., Graced, J. B., and Powell, J. R. (2016). From patterns to causal understanding: Structural equation modeling (SEM) in soil ecology. *J. Pedobi.* 58, 65–72.

Elser, J. J., Fagan, W. F., Denno, R. F., Dobberfuhl, D. R., Folarin, A., Huberty, A., et al. (2000). Nutritional constraints in terrestrial and freshwater food webs. *Nature* 408, 578–580.

Fan, H., Wu, J., Liu, W., Yuan, Y., Hu, L., and Cai, Q. (2015). Linkages of plant and soil C:N:P stoichiometry and their relationships to forest growth in subtropical plantations. *Plant Soil* 392, 127–138.

Fernández-Calviño, D., Rousk, J., Brookes, P. C., and Bååth, E. (2011). Bacterial pH-optima for growth track soil pH, but are higher than expected at low pH. *Soil Biol. Biochem.* 43, 1569–1575.

Guo, Q. Q., Fang, J. P., and Bian, D. (2009). Effect of different disturbances on structural characteristics of *Sophora moorcroftiana* communities. *Acta Bot. Bor-Occid. Sin.* 29, 1670–1677.

Guo, Q. Q., Zhang, W. H., and Li, H. E. (2014). Comparison of photosynthesis and antioxidative protection in *Sophora moorcroftiana* and *Caragana maximovicziana* under water stress. *J. Arid Land* 6, 637–645.

Güsewell, S. (2004). N:P ratios in terrestrial plants: variation and functional significance. *New Phytol.* 164, 243–266.

Güsewell, S., and Verhoeven, J. T. A. (2006). Litter N:P ratios indicate whether n or p limits the decomposability of graminoid leaf litter. *Plant Soil.* 287, 131–143.

Han, W., Fang, J., Guo, D., and Zhang, Y. (2005). Leaves nitrogen and phosphorus stoichiometry across 753 terrestrial plant species in China. *New Phytol.* 168, 377–385.

He, M. Z., Dijkstra, F. A., Zhang, K., Li, X. R., Tan, H. J., Gao, Y. H., et al. (2014). Leaf nitrogen and phosphorus of temperate desert plants in response to climate and soil nutrient availability. *Sci. Rep.* 4, 6932.

Higgins, K. F., Jenkins, K. J., Clambey, G. K., Uresk, D. W., Naugle, D. E., Klaver, R. W., et al. (2012). Vegetation sampling and measurement. In: Silvy, N.J. (Ed.), *Techniques for Wildlife Investigations and Management*. Ed. N. J. Silvy (John Hopkins University Press), 381–409.

Hortal, S., Bastida, F., Armas, C., Lozano, Y. M., Moreno, J. L., Garcia, C., et al. (2013). Soil microbial community under a nurse-plant species changes in composition, biomass and activity as the nurse grows. *Soil Biol. Biochem.* 64, 139–146.

Huang, X. M., Liu, S. R., Wang, H., Hu, Z. D., Li, Z. G., and You, Y. M. (2014). Changes of soil microbial biomass carbon and community composition through mixing nitrogen-fixing species with *Eucalyptus urophylla* in subtropical China. *Soil Biol. Biochem.* 73, 42–48.

Huang, W., Liu, J., Wang, Y. P., Zhou, G., Han, T., and Li, Y. (2013). Increasing phosphorus limitation along three successional forests in southern China. *Plant Soil* 364, 181–191.

Jiao, L., Lu, N., Gao, G. Y., Wang, S., Jin, T. T., Zhang, L. W., et al. (2016). Comparison of transpiration between different aged black locust (*Robinia pseudoacacia*) trees on the semi-arid loess plateau, China. *J. Arid Land* 8, 604–617.

Joergensen, R. G., and Mueller, T. (1996). The fumigation-extraction method to estimate soilmicrobial biomass: calibration of the kEN value. *Soil Biol. Biochem.* 28, 33–37.

Koerselman, W., and Meuleman, A. F. M. (1996). The vegetation N:P ratio: a new tool to detect the nature of nutrient limitation. *J. Appl. Ecol.* 33, 1441.

Liao, C. R., Li, H. D., Lv, G. P., Tian, M. R., Tian, J. R., Shi, H. H., et al. (2021). Stability and micro-topographic effects of *Sophora moorcroftiana* population on a restored alluvial fan, southern Tibetan plateau. *Land Degrad. Dev.* 32, 2037–2049.

Li, X., Jiang, D., Zhou, Q., and Oshida, T. (2014). Soil seed bank characteristics beneath an age sequence of caragana microphylla shrubs in the horqin sandy land region of northeastern China. *Land Degrad. Dev.* 253, 236–243.

Liu, Y., Fang, Y., and An, S. S. (2020). How C:N:P stoichiometry in soils and plants responds to succession in *Robinia pseudoacacia* forests on the loess plateau, China. *For. Ecol. Manage.* 475, 118394.

Liu, R., and Wang, D. (2021). C:N:P stoichiometric characteristics and seasonal dynamics of leaf-root-litter-soil in plantations on the loess plateau. *Ecol. Indic.* 127, 107772.

Li, Y., Wang, S., Jiang, L., Zhang, L., Cui, S., Meng, F., et al. (2016). Changes of soil microbial community under different degraded gradients of alpine meadow. *Agric. Ecosyst. Environ.* 222, 213–222.

Luo, Y., Peng, Q. W., Li, K. H., Gong, Y. M., Liu, Y. Y., and Han, W. X. (2021). Patterns of nitrogen and phosphorus stoichiometry among leaf, stem and root of desert plants and responses to climate and soil factors in xinjiang, China. *Catena* 199, 105100.

Manzoni, S., Jackson, R. B., Trofymow, J. A., and Porporato, A. (2008). The global stoichiometry of litter nitrogen mineralization. *Science* 321, 684–686.

McGroddy, M. E., Daufresne, T., and Hedin, L. O. (2004). Scaling of C:N:P stoichiometry in forests worldwide: implications of terrestrial redfield-type ratios. *Ecology* 85, 2390–2401.

Mooshammer, M., Wanek, W., Zechmeister-Boltenstern, S., and Richter, A. (2014). Stoichiometric imbalances between terrestrial decomposer communities and their resources: mechanisms and implications of microbial adaptations to their resources. *Front. Microbiol.* 5, 22.

Parton, W., Silver, W. L., and Burker, I. C. (2007). Gloabal-scale similarities in nitrogen release patterns during longterm decomposition. *Science* 315, 361–364.

Peng, X. D., Dai, Q. H., Ding, G. J., Shi, D. M., and Li, C. M. (2020). Impact of vegetation restoration on soil properties in near-surface fissures located in karst rocky desertification regions. *Soil Till. Res.* 200, 104620.

Pii, Y., Mimmo, T., Tomasi, N., Terzano, R., Cesco, S., and Crecchio, C. (2015). Microbial interactions in the rhizosphere: beneficial influences of plant growth-promoting rhizobacteria on nutrient acquisition process. *A review. Biol. Fertil. Soils* 51, 403–415.

Plum, C., Husener, M., and Hillebrand, H. (2015). Multiple vs. single phytoplankton species alter stoichiometry of trophic interaction with zooplankton. *Ecology* 96, 3075–3089.

Pugnaire, F. I., Haase, P., Puigdefábregas, J., Cueto, M., Clark, S. C., Incoll, L. D., et al. (1996). Facilitation and succession under the canopy of a leguminous shrub, *Retama sphaerocarpa*, in a semi-arid environment in south-East Spain. *Oikos* 76, 455.

Qiao, Y., Wang, J., Liu, H., Huang, K., Yang, Q., Lu, R., et al. (2020). Depth-dependent soil c-N-P stoichiometry in a mature subtropical broadleaf forest. *Geoderma* 370, 114357.

Qi, D. D., Feng, F. J., Lu, C., and Fu, Y. M. (2022). C:N:P stoichiometry of different soil components after the transition of temperate primary coniferous and broad-leaved mixed forests to secondary forests. *Soil Till. Res.* 216, 105260.

Reich, P. B. (2005). Global biogeography of plant chemistry: filling in the blanks. *New Phytol.* 168, 263–266.

Reich, P. B., and Oleksyn, J. (2004). Global patterns of plant leaf n and p in relation to temperature and latitude. *Proc. Natl. Acad. Sci. U. S. A.* 101, 11001–11006.

Reich, P. B., Walters, M. B., and Ellsworth, D. S. (1997). From tropics to tundra: Global convergence in plant functioning. *Proc. Natl. Acad. Sci. U. S. A.* 94, 13730–13734.

Ren, C. J., Zhao, F. Z., Kang, D., Yang, G. H., Han, X. H., Tong, X. G., et al. (2016). Linkages of C:N:P stoichiometry and bacterial community in soil following afforestation of former farmland. *For. Ecol. Manage.* 376, 59–66.

Robbins, C. J., Matthaeus, W. J., Cook, S. C., Housley, L. M., Robison, S. E., Garbarino, M. A., et al. (2019). Leaf litter identity alters the timing of lotic nutrient dynamics. *Freshw. Biol.* 64, 2247–2259.

Roem, W. J., and Berendse, F. (2000). Soil acidity and nutrient supply ratio as possible factors determining changes in plant species diversity in grassland and heathland communities. *Biol. Conserv.* 92, 151–161.

Schade, J. D., Kyle, M., Hobbie, S. E., Fagan, W. F., and Elser, J. J. (2003). Stoichiometric tracking of soil nutrients by a desert insect herbivore. *Ecol. Lett.* 6, 96–101.

Schermelleh-Engel, K., Moosbrugger, H., and Müller, H. (2003). Evaluating the fit of structural equation models, tests of significance descriptive good-ness-of-fit measures. *Methods psychol. Res.* 8, 23–74.

Shen, W. S., Li, H. D., Sun, M., and Jiang, J. (2012). Dynamics of aeolian sandy land in the yarlung zangbo river basin of Tibet, China from 1975 to 2008. *Glob. Planet. Change* 86–87, 37–44.

Sterner, R. W., and Elser, J. J. (2002). *Ecological stoichiometry: The biology of elements from molecules to the biosphere* (Princeton: Princeton University Press).

Sun, J., Gao, P., Li, C., Wang, R., Niu, X., and Wang, B. (2019). Ecological stoichiometry characteristics of the leaf–litter–soil continuum of *Quercus acutissima* carr. and *Pinus densiflora* sieb. in northern China. *Environ. Earth Sci.* 78, 20.

Tilman, D. (1996). Biodiversity: population versus ecosystem stability. *Ecology* 77, 350–363.

Vance, E. D., Brookes, P. C., and Jenkinson, D. S. (1987). An extraction method for measuring soil microbial biomass c. *Soil Biol. Biochem.* 19, 703–707.

Villalobos-Vega, R., Goldstein, G., Haridasan, M., Franco, A. C., Miralles-Wilhelm, F., Scholz, F. G., et al. (2011). Leaf litter manipulations alter soil physicochemical properties and tree growth in a Neotropical savanna. *Plant Soil.* 346, 385–397.

Walker, T. W., and Syers, J. K. (1976). The fate of phosphorus during pedogenesis. *Geoderma* 15, 1–19.

Wang, Y. C., Chu, L., Daryanto, S., Lu, L., Ala, M., and Wang, L. (2019). Sand dune stabilization changes the vegetation characteristics and soil seed bank and their correlations with environmental factors. *Sci. Total Environ.* 648, 500–507.

Wang, Y. H., Li, S. F., Lang, X. D., Huang, X. B., and Su, J. R. (2022a). Effects of microtopography on soil fungal community diversity, composition, and assembly in a subtropical monsoon evergreen broadleaf forest of southwest China. *Catena* 211, 106025.

Wang, Z. Q., Zhao, M. Y., Yan, Z. B., Yang, Y. H., Niklas, K. J., Huang, H., et al. (2022b). Global patterns and predictors of soil microbial biomass carbon, nitrogen, and phosphorus in terrestrial ecosystems. *Catena* 211, 106037.

Wu, J., He, Z. L., Wei, W. X., O'Donnell, A. G., and Syers, J. K. (2000). Quantifying microbial biomass phosphorus in acid soils. *Biol. Fertil. Soils.* 32, 500–507.

Xiao, C., Janssens, I. A., Zhou, Y., Su, J., Liang, Y., and Guenet, B. (2015). Strong stoichiometric resilience after litter manipulation experiments; a case study in a Chinese grassland. *Biogeosciences* 12, 757–767.

Xiao, G., Li, T., Zhang, X., Yu, H., Huang, H., and Gupta, D. K. (2009). Uptake and accumulation of phosphorus by dominant plant species growing in a phosphorus mining area. *J. Hazard. Mater.* 171, 542–550.

Xu, X. F., Thornton, P. E., and Post, W. M. (2013). A global analysis of soil microbial biomass carbon, nitrogen and phosphorus in terrestrial ecosystems. *Glob. Ecol. Biogeogr.* 22, 737–749.

Yang, Y., and Liu, B. R. (2019). Effects of planting *Caragana* shrubs on soil nutrients and stoichiometries in desert steppe of Northwest China. *Catena* 183, 104213.

Yang, Y., Liu, B. R., and An, S. S. (2018). Ecological stoichiometry in leaves, roots, litters and soil among different plant communities in a desertified region of northern China. *Catena* 166, 328–338.

Yu, J., and Steinberger, Y. (2012). Vertical distribution of soil microbial biomass and its association with shrubs from the Negev desert. *J. Arid Environ.* 78, 110–118.

Zechmeister-Boltenstern, S., Keiblinger, K. M., Mooshammer, M., Pe˜nuelas, J., Richter, A., Sardans, J., et al. (2015). The application of ecological stoichiometry to plant–microbial–soil organic matter transformations. *Ecol. Monogr.* 85, 133–155.

Zhang, W., Liu, W. C., Xu, M. P., Deng, J., Han, X. H., Yang, G. H., et al. (2019). Response of forest growth to C:N:P stoichiometry in plants and soils during *Robinia pseudoacacia* afforestation on the loess plateau, China. *Geoderma* 337, 280–289.

Zhang, X. M., Wang, Y. D., Zhao, Y., Xu, X. W., Lei, J. Q., and Hill, R. L. (2017). Litter decomposition and nutrient dynamics of three woody halophytes in the taklimakan desert highway shelterbelt. *Arid Land Res. Manage.* 31, 335–351.

Zhao, F. Z., Bai, L., Wang, J. Y., Deng, J., Ren, C. J., Han, X. H., et al. (2019). Change in soil bacterial community during secondary succession depend on plant and soil characteristics. *Catena* 173, 246–252.

Zhao, W. Z., Zhang, Z. H., and Li, Q. Y. (2007). Growth and reproduction of *Sophora moorcroftiana* responding to altitude and sand burial in the middle Tibet. *Environ. Geol.* 53, 11–17.

frontiers | Frontiers in Plant Science

TYPE Mini Review
PUBLISHED 12 January 2023
DOI 10.3389/fpls.2022.1037972

OPEN ACCESS

EDITED BY
Boris Rewald,
University of Natural Resources and Life Sciences Vienna, Austria

REVIEWED BY
Junpeng Mu,
Mianyang Normal University, China

*CORRESPONDENCE
Xiao Ying Gong
xgong@fjnu.edu.cn

SPECIALTY SECTION
This article was submitted to Functional Plant Ecology, a section of the journal Frontiers in Plant Science

RECEIVED 06 September 2022
ACCEPTED 19 December 2022
PUBLISHED 12 January 2023

CITATION
Ma WT, Yu YZ, Wang X and Gong XY (2023) Estimation of intrinsic water-use efficiency from $\delta^{13}C$ signature of C_3 leaves: Assumptions and uncertainty.
Front. Plant Sci. 13:1037972.
doi: 10.3389/fpls.2022.1037972

Estimation of intrinsic water-use efficiency from $\delta^{13}C$ signature of C_3 leaves: Assumptions and uncertainty

Wei Ting Ma[1], Yong Zhi Yu[1], Xuming Wang[1,2] and Xiao Ying Gong[1,2,3]*

[1]Key Laboratory for Subtropical Mountain Ecology (Ministry of Science and Technology and Fujian Province Funded), College of Geographical Sciences, Fujian Normal University, Fuzhou, China, [2]Key Laboratory for Humid Subtropical Eco-Geographical Processes of the Ministry of Education, Fujian Normal University, Fuzhou, China, [3]Fujian Provincial Key Laboratory for Plant Eco-physiology, Fuzhou, China

Carbon isotope composition ($\delta^{13}C$) has been widely used to estimate the intrinsic water-use efficiency (iWUE) of plants in ecosystems around the world, providing an ultimate record of the functional response of plants to climate change. This approach relies on established relationships between leaf gas exchange and isotopic discrimination, which are reflected in different formulations of ^{13}C-based iWUE models. In the current literature, most studies have utilized the simple, linear equation of photosynthetic discrimination to estimate iWUE. However, recent studies demonstrated that using this linear model for quantitative studies of iWUE could be problematic. Despite these advances, there is a scarcity of review papers that have comprehensively reviewed the theoretical basis, assumptions, and uncertainty of ^{13}C-based iWUE models. Here, we 1) present the theoretical basis of ^{13}C-based iWUE models: the classical model ($iWUE_{sim}$), the comprehensive model ($iWUE_{com}$), and the model incorporating mesophyll conductance ($iWUE_{mes}$); 2) discuss the limitations of the widely used $iWUE_{sim}$ model; 3) and make suggestions on the application of the $iWUE_{mes}$ model. Finally, we suggest that a mechanistic understanding of mesophyll conductance associated effects and post-photosynthetic fractionation are the bottlenecks for improving the ^{13}C-based estimation of iWUE.

KEYWORDS

water-use efficiency, carbon isotope discrimination, mesophyll conductance, post-photosynthetic fractionation, climate change, photosynthesis

Introduction

During photosynthesis, plant stomata act as a control valve for the diffusion of CO_2 and water vapor, regulating the rates of water and carbon exchange between the biosphere and the atmosphere (de Boer et al., 2011; Adams et al., 2020; Walker et al., 2021). Intrinsic water-use efficiency (iWUE), defined as the ratio of net photosynthetic rate (A_n) to stomatal conductance for water vapor (g_{sw}), plays a key role in quantifying carbon uptake and water loss at leaf to continental scales (Seibt et al., 2008; Keenan et al., 2013). The response of iWUE is fundamental to climate change research since small changes in iWUE can have profound impacts on global carbon and water cycles. Furthermore, iWUE can provide insights into the mechanisms of plant physiological responses to climate change and support the screening and breeding of climate-resilient crops (Farquhar and Richards, 1984; von Caemmerer et al., 2014; Gresset et al., 2014). Central to these research domains is the quantification of iWUE.

Stable carbon isotope discrimination (Δ) can be used as an integrated measure of iWUE in C_3 plants (Farquhar et al., 1989). Plants discriminate against ^{13}C in favour of ^{12}C during photosynthetic CO_2 assimilation in C_3 leaves, and the variation in carbon isotope composition ($\delta^{13}C$) from source CO_2 to photosynthetic products (e.g., bulk leaf organic carbon or sugars) is termed as Δ, following Farquhar et al. (1982b); Farquhar et al. (1989):

$$\Delta = \frac{\delta^{13}C_a - \delta^{13}C_p}{1 + \delta^{13}C_p} \quad \text{Equation 1}$$

where atmospheric $\delta^{13}C_a$ is approximately -7~-8‰ during the 20th century. Δ can also be estimated from $\delta^{13}C$ of CO_2 entering (δ_{in} and C_{in}) and leaving (δ_{out} and C_{out}) the cuvette during gas exchange, termed as online $^{12}C/^{13}C$ discrimination (Evans et al., 1986):

$$\Delta_{online} = \frac{\xi(\delta_{out} - \delta_{in})}{1 + \delta_{out} - \xi(\delta_{out} - \delta_{in})} \quad \text{Equation 2}$$

where $\xi = C_{in}/(C_{in}-C_{out})$. In this way, Δ can be measured nondestructively to probe real-time responses of photosynthesis at high temporal resolution. Changes in photosynthetic parameters (A_n and g_s) are captured in Δ_{online} and the isotopic signatures are further imprinted on plant tissues during biosynthesis. As such, biomass-based Δ reflects physiological status of plants throughout the growth period of plant tissues (Cernusak et al., 2013; Soh et al., 2019). Different from classical approaches such as gas exchange or growth analysis, biomass-based Δ can be applied retrospectively, providing a useful record of iWUE at large spatial and temporal scales (Frank et al., 2015; Adams et al., 2020; Gong et al., 2022).

Inferring iWUE from isotopic records relies on theoretical models. In the current literature, most studies have utilized the simple, linear equation of photosynthetic discrimination to estimate iWUE. However, it can be problematic to interpret iWUE using this linear model which ignores effects other than diffusion through stomata and carboxylation. For instance, Seibt et al. (2008) suggested that the uncertainty in iWUE-^{13}C models was related to the simplification of mesophyll conductance (g_m). g_m represents the conductance to CO_2 diffusion from the intercellular space to the carboxylation site in chloroplasts, a key limiting factor of photosynthesis in addition to stomatal conductance and biochemical capacity (Tholen et al., 2012; Stangl et al., 2019). However, recent advances in $\delta^{13}C$-based iWUE estimation have not been systematically reviewed. The main objective of this mini review is to concisely summarize the theoretical basis and uncertainties of $\delta^{13}C$-based iWUE models. We (i) present different formulations of Δ and the associated assumptions, (ii) present Δ-based iWUE models derived from those formulations: the classical model ($iWUE_{sim}$), the comprehensive model ($iWUE_{com}$), the model incorporating g_m ($iWUE_{mes}$), (iii) discuss the limitations of the widely used $iWUE_{sim}$ model; and make suggestions on the application of the $iWUE_{mes}$ model.

Comprehensive model of photosynthetic ^{13}C discrimination and simplifications

A comprehensive description of ^{13}C discrimination (Δ_{com}) during C_3 photosynthesis was given by Farquhar et al. (1982b) and extended to include ternary effects of transpiration on CO_2 assimilation by Farquhar and Cernusak (2012):

$$\Delta_{com} = \frac{1}{1-t}\left(a_{ac}\frac{C_a - C_i}{C_a}\right) + \frac{1+t}{1-t}\left(a_m\frac{C_i - C_c}{C_a} + b\frac{C_c}{C_a} - \frac{\alpha_b}{\alpha_e}e\frac{R_d}{V_c}\frac{C_c}{C_a} - \frac{\alpha_b}{\alpha_f}f\frac{\Gamma^*}{C_a}\right) \quad \text{Equation 3}$$

and

$$t = \frac{(1 + a_{ac})E}{2g_{ac}} \quad \text{Equation 4}$$

$$a_{ac} = \frac{a_b(C_a - C_s) + a_s(C_s - C_i)}{C_a - C_i} \quad \text{Equation 5}$$

where a_b (2.9‰) and a_s (4.4‰) are fractionations associated with the diffusion of CO_2 through leaf boundary layer and in the air, respectively. a_m (1.8‰) is the fractionation associated with the dissolution and diffusion of CO_2 in mesophyll (see Table S1 for the list of parameters). C_a, C_s, C_i and C_c represent the mole fraction of CO_2 in air, at leaf surface, in the intercellular spaces and chloroplast, respectively (Figure 1). Δ_{com} can be separated into a series of fractionation components of leaf boundary layer conductance

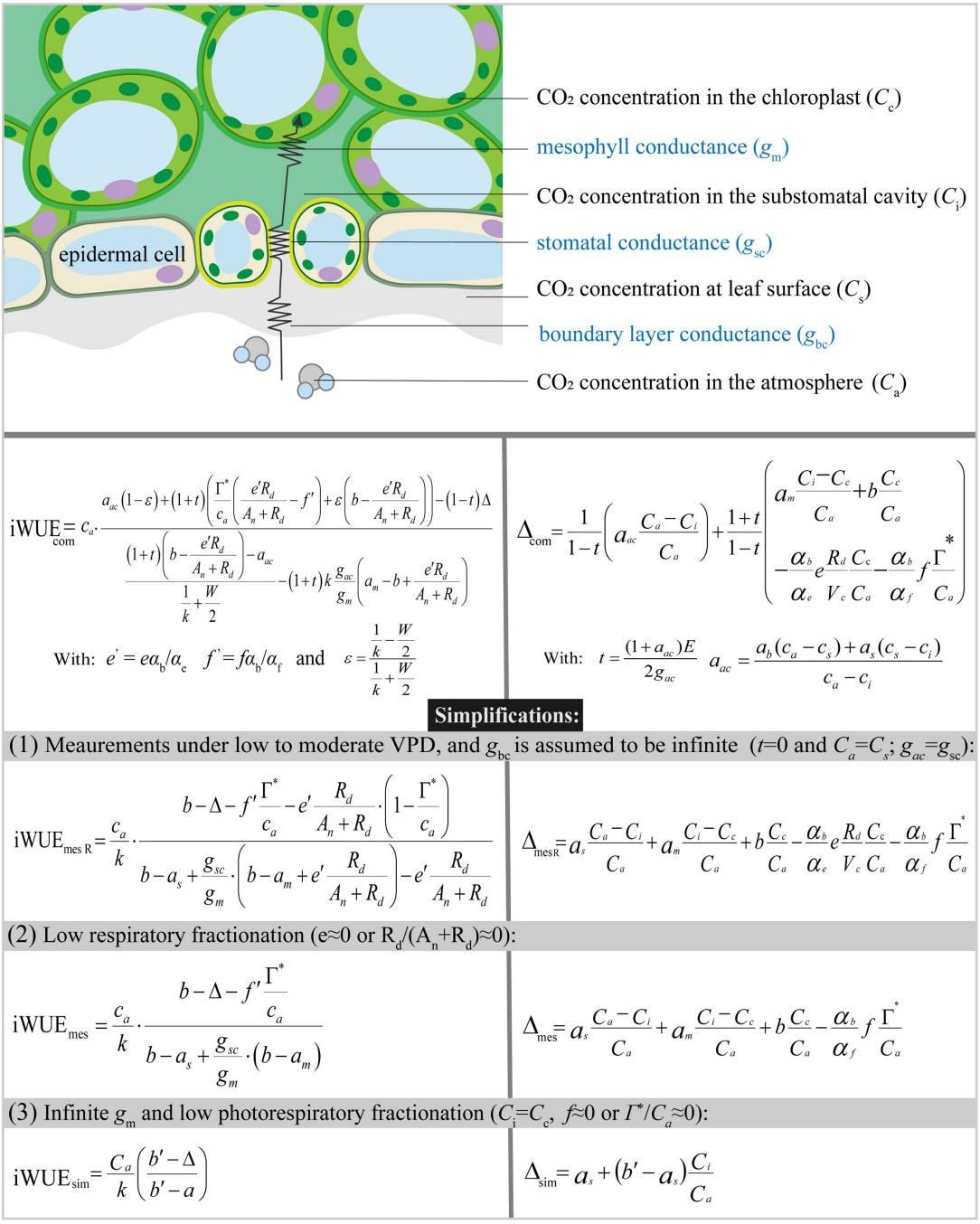

FIGURE 1
Diagram of the CO_2 diffusion pathway in C_3 leaves and different formulations of iWUE ($iWUE_{com}$, $iWUE_{mes\ R}$, $iWUE_{mes}$, and $iWUE_{sim}$) derived from the Farquhar et al. model for photosynthetic ^{13}C discrimination.

(Δ_{gbc}), stomatal conductance (Δ_{gsc}), mesophyll conductance (Δ_{gm}), Rubisco (ribulose-1,5-bisphosphate carboxylase/oxygenase) carboxylation (Δ_b), day respiration (Δ_e), and photorespiration (Δ_f). Note that t is included to account for the ternary effects of transpiration rate (E) on photosynthetic discrimination (Farquhar and Cernusak, 2012). Usually, the effect of t is small and can be omitted under low or moderate vapor pressure deficit (VPD) (Farquhar and Cernusak, 2012; Evans and Caemmerer, 2013). If Δ_{gbc} is also omitted (C_a=C_s and g_{ac}=g_{sc}), the Δ_{com} model is simplified as:

$$\Delta_{\text{mes R}} = a_s\frac{C_a - C_i}{C_a} + a_m\frac{C_i - C_c}{C_a} + b\frac{C_c}{C_a} - \frac{\alpha_b}{\alpha_e}e\frac{R_d}{V_c}\frac{C_c}{C_a} - \frac{\alpha_b}{\alpha_f}f\frac{\Gamma^*}{C_a} \quad \text{Equation 6}$$

where the subscript "mes R" indicates that the expression takes mesophyll conductance, day respiration and photorespiration into account.

Δ_e, the respiratory contribution to discrimination is mainly determined by respiratory fractionation (e), and R_d/(An+ R_d). Δ_e has rarely been accurately quantified largely due to the difficulty of estimating R_d (Tcherkez et al., 2017; Gong et al., 2018). Moreover, fractionation of day respiration has rarely been reported, and e estimated from respiration in the dark varies between 0 and -6‰ (Ghashghaie et al., 2003; Tcherkez et al., 2010). Under natural conditions, Δ_e is usually small and negligible (Seibt et al., 2008; Ubierna and Farquhar, 2014). Notably, a significant apparent respiratory fractionation may occur when the CO_2 source used for combined gas exchange and isotopic measurements has a $\delta^{13}C$ differed from that of the ambient air (Gillon and Griffiths, 1997; Gong et al., 2015). Under such conditions, e should be corrected to account for the isotopic disequilibria between photosynthetic and respiratory fluxes (Wingate et al., 2007; Gong et al., 2015). Assuming Δ_e=0, Equation 6 can be simplified as:

$$\Delta_{\text{mes}} = a_s\frac{C_a - C_i}{C_a} + a_m\frac{C_i - C_c}{C_a} + b\frac{C_c}{C_a} - \frac{\alpha_b}{\alpha_f}f\frac{\Gamma^*}{C_a} \quad \text{Equation 7}$$

C_c is usually unknown since its calculation requires g_m which cannot be directly measured. g_m is assumed to be infinite in early studies (for a review see Flexas et al., 2012); that is, CO_2 mole fraction in the chloroplast is equal to that in the intercellular space. Assuming C_i=C_c and Δ_f=0, Equation 7 is simplified as:

$$\Delta_{\text{sim}} = a_s + \left(b' - a_s\right)\frac{C_i}{C_a} \quad \text{Equation 8}$$

Comprehensive model of iWUE and simplifications

The comprehensive model of iWUE which includes all fractionation components of Equation 3 was first derived by Ma et al. (2021):

$$\text{iWUE}_{\text{com}} = c_a\frac{a_{ac}(1-\epsilon) + (1+t)\left[\frac{\Gamma^*}{c_a}\left(\frac{e'R_d}{A_n+R_d} - f'\right) + \epsilon\left(b - \frac{e'R_d}{A_n+R_d}\right)\right] - (1-t)\Delta}{\frac{(1+t)\left(b - \frac{e'R_d}{A_n+R_d}\right) - a_{ac}}{\frac{1}{k}+\frac{W}{2}} - (1+t)k\frac{g_{ac}}{g_m}\left(a_m - b + \frac{e'R_d}{A_n+R_d}\right)} \quad \text{Equation 9}$$

where e'=ea_b/a_e, f'=fa_b/a_f and ϵ=(1/k-W/2)/(1/k+W/2). This formulation is particularly useful for assessing the contribution of each fractionation component to iWUE estimates. Ma et al. (2021) performed sensitivity tests using theoretical data of the standard photosynthetic scenarios. Their results indicated that ternary correction and Δ_{gbc} had little influence on iWUE_{com} estimates (error< 2 μmol mol^{-1}), which is in agreement with Seibt et al. (2008). Neglecting the contribution of t and Δ_{gbc}, Equation 9 can be simplified as:

$$\text{iWUE}_{\text{mes R}} = \frac{c_a}{k}\cdot\frac{b - \Delta - f'\frac{\Gamma^*}{c_a} - e'\frac{R_d}{A_n+R_d}\left(1 - \frac{\Gamma^*}{c_a}\right)}{b - a_s + \frac{g_{sc}}{g_m}\left(b - a_m + e'\frac{R_d}{A_n+R_d}\right) - e'\frac{R_d}{A_n+R_d}} \quad \text{Equation 10}$$

Δ_e in the $\text{iWUE}_{\text{mes R}}$ model could be ignored as it caused an error of less than 2 μmol mol^{-1} in typical photosynthetic scenarios (Ma et al., 2021). Excluding the contribution of day respiratory, Equation 10 can be simplified as:

$$\text{iWUE}_{\text{mes}} = \frac{c_a}{k}\cdot\frac{b - \Delta - f'\frac{\Gamma^*}{c_a}}{b - a_s + \frac{g_{sc}}{g_m}(b - a_m)} \quad \text{Equation 11}$$

The iWUE_{mes} model provided iWUE estimates that are numerically very similar with iWUE_{com} (error< 3 μmol mol^{-1}) (Ma et al., 2021). Neglecting the contribution of g_m and photorespiration, the simplified equation for iWUE is given as:

$$\text{iWUE}_{\text{sim}} = \frac{C_a}{k}\left(\frac{b' - \Delta}{b' - a}\right) \quad \text{Equation 12}$$

This linear relationship between iWUE and photosynthetic ^{13}C discrimination is the most used to estimate iWUE, however, the limitations of this formulation have been raised (Seibt et al., 2008; Ubierna and Farquhar, 2014; Ma et al., 2021).

Uncertainty in iWUE_{sim} estimation associated with mesophyll conductance

Experimental evidence shows that g_m exerts a significant limitation on CO_2 diffusion and leads to a significant drawdown from C_i to C_c (Loreto et al., 1992; Flexas et al., 2008; Cano et al., 2014). It is apparent from Equation 11 that, assuming an infinite g_m will lead to overestimation of iWUE, this is supported by experimental observations (Barbour et al., 2010; Stangl et al., 2019; Adams et al., 2020). Experimental results showed that the relationship between Δ and water-use efficiency is at least partly a function of g_m (Warren and Adams, 2006). Therefore, it is important to incorporate g_m in the parameterization of the iWUE model. Ma et al. (2021) showed that iWUE_{sim} overestimated iWUE by c. 65%. Importantly, the magnitude of overestimation is dependent on Δ, making correction using empirical relations difficult. These results raise concerns regarding the accuracy of iWUE_{sim} estimations.

The overestimation of the $iWUE_{sim}$ model has also been observed in recent studies using ^{13}C series of environmental archives (Baca Cabrera et al., 2021; Bing et al., 2022). More importantly, $iWUE_{sim}$ model could provide biased estimations of historical iWUE trend. Gong et al. (2022) analyzed tree ring ^{13}C series across the globe using the $iWUE_{mes}$ model, and reported that $iWUE_{sim}$ model significantly overestimated iWUE (by c. 100%) and the rate of iWUE gain with time or C_a (by c. 70%) during the 20th century. This finding has been confirmed by studies carried out in distinct ecosystems (Bing et al., 2022; Mathias and Hudiburg, 2022). Failure to consider g_m must lead to an overestimated historical trend as implied by the partial derivative of $iWUE_{mes}$ (Equation 11) (Gong et al., 2022):

$$\frac{diWUE}{dC_a} = \frac{b-\Delta}{k\left(\frac{g_{sc}}{g_m}(b-a_m)+b-a_s\right)} \qquad \text{Equation 13}$$

Given that ^{13}C series of environmental archives (e.g. tree rings) provide a unique proxy for benchmarking the output of land surface models (Frank et al., 2015; Wang et al., 2017; Lavergne et al., 2022), cautions should be paid when $iWUE_{sim}$ model is used to predict historical trend of iWUE.

Uncertainty in $iWUE_{sim}$ estimation associated with *b'*

The value and physiological meaning of *b'* in the equation of Δ_{sim} or $iWUE_{sim}$ remain subjects of debate. Initially, Farquhar et al. (1982a) proposed that *b'* (27‰) could be derived from early *in vitro* estimations of Rubisco carboxylation. As it agreed well with the relationship between measured biomass-based Δ and C_i/C_a, it was interpreted as a fitted value. However, when measured Δ from online instantaneous measurements was used to fit Equation 8, the fitted *b'* appears to be lower than 27‰ (Caemmerer and Evans, 1991; Ma et al., 2021).

b' was also explained as the net fractionation caused by Rubisco and PEPC (phosphoenolpyruvate carboxylase). Farquhar and Richards (1984) described *b'* as a function of relative contribution of Rubisco and PEPC carboxylation:

$$b' = (1-\beta)b + \beta b_4 \qquad \text{Equation 14}$$

where *b* (29-30‰) and b_4 (usually taken as -5.7‰ at 25°C) are fractionation factors of Rubisco and PEPC carboxylation, respectively. β is the proportion of carbon fixation through PEPC carboxylation. PEPC uses HCO_3^- produced by CO_2 hydration as the substrate for the synthesis of aspartate or malate, which is important for the control of cellular pH (Davies, 1979). Generally, carboxylation by Rubisco contributes a greater fraction of carbon in plants and respiratory substrates. But it is also suggested that the PEPC carboxylation could be important under the conditions of low stomatal conductance or carboxylation in darkness (Ikeda and Yamada, 1981; Gupta et al., 1994; Hibberd and Quick, 2002). Furthermore, several studies have revealed that N source and concentration were potential factors affecting carbon fixation by PEPC, which indicates that *b'* could vary with nitrogen metabolism (Raven and Farquhar, 1990; Douthe et al., 2012; Lian et al., 2021). That is, Equation 14 is not particularly useful for iWUE estimation because β is variable and difficult to quantify.

b' has also been described by Ubierna and Farquhar (2014) as a parameter that included carboxylation, mesophyll conductance, and photorespiration:

$$b' \cong b\frac{C_c}{C_i} + a_m\left(1-\frac{C_c}{C_i}\right) - f\frac{\Gamma^*}{C_a} \qquad \text{Equation 15}$$

According to Equation 15, *b'* is largely dependent on C_c/C_i which is modulated by g_m. It should be noted that the most used *b'*=27‰ is consistent with the C_c/C_i value of 0.9, higher than the common values of 0.7-0.8 (Caemmerer and Evans, 1991; Warren et al., 2003). So far, Equations 14 and 15 have only been used to discuss the potential origin of variation in *b'*, but have not been incorporated in the model of iWUE estimation. In short, there is still no consensus concerning the interpretation of *b'*, and current discussion on *b'* (Equations 14, 15) illustrated that it should not be treated as a constant value of 27‰.

Uncertainty in iWUE associated with post-photosynthetic fractionation

Post-photosynthetic fractionation (Δ_{post}) includes the discrimination processes that follow photosynthetic carbon fixation, altering $\delta^{13}C$ signals in plant organs and leaves at different development stages (Badeck et al., 2005; Vogado et al., 2020). In general, heterotrophic organs (branches, stems and roots) are ^{13}C-enriched compared with autotrophic organs (leaves) (Badeck et al., 2005; Bowling et al., 2008; Cernusak et al., 2009; Lamade et al., 2016), and the immature leaves (heterotrophic phase) are ^{13}C-enriched (by *c.* 2‰) compared to mature leaves (autotrophic phase) in both deciduous and evergreen species (Lamade et al., 2009; Vogado et al., 2020). However, the contribution of Δ_{post} to $\delta^{13}C$ of plant tissues and its influence on iWUE estimation are poorly understood.

Several studies has accounted for Δ_{post} to estimate iWUE (Table S2). Gimeno et al. (2021) found an improvement in correlation between iWUE estimated from gas exchange and that from Δ when g_m and Δ_{post} were accounted for. In that study, Δ_{post} was taken as -2.5‰ estimated from the $\delta^{13}C$ difference between phloem contents and whole-tree photosynthesis. Similarly, $\delta^{13}C$ of wood and cellulose have been corrected by -3.2‰ and -1.3‰, respectively, to account for the offset from leaf $\delta^{13}C$ (Thomas et al., 2013; Brownlee et al., 2016). In other studies, iWUE was calculated from tree-ring with a $\delta^{13}C$ offset of

-2‰ to account for Δ_{post} (Michelot et al., 2011; Frank et al., 2015). Without correcting a Δ_{post} of about 2.5‰, iWUE estimated from the $\delta^{13}C$ of tree-ring could be overestimated by 20% (Gessler et al., 2009).

The likely mechanisms underlying Δ_{post} include fractionation associated with respiration, transport and mixing of assimilates (Tcherkez et al., 2003; Brüggemann et al., 2011; Bögelein et al., 2019). Respiratory fractionation ranges from -6 to 0‰ in various species (Duranceau et al., 1999; Ghashghaie et al., 2001; Tcherkez et al., 2003). Also, there are some variations in the apparent fractionation during transport processes (e.g., day-night differences in $\delta^{13}C$ of leaf-export organic matter and different leaf-to-phloem $\delta^{13}C$ signatures along vertical canopy gradients) and very few direct measurements of isotopic differences between components at molecule/atom scale (Gessler et al., 2008; Mauve et al., 2009; Gilbert et al., 2011; Gilbert et al., 2012; Bögelein et al., 2019). In addition, post-photosynthetic fractionation is complicated by ontogenic effects (e.g., size, height, and age of individuals) that can confound the relationship between iWUE and environmental factors (Vadeboncoeur et al., 2020). That is, the influence of Δ_{post} could accumulate over time and lead to age-dependent patterns (Cernusak et al., 2009). Therefore, using a constant, empirical value of Δ_{post} could be unreliable. A mechanistic description of Δ_{post} should be very useful to improve the iWUE estimates, which requires further study on the fractionations associated with respiration, transport and allocation of assimilates.

$iWUE_{mes}$, a useful, simplified model for estimating iWUE

$iWUE_{mes}$ takes the influence of mesophyll conductance and photorespiratory fractionation into account. We propose to use the $iWUE_{mes}$ model (Equation 11) since it considers the components that have a significant influence on the iWUE estimation. In particular, it includes g_m effect which is known to affect iWUE prediction.

Parameterizing the $iWUE_{mes}$ model requires g_{sc}/g_m rather than g_m (Ma et al., 2021). Some studies use a constant g_m in the equation to estimate iWUE (Keeling et al., 2017), which makes more sense than disregarding g_m. However, the assumption of constant g_m is not supported by experimental evidence. The positive relationships between g_{sc} and g_m have been reported in many studies (Flexas et al., 2013; Gong et al., 2018), and this relationship is rather conserved across levels of CO_2, irradiance, and drought stress and functionally distinct species (Flexas et al., 2008; Ma et al., 2021; Gong et al., 2022). Incorporating the g_{sc}/g_m ratio improves the predictive accuracy of the iWUE model, as demonstrated in gas exchange experiments (Ma et al., 2021). Without knowing g_m, it is preferable to use the average g_{sc}/g_m of 0.79 (± 0.07) derived from a global synthesis to parameterize the $iWUE_{mes}$ model rather than using the $iWUE_{sim}$ model.

We acknowledge that using a constant g_{sc}/g_m is not always adequate. As more g_m data become available, interspecific differences in g_{sc}/g_m can be identified and should be accounted for in the estimated iWUE. Theoretically, species-specific g_{sc}/g_m is more appropriate to be used in the $iWUE_{mes}$ estimation. It is also noteworthy that short-term responses of g_m are still not well defined, implying that neglecting short-term variation in g_{sc}/g_m might lead to errors in estimating iWUE at nonsteady-states, thus should be addressed in further work. Moreover, the $iWUE_{mes}$ model does not account for the post-photosynthetic fractionation, due to a lack of knowledge on post-photosynthetic fractionation. Therefore, we recommend for biomass-based analyses to distinguish the age of organs to minimize the influence of post-photosynthetic fractionation.

Conclusion remarks

The comprehensive model of photosynthetic ^{13}C discrimination of Farquhar and Cernusak (2012) is a synthesis of current understanding, and provides the theoretical basis for estimating iWUE from the ^{13}C composition of plant materials. The classical $iWUE_{sim}$ model has been shown to strongly overestimate iWUE and its historical trends due to the neglect of g_m associated effect, limiting its use in quantitative studies. $iWUE_{mes}$ is suggested as a useful, simplified model for quantitative estimation of iWUE, which has been included in a standardized, open-source tool (R package) for calculation of iWUE from stable isotope signatures (Mathias and Hudiburg, 2022). Nonetheless, the formulation of $iWUE_{mes}$ could still be further improved. For example, a fixed, empirical g_{sc}/g_m value could be replaced by species-specific values or mechanistic relationships derived from experimental results. ^{13}C discrimination of plant material, combining with appropriate iWUE models, is also an ultimate tool for screening genetic resources to enhance the iWUE of crops under climate change scenarios. One of the primary questions is how g_{sc} and g_m of plants will respond to changes in temperature, water availability, and carbon dioxide concentration. Furthermore, the response of post-photosynthetic fractionation to climate change factors remains unknown. We conclude that mechanistic descriptions of g_m associated effect and post-photosynthetic fractionation are the bottlenecks for improving the ^{13}C-based estimation of iWUE.

Author contributions

XG conceptualized the topic of this review, WM and YY wrote the first draft, and all authors contributed to the writing

and revision of the manuscript. All authors contributed to the article and approved the submitted version.

Funding

This work was supported by the National Natural Science Foundation of China (NSFC 31870377, 32120103005, 32201277).

Conflict of interest

The authors declare that the research was conducted in the absence of any commercial or financial relationships that could be construed as a potential conflict of interest.

Publisher's note

Supplementary material

The Supplementary Material for this article can be found online at: https://www.frontiersin.org/articles/10.3389/fpls.2022.1037972/full#supplementary-material

References

Adams, M. A., Buckley, T. N., and Turnbull, T. L. (2020). Diminishing CO_2-driven gains in water-use efficiency of global forests. *Nat. Clim. Change* 10 (5), 466–471. doi: 10.1038/s41558-020-0747-7

Baca Cabrera, J. C., Hirl, R. T., Schäufele, R., Macdonald, A., and Schnyder, H. (2021). Stomatal conductance limited the CO_2 response of grassland in the last century. *BMC Biol.* 19 (1), 50. doi: 10.1186/s12915-021-00988-4

Badeck, F. W., Tcherkez, G., Nogués, S., Piel, C., and Ghashghaie, J. (2005). Post-photosynthetic fractionation of stable carbon isotopes between plant organs–a widespread phenomenon. *Rapid Commun. Mass Spectrom* 19 (11), 1381–1391. doi: 10.1002/rcm.1912

Barbour, M. M., Warren, C. R., Farquhar, G. D., Forrester, G., and Brown, H. (2010). Variability in mesophyll conductance between barley genotypes, and effects on transpiration efficiency and carbon isotope discrimination. *Plant Cell Environ.* 33 (7), 1176–1185. doi: 10.1111/j.1365-3040.2010.02138.x

Bing, X., Fang, K., Gong, X., Wang, W., Xu, C., Li, M., et al. (2022). The intra-annual intrinsic water use efficiency dynamics based on an improved model. *Clim Change* 172 (1), 16. doi: 10.1007/s10584-022-03368-1

Bögelein, R., Lehmann, M. M., and Thomas, F. M. (2019). Differences in carbon isotope leaf-to-phloem fractionation and mixing patterns along a vertical gradient in mature European beech and Douglas fir. *New Phytol.* 222 (4), 1803–1815. doi: 10.1111/nph.15735

Bowling, D. R., Pataki, D. E., and Randerson, J. T. (2008). Carbon isotopes in terrestrial ecosystem pools and CO_2 fluxes. *New Phytol.* 178 (1), 24–40. doi: 10.1111/j.1469-8137.2007.02342.x

Brownlee, A. H., Sullivan, P. F., Csank, A. Z., Sveinbjörnsson, B., and Ellison, S. B. Z. (2016). Drought-induced stomatal closure probably cannot explain divergent white spruce growth in the brooks range, Alaska, USA. *Ecology* 97 (1), 145–159. doi: 10.1890/15-0338.1

Brüggemann, N., Gessler, A., Kayler, Z., Keel, S. G., Badeck, F., Barthel, M., et al. (2011). Carbon allocation and carbon isotope fluxes in the plant-soil-atmosphere continuum: A review. *Biogeosciences* 8 (11), 3457–3489. doi: 10.5194/bg-8-3457-2011

Caemmerer, S.v., and Evans, J. R. (1991). Determination of the average partial pressure of CO_2 in chloroplasts from leaves of several C_3 plants. *Aust. J. Plant Physiol.* 18 (3), 287–305. doi: 10.1071/PP9910287

von Caemmerer, S.v., Ghannoum, O., Pengelly, J. J. L., and Cousins, A. B. (2014). Carbon isotope discrimination as a tool to explore C_4 photosynthesis. *J. Exp. Bot.* 65 (13), 3459–3470. doi: 10.1093/jxb/eru127

Cano, F. J., Lopez, R., and Warren, C. R. (2014). Implications of the mesophyll conductance to CO_2 for photosynthesis and water-use efficiency during long-term water stress and recovery in two contrasting eucalyptus species. *Plant Cell Environ.* 37 (11), 2470–2490. doi: 10.1111/pce.12325

Cernusak, L. A., Tcherkez, G., Keitel, C., Cornwell, W. K., Santiago, L. S., Knohl, A., et al. (2009). Why are non-photosynthetic tissues generally $_{13}C$ enriched compared with leaves in C_3 plants? Review and synthesis of current hypotheses. *Funct. Plant Biol.* 36 (3), 199–213. doi: 10.1071/FP08216

Cernusak, L. A., Ubierna, N., Winter, K., Holtum, J. A. M., Marshall, J. D., and Farquhar, G. D. (2013). Environmental and physiological determinants of carbon isotope discrimination in terrestrial plants. *New Phytol.* 200 (4), 950–965. doi: 10.1111/nph.12423

Davies, D. D. (1979). The central role of phosphoenolpyruvate in plant metabolism. *Ann. Rev. Plant Physiol.* 30 (1), 131–158. doi: 10.1146/annurev.pp.30.060179.001023

de Boer, H. J., Lammertsma, E. I., Wagner-Cremer, F., Dilcher, D. L., Wassen, M. J., and Dekker, S. C. (2011). Climate forcing due to optimization of maximal leaf conductance in subtropical vegetation under rising CO_2. *Proc. Natl. Acad. Sci. U.S.A.* 108 (10), 4041–4046. doi: 10.1073/pnas.1100555108

Douthe, C., Dreyer, E., Brendel, O., and Warren, C. R. (2012). Is mesophyll conductance to CO_2 in leaves of three eucalyptus species sensitive to short-term changes of irradiance under ambient as well as low O_2? *Funct. Plant Biol.* 39 (5), 435–448. doi: 10.1071/FP11190

Duranceau, M., Ghashghaie, J., Badeck, F., Deleens, E., and Cornic, G. (1999). δ13C of CO_2 respired in the dark in relation to $\delta_{13}C$ of leaf carbohydrates in phaseolus *vulgaris* L. under progressive drought. *Plant Cell Environ.* 22 (5), 515–523. doi: 10.1046/j.1365-3040.1999.00420.x

Evans, J. R., and Caemmerer, S. V. (2013). Temperature response of carbon isotope discrimination and mesophyll conductance in tobacco. *Plant Cell Environ.* 36 (4), 745–756. doi: 10.1111/j.1365-3040.2012.02591.x

Evans, J. R., Sharkey, T. D., Berry, J. A., and Farquhar, G. D. (1986). Carbon isotope discrimination measured concurrently with gas exchange to investigate CO_2 diffusion in leaves of higher plants. *Aust. J. Plant Physiol.* 13 (2), 281–292. doi: 10.1071/PP9860281

Farquhar, G. D., Ball, M. C., von Caemmerer, S., and Roksandic, Z. (1982a). Effect of salinity and humidity on $\delta_{13}C$ value of halophytes–evidence for diffusional isotope fractionation determined by the ratio of intercellular/atmospheric partial pressure of CO_2 under different environmental conditions. *Oecologia* 52 (1), 121–124. doi: 10.1007/BF00349020

Farquhar, G. D., and Cernusak, L. A. (2012). Ternary effects on the gas exchange of isotopologues of carbon dioxide. *Plant Cell Environ.* 35 (7), 1221–1231. doi: 10.1111/j.1365-3040.2012.02484.x

Farquhar, G. D., Ehleringer, J. R., and Hubick, K. T. (1989). Carbon isotope discrimination and photosynthesis. *Annu. Rev. Plant Physiol. Plant Mol. Biol.* 40 (1), 503–537. doi: 10.1146/annurev.pp.40.060189.002443

Farquhar, G. D., O'Leary, M. H., and Berry, J. A. (1982b). On the relationship between carbon isotope discrimination and the intercellular carbon dioxide concentration in leaves. *Aust. J. Plant Physiol.* 9 (2), 121–137. doi: 10.1071/PP9820121

Farquhar, G. D., and Richards, R. A. (1984). Isotopic composition of plant carbon correlates with water-use efficiency of wheat genotypes. *Aust. J. Plant Physiol.* 11 (6), 539–552. doi: 10.1071/PP9840539

Flexas, J., Barbour, M. M., Brendel, O., Cabrera, H. M., Carriquí, M., Díaz-Espejo, A., et al. (2012). Mesophyll diffusion conductance to CO2: an

unappreciated central player in photosynthesis. *Plant Sci.* 193-194, 70–84. doi: 10.1016/j.plantsci.2012.05.009

Flexas, J., Niinemets, Ü., Gallé, A., Barbour, M. M., Centritto, M., Diaz-Espejo, A., et al. (2013). Diffusional conductances to CO2 as a target for increasing photosynthesis and photosynthetic water-use efficiency. *Photosynth. Res.* 117 (1-3), 45–59. doi: 10.1007/s11120-013-9844-z

Flexas, J., Ribas-Carbo, M., Diaz-Espejo, A., Galmes, J., and Medrano, H. (2008). Mesophyll conductance to CO_2: Current knowledge and future prospects. *Plant Cell Environ.* 31 (5), 602–621. doi: 10.1111/j.1365-3040.2007.01757.x

Frank, D. C., Poulter, B., Saurer, M., Esper, J., Huntingford, C., Helle, G., et al. (2015). Water-use efficiency and transpiration across European forests during the anthropocene. *Nat. Clim. Change* 5 (6), 579–583. doi: 10.1038/nclimate2614

Gessler, A., Brandes, E., Buchmann, N., Helle, G., Rennenberg, H., and Barnard, R. L. (2009). Tracing carbon and oxygen isotope signals from newly assimilated sugars in the leaves to the tree-ring archive. *Plant Cell Environ.* 32, 780–795. doi: 10.1111/j.1365-3040.2009.01957.x

Gessler, A., Tcherkez, G., Peuke, A. D., Ghashghaie, J., and Farquhar, G. D. (2008). Experimental evidence for diel variations of the carbon isotope composition in leaf, stem and phloem sap organic matter in ricinus communis. *Plant Cell Environ.* 31 (7), 941–953. doi: 10.1111/j.1365-3040.2008.01806.x

Ghashghaie, J., Badeck, F.-W., Lanigan, G., Nogués, S., Tcherkez, G., Deléens, E., et al. (2003). Carbon isotope fractionation during dark respiration and photorespiration in C_3 plants. *Phytochem. Rev.* 2 (1), 145–161. doi: 10.1023/B:PHYT.0000004326.00711.ca

Ghashghaie, J., Duranceau, M., Badeck, F.-W., Cornic, G., Adeline, M.-T., and Deleens, E. (2001). $\delta_{13}C$ of CO_2 respired in the dark in relation to $\delta_{13}C$ of leaf metabolites: comparison between nicotiana sylvestris and helianthus annuus under drought. *Plant Cell Environ.* 24 (5), 505–515. doi: 10.1046/j.1365-3040.2001.00699.x

Gilbert, A., Robins, R. J., Remaud, G. S., and Tcherkez, G. G. (2012). Intramolecular $_{13}C$ pattern in hexoses from autotrophic and heterotrophic C_3 plant tissues. *Proc. Natl. Acad. Sci. U.S.A.* 109, 18204–18209. doi: 10.1073/pnas.1211149109

Gilbert, A., Silvestre, V., Robins, R. J., Tcherkez, G., and Remaud, G. S. (2011). A $_{13}C$ NMR spectrometric method for the determination of intramolecular $\delta_{13}C$ values in fructose from plant sucrose samples. *New Phytol.* 191, 579–588. doi: 10.1111/j.1469-8137.2011.03690.x

Gillon, J. S., and Griffiths, H. (1997). The influence of (photo)respiration on carbon isotope discrimination in plants. *Plant Cell Environ.* 20 (10), 1217–1230. doi: 10.1046/j.1365-3040.1997.d01-24.x

Gimeno, T. E., Campany, C. E., Drake, J. E., Barton, C. V. M., Tjoelker, M. G., Ubierna, N., et al. (2021). Whole-tree mesophyll conductance reconciles isotopic and gas-exchange estimates of water-use efficiency. *New Phytol.* 229 (5), 2535–2547. doi: 10.1111/nph.17088

Gong, X. Y., Ma, W. T., Yu, Y. Z., Fang, K., Yang, Y., Tcherkez, G., et al. (2022). Overestimated gains in water-use efficiency by global forests. *Global Change Biol.* 28 (16), 4923–4934. doi: 10.1111/gcb.16221

Gong, X. Y., Schäufele, R., Feneis, W., and Schnyder, H. (2015). 13CO2/12CO2 exchange fluxes in a clamp-on leaf cuvette: disentangling artefacts and flux components. *Plant Cell Environ.* 38 (11), 2417–2432. doi: 10.1111/pce.12564

Gong, X. Y., Tcherkez, G., Wenig, J., Schäufele, R., and Schnyder, H. (2018). Determination of leaf respiration in the light: Comparison between an isotopic disequilibrium method and the laisk method. *New Phytol.* 218 (4), 1371–1382. doi: 10.1111/nph.15126

Gresset, S., Westermeier, P., Rademacher, S., Ouzunova, M., Presterl, T., Westhoff, P., et al. (2014). Stable carbon isotope discrimination is under genetic control in the C_4 species maize with several genomic regions influencing trait expression. *Plant Physiol.* 164 (1), 131–143. doi: 10.1104/pp.113.224816

Gupta, S., Ku, M., Lin, J.-H., Zhang, D., and Edwards, G. (1994). Light/dark modulation of phosphoenolpyruvate carboxylase in C_3 and C_4 species. *Photosynth. Res.* 42, 133–143. doi: 10.1007/BF02187124

Hibberd, J. M., and Quick, W. P. (2002). Characteristics of C_4 photosynthesis in stems and petioles of C_3 flowering plants. *Nature* 415 (6870), 451–454. doi: 10.1038/415451a

Ikeda, M., and Yamada, Y. (1981). Dark CO2 fixation in leaves of tomato plants grown with ammonium and nitrate as nitrogen sources. *Plant Soil* 60 (2), 213–222. doi: 10.1007/BF02374106

Keeling, R. F., Graven, H. D., Welp, L. R., Resplandy, L., Bi, J., Piper, S. C., et al. (2017). Atmospheric evidence for a global secular increase in carbon isotopic discrimination of land photosynthesis. *Proc. Natl. Acad. Sci. U.S.A.* 114 (39), 10361–10366. doi: 10.1073/pnas.1619240114

Keenan, T. F., Hollinger, D. Y., Bohrer, G., Dragoni, D., Munger, J. W., Schmid, H. P., et al. (2013). Increase in forest water-use efficiency as atmospheric carbon dioxide concentrations rise. *Nature* 499 (7458), 324–327. doi: 10.1038/nature12291

Lamade, E., Setiyo, I. E., Girard, S., and Ghashghaie, J. (2009). Changes in $_{13}C/_{12}C$ of oil palm leaves to understand carbon use during their passage from heterotrophy to autotrophy. *Rapid Commun. Mass Spectrom* 23 (16), 2586–2596. doi: 10.1002/rcm.4169

Lamade, E., Tcherkez, G., Darlan, N. H., Rodrigues, R. L., Fresneau, C., Mauve, C., et al. (2016). Natural 13C distribution in oil palm (*Elaeis guineensis* jacq.) and consequences for allocation pattern. *Plant Cell Environ.* 39 (1), 199–212. doi: 10.1111/pce.12606

Lavergne, A., Hemming, D., Prentice, I. C., Guerrieri, R., Oliver, R. J., and Graven, H. (2022). Global decadal variability of plant carbon isotope discrimination and its link to gross primary production. *Global Change Biol.* 28 (2), 524–541. doi: 10.1111/gcb.15924

Lian, L., Lin, Y., Wei, Y., He, W., Cai, Q., Huang, W., et al. (2021). PEPC of sugarcane regulated glutathione s-transferase and altered carbon–nitrogen metabolism under different n source concentrations in oryza sativa. *BMC Plant Biol.* 21, 287. doi: 10.1186/s12870-021-03071-w

Loreto, F., Harley, P. C., Di Marco, G., and Sharkey, T. D. (1992). Estimation of mesophyll conductance to CO_2 flux by three different methods. *Plant Physiol.* 98 (4), 1437–1443. doi: 10.1104/pp.98.4.1437

Ma, W. T., Tcherkez, G., Wang, X. M., Schäufele, R., Schnyder, H., Yang, Y., et al. (2021). Accounting for mesophyll conductance substantially improves $_{13}C$-based estimates of intrinsic water-use efficiency. *New Phytol.* 229 (3), 1326–1338. doi: 10.1111/nph.16958

Mathias, J. M., and Hudiburg, T. W. (2022). isocalcR: An r package to streamline and standardize stable isotope calculations in ecological research. *Global Change Biol.* 28 (24), 7428–7436. doi: 10.1111/gcb.16407

Mauve, C., Bleton, J., Bathellier, C., Lelarge-Trouverie, C., Guérard, F., Ghashghaie, J., et al. (2009). Kinetic $_{12}C/_{13}C$ isotope fractionation by invertase: evidence for a small *in vitro* isotope effect and comparison of two techniques for the isotopic analysis of carbohydrates. *Rapid Commun. Mass Spectrom* 23, 2499–2506. doi: 10.1002/rcm.4068

Michelot, A., Eglin, T., Dufrêne, E., Lelarge-Trouverie, C., and Damesin, C. (2011). Comparison of seasonal variations in water-use efficiency calculated from the carbon isotope composition of tree rings and flux data in a temperate forest. *Plant Cell Environ.* 34 (2), 230–244. doi: 10.1111/j.1365-3040.2010.02238.x

Raven, J. A., and Farquhar, G. D. (1990). The influence of n metabolism and organic acid synthesis on the natural abundance of isotopes of carbon in plants. *New Phytol.* 116 (3), 505–529. doi: 10.1111/j.1469-8137.1990.tb00536.x

Seibt, U., Rajabi, A., Griffiths, H., and Berry, J. A. (2008). Carbon isotopes and water use efficiency: sense and sensitivity. *Oecologia* 155 (3), 441–454. doi: 10.1007/s00442-007-0932-7

Soh, W. K., Yiotis, C., Murray, M., Parnell, A., Wright, I. J., Spicer, R. A., et al. (2019). Rising CO_2 drives divergence in water use efficiency of evergreen and deciduous plants. *Sci. Adv.* 5 (12), eaax7906. doi: 10.1126/sciadv.aax7906

Stangl, Z. R., Tarvainen, L., Wallin, G., Ubierna, N., Räntfors, M., and Marshall, J. D. (2019). Diurnal variation in mesophyll conductance and its influence on modelled water-use efficiency in a mature boreal pinus sylvestris stand. *Photosynth. Res.* 141 (no. 1), 53–63. doi: 10.1007/s11120-019-00645-6

Tcherkez, G., Gauthier, P., Buckley, T. N., Busch, F. A., Barbour, M. M., Bruhn, D., et al. (2017). Leaf day respiration: low CO_2 flux but high significance for metabolism and carbon balance. *New Phytol.* 216 (4), 986–1001. doi: 10.1111/nph.14816

Tcherkez, G., Nogués, S., Bleton, J., Cornic, G., Badeck, F., and Ghashghaie, J. (2003). Metabolic origin of carbon isotope composition of leaf dark-respired CO_2 in french bean. *Plant Physiol.* 131 (1), 237–244. doi: 10.1104/pp.013078

Tcherkez, G., Schäufele, R., Nogués, S., Piel, C., Boom, A., Lanigan, G., et al. (2010). On the $_{13}C/_{12}C$ isotopic signal of day and night respiration at the mesocosm level. *Plant Cell Environ.* 33 (6), 900–913. doi: 10.1111/j.1365-3040.2010.02115.x

Tholen, D., Ethier, G., Genty, B., Pepin, S., and Zhu, X. G. (2012). Variable mesophyll conductance revisited: Theoretical background and experimental implications. *Plant Cell Environ.* 35 (12), 2087–2103. doi: 10.1111/j.1365-3040.2012.02538.x

Thomas, R. B., Spal, S. E., Smith, K. R., and Nippert, J. B. (2013). Evidence of recovery of juniperus virginiana trees from sulfur pollution after the clean air act. *Proc. Natl. Acad. Sci. U.S.A.* 110, 15319–15324. doi: 10.1073/pnas.1308115110

Ubierna, N., and Farquhar, G. (2014). Advances in measurements and models of photosynthetic carbon isotope discrimination in C_3 plants. *Plant Cell Environ.* 37. (7), 1494–1498. doi: 10.1111/pce.12346

Vadeboncoeur, M. A., Jennings, K. A., Ouimette, A. P., and Asbjornsen, H. (2020). Correcting tree-ring $\delta_{13}C$ time series for tree-size effects in eight temperate tree species. *Tree Physiol.* 40 (3), 333–349. doi: 10.1093/treephys/tpz138

Vogado, N. O., Winter, K., Ubierna, N., Farquhar, G. D., and Cernusak, L. A. (2020). Directional change in leaf dry matter $\delta_{13}C$ during leaf development is widespread in C3 plants. *Ann. Bot.* 126 (6), 981–990. doi: 10.1093/aob/mcaa114

Walker, A. P., De Kauwe, M. G., Bastos, A., Belmecheri, S., Georgiou, K., Keeling, R. F., et al. (2021). Integrating the evidence for a terrestrial carbon sink caused by increasing atmospheric CO2. *New Phytol.* 229 (5), 2413–2445. doi: 10.1111/nph.16866

Wang, H., Prentice, I. C., Keenan, T. F., Davis, T. W., Wright, I. J., Cornwell, W. K., et al. (2017). Towards a universal model for carbon dioxide uptake by plants. *Nat. Plants* 3 (9), 734–741. doi: 10.1038/s41477-017-0006-8

Warren, C. R., and Adams, M. A. (2006). Internal conductance does not scale with photosynthetic capacity: implications for carbon isotope discrimination and the economics of water and nitrogen use in photosynthesis. *Plant Cell Environ.* 29 (2), 192–201. doi: 10.1111/j.1365-3040.2005.01412.x

Warren, C. R., Ethier, G. J., Livingston, N. J., Grant, N. J., Turpin, D. H., Harrison, D. L., et al. (2003). Transfer conductance in second growth Douglas-fir (*Pseudotsuga menziesii* (Mirb.)Franco) canopies. *Plant Cell Environ.* 26 (8), 1215–1227. doi: 10.1046/j.1365-3040.2003.01044.x

Wingate, L., Seibt, U., Moncrieff, J. B., Jarvis, P. G., and Lloyd, J. (2007). Variations in $_{13}C$ discrimination during CO_2 exchange by picea sitchensis branches in the field. *Plant Cell Environ.* 30 (5), 600–616. doi: 10.1111/j.1365-3040.2007.01647.x

frontiers | Frontiers in Plant Science

TYPE Original Research
PUBLISHED 24 January 2023
DOI 10.3389/fpls.2023.1099217

OPEN ACCESS

EDITED BY
Boris Rewald,
University of Natural Resources and Life SciencesVienna, Austria

REVIEWED BY
Gaochao Cai,
Sun Yat-sen University, China
Maierdang Keyimu,
Xinjiang Institute of Ecology and Geography, Chinese Academy of Sciences (CAS), China

*CORRESPONDENCE
Jianhua Si
jianhuas@lzb.ac.cn

SPECIALTY SECTION
This article was submitted to Functional Plant Ecology, a section of the journal Frontiers in Plant Science

RECEIVED 15 November 2022
ACCEPTED 10 January 2023
PUBLISHED 24 January 2023

CITATION
Zhou D, Si J, He X, Jia B, Zhao C, Wang C, Qin J, Zhu X and Liu Z (2023) Response of soil water content temporal stability to stand age of *Haloxylon ammodendron* plantation in Alxa Desert, China. *Front. Plant Sci.* 14:1099217. doi: 10.3389/fpls.2023.1099217

Response of soil water content temporal stability to stand age of *Haloxylon ammodendron* plantation in Alxa Desert, China

Dongmeng Zhou[1,2], Jianhua Si[1]*, Xiaohui He[1,2,3], Bing Jia[1], Chunyan Zhao[1], Chunlin Wang[1,2], Jie Qin[1,2], Xinglin Zhu[1,2] and Zijin Liu[1,2]

[1]Key Laboratory of Eco-Hydrology of Inland River Basin, Northwest Institute of Eco-Environment and Resources, Chinese Academy of Sciences, Lanzhou, China, [2]University of Chinese Academy of Sciences, Beijing, China, [3]Faculty of Resources and Environment, Baotou Teachers' College, Inner Mongolia University of Science and Technology, Baotou, China

Afforestation as an effective measure for wind and sand control has achieved remarkable results in northern China, and has also greatly changed the land use and vegetation characteristics of the region. It is important to study the spatial and temporal dynamics of soil water content (SWC) in different afforestation years and its temporal stability to understand the dynamic characteristics of SWC during afforestation. In order to reveal the spatiotemporal dynamic characteristics of SWC in desert area *Haloxylon ammodendron (HA)*plantations, in this study, five restorative-aged *HA* plantations in desert areas were selected and their SWC was measured in stratified layers for the 0–400 cm soil profile; we also analyzed the spatiotemporal dynamics and temporal stability of the SWC. The results showed that the SWC of *HA* plantations decreased with the increase in planting age in the measurement period, and the SWC of deep layers increased by more than that of shallow layers with planting age. Spearman's rank correlation coefficients for SWC of 0–400 cm in both 5- and 11-year-old HA plantations reached above 0.8 and were highly significantly correlated; the temporal stability of SWC tends to increase as the depth of the soil layer deepens. In contrast, the temporal stability of SWC in deeper layers (200–400 cm) of 22-, 34- and 46-year-old stands showed a decreasing trend with depth. Based on the relative difference analysis, representative sampling points can be selected to monitor the regional average SWC, but for older *HA* plantations, the uncertainty factor of stand age should be considered in the regional moisture simulation. This study verified that it is feasible to simulate large-scale SWC in fewer observations for *HA* plantations younger than 11 years old, while large errors exist for older stands, especially for deeper soils. This will help soil moisture management in *HA* plantations in arid desert areas.

KEYWORDS

soil water content, *Haloxylon ammodendron* plantations, temporal stability, spatiotemporal variability, stand age

Abbreviations: SWC, soil water content; HA, Haloxylon ammodendron; CV, coefficient of variation; MRD, mean relative difference; SDRD, standard deviation of relative difference; RSL, Representative sampling locations.

1 Introduction

This study area is located in northwestern China, at the southern edge of the Badain Jaran Desert, which has long suffered from wind and sand. In order to effectively curb wind and sand hazards and prevent the further expansion of sandy land, China has launched a number of major ecological construction projects in wind and sand hazards, such as the "3-North Shelter Forest Program" and the "Grain for Green" program with artificial vegetation construction as the main ecological restoration measure. The vegetation represented by *Haloxylon ammodendron* (HA) plantations is increasingly restricted by soil water content (SWC), especially as the large area of *HA* plantations has a more obvious soil drying phenomenon, which seriously affects the water cycle process in the study area (Kang et al., 2021; Zhou et al., 2022). Therefore, it is important to understand the hydrological effect of SWC after afforestation for the water cycle and eco-hydrological process of terrestrial ecosystems. SWC is at the core of functioning sandy ecosystems in arid and semi-arid regions, driving the material cycle and energy flow in the soil–vegetation–atmosphere continuum, and its dynamic changes affect hydrological and ecological processes such as precipitation infiltration, vegetation transpiration and solute transport (Vereecken et al., 2015; Zhang et al., 2016). SWC has strong spatial and temporal variability due to topography, elevation, soil texture and climate (Hu et al., 2010; Heathman et al., 2012). Related studies also indicate that vegetation affects the spatial distribution of SWC, enhancing or reducing the spatial heterogeneity of SWC to some extent (Li et al., 2008; Cho and Choi, 2014), and the variability of SWC also responds to vegetation growth succession and spatial patterns to varying degrees (Van Pelt and Wierenga, 2001). Therefore, a quantitative study of the spatial variability of SWC is essential to grasp the regional ecohydrological dynamics.

Although soil water has strong spatial and temporal variability, previous studies have shown that SWC is characterized by temporal stability (Brocca et al., 2009; Brocca et al., 2010). Vachaud et al. (1985) found that the spatial structure of SWC is continuous in time when external factors such as soil structure and topography remain stable, and that certain sampling points can represent regional average SWC conditions; this phenomenon was subsequently defined as the temporal stability of SWC. Since then, the temporal stability of SWC has been widely used to identify the average SWC condition in the field (Huang et al., 2020; Zhou et al., 2020; Quan et al., 2021) to simulate hydrological variables (Nasta et al., 2018). The temporal stability of SWC is influenced by numerous elements, such as the length of the observation period (Zhang et al., 2018) and the type of land use (Liu and Shao, 2014; Zhang et al., 2016). Liu and Shao (Liu and Shao, 2014) reported a significant effect of different land use types on SWC in the 0–4 m profile and further validated the feasibility of representative sampling points for estimating the average SWC. Zhang et al. (Zhang et al., 2016) reported that in the spring wheat–shelterbelt–maize agroforestry ecosystem, SWC relationships between adjacent land use types were explored by determining the most time-stable locations of each soil profile for different land use types. Jia and Shao (Jia and Shao, 2013) reported that vegetation cover and above-ground biomass are the main factors affecting the temporal stability of SWC, and further concluded that sampling in slopes may produce better results when the temporal stability theory is applied to slopes.

The above findings indicate that the study of temporal stability of SWC is more meaningful in the context of non-homogeneous soils, and that vegetation factors profoundly affect temporal stability and differ for different soil depths. As a key area for revegetation in the Alxa desert region, artificial revegetation has greatly changed the land use and vegetation characteristics of the region, and the effect of this huge disturbance on the temporal variability and temporal stability of SWC is yet to be studied. Specifically, this study aimed to: (1) explore the response of SWC to stand age in HA plantations;(2) reveal the spatiotemporal dynamic characteristics of SWC in desert area. This study provide a theoretical basis for water resource management and vegetation construction in the region.

2 Materials and methods

2.1 Description of study site

The Alxa desert area is located in northwestern China (97°10′E-106°52′E,37°21′N-42°47′N). The region has an arid climate. The sunshine is sufficient and the annual sunshine hours are 2993 to 3345h. The annual average temperature is 6.8-8.8°, with extreme minimum and maximum temperatures of -36.4° and 41.7° respectively. The temperature has a large diurnal temperature difference and significant seasonal changes. The frost-free period is 130-165 d. The average annual precipitation is 39.3-85.6 mm, with precipitation from July to September accounting for about 90% of the year. The water table is 80-120 m, and there are no river confluences. Due to the drought tolerance and high survival rate of HA, the Chinese government planted HA in large quantities in the study area around the 1970s for wind and sand control, and it has played a vital role in the improvement of the ecological environment in the area.

2.2 Experimental design and measurements

Since 1975, afforestation projects have been carried out every year in Alxa desert. In this study, the HA planted in 1975,1987,1999,2010 and 2016 were selected according to the principle of consistency of soil texture. Then, five representative sample plots of 5-, 11-, 22-, 34- and 46-year-olds were selected in the study area with a 10-year age gradient, 50m*50m sample plots were delineated in each plantation and 3 replicate samples were collected at the center of the sample plots in May–September 2021 in 20 cm stratification. The 0-400 cm soil profile was sampled in 20 cm layers, and three duplicate samples were collected from each sample site. And put the soil sample into the aluminum box back to the laboratory for drying method to measure the SWC. Three undisturbed soil samples were collected with a ring knife near the sampling point for the determination of soil hydraulic characteristics such as soil bulk density and field water capacity, and sample plots were investigated at the same time (Table 1). The selected plots were all planted in a standardized "two rows and one strip "planting mode. There was no other vegetation around, so the study was not interfered with by the planting density and other vegetation on the experimental results.

TABLE 1 Characteristics of *Haloxylon ammodendron* (HA) plantation lands at different plots.

Parameters of sites	Plot 1	Plot 2	Plot 3	Plot 4	Plot 5	Plot 6
Planting Age (a)	5	11	22	34	46	Wasteland
Year of planting	2016	2010	1999	1987	1975	/
Altitude (m)	1204.86	1204.95	1203.69	1203.66	1204.37	1203.97
Clay Volume Fraction (%)	11.07	11.61	11.73	11.16	10.97	10.31
Silt Volume Fraction (%)	13.57	15.95	14.26	13.19	12.80	15.18
Sand Volume Fraction (%)	75.36	72.44	74.01	75.65	76.23	74.51
Diameter at breast height(cm)	3.5 ± 1.2	8.9 ± 3.8	12.4 ± 5.5	16.5 ± 6.2	22.1 ± 7.5	/
Mean tree height/(cm)	55 ± 12	140 ± 28	220 ± 46	370 ± 63	420 ± 81	/
Tree density/(Tree/hm^2)	230	230	230	230	230	/
Bulk Density/(g/cm^3)	1.53	1.53	1.52	1.53	1.54	1.53

2.3 Statistical analysis

Soil water storage is the amount of soil water stored in a certain unit volume. In this study, based on the observed depth of 0–400 cm soil depth, the soil water storage per unit volume of 0–400 cm soil depth is given by:

$$SWS_i = \sum_{i=1}^{20} SVWC_i d_i \quad (1)$$

$$\overline{SVWC_j} = \frac{1}{20}\sum_{i=1}^{20} SVWC_{ij} \quad (2)$$

where SWS_i is a soil water storage of 0–400 cm from point i (i=1,…, n) (mm), $SVWC_i$ is the soil volumetric water content (cm3cm-3), d_i is the soil depth (mm), and $\overline{SVWC_j}$ is the average soil volumetric water content at time j (j=1,…,m) (cm3cm-3), The number of soil layers observed in this study is 20. According to Vachaud et al. (1985), the relative difference (RD) and standard deviation (SD) of each observation can characterize the temporal stability of SWC. The RD_{ij} and SD of SWS_{ij} at any observation at point i (i=1,…,m) at time j (j=1,…,m) are given by:

$$RD_{ij} = \frac{SVWC_{ij} - \overline{SVWC_j}}{\overline{SVWC_j}} \quad (3)$$

$$SD = \sum_{i=1}^{m}\sqrt{\frac{SVWC_{ij} - \overline{SVWC_j}}{m-1}} \quad (4)$$

where $SVWC_{ij}$ is SVWC at point i (i=1,…,m) at time j (j=1,…,m) (cm3cm-3), $\overline{SVWC_j}$ is the average SVWC at time j (j=1,…,m) (cm3cm-3), and m is the number of measurements. The mean relative difference MRD_i and its corresponding standard deviation $SDRD_i$ are given by:

$$MRD_i = \frac{1}{m}\sum_{j=1}^{m} RD_{ij} \quad (5)$$

$$SDRD_i = \sqrt{\frac{1}{m-1}\sum_{i=1}^{m}\left(RD_{ij} - MRD_i\right)^2} \quad (6)$$

According to Zhao et al. (Zhao et al., 2010), we compared the temporal stability of SWC at different soil depths in different restoration years of HA plantations by comparing the index of temporal stability at depth i ($ITSD_i$) to find the highest temporal stability point. The observation point with the highest temporal stability, which is representative of the average SWC condition and $ITSD_i$, is given by:

$$ITSD_i = \sqrt{MRD_i^2 + SDRD_i^2} \quad (7)$$

Spearman's rank correlation coefficient r_s was used to analyze the stability of the rank change over time for different observations during the growing season:

$$r_s = 1 - 6\sum_{i=1}^{n}\frac{\left(R_{ij} - R_{il}\right)^2}{n(n^2-1)} \quad (8)$$

where R_{ij} is the rank of the SWC at point i at time j,R_{il} is the rank of the SWC at point i at time l, and n is the total number of observation points. Dummy Figure 1

3 Results and discussion

3.1 Distribution characteristics of SWC variability

Stand age influenced the spatial and temporal distribution of soil water to some extent, and that the age factor gradually overshadowed the soil depth factor as the stand age increased. Table 2 shows the spatial statistical characteristics of the mean SWC, standard deviation and coefficient of variation (CV) of the 0–400 cm soil layer profile in each HA plantation. The standard deviation and CV of SWC in each soil layer showed a general trend of increasing with the deepening of the soil layer. From Figure 2, it can be seen that the CV of SWC changed irregularly for 5-,11-, and 22- year-old of HA plantations, but the CV of SWC of 34- and 46-year-old HA plantations tends to increase with the deepening of the soil layer, It is indicated that the spatial variability of SWC increases with the deepening of the soil layer for 34- and 46-year-old of HA plantations. Li et al. (2015)

10.3389/fpls.2023.1099217

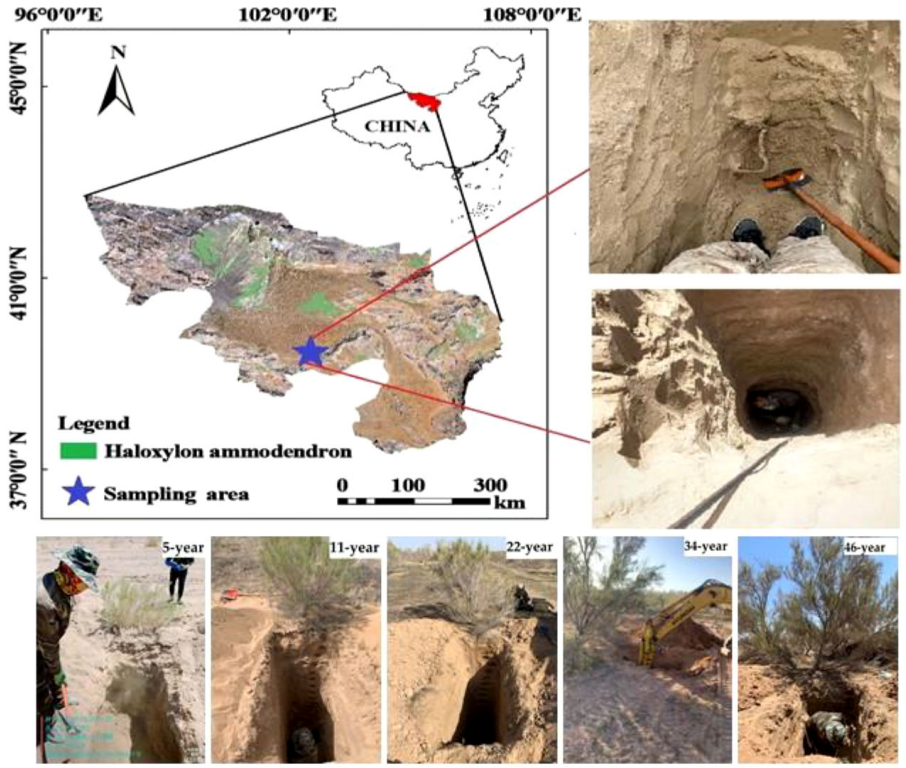

FIGURE 1
Location of the study area.

reached similar conclusions on the Loess Plateau, the spatial distribution of SWC depends largely on structural factors such as climate, topography and soil texture, while stochastic factors such as vegetation recovery and human activity increase the spatial variability of SWC (Zhao et al., 2018). The sampling area is located at the southern edge of the Badain Jaran Desert, and is less disturbed by human and animal activities, the spatial variability of SWC was increase as the soil layer deepened for 34- and 46-year-old HA

TABLE 2 Spatial statistical characteristics of temporal average, standard deviation and coefficient of variation (CV) of SWC in different soil layers.

Planting Age (a)	Variable	Soil depth (cm)			
		0–100 cm	100–200 cm	200–300 cm	300–400 cm
5	Mean SWC	7.56	6.34	7.29	8.41
	Standard deviation	0.59	0.45	0.85	0.71
	CV	7.56	7.04	11.68	8.47
11	Mean SWC	7.65	6.20	6.04	7.40
	Standard deviation	0.48	0.37	0.50	0.58
	CV	6.43	5.94	8.49	7.99
22	Mean SWC	7.48	5.95	5.36	6.40
	Standard deviation	0.57	0.45	0.49	0.54
	CV	7.65	7.54	9.24	8.60
34	Mean SWC	6.71	5.36	4.13	4.65
	Standard deviation	0.55	0.44	0.45	0.52
	CV	8.21	8.16	10.80	11.35
46	Mean SWC	6.33	2.87	2.42	2.36
	Standard deviation	0.42	0.39	0.39	0.36
	CV	6.71	14.11	16.10	15.34

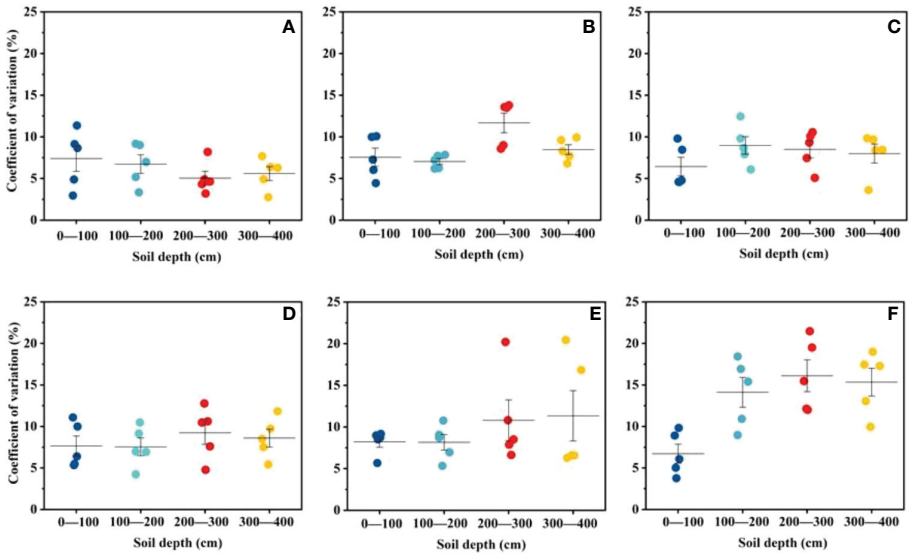

FIGURE 2
A scatterplot of SWC coefficient of variability for each soil layer in HA plantation forested land at different ages: **(A)** wasteland, **(B)** 5, **(C)** 11, **(D)** 22, **(E)** 34 and **(F)** 46 years. Different colors represent different soil depths: blue (0-100 cm), green (100-200 cm), red (200-300 cm), yellow (300-400 cm).

plantations. Nan et al. (2019) quantified the soil water depletion of artificial *Robinia pseudoacacia* forest of different ages (5, 20, and 40 years) on the Loess Plateau. His research showed that soil water consumption was divided into two stages, the first stage was that the artificial *Robinia pseudoacacia* forest gradually transited from shallow soil layer to deep soil layer with the increase of age, the second stage is the transition from the deep soil to the shallow soil when the deep soil water consumption reaches a certain threshold. However, this study found that the soil water consumption was similar to the first stage of the above research with the increase of the age of the HA plantation, but the rule of the second stage did not appear. The reason for this difference may be that the sampling depth of this study is relatively shallow (400 cm), and the sampling depth has not yet reached the conversion threshold of soil water consumption. According to Zeng et al. (2011), it was found that the root system of aged HA can grow vertically down to 800 cm, which also verified the above hypothesis. Future studies should carry out deeper soil layer research for aging HA. It also helps to reveal the relationship between artificial vegetation growth and soil water consumption.

3.2 The spatiotemporal behavior of SWC

The SWC showed a trend of decreasing with increasing years of HA plantations, and the variation of SWC with plant years was greater in the deep layer than in the shallow layer. Figure 3 shows the variation trend of SWC with depth in the HA plantation profile at each stand age; it can be seen that the SWC in the surface layer (0–100 cm) did not vary much with stand age during the study period and was at a high level relative to the deeper layers, fluctuating in the range of 0.06-0.09 cm^3cm^{-3}. The SWC in the 100–400 cm soil layer varied greatly with the age of the forest, fluctuating between 0.02-0.09 cm^3cm^{-3}, with the SWC in the 100–400 cm soil layer decreasing with depth in the 46-year-old HA plantations. The SWC in 11-, 22- and 34-year-old HA plantations showed a decreasing trend with a depth from 0 to 300 cm, but there was an "inflection point" from 300 to 400 cm, where the SWC increased with depth and the "inflection point" in 5-year-old HA plantations occurred at a more shallow level (100–200 cm). Hu et al. (2010) used soil water storage data in the Loess Plateau to identify temporal stability points, and found that artificial vegetation significantly affected deep soil water. Gao and Shao (2012) conducted research on 0-300 cm soil layer SWC in the Loess Plateau and found that the change rate of SWC in deep soil was lower than that in shallow soil, which was contrary to the conclusion of this study. These differences are due to the different types of trees, shrubs and herbs that were focused on in the study of Gao and Shao (2012). The present study is consistent with Hu et al. (2010), which was conducted on a mono-vegetated hillside. Compared to trees and shrubs, herbs consume less water at shallow depths, and the effect of vegetation factors on SWC varies with soil depth. The vegetation factors interfered with the regularity of SWC variation with depth, resulting in large differences in vertical soil profile variations under different vegetation types. In addition, this study area is located in an arid desert area with little human activity, which reduces the influence of human activity and other factors on the soil surface moisture changes. HA plantations are planted for a long period of time (46 years) and HA is a deep-rooted plant (Gong et al., 2019); the SWC in the 200–400 cm soil layer is more influenced by root water consumption, which also leads to the deep SWC changing with planting. The SWC in the 200–400 cm soil layer is more influenced by root water consumption, which leads to a greater variation of SWC in the deep layer than in the shallow layer with planting age.

Figure 3 shows that there is no significant decrease in SWC in the 0–100 cm soil profile for all stand ages, while the SWC in 200–400 cm decreases significantly after more than 11 years of HA plantations. Moradi et al. (2017) assessed the impact of afforestation on soil physical and chemical properties and SWC in south-west Iran, and found that afforestation improved soil conditions but significantly

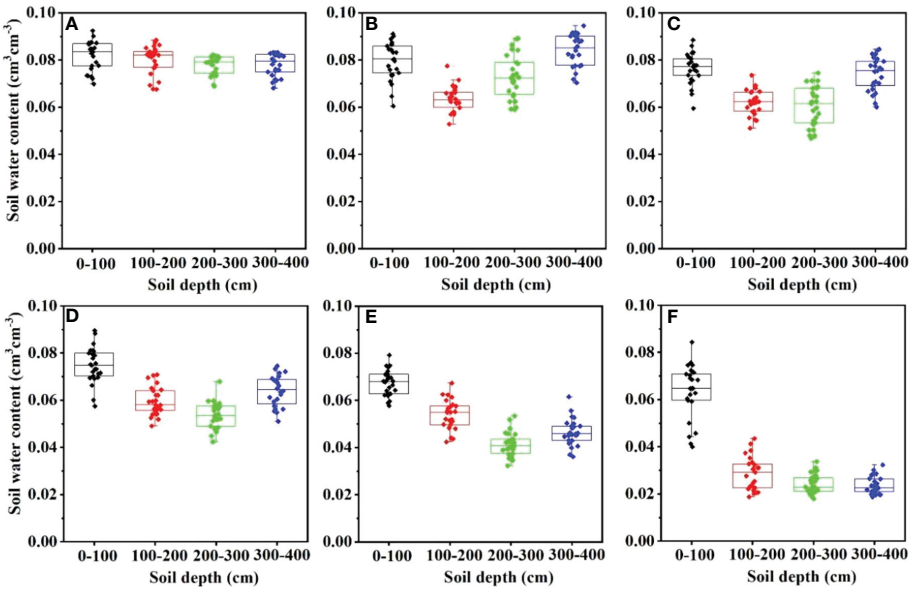

FIGURE 3
A boxplot of the vertical distribution of soil water content (SWC) in HA plantations: **(A)** wasteland, **(B)** 5-year-old, **(C)** 11-year-old, **(D)** 22-year-old, **(E)** 34-year-old and **(F)** 46-year-old.

depleted SWC. Haque et al. (1999) studied differences in SWC in three different plantations in the North-East of Scotland. The results showed that, compared with the control group, the early growth stage had little effect on SWC, while the late growth stage made the soil dry. Wang et al. (2021) reached similar conclusion in HA plantations of different planting years in the desert oasis transition zone of the Hexi Corridor. Guo et al. (2016), however, found that the SWC in HA plantations significantly increased in the 260 cm soil layer. The main reason for the difference is that Guo et al. (2016) selected HA plantations which were 3 years old; compared with the short planting period in this study, the root depth of HA plantations in 3-year-old stands is shallow. In comparison, Wang et al. (2021) selected HA planting years similar to the present study. The reason for this phenomenon is that precipitation is low and evaporation is high in the study area. The less precipitation mainly occurs in short precipitation periods, and the infiltration process of precipitation is mainly concentrated in the soil layer within 60 cm. Therefore, shallow soils can be recharged by precipitation, while deep soil water recharge is not significant. (Yang and Zhao, 2014). Furthermore, the transpiration water consumption of HA is much higher than the precipitation (Chang et al., 2007); after 22 years of planting in particular, the excessive consumption of deep soil water by HA roots further leads to SWC deterioration.

3.3 Temporal stability of SWC

3.3.1 Spearman's rank correlation coefficient

For different stand ages, the correlation coefficients tended to decrease with increasing stand age, but in general the correlation coefficients were greater than 0.5 and highly significant ($P<0.01$). Spearman's rank correlation coefficient of SWC at each sampling point can characterize the temporal stability of the study area as a whole. Figure 4 shows Spearman's rank correlation coefficient matrix of SWC at 0–400 cm depth for different observation dates in the study area. As depicted in Table 2, the correlation coefficient between August 12 and the other measurement dates is small, between 0.631 and 0.828, and the correlation coefficient between the remaining dates is large. The reason for this discrepancy may be due to the large variation in SWC due to the larger rainfall in the week before the July 12 sampling, resulting in a smaller correlation coefficient. The study of Xin et al. (Xin et al., 2008) on the temporal stability of soil water uptake also found that the temporal stability of soil water was worst when the soil was alternately dry and wet. This indicates that the spatial distribution of SWC at 0–400 cm depth in *HA* plantations in the study area is characterized by temporal stability within the study time; Grant et al. (2004), However, it should be noted that the temporal stability showed a trend of time-dependent variation, The closer the sampling time, the greater the correlation coefficient. This result indicates that the duration of temporal stability of SWC is limited, which is a similar conclusion in other studies with interannual observation scales (Penna et al., 2013; Zhang and Shao, 2013a). This study was conducted based on one growing season of *HA* plantations, and for future studies, a longer time series can be considered to explore the effective period of temporal stability.

3.3.2 Relative difference analysis

Deep SWC in favor of maintaining a higher temporal stability. However, with the introduction of artificial vegetation, the growth of stand age gradually overshadows the soil depth factor, making the temporal stability of deep SWC lower. Figure 5 shows the mean relative difference (MRD) values of SWC at each sampling point in different soil layers in descending order, and the corresponding time index of temporal stability at depth curves; the vertical error line is the standard deviation of relative difference (SDRD) at each sampling point. The MRD of SWC of 5- and 11-year-old *HA* plantations

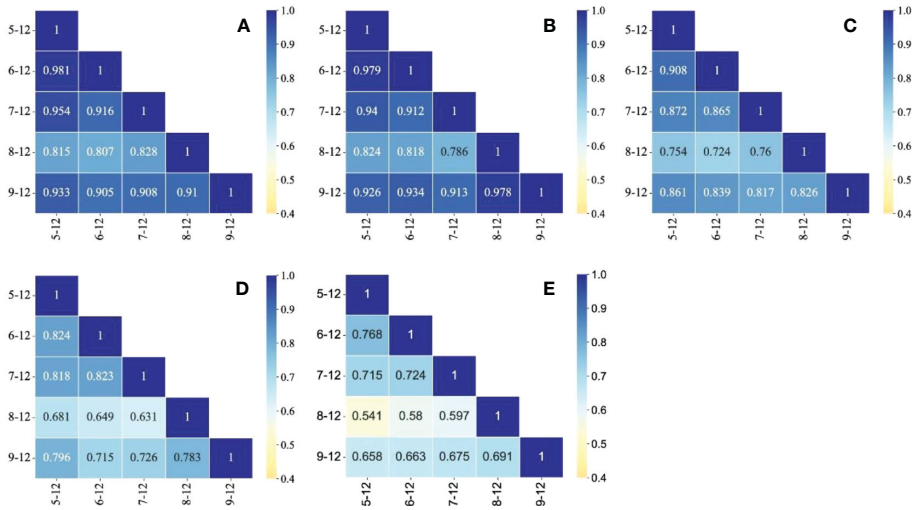

FIGURE 4
Spearman's rank correlation coefficient heat map of 0-400 cm SWC in *HA* plantations: **(A)** 5-year-old, **(B)** 11-year-old, **(C)** 22-year-old, **(D)** 34-year-old and **(E)** 46-year-old.

showed a trend of increasing and then decreasing; for the shallow layer, the MRD increased gradually probably because the spatial variability of SWC increased as the soil layer deepened (Jia and Shao, 2013). The MRD of SWC in the deeper soil layers decreases, probably due to the young age of the *HA* plantations and the failure of the root system to grow into the deeper soil layers. For the 22-, 34- and 46-year-old *HA* plantations, the MRD in SWC increased with the increasing depth of the soil layer, and the same conclusion was reached in the CV analysis above. The stronger the spatial variability, the more dispersed the distribution of water content at each sampling point, and the greater the deviation from the average value will be; Zhang and Shao (2013) selected two plots with different soil textures in northwest China, and evaluated the spatial distribution of SWC. The results showed that the deeper the soil depth, the greater the MRD of SWC, which was similar to the conclusion of this study. In a gravel–mulch field in northwestern China, in relation to the spatial and temporal stability of SWC, Zhao et al. (Zhao et al., 2017) found that the MRD decreases with increasing soil depth; the reason for this difference lies in its small research scope (32*32 m), and the gravel–mulch field soil has a homogeneous texture and uniform sand and gravel cover, resulting in its weak spatial variability of SWC. Li et al. (Li et al., 2015) found that the fluctuation range of the MRD may be related to the study scale, test placement, sampling method, etc. With the expansion of the study area, the more complex the corresponding soil properties, topography and vegetation cover, the stronger the spatial variability of SWC, and the range of the MRD also increases (Martinez-Fernandez et al., 2003). Spatial variability is the result of the interaction of different dominant factors at different spatial scales, and in the process of scale transformation, the influencing factors also change, so the results of studies at different scales vary (Sun et al., 2022). Therefore, for specific research objects, the sampling scale range and sampling granularity need to be considered in order to have a better explanation of the spatial heterogeneity of SWC (Fagan et al., 2003). Figure 4 also shows that the MRD is asymmetric, with negative absolute values greater than positive values, due to the fact that the SWC at more sampling points is less than the mean value, probably because the soil at the measurement site has a gravel content, which is not conducive to water retention.

The magnitude of the SDRD can characterize the degree of temporal stability of SWC at the sampling point; the smaller the SDRD, the higher the temporal stability. Figure 4 shows that 5-,11- and 22-year-old HA plantations is in line with the trend of decreasing SDRD with soil depth deepening, but not at ages 34 and 46, indicating that deep soil water of HA plantations at the age of 5,11, and 22 is not disturbed by vegetation and has higher temporal stability. However, SWC in the deep layer of HA at 34-,46-year-old was greatly disturbed by vegetation, so the temporal stability of SWC did not show a decreasing trend with soil depth., which was consistent with the MRD analysis above. Temporal stability of SWC is the result of the interaction of many factors such as vegetation, topography, climate and soil (He et al., 2021). The study area is on the edge of the desert. The climate environment of low rainfall and high evaporation has its own special effects on the temporal stability of soil water; long time soil freezing makes the mid-soil flow a predominantly vertical movement; meanwhile, the soil dry layer induced by vegetation water depletion hinders the vertical movement of soil water and limits the recharge of deep soil water. Ding et al. (Ding et al., 2020) concluded that artificially restored vegetation has a certain impact on SWC in the rhizosphere, but it has less impact below the rhizosphere, mainly because the vegetation growth period is short and the vegetation characteristics of slow growth make its ecological water consumption low, and the precipitation basically meets the vegetation growth demand. However, this study found that as the growth years of *HA* plantations increased, it had a non-negligible effect on the changes of SWC dynamics; precipitation and evaporation are the most direct influencing factors of SWC, but there are large differences in response to different soil depths. Surface runoff caused by strong rainfall on the

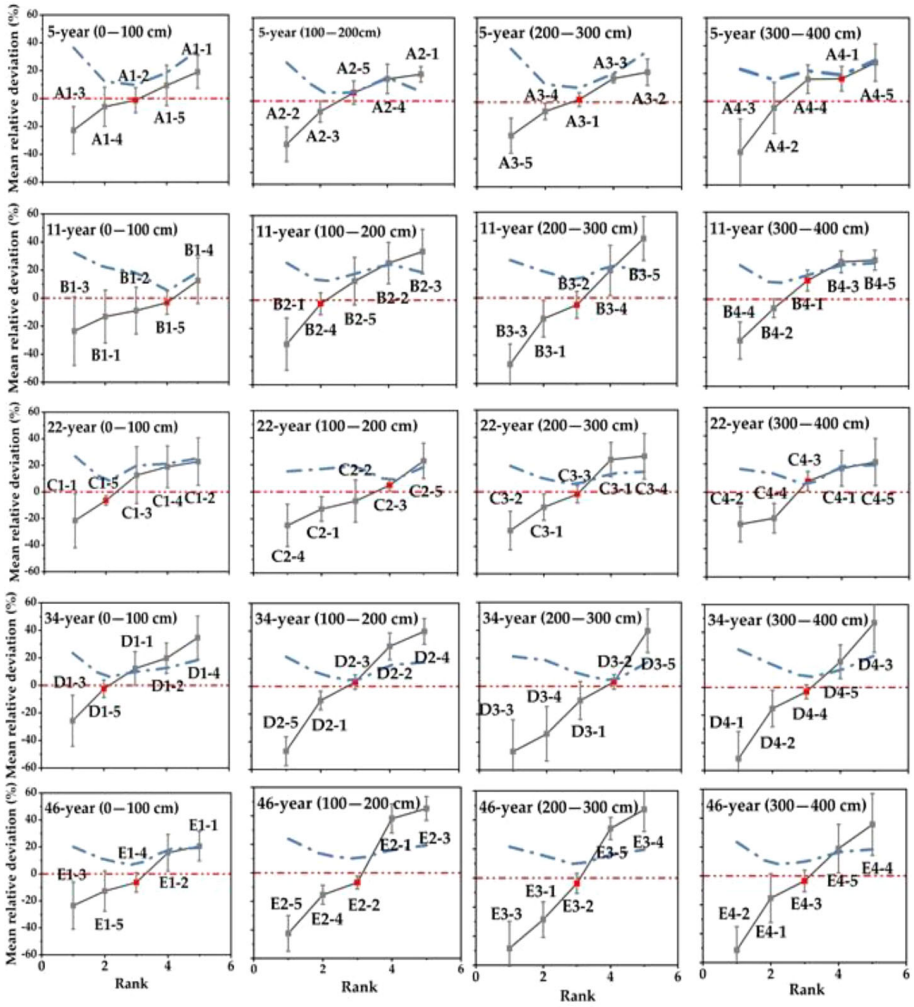

FIGURE 5
Ranked mean relative difference (MRD) of SWC in the diverse soil layers in HA plantations, the letters in the figure represent different stand ages: **(A)** 5-year-old, **(B)** 11-year-old, **(C)** 22-year-old, **(D)** 34-year-old and **(E)** 46-year-old. The numbers in the figure are the sample point numbers. The solid gray line indicates MRD, the red line is the baseline with an average relative deviation of 0. Error bars represent the standard deviation of relative difference (SDRD). The most time-stable locations are indicated by the red dots. The blue dotted line indicates index of temporal stability at depth.

slope surface replenishes surface SWC significantly; while it is not conducive to deep SWC infiltration and evaporative dissipation of surface SWC is large, the rough soil texture is weak in lifting deep SWC, and the combined factors lead to deep SWC in favor of maintaining a higher temporal stability. However, with the introduction of artificial vegetation, the growth of stand age gradually overshadows the soil depth factor, making the temporal stability of deep SWC lower.

The results of the above-mentioned study showed that the temporal stability of deep soil layers was higher than that of shallow layers, and the temporal stability characteristics of SWC were depth-dependent for *HA* plantations before 22 years of age. This is consistent with the results of related studies (Gao and Shao, 2012a). However, for older *HA* plantations there is an opposite performance in deeper soils (200–400 cm). It is worth to note that, limited by the experimental conditions, this study only studied SWC in HA plantation with a stand age of 5,11,22,34, and 46 years, and could not find a continuous stand that met the experimental conditions. Therefore, appropriate models should be selected for future research in order to evaluate SWC more accurately.

3.3.3 Representative sampling locations

The correlation with the mean value of SWC in the corresponding soil layer is high, and the average SWC of each soil layer in the study area can be estimated more accurately. Zhang et al. (Zhang et al., 2016) show that representative sampling locations (RSL) can be selected to estimate the regional average SWC according to the principle that the MRD is close to 0 and the SDRD is relatively small. To verify the reasonableness of the RSL, the SWC of each RSL was compared with the average SWC of each soil layer, and it was found that the SWC of each measurement point fluctuated slightly around the average SWC (Figure 6). Meanwhile, the regression analysis between the mean SWC values of different soil layers and the RSL during the observation period showed that the coefficient of determination R^2 of each soil layer from 0 to 400 cm varied in the ranges of 0.88–0.95, 0.60–0.95, 0.49–0.95 and 0.53–0.95, indicating that the correlation between the mean SWC values of each RSL and the corresponding soil layer was high. The correlation with the mean value of SWC in the corresponding soil layer is high, and the average SWC of each soil layer in the study area can be estimated more

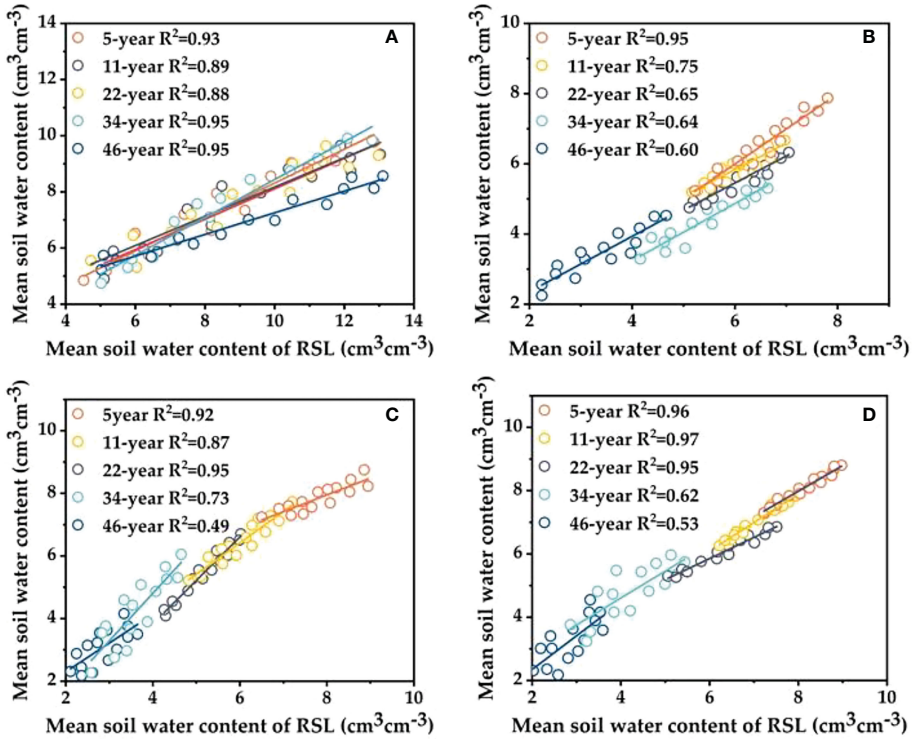

FIGURE 6
Comparisons of measured SWC at the most time-stable location with the estimated values in the four soil layers under five different stand ages: **(A)** 0—100 cm, **(B)** 100—200 cm, **(C)** 200—300 cm, **(D)** 300—400 cm.

accurately, but the temporal stability of the deep SWC gradually decreases with increasing growth years of *HA* plantations.

3.4 Implications for future afforestation activities

In order to prevent further desert expansion, China introduced many plant species in the 1970s (Ahrends et al., 2017). The excessive water consumption of artificial vegetation has broken the dynamic balance between precipitation and native vegetation, and many new environmental problems have emerged (Gao and Shao, 2012b; He et al., 2019). In recent years, there have been numerous studies showing that the massive consumption of soil water by artificial vegetation leads to a decrease in SWC and has a negative impact on vegetation growth, which in turn threatens the health of the ecosystem (Chang et al., 2007; Xin et al., 2008; Zhang and Shao, 2013).

In our field survey, we found that when the SWC dropped to 0.02-0.03 cm^3cm^{-3} after 30a of *HA* planting, the leaves fell off in large numbers and the individual biomass decreased significantly. Moreover, when the SWC was at 0.01-0.02 cm^3cm^{-3}, the sand-fixing plants appeared to decline; at about 1% the sand-fixing plants died in large numbers. Although *HA* can reduce the water consumption of aging photosynthetic organs by withering leaves and branches, the water scarcity of old leaves, branches and stems is extremely serious and has basically reached its limit. The further shedding of a large number of leaves and branches reduces its individual biomass and deteriorates its survival ability. Finally, the stems also dry up and break due to too little water in the plant. Therefore, based on the above findings, we suggest that moderate manual interventions, such as pruning of dead branches, proper irrigation and some level of crop flattening or intercropping after 30–40a of HA planting, may have positive implications for the revival and rejuvenation of *HA* plantations. It is worth noting that this study based on the same planting density on the SWC of different age HA plantations, to avoid the planting density to interfere with the results of the study. In the actual afforestation project, usually through adjusting the planting density to reduce the deep soil water consumption. Therefore, future research should further establish mechanism models through vegetation growth and soil water consumption to provide theoretical basis for rational afforestation engineering.

4 Conclusions

1. The SWC of 0-400 cm of *Haloxylon ammodendron* plantations t in the study area showed a decreasing trend with the increase of HA planting age, and the HA plantations consumed mainly shallow soil water in 5- and 11-year-old stands, while 22-,34-and 46- year-old consumed mainly deep soil water.

2. The distribution of SWC at 0-400 cm depth in the *HA* plantations in the study area was characterized by temporal stability during the study time period, but it should be noted that the temporal stability showed a time-dependent trend, with the correlation coefficient increasing the closer the sampling time and tending to

decrease as the time interval increased. This result indicates that the duration of temporal stability of SWC is limited.

3. Afforestation (e.g., *Haloxylon ammodendron*) is an important measure to prevent wind and sand fixation in desert areas, which is of great significance to the sustainable development of the ecosystem. Our study found that the age of vegetation has an important influence on the deep SWC dynamics, and with the increase of forest age, the water depletion of vegetation roots leads to the degradation of SWC in the study area, and the temporal stability also decreases with the increase of forest age and soil depth, therefore, in the future afforestation work in the Alxa desert area, appropriate moisture control measures should be taken for *HA* plantations of advanced forest age.

Data availability statement

The original contributions presented in the study are included in the article/Supplementary Material. Further inquiries can be directed to the corresponding author.

Author contributions

DZ: conceptualization, data curation, investigation, methodology, formal analysis, roles/writing—original draft, writing—review and editing. JS: conceptualization, data curation, formal analysis, funding acquisition, methodology. BJ: investigation. CZ: conceptualization, data curation, formal analysis, investigation. JQ: investigation, XH: investigation. CW: investigation. XZ: investigation. ZL: investigation. All authors read and approved the final manuscript. All authors contributed to the article and approved the submitted version.

Funding

This study was supported by the Major Science and Technology Project in Inner Mongolia Autonomous region of China (No. Zdzx2018057), the Innovation Cross Team Project of Chinese Academy of Sciences, CAS (No. JCTD-2019-19), Transformation Projects of Scientific and Technological Achievements in Inner Mongolia Autonomous region of China (No. 2021CG0046), and the National Natural Science Foundation of China (No. 42001038).

Conflict of interest

The authors declare that the research was conducted in the absence of any commercial or financial relationships that could be construed as a potential conflict of interest.

Publisher's note

Supplementary material

The Supplementary Material for this article can be found online at: https://www.frontiersin.org/articles/10.3389/fpls.2023.1099217/full#supplementary-material

References

Ahrends, A., Hollingsworth, P. M., Beckschaefer, P., Chen, H., Zomer, R. J., Zhang, L., et al. (2017). China's fight to halt tree cover loss. *Proc. Of R. Soc. B-Biological Sci.* 284 (1854). doi: 10.1098/rspb.2016.2559

Brocca, L., Melone, F., Moramarco, T., and Morbidelli, R. (2009). Soil moisture temporal stability over experimental areas in central Italy. *Geoderma* 148 (3), 364–374. doi: 10.1016/j.geoderma.2008.11.004

Brocca, L., Melone, F., Moramarco, T., and Morbidelli, R. (2010). Spatial-temporal variability of soil moisture and its estimation across scales. *Water Resour. Res.* 46 (2). doi: 10.1029/2009WR008016

Chang, X., Zhao, W., and Zhang, Z. (2007). Water consumption characteristic of haloxylon ammodendron for sand binding in desert area. *Acta Ecological Sin.* 27 (5), 1826–1837. doi: 10.1016/S1872-2032(07)60017-1

Cho, E., and Choi, M. (2014). Regional scale spatio-temporal variability of soil moisture and its relationship with meteorological factors over the Korean peninsula. *J. Hydrology* 516, 317–329. doi: 10.1016/j.jhydrol.2013.12.053

Ding, C., Wang, D., He, K., Li, P., Zhang, P., and Liang, S. (2020). Study of temporal stability of soil moisture on hillslope in loess regions of China. *Acta Ecological Sin.* 40 (1), 151–160. doi: 10.5846/stxb201809272104

Fagan, W. F., Fortin, M. J., and Soykan, C. (2003). Integrating edge detection and dynamic modeling in quantitative analyses of ecological boundaries. *Bioscience* 53 (8), 730–738. doi: 10.1641/0006-3568(2003)053[0730:IEDADM]2.0.CO;2

Gao, L., and Shao, M. (2012). Temporal stability of soil water storage in diverse soil layers. *Catena* 95, 24–32. doi: 10.1016/j.catena.2012.02.020

Gong, X., Lu, G., He, X., Sarkar, B., and Yang, X. (2019). High air humidity causes atmospheric water absorption *via* assimilating branches in the deep-rooted tree haloxylon ammodendron in an arid desert region of Northwest China. *Front. In Plant Sci.* 10. doi: 10.3389/fpls.2019.00573

Grant, L., Seyfried, M., and McNamara, J. (2004). Spatial variation and temporal stability of soil water in a snow-dominated, mountain catchment. *Hydrological Processes* 18 (18), 3493–3511. doi: 10.1002/hyp.5798

Guo, J., Li, C., Zeng, F., Zhang, B., Liu, B., and Guo, Z. (2016). Relationship between root biomass distribution and soil moisture, nutrient for two desert plant species. *Arid Zone Res.* 33 (1), 166–171. doi: 10.13866/j.azr.2016.01.21

Haque, S., Billett, M. F., Grayston, S., and Ord, B. G. (1999). Effects of afforestation on ammonification and nitrification rates in former agricultural soils. *Soil Use Manage.* 15 (2), 117–122. doi: 10.1111/j.1475-2743.1999.tb00074.x

Heathman, G. C., Cosh, M. H., Merwade, V., and Han, E. (2012). Multi-scale temporal stability analysis of surface and subsurface soil moisture within the upper cedar creek watershed, Indiana. *Catena* 95, 91–103. doi: 10.1016/j.catena.2012.03.008

He, F., Tong, Z., Hannaway, D. B., and Li, X. (2021). Erratic precipitation and clipping frequency reshape the community structure and species stability of leymus chinensis steppe. *Ecol. Indic.* 133. doi: 10.1016/j.ecolind.2021.108432

He, Z., Zhao, M., Zhu, X., Du, J., Chen, L., Lin, P., et al. (2019). Temporal stability of soil water storage in multiple soil layers in high-elevation forests. *J. Hydrology* 569, 532–545. doi: 10.1016/j.jhydrol.2018.12.024

Huang, M., Liu, X., and Zhou, S. (2020). Asynchrony among species and functional groups and temporal stability under perturbations: Patterns and consequences. *J. Ecol.* 108 (5), 2038–2046. doi: 10.1111/1365-2745.13418

Hu, W., Shao, M., and Reichardt, K. (2010). Using a new criterion to identify sites for mean soil water storage evaluation. *Soil Sci. Soc. America J.* 74 (3), 762–773. doi: 10.2136/sssaj2009.0235

Jia, Y., and Shao, M. (2013). Temporal stability of soil water storage under four types of revegetation on the northern loess plateau of China. *Agric. Water Manage.* 117, 33–42. doi: 10.1016/j.agwat.2012.10.013

Kang, J., Yu, J., Zhang, J., Xu, J., and Wang, S. (2021). Na Compound fertiliser improves growth performance, drought resistance, and water-saving efficiency of the succulent xerophyte haloxylon ammodendron in the alxa desert region of China. *Aust. J. Bot.* 69 (5), 318–327. doi: 10.1071/BT20107

Li, X., Shao, M., Jia, X., and Wei, X. (2015). Landscape-scale temporal stability of soil water storage within profiles on the semiarid loess plateau of China. *J. Soils And Sediments* 15 (4), 949–961. doi: 10.1007/s11368-015-1059-9

Liu, B., and Shao, M. (2014). Estimation of soil water storage using temporal stability in four land uses over 10 years on the loess plateau, China. *J. Hydrology* 517, 974–984. doi: 10.1016/j.jhydrol.2014.06.003

Li, P., Wang, N., He, W., Kruesi, B. O., Gao, S., Zhang, S., et al. (2008). Fertile islands under artemisia ordosica in inland dunes of northern China: Effects of habitats and plant developmental stages. *J. Arid Environments* 72 (6), 953–963. doi: 10.1016/j.jaridenv.2007.11.004

Martinez-Fernandez, J., and Ceballos, A. (2003). Temporal stability of soil moisture in a large-field experiment in Spain. *Soil Sci. Soc. America J.* 67 (6), 1647–1656. doi: 10.2136/sssaj2003.1647

Moradi, M., Naji, H. R., Imani, F., Behbahani, S. M., and Ahmadi, M. T. (2017). Arbuscular mycorrhizal fungi changes by afforestation in sand dunes. *J. Arid Environments* 140, 14–19. doi: 10.1016/j.jaridenv.2017.01.006

Nan, G. W., Wang, N., Jiao, L., Zhu, Y. M., and Sun, H. (2019). A new exploration for accurately quantifying the effect of afforestation on soil moisture: A case study of artificial *robinia pseudoacacia* in the loess plateau (China). *For. Ecol. Manage.* 433, 459–466. doi: 10.1016/j.foreco.2018.10.029

Nasta, P., Sica, B., Mazzitelli, C., Di Fiore, P., Lazzaro, U., Palladino, M., et al. (2018). How effective is information on soil-landscape units for determining spatio-temporal variability of near-surface soil moisture? *J. Agric. Eng.* 49 (3), 174–182. doi: 10.4081/jae.2018.822

Penna, D., Brocca, L., Borga, M., and Dalla Fontana, G. (2013). Soil moisture temporal stability at different depths on two alpine hillslopes during wet and dry periods. *J. Hydrology* 477, 55–71. doi: 10.1016/j.jhydrol.2012.10.052

Quan, Q., Zhang, F., Jiang, L., Chen, H. Y. H., Wang, J., Ma, F., et al. (2021). High-level rather than low-level warming destabilizes plant community biomass production. *J. Ecol.* 109 (4), 1607–1617. doi: 10.1111/1365-2745.13583

Sun, G., Zhu, Y., Ye, M., Yang, Y., Yang, J., Mao, W., et al. (2022). Regional soil salinity spatiotemporal dynamics and improved temporal stability analysis in arid agricultural areas. *J. Of Soils Sediments* 1), 272–292. doi: 10.1007/s11368-021-03074-y

Vachaud, G., Desilans, A. P., Balabanis, P., and Vauclin, M. (1985). Temporal stability of spatially measured soil-water probability density-function. *Soil Sci. Soc. America J.* 49 (4), 822–828. doi: 10.2136/sssaj1985.03615995004900040006x

Van Pelt, R. S., and Wierenga, P. J. (2001). Temporal stability of spatially measured soil matric potential probability density function. *Soil Sci. Soc. America J.* 65 (3), 668–677. doi: 10.2136/sssaj2001.653668x

Vereecken, H., Huisman, J. A., Franssen, H. J. H., Brueggemann, N., Bogena, H. R., Kollet, S., et al. (2015). Soil hydrology: Recent methodological advances, challenges, and perspectives. *Water Resour. Res.* 51 (4), 2616–2633. doi: 10.1002/2014WR016852

Wang, G., Chen, Z., Shen, Y., and Yang, X. (2021). Efficient prediction of profile mean soil water content for hillslope-scale caragana korshinskii plantation using temporal stability analysis. *Catena* 206. doi: 10.1016/j.catena.2021.105491

Xin, X., Zhang, J., and Zhu, A. (2008). Temporal stability of spatial distribution pattern of soil water tension at different scales. *Trans. Chin. Soc. Agric. Eng.* 24 (5), 15–19. doi: 10.3901/JME.2008.09.177

Yang, Q., and Zhao, W. (2014). Responses of leaf stomatal conductance and gas exchange of haloxylon ammodendronto typical precipitation event in the hexi corridor. *J. Desert Res.* 34 (2), 419–425. doi: 10.7522/j.issn.1000-694X.2013.00333

Zeng, C., Shao, M. A., Wang, Q. J., and Zhang, J. (2011). Effects of land use on temporal-spatial variability of soil water and soil-water conservation. *Acta Agriculturae Scandinavica Section B-Soil Plant Sci.* 61 (1), 1–13. doi: 10.1080/09064710903352589

Zhang, Y., Huang, M., Hu, W., Suo, L., Duan, L., and Wu, L. (2018). How shallow and how many points of measurements are sufficient to estimate the deep profile mean soil water content of a hillslope in the loess plateau? *Geoderma* 314, 85–94. doi: 10.1016/j.geoderma.2017.11.013

Zhang, P., and Shao, M. (2013). Temporal stability of surface soil moisture in a desert area of northwestern China. *J. Hydrology* 505, 91–101. doi: 10.1016/j.jhydrol.2013.08.045

Zhang, P., Shao, M., and Zhang, X. (2016). Temporal stability of soil moisture on two transects in a desert area of northwestern China. *Environ. Earth Sci.* 75 (2). doi: 10.1007/s12665-015-4914-5

Zhang, Y., Xiao, Q., and Huang, M. (2016). Temporal stability analysis identifies soil water relations under different land use types in an oasis agroforestry ecosystem. *Geoderma* 271, 150–160. doi: 10.1016/j.geoderma.2016.02.023

Zhao, W., Cui, Z., Zhang, J., and Jin, J. (2017). Temporal stability and variability of soil-water content in a gravel mulched field in northwestern China. *J. Hydrology* 552, 249–257. doi: 10.1016/j.jhydrol.2017.06.031

Zhao, Y., Peth, S., Wang, X.Y., et al (2010). Controls of surface soil moisture spatial patterns and their temporal stability in a semi-arid steppe. *HYDROLOGICAL PROCESSES*, 24 (18), 2507–2519. doi: 10.1002/hyp.7665

Zhao, Y. N., Zhou, Y. R., and Wang, H. M. (2018). Spatial heterogeneity of soil water content under introduced shrub (Caragana korshinskii) in desert grassland of the eastern ningxia, China. *Ying yong sheng tai xue bao = J. Appl. Ecol.* 29 (11), 3577–3586. doi: 10.13287/j.1001-9332.201811.001

Zhou, D., Si, J., He, X., Jia, B., Zhao, C., Wang, C., et al. (2022). The process of soil desiccation under haloxylon ammodendron plantations: A case study of the alxa legue desert, China. *Plants-Basel* 11 (3). doi: 10.3390/plants11030235

Zhou, M., Yang, Q., Zhang, H., Yao, X., Zeng, W., and Wang, W. (2020). Plant community temporal stability in response to nitrogen addition among different degraded grasslands. *Sci. Total Environ.* 729. doi: 10.1016/j.scitotenv.2020.138886

frontiers | Frontiers in Plant Science

TYPE Original Research
PUBLISHED 02 June 2023
DOI 10.3389/fpls.2023.1099139

OPEN ACCESS

EDITED BY
Antonio (Antonello) Montagnoli,
University of Insubria, Italy

REVIEWED BY
Yulong Zheng,
Chinese Academy of Sciences (CAS), China
Rishikesh Singh,
Panjab University, India

*CORRESPONDENCE
Jinfu Liu
fjljf@fafu.edu.cn
Zhongsheng He
jxhzs85@fafu.edu.cn

RECEIVED 15 November 2022
ACCEPTED 10 May 2023
PUBLISHED 02 June 2023

CITATION
Zhu J, Jiang L, Chen L, Jin X, Xing C, Liu J, Yang Y and He Z (2023) Tree seedling growth allocation of *Castanopsis kawakamii* is determined by seed-relative positions. *Front. Plant Sci.* 14:1099139. doi: 10.3389/fpls.2023.1099139

Tree seedling growth allocation of *Castanopsis kawakamii* is determined by seed-relative positions

Jing Zhu[1], Lan Jiang[1], Lyuyi Chen[2], Xing Jin[1], Cong Xing[1], Jinfu Liu[1*], Yongchuan Yang[3] and Zhongsheng He[1*]

[1]Key Laboratory of Fujian Universities for Ecology and Resource Statistics, College of Forestry, Fujian Agriculture and Forestry University, Fuzhou, China, [2]Entomology and Nematology Department, University of Florida, Gainesville, FL, United States, [3]College of Environment and Ecology, Chongqing University, Chongqing, China

Plants allocate growth to different organs as a strategy to obtain limiting resources in different environments. Tree seeds that fall from a mother tree settle on, within, or below the forest floor and litter layer, and their relative positions can determine seedling biomass and nutrient allocation and ultimately affect survival to the sapling stage. However, how emerged seedling biomass and nutrients of each organ are affected by seeds in different positions is not yet completely understood in subtropical forests. Therefore, an experiment was conducted with seeds positioned above the litter layers of different thicknesses, on the forest floor, and beneath the litter layer, and the influences of seed position on biomass allocation and nutrient use efficiency of emerged seedlings of *Castanopsis kawakamii* was examined. The aim of the study was to determine the optimal seed position to promote regeneration. Allocation strategies were well coordinated in the emerged seedlings from different seed positions. Seedlings from seeds positioned above litter layers of different thicknesses (~40 and 80 g of litter) allocated growth to leaf tissue at the expense of root tissue (lower root mass fraction) and increased nitrogen (N) and phosphorus (P) accumulation and nutrient use efficiency. Seedlings from seeds positioned beneath a deep litter layer allocated most growth to roots (high root: shoot ratio, root mass fraction) to capture available resources at the expense of leaf growth. Seedlings from seeds positioned on the forest floor allocated most growth to roots to obtain limiting resources. Further, we also found that these traits were clustered into three groups based on trait similarity, and the cumulative interpretation rate was 74.2%. Thus, seed relative positions significantly affected seedling growth by altering the allocation of resources to different organs. The different strategies indicated that root N:P ratios (entropy weight vector was 0.078) and P nutrient use efficiency were essential factors affecting seedling growth in the subtropical forest. Of the seed positions analyzed, beneath a moderate litter layer (~40 g of litter) was the most suitable position for the growth and survival of *Castanopsis* seedlings. In future studies, field and lab experiments will be combined to reveal the mechanisms underlying forest regeneration.

KEYWORDS

biomass allocation, *Castanopsis* plant, nutrient use efficiency, plant traits, seedling adaptability, trade-off strategy

1 Introduction

Plants achieve rapid growth by altering allocation strategies to capture the most available resources (i.e., water, light, and nutrients). For example, plants allocate growth to shoots or roots to, respectively, capture light or soil water and nutrients, which indirectly affects plant regeneration (Umaña et al., 2020). In forest ecosystems, seedlings are the most vulnerable stage in plant life histories (Yang et al., 2015), and the early developmental stages of seedlings are more sensitive to environmental alterations than adult stages (Wellstein, 2015). Further, forest community dynamics are unpredictable in subtropical forests due to the complex interaction among tree seedling growth, traits allocation of each organ, and environmental conditions (Bhadouria et al., 2017). Thus, understanding how seedling allocation responds to variations in the environment is a major goal in forest regeneration.

Litter or soil is the initial physical environment that seeds contact after falling from a tree (Ruprecht and Szabó, 2012; Werden et al., 2020), and seeds can settle on, within, or beneath the forest floor and litter layer (Wellstein, 2015). Seeds settle on the forest floor by animal dispersal or gravity (Huang et al., 2021; Perea et al., 2021), and then experience strong but effective photosynthetic radiation (high-intensity light). In this case, emerged seedlings prioritize the investment of resources into roots to expand root area to absorb and store water (water limitation theory) (Ma et al., 2021), thereby altering above- and belowground allocation patterns of seedlings (Umaña et al., 2021). Seeds also settle on top of the litter layer because the physical barrier of litter prevents seeds from reaching the soil (Rotundo and Aguiar, 2005; Nuñez et al., 2021). In this case, the roots of emerged seedlings cannot contact the soil, which affects seedling establishment (Rotundo and Aguiar, 2005). When litter input occurs after seed rain, seeds settle beneath the litter layer. The physical barrier caused by litter must be penetrated for seedling emergence, which alters resource allocation (Donath and Eckstein, 2011). A forest litter layer can reduce light intensity and quality, and regulate the physical and chemical environmental factors, e.g., soil moisture and nutrients, leading to less active heat exchange between the forest floor and canopy (Ruprecht et al., 2010). In this case, litter facilitates seedling growth by providing rich nutrient resources [e.g., nitrogen (N) and phosphorus (P)] (Quested and Eriksson, 2006), and provides important protection and buffering effects for early plant regeneration (Zhang et al., 2022). However, litter also restricts seedling establishment (Zhang et al., 2022), and deep litter can act as a mechanical barrier that causes the extinction of light, which affects seedling emergence (Loydi et al., 2015). Ellsworth et al. (2004) also observed that photosynthetically active radiation reaching the forest floor decreases under deep litter layer. Therefore, under the deep litter, the litter layer negatively affects seedling settlement (Zhu et al., 2022b). Thus, understanding how seed relative positions in relation to the litter layer and forest floor affect the trade-offs between above- and belowground allocation of emerged seedlings will help to clarify plant resource acquisition strategies.

Castanopsis is a common tree genus in subtropical evergreen broad-leaved forests and is widely used in forest restoration (Du et al., 2007; Yang et al., 2015). The regeneration dynamics of *Castanopsis* plants directly affect future species composition and community structure of subtropical forest ecosystems (Huang et al., 2020). In this study, we focus on seedlings since it represents an important demographic bottleneck for forest communities, and whether seedlings survive determines the success of natural regeneration (Walck et al., 2011; Yang et al., 2015; Umaña et al., 2016). The *Castanopsis kawakamii* Nature Reserve in Sanming City includes the typical evergreen broad-leaved tree species in subtropical forests throughout southeastern China (He et al., 2019). The canopy is closed because of the high forest biodiversity. There is a deep litter layer in the understory, and seed relative positions are the most common factor affecting seedling recruitment and turnover rate from seedlings to saplings (He et al., 2020). However, the effects of seed relative positions in the litter layer on emerged seedling growth remain unclear. Because of the effects of seed relative positions, regeneration dynamics and recovery strategies of seedlings in the understory are typically uncertain (He et al., 2019; He et al., 2020; Zhu et al., 2022b), presenting a challenge to forest management.

Thus, *Castanopsis kawakamii*, one of the most widely distributed dominant tree species in natural evergreen broad-leaved subtropical forest communities, was selected as the research object in this study. This study examined whether differences in allocation to seedling shoots and roots resulting from seed relative positions affected natural regeneration in subtropical forests (Figure 1). To understand the relationship between seedling allocation and regeneration, it is essential to determine how seed position in relation to the forest floor and litter layer alters allocation to seedling shoots and roots. Determining how seed position affects seedling resource allocation can help to identify the most suitable seed position for seedling regeneration in a subtropical forest. Therefore, seedling above- and belowground biomass and nutrient content traits were measured to reveal how seed positions affect seedling resource allocation.

2 Materials and methods

2.1 Site description

The study site was located in the *Castanopsis kawakamii* Nature Reserve in Sanming City, Fujian Province, China (26°07′–26°12′N, 117°24′–117°29′E). The region has a subtropical monsoon climate (He et al., 2019; He et al., 2020). The average annual temperature is 19.5°C, and the average annual precipitation is 1,500 mm. Canopy closure is approximately 80% across the region (He et al., 2019). Vegetation is typical subtropical evergreen broad-leaved forests, with the tree layer co-dominated by *C. kawakamii* (average age > 100 years), *Litsea subcoriacea*, and *Schima superba* (He et al., 2020; Zhu et al., 2022a).

2.2 Collection of materials

In March 2018, 10 sampling plots dominated by *C. kawakamii* were established in the *Castanopsis kawakamii* Nature Reserve. Five

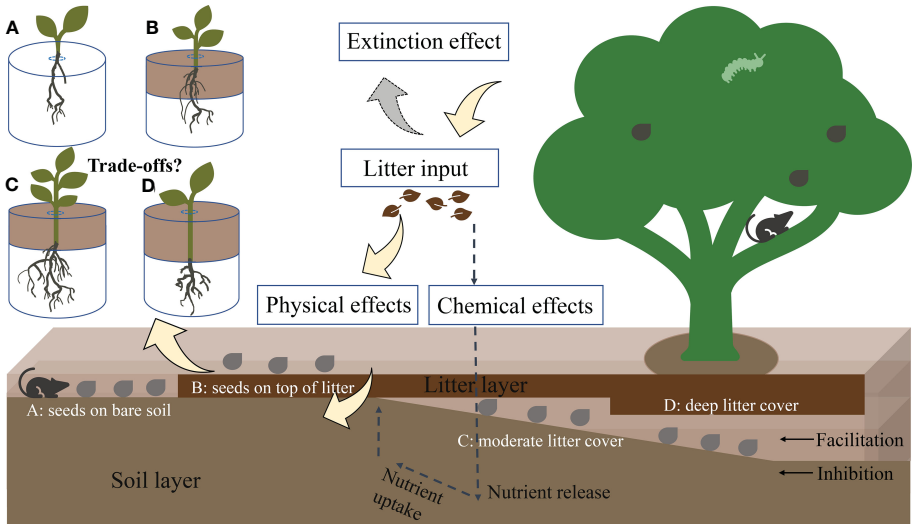

FIGURE 1
Conceptual model of the physical effects of litter, which cause seed positions to facilitate or inhibit plant regeneration. Yellow, gray, and dashed arrows represent the physical effects of litter, light extinction effects, and possible chemical effects/feedbacks of litter, respectively. Gray points represent seeds fallen from mother trees. **(A–D)** describe different positions of seeds that fall from mother trees. After germinating, seedlings from different seed positions have different growth patterns because of litter thickness and associated physical effects. Experimental design: **(A)** seeds positioned on the forest floor (without litter), **(B)** seeds positioned on top of litter, **(C)** seeds positioned beneath moderate litter cover (2 and 4 cm), and **(D)** seeds positioned beneath the deep litter cover (6 and 8 cm).

1 m × 1 m litter traps were placed 1 m above the forest floor in each plot (Zhu et al., 2022b). To reduce the experimental error caused by differences in litter types, litter from the traps was collected once a month, mixed in the laboratory, and then oven-dried to a constant weight at 65°C for 72 h.

From October to December 2018 (depending on the peak seed fall period), full and intact seeds were collected and then stored in sand. Before conducting a germination experiment, we placed seeds in distilled water for 3 h, removed the floating and inferior seeds, and selected the intact and pest-free seeds for disinfection using 0.5% $KMnO_4$. For specific details, see Zhu et al. (2022a).

The relatively thick humus layer (0–10 cm) and intricate plant roots systems on the forest floor of the *C. kawakamii* natural forest prevented seeds from always contacting the forest floor. Thus, soil was collected from a depth of 10–40 cm in each sample plot. The soil from each plot was a mixture of soil from the east, south, west, north, and center positions of each plot. The soil was passed through a 5-mm sieve to remove roots and stones. The soil was then sterilized in an autoclave for 30 min at 120°C to reduce the probability of seeds in the soil being infected by pathogens (Liang et al., 2019).

2.3 Experimental design

A germination experiment was conducted in a large indoor laboratory in January 2019. Germination pots measured 38.5 cm × 27.5 cm × 14 cm, and litter weight was calculated according to pot volume. A completely randomized experimental design included seven seed-position treatments. Seeds positioned above the litter layers included one positioned in a 2 cm thick litter layer (~40 g of litter) and one positioned in a 4 cm thick litter layer (~80 g of litter). That is, seeds were in direct contact with the litter layer. Seeds' relative positions on the forest floor or beneath the litter layer meant direct contact between the seeds and forest soil. Seeds positioned on the forest floor without litter cover layer. Seeds positioned beneath the litter layer meant that they are covered by 2 cm (~40 g of litter), 4 cm (~80 g of litter), 6 cm (~120 g of litter), and 8 cm (~160 g of litter) of litter (Zhu et al., 2022b). Each position included three experimental pots, and each pot was sown with 50 seeds of uniform size (2.062 ± 0.06 g). Thus, the experiment included a total of 21 experimental pots. Litter thickness was determined by weight, and the thickness of litter at each position was kept as consistent as possible during the study. Seeds began to germinate in mid-February, and germination was complete in mid-April 2019. Emerged seedlings, i.e., those that successfully penetrated through the litter cover, were counted every three days until the number of emerged seedlings did not increase on three consecutive days (Wellstein, 2015). Seedlings were cultivated for 6 months after emergence to measure above- and belowground traits. Pots received the same amount of water (200 mL/pot) every two days and were moved regularly to ensure similar environmental conditions for all pots during seedling growth (Zhu et al., 2022b). Soil moisture was determined based on the average annual humidity of the *C. kawakamii* natural forest (18%–27%) (Wang et al., 2021b), and litter thickness reached the mean annual value of litter in the natural forest of *C. kawakamii* (432.5–922.5 g/m^2).

2.4 Seedling biomass

In December 2019, functional traits were measured on individual seedlings. Three surviving individual seedlings in each

experimental pot were harvested to measure biomass and nutrients. Fully expanded leaves of seedlings without obvious pests and diseases were selected, and roots were separated from the main stems and leaves. Each organ was carefully cleaned of soil with deionized water, ensuring the integrity of roots as much as possible. Plants' tissues were placed in marked envelopes and returned to the laboratory for further analysis. Roots, stems, and leaves were oven-dried to constant weight at 65°C for 72 h, and dry matter mass (0.0001 g) was determined to calculate traits related to biomass allocation. Root: shoot ratio was calculated as root biomass divided by the sum of stem and leaf biomass. Mass partitioning into photosynthetic and non-photosynthetic tissues was calculated as photosynthetic tissue (leaf biomass) divided by non-photosynthetic tissue (sum of stem and root biomass) (Umaña et al., 2020). Total plant biomass was the sum of root, stem, and leaf biomass. Root mass fraction, stem mass fraction, and leaf mass fraction were calculated as root, stem, and leaf biomass divided by the total plant biomass, respectively (Shen et al., 2019b). The mean value was determined from the three surviving individual seedlings in each experimental pot (n = 3) and was regarded as one available value.

2.5 Nutrient contents

Dried seedling roots, stems, and leaves were crushed by mortar and sieved through a 0.15-mm mesh. Total N contents of roots, stems, and leaves were determined by an elemental analyzer (VARIO MAX CUBE, Elementar Analysensysteme GmbH, Germany), and total P contents were determined by inductively coupled plasma emission spectrometer (ICP-OES, PE OPTIMA 8000, PerkinElmer Inc., USA). The N:P ratios in root, stem, and leaf were calculated as N contents divided by P contents of the different tissues. The total N and P contents of plants were determined by biomass-weighted mean values of N and P contents of leaves, stems, and roots. Total N and P accumulation were determined by multiplying total plant biomass and total nutrient contents. Plant nutrient use efficiency was calculated as total plant biomass divided by total plant nutrient content (Bridgham and Pastor, 1995).

2.6 Statistical analyses

To analyze differences in biomass and nutrient allocation of emerged seedlings from different seed positions, the normality of all variables was first tested using the "shapiro.test" function. Then, "aov" and "duncan.test" functions in the "agricolae" package were used to identify significant differences among means of seedling traits from different seed positions (de Mendiburu, 2009). To assess relationships within data, effect size and 95% confidence interval (CI) were also tested for significant differences, and 'effect size' was replaced with 'mean difference' to estimate the magnitude of an effect (Nakagawa and Cuthill, 2007). Pearson correlation analysis was performed using the "corrplot" package (Friendly, 2002) to examine correlations between biomass and nutrient contents of different organs.

To consider the similarity between individuals and reduce the dimension of a primary matrix containing mixed types of variables in each organ of *C. kawakamii* seedlings, biomass and nutrient contents were incorporated into a principal component analysis (PCA) using the "prcomp" function from the "factoextra" package, and the first two dimensions were extracted (Kassambara and Mundt, 2017). The analysis was also used to identify the adaptive strategies of seedlings from seeds in different positions. Furthermore, k-means cluster analysis was used to group similar traits in the "cluster" package based on the nearest neighbor method, and the "factoextra" package was used to determine the optimal number of clusters (Kassambara and Mundt, 2017). The number of points of categorical variables was also extracted, and figures were prepared using the "prcomp" function to classify differences among seed positions. The primary matrix included 19 quantitative variables (including mass partitioning into photosynthetic and non-photosynthetic tissues, root: shoot ratio, total biomass, root mass fraction, stem mass fraction, leaf mass fraction, N and P contents of each organ, N:P ratios of root, stem, and leaf, N accumulation, P accumulation, N nutrient use efficiency, and P nutrient use efficiency) for the seven seed positions. The software R 3.5.3 was used for statistical analyses and the preparation of figures (R Development Core Team, 2020).

To determine the most suitable seed position for *C. kawakamii* seedling growth, the maximum difference normalization method was used to eliminate the effects of different trait dimensions (Zou et al., 2006). The entropy method was used to determine the objective weight of the abovementioned traits in fuzzy synthetic evaluation (Zou et al., 2006). Positive indices were those with high trait values indicating low-stress levels. However, the allocation of biomass and nutrient contents of roots, stems, and leaves represented plant adaptation strategies and explained the degree of environmental stress. Increases in values of different traits indicate plant priorities in obtaining resources. Thus, in this study, all traits were considered positive indicators, and in a synthesis of all the influencing factors, trait entropy weights were calculated. With this approach, comprehensive evaluation scores of different seed positions were obtained (Zou et al., 2006; Zhong et al., 2021), and the most suitable seed position for seedling growth was determined.

3 Results

3.1 Biomass allocation to roots, stems, and leaves

Plant biomass allocation in *C. kawakamii* seedlings from different seed positions was significantly different (Figures 2, S1; Table S1). Total biomass (Figure 2A), root mass fraction (Figure 2B), stem mass fraction (Figure 2C), and root: shoot ratio (Figure S1) of seedlings from seed positions above the litter layer were lower than those of seedlings from seed positions beneath litter layer, with leaf mass fraction being the exception (Figure 2D). Biomass values varied significantly with increasing thickness of the litter layer, and root mass fraction (Figure 2B), stem mass fraction (Figure 2C), and root: shoot ratio (Figure S1) of seedlings from seeds positioned beneath the deep litter cover were higher than those of seedlings from other seed positions.

10.3389/fpls.2023.1099139

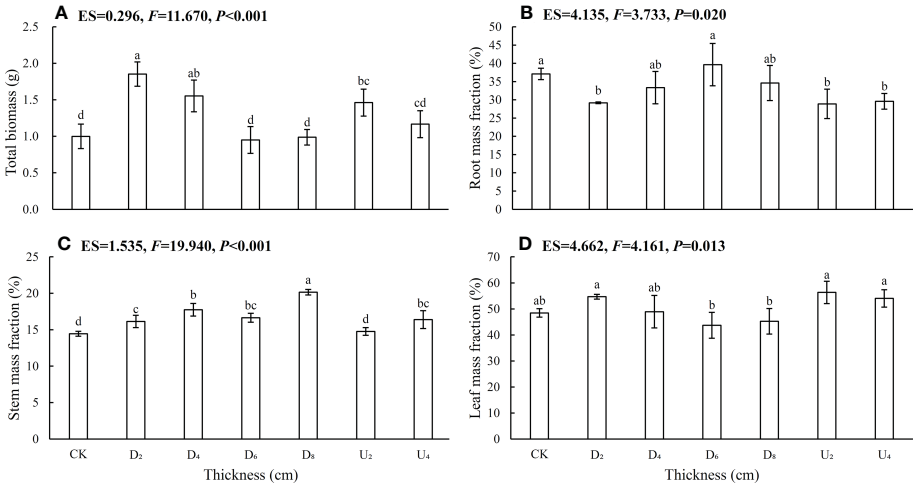

FIGURE 2
Seedling **(A)** total plant biomass, **(B)** root mass fraction, **(C)** stem mass fraction, and **(D)** leaf mass fraction. CK represents emerged seedlings from seeds positioned on the forest floor (bare soil); D_2, D_4, D_6, and D_8 represent emerged seedlings from seeds positioned beneath the litter layer with a cover of 2 cm, 4 cm, 6 cm, and 8 cm of litter, respectively; U_2 and U_4 represent emerged seedlings from seeds positioned above litter that is 2 cm and 4 cm thick, respectively. Different lowercase letters (a, b) indicate significant differences (P < 0.05). ES indicates the effect size; P indicates the probability value; F indicates the F-test value; and error bars represent one standard deviation, with the same below, and df = 6.

3.2 Nitrogen and phosphorus contents in roots, stems, and leaves

In different seed positions, leaf N contents and N:P ratios were overall higher than those in root and stem tissues (Figures 3, 4; Table S1), whereas P contents were lowest in leaves, intermediate in stems, and highest in roots. In addition, N contents of roots, stems, and leaves of seedlings from seeds positioned under the deep litter layer and on the forest floor were overall higher than those in seedlings from other seed positions (Figures 3A, C, E). Furthermore, P contents of root, stem, and leaf tissues under moderate amounts of litter layer (~40 and 80 g of litter) were overall lower than those in seedlings from other seed positions (Figures 3B, D, F), whereas N:P ratios were not (Figures 4A–C). Phosphorus contents of the shoot

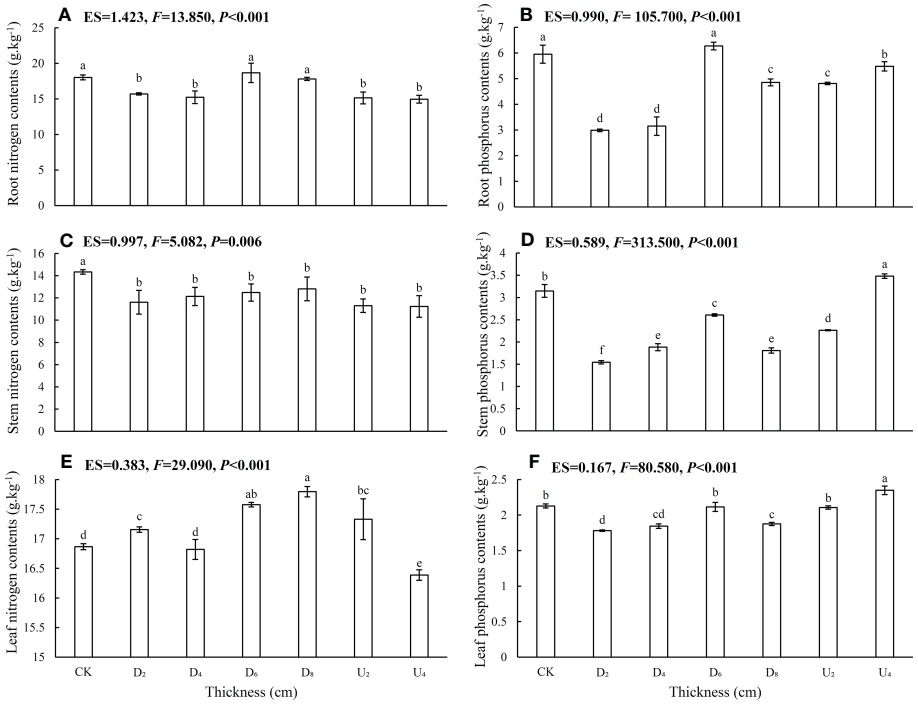

FIGURE 3
Nitrogen and phosphorus contents in roots, stems, and leaves of *Castanopsis kawakamii* seedlings. **(A)** Root nitrogen contents, **(B)** root phosphorus contents, **(C)** stem nitrogen contents, **(D)** stem phosphorus contents, **(E)** leaf nitrogen contents, and **(F)** leaf phosphorus contents of seedling. Different lowercase letters (a, b) indicate significant differences (P<0.05).

10.3389/fpls.2023.1099139

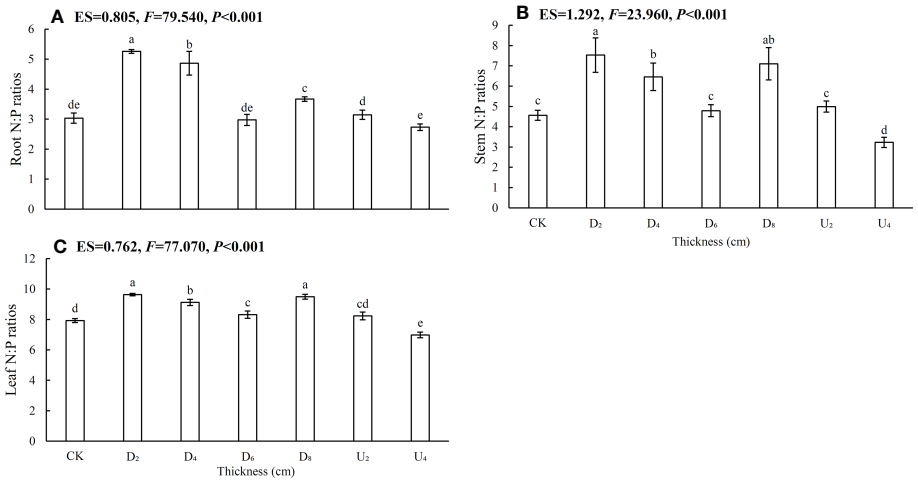

FIGURE 4
Nitrogen, phosphorus ratios in **(A)** roots, **(B)** stems, and **(C)** and leaves of *Castanopsis kawakamii* seedlings. Different lowercase letters (a, b) indicate significant differences (P<0.05).

and root tissues of seedlings from seeds positioned above the litter layer were higher than those of seedlings from seeds positioned beneath the litter layer.

3.3 Nutrient accumulation and nutrient use efficiency

Seed positions altered whole-plant N and P accumulation and nutrient use efficiency (Figure 5; Table S1). N accumulation, N and P nutrient use efficiencies of seedlings from seeds positioned under moderate litter layers (~40 and 80 g of litter) were overall higher than those of seedlings from other seed positions, whereas seedling P accumulation was lower than that from seeds positioned above the litter layer. Nutrient accumulation and use efficiency of emerged seedlings from seeds positioned beneath the deep litter layer and on the forest floor were lower than those of seedlings from seeds in other positions.

3.4 Correlations between biomass and nutrient contents

Biomass allocation to each organ was highly significantly correlated with nutrient contents (Figure S2). In a PCA, the first two dimensions explained 74.2% of the variability (Figure 6A). The first dimension (Dim 1) of the PCA accounted for 44.6% of the variance and indicated relatively high P nutrient use efficiency, root N:P ratios, N nutrient use efficiency, total biomass, and N accumulation, and relatively low root P contents were positively correlated (Figure S3A). The second dimension (Dim 2) captured 29.6% of the variance and indicated relatively low leaf N:P ratios, stem N:P ratios, and leaf N contents were negatively correlated (Figure S3B).

The nearest neighbor method was used to cluster seedlings from different seed positions according to close and distant relations of trait similarity, and seedlings from seed positions with the greatest trait similarity were clustered together (Figure 6B). Principal components were extracted from biomass and nutrient indices, which were then clustered into three groups. One group included emerged seedlings from seeds positioned at different depths beneath the moderate litter layer (~40 and 80 g of litter), which had higher total biomass, nutrient accumulation, and nutrient use efficiency than seedlings in the other groups. A second group included seedlings from seeds positioned on the forest floor and beneath the deep litter layer, which had relatively high root biomass and nutrient contents. The third group included seedlings from seeds positioned on top of the litter layer, which all had high trait similarity.

3.5 A comprehensive evaluation of different seed positions

The entropy weight vectors of biomass and nutrient contents of emerged seedlings indicated that root N:P ratios had the highest entropy weight vector, whereas root mass fraction had the lowest entropy weight vector (Table S2). The comprehensive score of the seed position beneath moderate litter cover (~40 g of litter) was significantly higher than that for the other positions, indicating the position had the most significant positive effect on seedling growth (Figure 7; Table S1). However, the lowest comprehensive score was for the seed position above the litter layer (~80 g of litter), indicating that the position might inhibit seedling growth.

4 Discussion

4.1 Effects of seed position on trade-off strategies in seedling biomass allocation

In this study, the trade-offs involved in the above- and belowground biomass allocation strategies of seedlings were

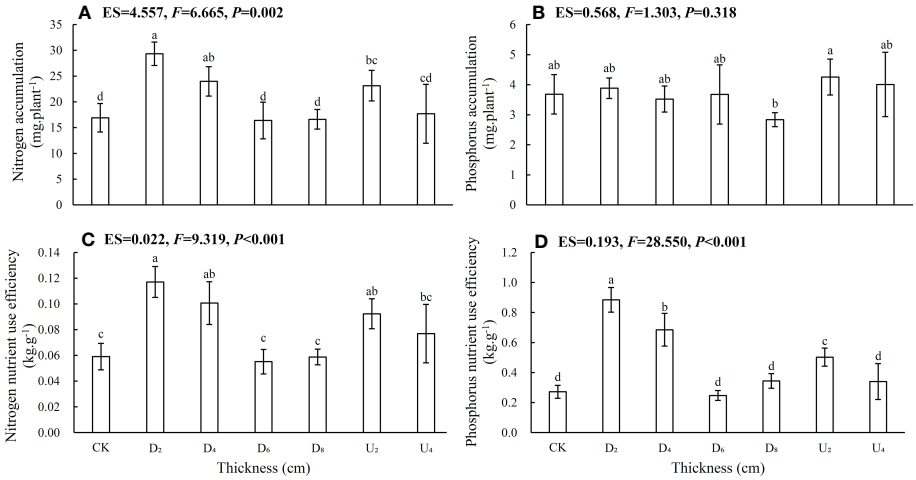

FIGURE 5
(A) Nitrogen accumulation, **(B)** phosphorus accumulation, **(C)** nitrogen nutrient use efficiency, and **(D)** phosphorus nutrient use efficiency of *Castanopsis kawakamii* seedlings. Different lowercase letters (a, b) indicate significant differences (P<0.05).

examined in response to seeds positioned on, within, and beneath the litter layer. Seedlings allocate growth to different tissues to increase the capture of the most limiting resource (Hodáňová, 1981), which ultimately affects the performance of individuals from different seed positions (Weemstra et al., 2021). Biomass allocation patterns indicated that seedlings from seeds positioned beneath the litter layer (~40 and 80 g of litter) had relatively high photosynthetic tissues at the expense of root tissues, whereas seedlings from seeds beneath the deep litter layer (~120 and 160 g of litter) decreased aboveground tissues by facilitating biomass allocation to belowground tissue. Therefore, when one organ receives additional resources, a decrease in investment in another organ is inevitable (Luo et al., 2020), indicating that plants take advantage of trait plasticity to maintain total growth. Litter acts as a physical barrier to seedling establishment (Wellstein, 2015), and the deep litter layer might cause respiration in biological mechanisms that cannot meet the needs for seedling photosynthesis (Zhang and Xi, 2021). To occupy a favorable position in the vertical direction, emerged seedlings from seeds positioned beneath the deep litter layer allocate additional carbohydrates to belowground tissue, and transfer excess nutrients to aboveground tissues to improve the acquisition of resources (Shen et al., 2019a; Ottaviani et al., 2020). Litter directly affects the light intensity reaching the forest floor, and indirectly leads to wilting or plant death (Sayer et al., 2006; Xia et al., 2019). Thus, when seedlings emerge from a seed position beneath a deep litter layer, the resulting variability in light intensity causes shifts in the ecological strategies that increase growth (Umaña et al., 2021). Under a deep litter layer, emerged seedlings increase

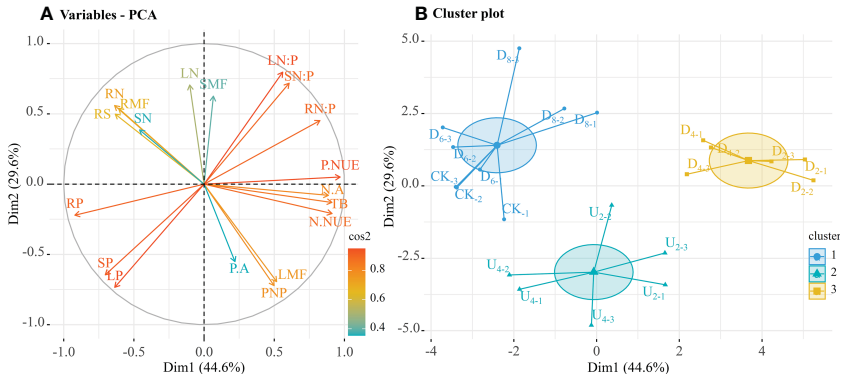

FIGURE 6
Relationship between biomass and nutrient contents in each organ of seedlings from seeds in different positions. **(A)** First two dimensions of principal component analysis. **(B)** Cluster analysis groups of individual categorical variables (seven seed positions). Cos2 value indicates the contribution of principal components, and cluster indicates the optimal number of clusters. The endpoint of cluster analysis was a set of clusters, with each cluster distinct from the others and objects within each cluster broadly similar to one another. Mass partitioning into photosynthetic and non-photosynthetic tissues (PNP), root/shoot ratio (RS), total plant biomass (TB), root mass fraction (RMF), stem mass fraction (SMF), leaf mass fraction (LMF). Root nitrogen contents (RN), stem N contents (SN), leaf N contents (LN), root phosphorus contents (RP), stem P contents (SP), and leaf P contents (LP). N:P ratios of roots (RN:P), N:P ratios of stems (SN:P), N:P ratios of leaves (LN:P); N accumulation (N.A), P accumulation (P.A), N nutrient use efficiency (N.NUE), and P nutrient use efficiency (P.NUE).

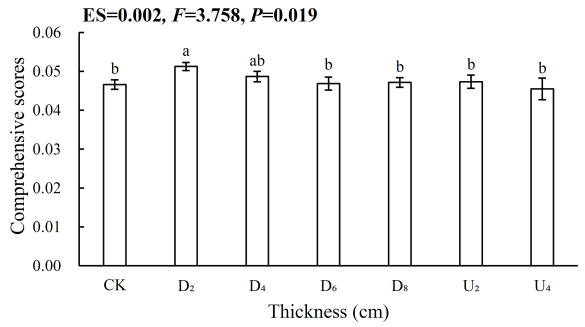

FIGURE 7
Comprehensive evaluation based on the entropy method for different seed positions. Different lowercase letters (a, b) indicate significant differences (P<0.05).

investments in root biomass at the expense of aboveground tissues to acquire the most available resources and optimize total growth (Hodáňová, 1981). In addition, the presence of a grass layer also plays a major role in tree seedlings' growth and establishment and competes with the roots of emerged seedlings for available soil resources, thus limiting the rapid seedling growth in this position (Bhadouria et al., 2020). However, litter can also block heat exchange between the soil and the external environment, prevent seedlings from being burned by high light intensities (Donath and Eckstein, 2011), release nutrients by decomposing, as well as reduce the possibility of seed predation (Wellstein, 2015). These interactive effects of light, nutrient availability caused by the litter layer, and the variations of relative positions contribute to seedling survival and recruitment (Bhadouria et al., 2020). When seedlings emerge from seeds positioned beneath or above a moderate litter layer (~40 g of litter), suitable environmental conditions can promote leaf carbon uptake and assimilation and thus facilitate leaf biomass accumulation to increase photosynthesis (de Groot et al., 2003). Simultaneously, plants can convert products of photosynthesis into resources that can be absorbed and used in natural regeneration (de Groot et al., 2003). Thus, in the case of seeds positioned beneath or above a moderate litter layer, the emerged seedlings altered the investment of each organ to receive the most available resources.

The biomass allocation strategy (i.e., relatively high root biomass) of seedlings from seeds positioned on the forest floor (i.e., bare soil) is consistent with the water limitation theory (Ma et al., 2021). When suffering from water limitation, plants always allocate more energy to belowground tissue to absorb and store water resources, and reduce leaf biomass to decrease water loss caused by transpiration (Ledo et al., 2018; Ma et al., 2021). In this study, emerged seedlings from seeds positioned on the forest floor invested in root biomass at the expense of leaf and stem tissues. The response was likely because rapid water evaporation easily transforms the forest floor into an arid environment, resulting in the lethal desiccation of seedlings (Wellstein, 2015). Furthermore, compared with seedlings germinating in the litter layer, emerged seedlings on the forest floor may be exposed to strong light intensity and experience burnt leaves (Ellsworth et al., 2004). In this position, emerged seedlings might increase allocation to roots to increase access to available resources and continue growth (Boonman et al., 2020). Thus, water balance and light intensity are critical factors in modulating the response of each organ to resource variation to maximize performance. In summary, to capture available resources, biomass allocation to each organ of seedling was well coordinated in different positions, which could lead to successful seedling recruitment.

4.2 Effects of seed position on trade-off strategies of seedling nutrient contents

Plant N and P contents and N:P ratios reflect the dynamic balance of nutrients and adaptation strategies of plants as affected by resource supply and demand (Koerselman and Meuleman, 1996; Jing et al., 2017), and are also closely associated with plant photosynthesis ability (de Groot et al., 2003). Generally, plants avoid damage in harsh environmental conditions and increase survival by maximizing organ strength (Shen et al., 2019b). In this study, emerged seedlings from seeds positioned beneath the deep litter layer generally had higher N and P contents than seedlings from other seed positions. This general pattern is consistent with the observations made by Donath and Eckstein (2011) and might be attributed to the strong positive correlation between litter thickness and light extinction (Sayer et al., 2006). With increasing litter thickness, light extinction directly offsets the photosynthetically active radiation received by plants (Xia et al., 2019). Emerged seedlings from seeds positioned beneath the deep litter layer increased investment in N and P contents to intercept light resources, and increase photosynthetic rates (Poorter et al., 2019). Nutrient contents are also transferred to roots to break through the litter mechanical barrier (Zhu et al., 2022b). Furthermore, the N and P contents of seedlings from seeds positioned on the forest floor were higher overall than that of seedlings from other seed positions. The likely cause of this result was that seedlings allocate more growth to root tissue to capture the most available resources (e.g., water or organic matter), thus achieving growth (Loydi et al., 2015; Yang et al., 2018). On the forest floor, water limitation decreases the adsorption and dissolution of inorganic P and blocks the upward transport of N and P because xylem embolisms form (He and Dijkstra, 2015; Yang, 2018). In this study, seedlings from seeds positioned on the forest floor had higher N and P contents in roots than in stems and leaves, which further confirmed the increased investment in root tissue. However, a moderate litter layer (~40 g of litter) overall decreased N and P contents of the shoot and root tissues compared with those of emerged seedlings from seeds positioned on the forest floor. Litter was assumed to alter the forest microenvironment (Donath and Eckstein, 2011) and minimize strong light radiation. In a moderate litter layer, litter reduces the evaporation rate of soil moisture and provides a shaded environment (Poorter et al., 2019), which further promotes seedling recruitment. In this case, seedlings accelerate the absorption and use of nutrient resources rather than balance supplies and demand to achieve rapid growth, which resulted in nutrient contents that were lower than those of other positions.

The N:P ratio is used to evaluate nutrient-limiting conditions in plants, and N:P ratio < 14, 14 < N:P ratios < 16, and N:P ratios >16

generally indicate limitations of N, both N and P, and P, respectively (Koerselman and Meuleman, 1996; Reich and Oleksyn, 2004; Han et al., 2005). In this study, N:P ratios (<14) were highest in leaves, intermediate in stems, and lowest in roots, which indicated that the growth of emerged seedlings was mainly limited by N (Figure 4). Leaf tissue synthesizes proteins via photosynthesis, and N-restricted seedlings obtain the most limited resource by increasing investment in leaves at the expense of non-photosynthetic tissues (Umaña et al., 2020). This trade-off directly leads to higher N:P ratios of leaves than of roots and stems. In this study, N:P ratios in each organ under a moderate litter layer were higher than those of other positions. The result indicated that the environment of the position was suitable for seedling growth because N and P contents were regulated, which can ultimately improve seedling survival (Han et al., 2005; Yang, 2018). The difference in position was likely because nutrients released by litter stimulated soil microbial activities through plant–soil feedback (Zhang et al., 2019; Wang et al., 2021a; Yang et al., 2021). When litter thickness exceeds the ability of a plant to adapt, physical effects caused by a deep litter layer may be a key factor inhibiting plant growth (Wellstein, 2015). Therefore, in a moderate litter layer, emerged seedlings alleviated nutrient limitations by altering N:P ratios (<14), which could directly influence seedling recruitment in subtropical forests.

4.3 Effects of seed position on seedling nutrient accumulation and use efficiency

Nutrient accumulation and use efficiency are important factors affecting plant regeneration and adaptation strategies (Han et al., 2005). A moderate litter layer (~40 g of litter) promoted N and P accumulation and nutrient use efficiencies in emerged seedlings (Figure 5). Such effects are likely associated with litter nutrient turnover rates and release (Berg, 2000). Rapidly decomposing litter increases soil nutrient availability for plant growth (Berg, 2000; Xu et al., 2013), thereby easing nutrient limitations for emerged seedlings. When decomposed slowly, litter maintains soil moisture and regulates soil temperature and relative humidity (Xu et al., 2013). This study concludes that the litter layer increased the diffusion of N and P in soil and thereby increased nutrient absorption and utilization by seedlings (Ellsworth et al., 2004). Thus, a moderate litter layer can provide an optimal growth environment for emerged seedlings in which roots assimilate and then shift N and P to other tissues (Boonman et al., 2020). In a moderate litter layer, seedlings can allocate growth to other tissues to compensate for the adverse effects of nutrient limitations by increasing nutrient accumulation and use efficiency and maintaining a nutrient balance (Yang et al., 2018). However, nutrient accumulation and use efficiency of emerged seedlings from seeds positioned beneath the deep litter layer were lower than those of seedlings in other positions. This result was likely caused by low amounts of nutrients released from litter (chemical effects) combined with mechanical barriers (physical effects). Physical effects are important factors affecting seedling emergence (Xu et al., 2013; Wellstein, 2015). When soil nutrients released by decomposing litter counteract the inhibition of physical barriers, seedlings from seeds positioned beneath a deep litter layer allocate additional growth to roots to expand the root area to absorb soil nutrients. Beneath a deep litter layer, plants can penetrate through litter cover to emerge and improve competitiveness (de Groot et al., 2003; Quested and Eriksson, 2006). Overall, seed relative positions influence the adaptability of emerged seedlings by altering nutrient accumulation and nutrient use efficiency of each organ.

4.4 Implications of trade-off strategies for regeneration in subtropical forests

In this study, relationships were explored between different positions of seeds and biomass and nutrient contents of seedlings of a dominant tree species to better understand how seed position affects regeneration in subtropical natural forests (Figures 6, S2). According to cluster analysis, biomass and nutrient allocation of emerged seedlings from seeds positioned above litter layers of different thicknesses, and those from seeds positioned beneath the deep litter layer and on the forest floor were clustered in one group. These results indicated that the variations of traits (biomass and nutrient) allocation were highly similar (Zhu et al., 2022b). Thus, emerged seedlings from these positions may increase the allocation to roots to obtain soil organic matter and water resources to adapt to an unfavorable environment, thus achieving rapid growth (Shen et al., 2019b). With continuous input, litter can regulate the physical and chemical environment of seed positions, and the amount of litter may be a critical factor in seedling regeneration (Wellstein, 2015). Similarly, to eliminate the negative effects caused by litter, emerged seedlings from seeds positioned beneath the deep litter layer expanded root area or increased leaf N contents to access limited resources and promote seedling growth. Comprehensive scores indicated that moderate litter cover (~40 g of litter) promoted the most seedling growth (Figure 7), and thus, positioning seeds in a moderately thick litter layer might be the best approach to regulate biomass and nutrient allocation of emerged seedlings in subtropical forests.

Root, stem, and leaf N:P ratios <14, as well as relatively high leaf N:P ratios and relatively low coefficients of variation (Figure S4), further confirmed the hypothesis that nutrient limitations for plant growth are best evaluated by leaf N:P ratios, compared with those of other tissues (Güsewell, 2004; He et al., 2008). A comprehensive evaluation of biomass and nutrient traits in seedlings from different seed positions demonstrated that the entropy weight vectors of root N:P ratios and P use efficiency were higher than those of other traits. The results further verified that P is the main factor affecting the rapid growth of plants during regeneration in subtropical evergreen broad-leaved forests (Han et al., 2005). It was also hypothesized that litter regulates the physical and chemical environment of seedlings during recruitment and that interactions between such effects may produce conflicting responses between above- and belowground biomass allocation (Figure 8). Thus, studying the biomass and nutrient allocation of seedlings from seeds positioned above, within, or beneath the forest floor and litter layer is a powerful approach to understanding forest regeneration. However, other

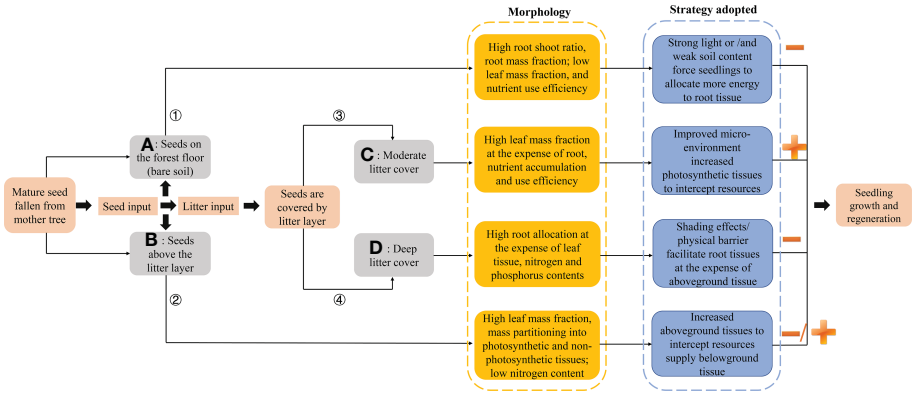

FIGURE 8
Trade-offs in seedling adaptability depend on seed positions. (1) Gray box represents seed positions; orange and blue boxes indicate morphological characteristics of emerged seedlings from seeds positioned on the forest floor and litter layer, and their adopted resource strategies, respectively. Addition (+) and subtraction **(-)** signs represent positive and negative effects, respectively, on seedling growth from seeds in different positions, whereas -/+ indicates first promotion and then inhibition of seedling growth in a position. (2) Main results: when mature seeds fall from mother trees, they may be positioned **(A)** on the forest floor (bare soil) or **(B)** above the litter layer. Seedlings from seeds positioned on the forest floor allocated growth to roots to achieve growth. With litter input, seedlings from seeds positioned in deep litter **(D)**/top of litter had relatively high leaf mass fraction at the expense of root investment. Moderate litter layer cover **(C)** (~40 g of litter) increased allocation to photosynthetic tissue at the expense of root tissue to promote the natural regeneration of seedlings in forests.

variables that affect the allocation strategies of seedlings, such as the soil environment and differences between lab and field experiments (He et al., 2020), were not tested in this study, although such variables may also be important in regulating seedling regeneration and thus deserve further study. Likewise, allocation strategies of seedlings in different age classes or habitats should be considered in future research. Finally, long-term responses in subtropical forests also need to be monitored.

5 Conclusion

To investigate factors affecting seedling regeneration in subtropical forests, this study explored the effects of different seed positions on above- and belowground biomass and nutrient contents of emerged seedlings of a dominant tree species. One critical finding was that biomass allocation in different organs was well coordinated. Emerged seedlings from seeds positioned above litter and beneath a moderate litter layer (~40 and 80 g of litter) had higher leaf allocation at the expense of root and stem tissues than seedlings from other positions. Emerged seedlings from seeds positioned beneath a deep litter layer (~120 and 160 g of litter) had higher root allocation at the expense of leaf tissue than seedlings from other positions, which was necessary to break through the physical barrier of litter. Biomass and nutrient allocation of emerged seedlings from seeds positioned on the forest floor indicated a decrease in investment in shoot tissue to achieve growth. Traits of biomass and nutrient were also comprehensively analyzed, and the analysis indicated that seedlings from seeds positioned beneath a moderate litter layer (~40 g of litter) facilitated the regeneration of a dominant tree species in the natural community, because those seedlings had relatively high N and P accumulation and nutrient use efficiency (N:P ratios < 14). Thus, protective mechanisms that occur in seeds positioned beneath a litter layer are particularly important for the natural regeneration of seedlings. In the future, seedling regeneration in subtropical natural forests could be promoted by adjusting litter thickness or adding N elements.

Data availability statement

The raw data supporting the conclusions of this article will be made available by the authors, without undue reservation.

Author contributions

JZ: conceptualization, formal analysis, investigation, methodology, writing–original draft, writing–review, and editing. LJ: investigation and formal analysis. LC: writing–review and editing. XJ: investigation. CX: investigation. JL: conceptualization, supervision, writing–review, editing, and funding acquisition. YY: writing–review and editing. ZH: conceptualization, supervision, writing–review, editing, and funding acquisition. All authors contributed to the article and approved the submitted version.

Funding

This work was sponsored by the National Natural Science Foundation of China (NSFC) [grant numbers 31700550, 31770678], the Fujian Province Forestry Science and Technology Project of China [grant number 2022FKJ21], and the Forestry Peak Discipline Construction Project of Fujian Agriculture and Forestry University of China [72202200205].

Acknowledgments

We wish to express our thanks for the support received from the *Castanopsis kawakamii* Nature Reserve in Sanming City, Fujian province, for allowing us to collect samples. We also thank Xuelin Wang, Xinguang Gu, Meihua Jia, and Qianru Xiao for their help during the experiment work.

Conflict of interest

The authors declare that the research was conducted in the absence of any commercial or financial relationships that could be construed as a potential conflict of interest.

Publisher's note

Supplementary material

The Supplementary Material for this article can be found online at: https://www.frontiersin.org/articles/10.3389/fpls.2023.1099139/full#supplementary-material

References

Berg, B. (2000). Litter decomposition and organic matter turnover in northern forest soils. *For. Ecol. Manage.* 133, 13–22. doi: 10.1016/S0378-1127(99)00294-7

Bhadouria, R., Srivastava, P., Singh, R., Tripathi, S., Singh, H., and Raghubanshi, A. S. (2017). Tree seedling establishment in dry tropics: an urgent need of interaction studies. *Environ. Syst. Decis.* 37, 88–100. doi: 10.1007/s10669-017-9625-x

Bhadouria, R., Srivastava, P., Singh, R., Tripathi, S., Verma, P., and Raghubanshi, A. S. (2020). Effects of grass competition on tree seedlings growth under different light and nutrient availability conditions in tropical dry forests in India. *Ecol. Res.* 35, 807–818. doi: 10.1111/1440-1703.12131

Boonman, C. C. F., van Langevelde, F., Oliveras, I., Couédon, J., Luijken, N., Martini, D., et al. (2020). On the importance of root traits in seedlings of tropical tree species. *New Phytol.* 227, 156–167. doi: 10.1111/nph.16370

Bridgham, S. D., and Pastor, J. (1995). Nutrient-use efficiency: a litterfall index, a model, and a test along a nutrient availability. *Am. Nat.* 145, 1–21. doi: 10.1086/285725

de Groot, C. C., van den Boogaard, R., Marcelis, L. F. M., Harbinson, J., and Lambers, H. (2003). Contrasting effects of n and p deprivation on the regulation of photosynthesis in tomato plants in relation to feedback limitation. *J. Exp. Bot.* 54, 1957–1967. doi: 10.1093/jxb/erg193

de Mendiburu, F. (2009). *Una herramienta de analisis estadistico para la investigacion agricola. master's thesis* (Rímac, Peru: Universidad Nacional de Ingenieria (UNI-PERU).

Donath, T. W., and Eckstein, R. L. (2011). Litter effects on seedling establishment interact with seed position and earthworm activity. *Plant Biol.* 14, 163–170. doi: 10.1111/j.1438-8677.2011.00490.x

Du, X. J., Guo, Q. F., Gao, X. M., and Ma, K. P. (2007). Seed rain, soil seed bank, seed loss and regeneration of *Castanopsis fargesii* (Fagaceae) in a subtropical evergreen broad-leaved forest. *For. Ecol. Manage.* 238, 212–219. doi: 10.1016/j.foreco.2006.10.018

Ellsworth, J. W., Harrington, R. A., and Fownes, J. H. (2004). Seedling emergence, growth, and allocation of oriental bittersweet: effects of seed input, seed bank, and forest floor litter. *For. Ecol. Manage.* 190, 255–264. doi: 10.1016/j.foreco.2003.10.015

Friendly, M. (2002). Corrgrams: exploratory displays for correlation matrices. *Am. Stat.* 56, 316–324. doi: 10.1198/000313002533

Güsewell, S. (2004). N:P ratios in terrestrial plants: variation and functional significance. *New Phytol.* 164, 243–266. doi: 10.1111/j.1469-8137.2004.01192.x

Han, W. X., Fang, J. Y., Guo, D. L., and Zhang, Y. (2005). Leaf nitrogen and phosphorus stoichiometry across 753 terrestrial plant species in China. *New Phytol.* 168, 377–385. doi: 10.1111/j.1469-8137.2005.01530.x

He, M. Z., and Dijkstra, F. A. (2015). Drought effect on plant nitrogen and phosphorus: a meta-analysis. *New Phytol.* 204, 924–931. doi: 10.1111/nph.12952

He, Z. S., Wang, L.J., Jiang, L., Wang, Z., Liu, J.F., Xu, D.W., et al. (2019). Effect of microenvironment on species distribution patterns in the regeneration layer of forest gaps and non-gaps in a subtropical natural forest, China. *Forests* 10, 90. doi: 10.3390/f10020090

He, Z. S., Tang, R., Li, M. J., Jin, M. R., Xin, C., Liu, J. F., et al. (2020). Response of photosynthesis and chlorophyll fluorescence parameters of *Castanopsis kawakamii* seedlings to forest gaps. *Forests* 11, 21. doi: 10.3390/f11010021

He, J. S., Wang, L., Flynn, D. F. B., Wang, X. P., Ma, W. H., and Fang, J. Y. (2008). Leaf nitrogen: phosphorus stoichiometry across Chinese grassland biomes. *Oecologia* 155, 301–310. doi: 10.1007/s00442-007-0912-y

Hodáňová, D. (1981). Plant strategies and vegetation processes. *Biol. Plant* 23, 254. doi: 10.1007/BF02895358

Huang, L., Jin, C., Zhou, L. H., Song, K., Qian, S. H., Lin, D. M., et al. (2021). Benefit vs. cost trade-offs of masting across seed-to-seedling transition for a dominant subtropical forest species. *J. Ecol.* 109, 3087–3098. doi: 10.1111/1365-2745.13722

Huang, L., Zhou, L. H., Wang, J. M., Jin, C., Hu, S. W., Qian, S. H., et al. (2020). Short-term decline of *Castanopsis fargesii* adult trees promotes conspecific seedling regeneration: the complete process from seed production to seedling establishment. *Ecol. Evol.* 10, 10657–10671. doi: 10.1002/ece3.6719

Jing, H., Zhou, H. X., Wang, G. L., Xue, S., Liu, G. B., and Duan, M. C. (2017). Nitrogen addition changes the stoichiometry and growth rate of different organs in *Pinus tabuliformis* seedlings. *Front. Plant Sci.* 8. doi: 10.3389/fpls.2017.01922

Kassambara, A., and Mundt, F. (2017) *Factoextra: extract and visualize the results of multivariate data analyses. retrieved from*. Available at: http://www.sthda.com/english/rpkgs/factoextra.

Koerselman, W., and Meuleman, A. F. M. (1996). The vegetation N:P ratio: a new tool to detect the nature of nutrient limitation. *J. Appl. Ecol.* 33, 1441–1450. doi: 10.2307/2404783

Ledo, A., Paul, K. I., Burslem, D. F. R. P., Ewel, J. J., Barton, C., Battaglia, M., et al. (2018). Tree size and climatic water deficit control root to shoot ratio in individual trees globally. *New Phytol.* 217, 8–11. doi: 10.1111/nph.14863

Liang, M. X., Liu, X. B., Parker, I. M., Johnson, D., Zheng, Y., Luo, S., et al. (2019). Soil microbes drive phylogenetic diversity-productivity relationships in a subtropical forest. *Sci. Adv.* 5, eaax5088. doi: 10.1126/sciadv.aax5088

Loydi, A., Donath, T. W., Otte, A., and Eckstein, R. L. (2015). Negative and positive interactions among plants: effects of competitors and litter on seedling emergence and growth of forest and grassland species. *Plant Biol.* 17, 667–675. doi: 10.1111/plb.12287

Luo, Y. J., Wang, X. K., Ouyang, Z. Y., Lu, F., Feng, L. G., and Tao, J. (2020). A review of biomass equations for china's tree species. *Earth Syst. Sci. Data* 12, 21–40. doi: 10.5194/essd-12-21-2020

Ma, H. Z., Mo, L. D., Crowther, T. W., Maynard, D. S., van den Hoogen, J., Stocker, B. D., et al. (2021). The global distribution and environmental drivers of aboveground versus belowground plant biomass. *Nat. Ecol. Evol.* 5, 1110–1122. doi: 10.1038/s41559-021-01485-1

Nakagawa, S., and Cuthill, I. C. (2007). Effect size, confidence interval and statistical significance: a practical guide for biologists. *Biol. Rev.* 82, 591–605. doi: 10.1111/j.1469-185X.2007.00027.x

Nuñez, N. H., Chazdon, R. L., and Russo, S. E. (2021). Seed rain–successional feedbacks in wet tropical forests. *Ecology* 102, e03362. doi: 10.1002/ecy.3362

Ottaviani, G., Molina-Venegas, R., Charles-Dominique, T., Chelli, S., Campetella, G., Canullo, R., et al. (2020). The neglected belowground dimension of plant dominance. *Trends Ecol. Evol.* 35, 763–766. doi: 10.1016/j.tree.2020.06.006

Perea, A. J., Wiegand, T., Garrido, J. L., Rey, P. J., and Alcántara, J. M. (2021). Legacy effects of seed dispersal mechanisms shape the spatial interaction network of plant species in Mediterranean forests. *J. Ecol.* 109, 3670–3684. doi: 10.1111/1365-2745.13744

Poorter, H., Ülo, N., Ntagkas, N., Siebenkäs, A., Mäenpää, M., Matsubara, S., et al. (2019). A meta-analysis of plant responses to light intensity for 70 traits ranging from molecules to whole plant performance. *New Phytol.* 223, 1073–1105. doi: 10.1111/nph.15754

Quested, H., and Eriksson, Q. (2006). Litter species composition influences the performance of seedlings of grassland herbs. *Funct. Ecol.* 20, 522–532. doi: 10.1111/j.1365-2435.2006.01131.x

R Delopment Core Team (2020). *R: a language and environment for statistical computing* (Vienna, Austria: R Foundation for Statistical Computing). Available at: http://www.R-project.org/.+

Reich, P. B., and Oleksyn, J. (2004). Global patterns of plant leaf n and p in relation to temperature and latitude. *Proc. Natl. Acad. Sci. U.S.A.* 101, 11001–11006. doi: 10.1073/pnas.0403588101

Rotundo, J. L., and Aguiar, M. R. (2005). Litter effects on plant regeneration in arid lands: a complex balance between seed retention, seed longevity and soil-seed contact. *J. Ecol.* 93, 829–838. doi: 10.1111/j.1365-2745.2005.01022.x

Ruprecht, E., Józsa, J., Ölvedi, T. B., and Simon, J. (2010). Differential effects of several "litter" types on the germination of dry grassland species. *J. Veg. Sci.* 21, 1069–1081. doi: 10.1111/j.1654-1103.2010.01206.x

Ruprecht, E., and Szabó, A. (2012). Grass litter is a natural seed trap in long-term undisturbed grassland. *J. Veg. Sci.* 23, 495–504. doi: 10.1111/j.1654-1103.2011.01376.x

Sayer, E. J., Tanner, E. V. J., and Cheesman, A. W. (2006). Increased litterfall changes fine root distribution in a moist tropical forest. *Plant Soil* 281, 5–13. doi: 10.1007/s11104-005-6334-x

Shen, Y., Gilbert, G. S., Li, W. B., Fang, M., Lu, H. P., and Yu, S. X. (2019a). Linking aboveground traits to root traits and local environment: implications of the plant economics spectrum. *Front. Plant Sci.* 10. doi: 10.3389/fpls.2019.01412

Shen, Y., Umaña, M. N., Li, W. B., Fang, M., Chen, Y. X., Lu, H. P., et al. (2019b). Coordination of leaf, stem and root traits in determining seedling mortality in a subtropical forest. *For. Ecol. Manage.* 446, 285–292. doi: 10.1016/j.foreco.2019.05.032

Umaña, M. N., Arellano, G., Swenson, N. G., and Zambrano, J. (2021). Tree seedling trait optimization and growth in response to local-scale soil and light variability. *Ecology* 102, e03252. doi: 10.1002/ecy.3252

Umaña, M. N., Cao, M., Lin, L. X., Swenson, N. G., and Zhang, C. C. (2020). Trade-offs in above and belowground biomass allocation influencing seedling growth in a tropical forest. *J. Ecol.* 109, 1184–1193. doi: 10.1111/1365-2745.13543

Umaña, M. N., Forero-Montaña, J., Muscarella, R., Nytch, C. J., Thompson, J., Uriarte, M., et al. (2016). Interspecific functional convergence and divergence and intraspecific negative density dependence underlie the seed-to-seedling transition in tropical trees. *Am. Nat.* 187, 99–109. doi: 10.1086/684174

Walck, J. L., Hidayati, S. N., Dixon, K. W., Thompson, K., and Poschlod, P. (2011). Climate change and plant regeneration from seed. *Glob. Change Biol.* 17, 2145–2161. doi: 10.1111/j.1365-2486.2010.02368.x

Wang, X. L., Liu, J. F., He, Z. S., Xing, C., Zhu, J., Gu, X. G., et al. (2021b). Forest gaps mediate the structure and function of soil microbial community in a *Castanopsis kawakamii* forest. *Ecol. Indic.* 122, 107288. doi: 10.1016/j.ecolind.2020.107288

Wang, J. N., Xu, B., Wu, Y., Gao, J., Shi, F. S., and Wu, N. (2021a). Effect of inflorescence litter from distinct species and life forms on soil nutrients and microbial biomass in the eastern Tibetan plateau. *Glob. Ecol. Conserv.* 31, e01825. doi: 10.1016/j.gecco.2021.e01825

Weemstra, M., Zambrano, J., Allen, D., and Umaña, M. N. (2021). Tree growth increases through opposing above and belowground resource strategies. *J. Ecol.* 109, 3502–3512. doi: 10.1111/1365-2745.13729

Wellstein, C. (2015). Seed-litter-position drives seedling establishment in grassland species under recurrent drought. *Plant Biol.* 14, 1006–1010. doi: 10.1111/j.1438-8677.2012.00635.x

Werden, L. K., Holl, K. D., Rosales, J. A., Sylvester, J. M., and Zahawi, R. A. (2020). Effects of dispersal-and niche-based factors on tree recruitment in tropical wet forest restoration. *Ecol. Appl.* 30, e02139. doi: 10.1002/eap.2139

Xia, L., Song, X. Y., Fu, N., Cui, S. Y., Li, L. J., Li, H. Y., et al. (2019). Effects of forest litter cover on hydrological response of hillslopes in the loess plateau of China. *Catena* 181, 104076. doi: 10.1016/j.catena.2019.104076

Xu, S., Liu, L. L., and Sayer, E. J. (2013). Variability of above-ground litter inputs alters soil physicochemical and biological processes: a meta-analysis of litterfall-manipulation experiments. *Biogeosciences* 10, 7423–7433. doi: 10.5194/bg-10-7423-2013

Yang, H. (2018). Effects of nitrogen and phosphorus addition on leaf nutrient characteristics in a subtropical forest. *Trees* 32, 383–391. doi: 10.1007/s00468-017-1636-1

Yang, Y. C., Huang, L., Qian, S. H., and Fukuda, K. (2015). Completing the life history of *Castanopsis fargesii*: changes in the seed dispersal, seedling and sapling recruitment patterns. *Eur. J. For. Res.* 134, 1143–1154. doi: 10.1007/s10342-015-0916-9

Yang, Y., Liu, B. R., and An, S. S. (2018). Ecological stoichiometry in leaves, roots, litters and soil among different plant communities in a desertified region of northern China. *Catena* 166, 328–338. doi: 10.1016/j.catena.2018.04.018

Yang, X. L., Wang, X. T., Xiao, S., Liu, Z. Y., Zhou, X. H., Du, G. Z., et al. (2021). Dominant plants affect litter decomposition mainly through modifications of the soil microbial community. *Soil Biol. Biochem.* 161, 108399. doi: 10.1016/j.soilbio.2021.108399

Zhang, P., Li, B., Wu, J. H., and Hu, S. J. (2019). Invasive plants differentially affect soil biota through litter and rhizosphere pathways: a meta-analysis. *Ecol. Lett.* 22, 200–210. doi: 10.1111/ele.13181

Zhang, X. Y., Ni, X. Y., Heděnec, P., Yue, K., Wei, X. Y., Yang, J., et al. (2022). Litter facilitates plant development but restricts seedling establishment during vegetation regeneration. *Funct. Ecol.* 36, 3134–3147. doi: 10.1111/1365-2435.14200

Zhang, C. H., and Xi, N. X. (2021). Precipitation changes regulate plant and soil microbial biomass *via* plasticity in plant biomass allocation in grasslands: a meta-analysis. *Front. Plant Sci.* 12, 614968. doi: 10.3389/fpls.2021.614968

Zhong, C. H., Yang, Q. C., Liang, J., and Ma, H. Y. (2021). Fuzzy comprehensive evaluation with AHP and entropy methods and health risk assessment of groundwater in yinchuan basin, northwest China. *Environ. Res.* 204, 111956. doi: 10.1016/j.envres.2021.111956

Zhu, J., Jiang, L., Zhu, D. H., Xing, C., Jin, M. R., Liu, J. F., et al. (2022a). Forest gaps regulate seed germination rate and radicle growth of an endangered plant species in a subtropical natural forest. *Plant Diversity* 44, 445–454. doi: 10.1016/j.pld.2021.10.003

Zhu, J., Liu, J. F., Xing, C., Jiang, L., Wang, X. L., He, Z. S., et al. (2022b). Effect of seeds dispersal position on the root morphology and growth characteristics of *Castanopsis kawakamii* seedlings. *Acta Ecol. Sin.* 42, 4065–4075. doi: 10.5846/stxb202102060385

Zou, Z. H., Yi, Y., and Sun, J. N. (2006). Entropy method for determination of weight of evaluating indicators in fuzzy synthetic evaluation for water quality assessment. *J. Environ. Sci.* 18, 1020–1023. doi: 10.1016/S1001-0742(06)60032-6

Frontiers in Plant Science

Cultivates the science of plant biology and its applications

The most cited plant science journal, which advances our understanding of plant biology for sustainable food security, functional ecosystems and human health.

Discover the latest Research Topics

See more →

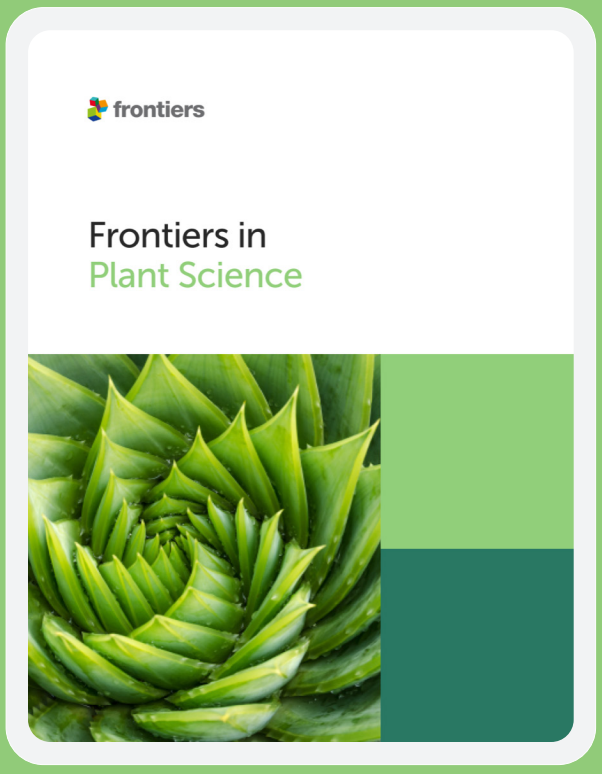

Frontiers

Avenue du Tribunal-Fédéral 34
1005 Lausanne, Switzerland
frontiersin.org

Contact us

+41 (0)21 510 17 00
frontiersin.org/about/contact